ASSEMBLY AND MECHANISM OF ACTION OF *SULFOLOBUS SOLFATARICUS* DNA REPLICATION COMPLEXES

by

Robert J. Bauer

Bachelor of Science, Indiana University of Pennsylvania, 2004

Submitted to the Graduate Faculty of the
Kenneth P. Dietrich School of Arts and Sciences in partial fulfillment
of the requirements for the degree of
Doctor of Philosophy

University of Pittsburgh

2014

ASSEMBLY AND MECHANISM OF ACTION OF *SULFOLOBUS SOLFATARICUS* DNA REPLICATION COMPLEXES

UNIVERSITY OF PITTSBURGH

DIETRICH SCHOOL OF ARTS AND SCIENCES

This dissertation was presented

by

Robert J. Bauer

It was defended on

May 21, 2014

and approved by

Sanford Asher, PhD, Professor, Department of Chemistry

Seth Horne, PhD, Assistant Professor, Department of Chemistry

Nicolas Sluis-Cremer, PhD, Associate Professor, Department of Medicine

Dissertation Advisor: Michael Trakselis, PhD, Assistant Professor, Department of Chemistry

ASSEMBLY AND MECHANISM OF ACTION OF *SULFOLOBUS SOLFATARICUS* DNA REPLICATION COMPLEXES

Robert J. Bauer, Ph.D.

The University of Pittsburgh, 2014

ABSTRACT

DNA replication enzymes are essential for the maintenance and propagation of genetic information which precisely governs the growth and development of our cells. Aberrant DNA replication processes have been implicated in a wide variety of human diseases, most notably cancer, and therefore, mechanistic understanding of DNA replication processes is paramount for the development of human therapeutic agents. The study of the eukaryotic replication system however, is difficult, as the system contains a large number of enzymes and regulatory factors making assembly of these systems for *in vitro* study complicated. Thus, in order to gain insight into the workings of the eukaryotic replication system, several model systems are used, where the complexity of the replication pathways is not as great.

The DNA replication system from the thermophilic archaeon *Sulfolobus solfataricus* is a recently identified model with components sharing high levels of sequence homology to their eukaryotic counterparts. This system is ideal for gaining insight into the mechanistic workings of DNA replication which can be translated to the eukaryotic system. A key advantage to the study of thermophilic enzymes is in the ability to utilize reaction temperatures far lower than the physiological conditions for the organisms. This results in slower kinetics with no significant change in overall function, allowing an easier discernment of the enzyme's mechanistic details.

I have contributed to the development of *Sulfolobus solfataricus* as a model system primarily through characterization of nucleotide transferase enzymes including DNA polymerases and primases. Firstly, I have determined that the DNA polymerase, *Sso*PolB3, possesses a low rate of synthesis and fidelity more similar to those involved in lesion bypass. Secondly, I characterized the assembly and mechanism of action *Sso*PolB1 replication holoenzyme which replicates in a distributive fashion similar to the eukaryotic Polδ holoenzyme, and maintains stimulated replication rates through rapid re-recruitment of the polymerase to the processivity clamp. Finally, I discovered and characterized the interactions of a unique primosome complex formed between the bacterial like DnaG primase and eukaryotic like MCM helicase. In all, my thesis provides for a more thorough understanding of the interactions, kinetics, and dynamics occurring at the replication fork.

TABLE OF CONTENTS

LIST OF TABLES

LIST OF FIGURES

PREFACE

This thesis is the culmination of all of the work and effort which I have put forth throughout my graduate career. I would like to take this opportunity to thank all of those who have helped shape me, over the course of 6 years, into not only the scientist, but also the person I have become.

I begin by thanking Dr. Michael Trakselis. My experiences as a graduate student working under the advisement of Dr. Trakselis have been the most enlightening and rewarding of my education, and having the opportunity to work for one of the most intelligent and dedicated people I have ever met has been nothing short of amazing. His in-depth knowledge, keen scientific insight, enthusiasm and constant re-assurance have allowed me to grow both personally and professionally, to heights I didn't believe possible. Dr. Trakselis has taught me everything I know about how to both perform and report research, and I thank him for his patience with all of my (likely annoying) questions.

I would also like to thank all of the members of the Trakselis laboratory that I have had the pleasure of working with over the years: Jonathan Bartko, Michael Begley, Sean Carney, Will Denq, Rodger Dilla, Brian Graham, Elizabeth Jeffries, Hsiang-kai Lin, Jessica Meyers, Andry Mikhekin, Parry Patel, Cory Rodgers, Ian Wolff, and Zhongfeng Zuo. Knowing and working with each and every one of you has been a privilege, and the times we have all shared together will be some that I will never forget. I appreciate the insights you all gave me on my own research and for providing me with the opportunity to improve my own knowledge by teaching many of you new techniques as well.

I would like to thank my committee members, Dr. Sanford Asher, Dr. Seth Horne, and Dr. Nicolas Sluis-Cremer, for their time, accommodation, and questions. I appreciate you taking time out of your schedules to be a part of the various meetings over the course of my graduate training, and of course for your involvement at my defense. I would also like to thank the University of Pittsburgh Chemistry Department and the awesome staff who have talked me through a great number of problems, many of which were of my own creation.

Finally I would like to thank my parents Mary Jane and Bernard Bauer, my brother Steven, and all of my friends for not only their support but also for putting up with me over the years. I know I am a pain much of the time! I couldn't have made it to where I am without you all, thank you for preventing me, what must have been a thousand times, from giving up.

1.0 ARCHAEAL DNA REPLICATION[1]

1.1 INTRODUTION

The DNA replication process revolves around the separation and subsequent copying of two anti-parallel parental template strands. This process is performed through the delicate interplay of a variety of different enzymes and accessory proteins to effectively synthesize DNA in a 5'-3' direction from each template strand with opposite polarity. Efficient DNA replication relies on both precise and uninterrupted DNA synthesis at the replication fork. As such, DNA replication polymerases in conjunction with a variety of accessory factors coordinate accurate synthesis in a discontinuous fashion on both the leading and lagging strands. This semiconservative DNA product contains one parental template strand and one newly synthesized complementary strand (**Figure 1.1**). Most organisms contain members from multiple DNA polymerase families including Archaea which provide a relevant model system for assessing the kinetics, dynamics, structure, and interactions of multiple DNA polymerases.

Studies over the past decade of DNA replication machinery have revealed that many components from Eukaryotes have evolved from a common ancestor in Archaea *(1)*. In particular, the archaeal DNA replication machinery is essentially a simplified eukaryotic vestige and provides an excellent experimental system for deciphering mechanisms of enzymatic action and evolutionary relationships. Although there are a number of similarities in sequence, structure, and function between Archaea and Eukaryotes, the link is not absolute, as Archaea also contain bacterial and archaeal-specific features.

---

[1] The bulk of the material for this chapter is derived from Trakselis, M.A. and **Bauer, R.J**. Archaeal DNA Polymerases: Enzymatic Abilities, Coordination, and Unique Properties, (Chapter 6) Nucleic Acid Polymerases, Murakami, K. and Trakselis, M.A. (Eds.), Berlin, Germany, Springer, 2013

Replication begins at a site on DNA termed the origin, where specific origin binding proteins called ORCs (Origin Recognition Complex) bind to and melt the DNA, allowing for the loading of helicases which are then responsible for unwinding the duplex DNA (**Figure 1.1**). Onto each of the now single stranded leading and lagging strands, single stranded binding proteins (SSBs) bind and coordinate binding of a DNA primase, which is responsible for de-novo synthesis of short RNA segments called primers.

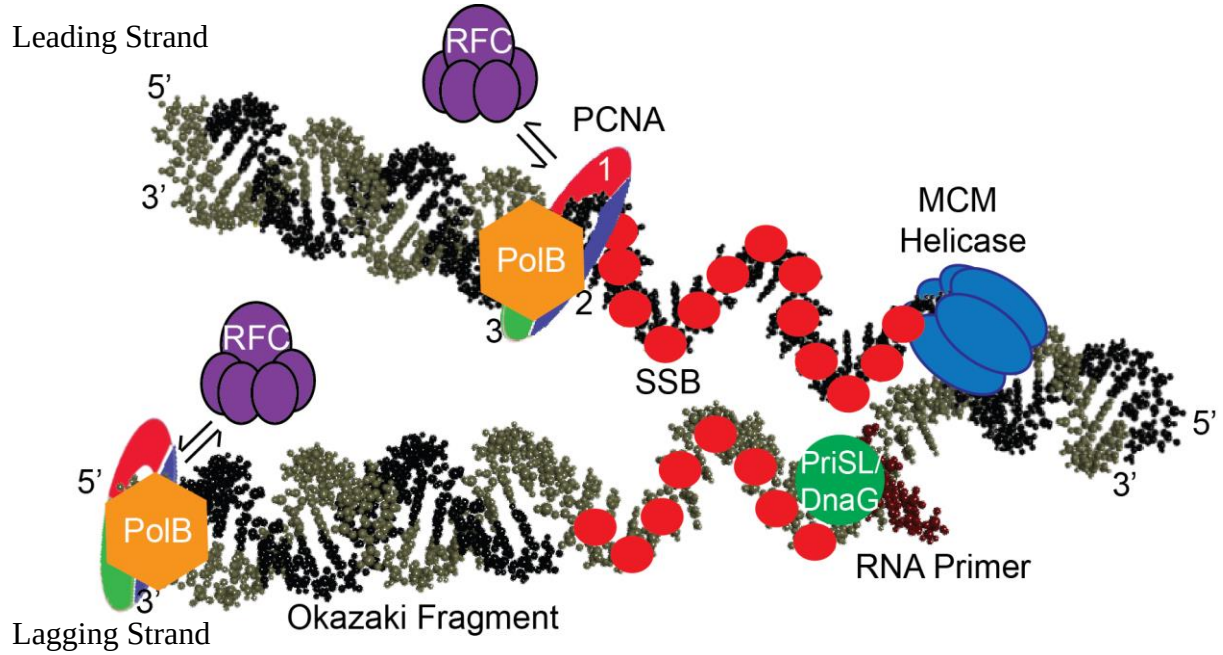

Figure 1.1: Archaeal Replisome

Depiction of both the leading strand (top) and lagging strand (bottom) replication processes. The helicase (MCM) is seen unwinding the duplex genomic DNA, which is then coated by single stranded binding protein (SSB) to prevent nuclease degradation until the daughter strand can be extended through by the replication holoenzyme (PCNA123, PolB, RFC). On the lagging strand the DNA Primase (PriSL/DnaG) is seen de-novo synthesizing an RNA primer.

These RNA primers are essential for the replication process as the DNA polymerases responsible for the bulk of DNA extension are unable to perform de-novo synthesis, instead require a primer-template for the subsequent attachment of deoxyribonucleotides (dNTPs). After creation of the primers, the replication holoenzyme is assembled, comprised of a replication DNA polymerase, processivity clamp, and potentially the ATP dependent clamp loader. This complex then elongates the leading strand in the 5'-3' direction, creating a contiguous complementary sequence. On the lagging strand, the DNA is also replicated in the 5'-3' direction creating short

discontinuous segments known as Okazaki fragments, which must later be joined together by a DNA ligase (**Figure 1.1**). The following chapter will describe the functions of these enzymes and their respective complexes in greater detail.

1.2 ARCHAEAL MCM HELICASE

The minichromosome maintenance (MCM) helicase unwinds double stranded DNA ahead of the replication fork, and is essential for the duplication of genomic DNA. It has been found that both the loading and activation of the MCM helicase are tightly regulated, and directly linked to cellular growth cycles. Deregulation of MCM function has been linked to genomic instability and development of cancer.[2, 3] In eukaryotes, the minichromosome maintenance (MCM) protein complex is composed of six unique protein subunits (MCM 2-7) and is essential for both initiation and elongation. Origins of replication are licensed when MCM proteins are loaded during G1 and unwinding of DNA commences once the cell transitions into S-phase.[4] In Archaea, the MCM complex is homohexameric, with high homology to each of the individual subunits from the eukaryotic system.[5] All MCM helicases are members of the AAA+ superfamily of enzymes, characterized by a conserved ATP binding and hydrolyzing motifs.[6]

Table 1.1: Helicases and Primases by Family

	Bacteria	**Archaea**	**Eukaryotes**
Helicase	DnaB	MCM	MCM 2-7
Primase	DnaG	DnaG and/or PriSL	Polα-Primase

MCM hexamers have a shared toroidal structure consisting of a central channel which encircles one strand of DNA. The N-terminal domain is used primarily for structural organization and processivity. The C-terminal AAA+ helicase domain contains most of the conserved residues and motifs required for ATP hydrolysis.[7-9] It has been observed that the N-terminal domain can coordinate with a neighboring subunit's C-terminal AAA+ helicase domain, through a conserved allosteric control loop. This loop plays a role in the regulation of MCM activity through facilitating communication between the domains in response to ATP binding and hydrolysis.[9, 10] Additionally

the N-terminal domain controls the directionality of the enzyme, as MCM , once loaded onto DNA traverse with 3'-5' polarity.[11] A mutant of *Sulfolobus solfataricus* MCM (*Sso*MCM) missing the N-terminal domain was observed to be much more promiscuous in its choice of substrates for DNA unwinding.[8] The unwinding of the helicase is driven by ATP hydrolysis within the C-terminal AAA+ helicase domain. The ATP binding site forms at the interface between two adjacent monomeric MCM subunits.[9] One monomer provides the P-loop responsible for stabilizing the phosphate groups, while the other interacts with the adenosine through conserved Walker A and B motifs.[9]

Several models for MCM helicase unwinding were proposed including: steric exclusion, strand extrusion, rotary pump and plowshare. In the steric exclusion model, which is a similar model to the model proposed for the prokaryotic DnaB helicase, the 5'-3' strand is excluded from entering the central channel. In the strand exclusion model, the 5'-3' strand is extruded from a side channel. This model is based on the change in size of the central channel from the C-terminal domain to the N-terminal domain, with only a single strand of DNA being able to fit through the N-terminal domains central channel.[12] In the rotary pump model, many hexameric MCM helicases bind at a replication origin and spread out along the genome. The helicases are anchored in place and rotate the DNA and unwind it through negative supercoiling.[13, 14] Finally, in the plowshare model, a rigid motif called the "plowshare" was proposed to be located at the end of the helicase. As the helicase translocated along the DNA, the plowshare would split the DNA, however this sort of motif is not present for Archaeal MCM helicases.[14] More recently, it has been shown that not only is the 5'-3' strand excluded from the central channel, it actually interacts with and wraps around the exterior of the hexameric helicase. This steric exclusion and wrapping (SEW) model is proposed to be the mechanism of unwinding for DnaB, MCM and perhaps other hexameric helicases.[15]

1.3 ARCHAEAL DNA PRIMASE FAMILIES AND FUNCTION

After the initial unwinding of duplex DNA at sites of origin, DNA replication begins with the *de novo* synthesis of short RNA primers in a template dependent manner by an RNA

polymerase which has been termed a primase. The synthesis of these short RNA primers is required in order for further extension by replicative DNA polymerases as they require the 3' –OH in order to add a subsequent nucleotide.[16] The synthesis of primers occurs at defined sites on both the leading and repeatedly on the lagging DNA strands to allow for further replication and synthesis of Okazaki fragments respectively. There are two primase families, DnaG, and Archaeo-Eukaryotic (AEP). Bacterial organisms typically contain primases which are of the DnaG family, while Eukaryotic organisms possess AEP primases. Archaea have been found to possess two separate primases DnaG (DnaG Family), and PriSL (AEP family) (**Table 1.1**).

1.3.1 DnaG Type Primases

The bacterial DnaG primase has three domains: the N-terminal Zn^{2+} binding domain, the catalytic domain (TOPRIM), and the C-terminal P16 helicase binding domain. The Zn^{2+} binding domain plays a regulatory role, controlling both DNA binding with regard to primer initiation and also the length of the primer.[17, 18] TOPRIM (TOpoisomerase-PRIMase) is a signature motif in DnaG-type primases, topoisomerase, and other nucleases.[16, 19] The TOPRIM domain is about 100 amino acids in length and contains two motifs, one centered on a glutamate and another which contains two highly conserved aspartates DxD, which have been shown to be responsible for coordination of a divalent cation (**Figure 1.2**). Both metal binding and the conserved glutamate were found to be essential for primase activity.[16] DnaG binding to DNA is generally weak and transient and occurs along an elusive positively charged region near the active site which orientates the DNA template.[20]

The C-terminal P16 domain of *Escherichia coli* DnaG (*Ec*DnaG) has been found to associate with the N-terminus of the DnaB helicase (*Ec*DnaB), forming the bacterial primosome complex that increases both priming and helicase activities.[21-24] This primase-helicase interaction and orientation has been seen in a variety of other bacterial and phage organisms[25-29] and is necessary for the repeated synthesis of primers on the lagging strand.[30] The strength of the interaction between the helicase and primase varies between organisms. In *E. coli*, this interaction was observed to be weak and transient, however in *Bacillus stearothermophilus*, the complex is stable. This potentially indicates that DnaG does not leave the replisome during lagging strand

DNA synthesis.[24, 30] In *E. coli*, the stoichiometry between DnaG and DnaB in the primosome has been observed to be 3:6 DnaG:DnaB.[31] However in other homologous systems the stoichiometry remains more unsettled including the T4 system where both 1:6 and 6:6 primase:helicase stoichiometries have been reported.[32, 33] It is clear from the available data that the stoichiometry of the primosome complex is not highly conserved in the prokaryotic system, but the interactions between enzymes direct coordinated unwinding and priming activities.

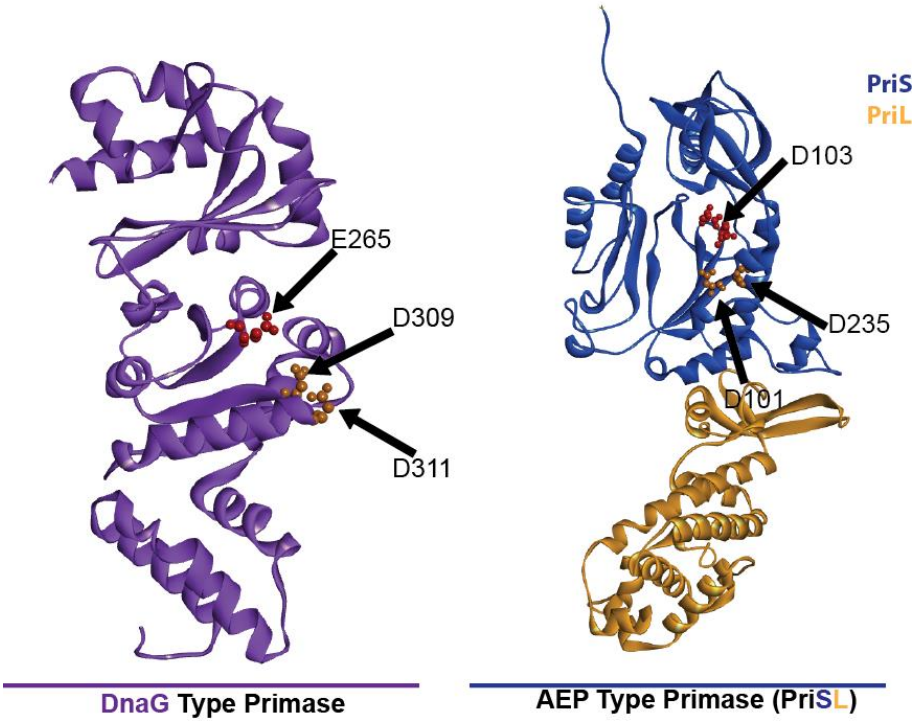

Figure 1.2: Primase Structures
The structures for the *E. coli* DnaG core catalytic domain (PDB: 1EQN), and *Sso*PriSL (PDB: 1ZT2), DNA primases. Pri small subunit catalytic subunit in conjunction with the large regulatory subunit. Active site residues for both structures are shown in CPK modeling format. Where the primary catalytic residue shown in red while divalent metal coordinating aspartates are shown in orange.

Primers synthesized by *Ec*DnaG are typically 11 nucleotides but can range from 2-14.[34] The mechanism of RNA synthesis as well as the protein interactions of *Ec*DnaG have been well studied.[18, 20, 35-44] Primer length is controlled through coordination of the two subunits of bacterial DnaG with the Zn^{2+} binding domain to regulate DNA template binding.[20, 23, 40, 45] DnaG primases

are known to have specific recognitions sequences upon which synthesis of RNA primers is initiated. In *E. coli*, this sequence was found to be 3'-(CTG)-5', however this recognition sequence appears to be species specific and is not well conserved in other homologous systems, for example in *Staphylococcus aureus* DnaG has the recognition sequence 3'-(CTA)-5', and to a weaker extent 3'-(GTA)-5'.[46]

DnaG type primases have also been found in archaeal organisms. Originally these enzymes were identified as a component of the RNA exosome complex in *Sulfolobus solfataricus*, where it was shown to stimulate degradation of a polyA substrate, and was determined to be important for efficient exosomal interaction with adenine-rich substrates.[47] The archaeal DnaG proteins were thought to be unable to perform as RNA primases due to their lack of both the N-terminal Zn^{2+} binding domain, as well as the C-terminal P16 helicase interacting domain, which are both observed in all bacterial DnaG enzymes. However, it was identified that *Sso*DnaG possesses divalent metal dependent RNA priming ability, resulting in the creation of 4 and 13 ribonucleotide products, similar to the 10 to 14 long products produced by *Ec*DnaG.[48] Surprisingly *Sso*DnaG was also found to possess robust DNA binding ability despite the lack of the Zn^{2+} N-terminal domain, thought to be important for DNA binding in the bacterial DnaG homologue. Interestingly, *Sulfolobus solfataricus* also possesses a separate Eukaryotic primase (PriSL) which is believed to be responsible for the synthesis of primers in the organism. However, significant expression of the DnaG gene has been detected *in vivo* in *Sulfolobus.*[49-52] This in conjunction with the primase ability of the enzyme potentially implicates both DnaG and PriSL in the synthesis of primers during DNA replication in *Sulfolobus.*

1.3.2 **AEP Type Primases**

The eukaryotic primase is a four subunit complex comprised of a small catalytic subunit (p48) and a large regulatory subunit (p58) that modulates binding and activity (**Figure 1.2**). These subunits are almost always found in complex with two other proteins, DNA polymerase α (p180) and polymerase B (p68), to form the polymerase α-primase complex (pol-prim).[53] This complex can synthesize RNA primers initially with minimal template specificity[54] and can then extend them by incorporating dNTPs by pol α and pol B. Eukaryotic primases may control primer length

(7-10 bases) through p58 regulation of binding to the ssDNA template that directs RNA synthesis by closing a hinge between p49/p58 subunits.[55, 56] The handoff of RNA primers larger than 7 nucleotides from p58 to pol α occurs by direct handoff within the complex for further extension into hybrid RNA-DNA products.[57, 58] The clamp loader complex (RFC) plays an important role in displacing polα after roughly 30 nucleotides for replacement with a more processive DNA polymerase holoenzyme complex that includes PCNA and either pol δ or pol ε.[59, 60]

AEP primases from Archaea contain only two of the four subunits of the pol α primosome (small catalytic, PriS, and large regulator, PriL, subunits) and have been characterized in *Pyrococcus*[61, 62], *Thermococcus kodakaraensis*[63], and *Sulfolobus solfataricus* (*Sso*).[64-66] An indirect link between PriSL and the MCM helicase is thought to be mediated by GINS23 to coordinate priming and unwinding activities in Archaea.[67] The DNA replication homology between Archaea and eukaryotes would predict that like other functional homologs, PriSL will fulfill the DNA priming role in Archaea as well.[5, 68]

In addition to RNA primer synthesis ranging from 2-500 nucleotides, these primases have surprisingly novel and unregulated DNA synthesis abilities producing oligonucleotide products greater than 7 kilobases. Temperature and slight differences in the affinity of NTP or dNTP may direct function towards RNA or DNA synthesis, respectively.[61, 64]. The PriS subunit shares significant structural and sequence homology to eukaryotic X-family DNA repair polymerases, most notably polymerase β [66, 69]. PriSL can also synthesize across discontinuous templates [65] in a similar manner to that of eukaryotic Pol μ, known to be involved in both base excision repair and double strand break (DSB) repair in humans. Archaea do not have a direct polymerase homolog from the X-family but the biochemical data suggests that PriSL may be a functional homolog (**Table 1.2**).

1.4 ARCHAEAL DNA POLYMERASE FAMILIES AND FUNCTION

The archaeal domain is subdivided minimally into several phyla with the largest two: Crenarchaeota (Erenarchaea) and Euryarchaeota (Euryarchaea), containing replication systems

with high homology to those found in eukaryotic systems. DNA polymerases have been classified into at least six different families. Compared with the 13 human DNA polymerases encompassing three different families, archaeal organisms generally have three to four DNA polymerases from two different families. Crenarchaea contain members from both the B- and Y-families, while Euryarchaea contain those belonging to B- and D-families (**Table 1.1**). DNA polymerases employed by archaeal organisms have high sequence, structural, and functional similarities to those found in eukaryotes yet, they have adapted for optimal function under extreme conditions, most notably high temperatures. The ease of purification, high conservation to eukaryotes, and adaptation for biotechnology applications have made archaeal polymerases models for studying processivity, protein interactions, lesion bypass, polymerase–exonuclease shuttling, and polymerase switching mechanisms essential to all domains of life.

1.4.1 Crenarchaeal B-Family DNA Replication Polymerases

B-family polymerases are typically robust and accurate enzymes, containing an N-terminal 3'-5' exonuclease and a C-terminal polymerase domain.[70, 71] The exonuclease domain increases selective nucleotide incorporation efficiencies generally by a factor of 10^2 up to 10^8 [72]. The polymerase domain is similar in structure to a right hand with fingers, thumb, and palm subdomains that act to bind the DNA template, orientate the incoming nucleotide, and catalyze polymerization through conformational changes between domains (**Figure 1.3**). The enzymes are typically not highly processive on their own, but possess the ability to form complexes with their respective processivity clamps (PCNAs), allowing for the incorporation of >10,000 nucleotides in a single binding event [73]. As a result, B-family enzymes are also thought to be the main replication polymerases in Crenarchaea and Euryarchaea.

Table 1.2: Archaeal Polymerase Family Members

	Archaeal Phyla				
Family	**Crenarchaeota**	**Euryarchaeota**	**Nanoarchaeota**	**Thaumarchaeota**	**Korachaeota**
A					
B	Pol B1 Pol B2 Pol B3	Pol B	Pol B	PolB	Pol BI Pol BII
C					
D		Pol D	Pol D	Pol D	Pol D
X	PriSL[1]	PriSL[1]	PriSL[1]	PriSL[1]	PriSL[1]
Y	Pol Y			Pol Y	

[1]AEP family of DNA primases with homology to X-family polymerases

Crenarchaea possess three B-family polymerases. PolB1 has robust synthesis activity, high nucleotide fidelity, an included exonuclease domain, and is considered to be the main DNA replication polymerase[74, 75]. PolB1 is evolutionary related to eukaryotic B-family polymerases (α, δ, ε, ζ) [76] but seems to have arisen after PolB2 and PolB3 in a gene duplication event (**Table 1.2**) [77]. PolB1 has a typical right hand conformation but includes two extra α-helices in the N-terminal domain that contact the fingers domain (**Figure 1.3**). It is proposed that these helices strengthen the contacts between the N and C-terminal domains for catalysis at high temperatures[71]. Alternatively, they could also play a role in promoting protein complex formation as seen for the trimeric PolB1 complex discussed below [78].

The exonuclease domain of *Sso*PolB1 contains an inherent 3'-5' proofreading ability that enhances the fidelity 14-fold [75] (**Figure 1.4**). Although PolB1 utilizes an induced fit mechanism for nucleotide incorporation [79], occasionally, it can make a mistake. The shuttling between the multiple active sites (pol and exo) has been examined in great detail in phage organisms with B-family polymerases and involves multiple steps including long range movement of the separated primer strand from the polymerase active site to the exonuclease site [80]. In crenarchaeal B-family polymerases, control of these two catalytic activities occurs intramolecularly, mediated by a flexible loop (Y-GG/A) in the palm domain[81, 82] (**Figure 1.3**). Most likely, the polymerase is able to efficiently achieve this feat by maintaining contact with their respective processivity clamps and allowing alternative holoenzyme conformations (discussed below). Mutation of the conserved aspartates in the exonuclease domain was instrumental in measuring the inherent fidelity of PoB1

[75] as well as other archaeal B-family polymerases [83]. Surprisingly, without an active exonuclease domain, PolB1exo$^-$ also exhibited a masked ability to extend ssDNA with a template independent and dependent terminal transferase activity [84]. Short 20 nucleotide ssDNA templates are extended in a template independent fashion initially adding 3-5 bases on the 3' end. Newly added DNA is then wrapped around and stabilized intramolecularly through incomplete base-paring interactions before template dependent slipping extension creates products greater than 7 kilobases in a mechanism akin to what has been shown for human X-family DNA polymerase μ and λ [85, 86].

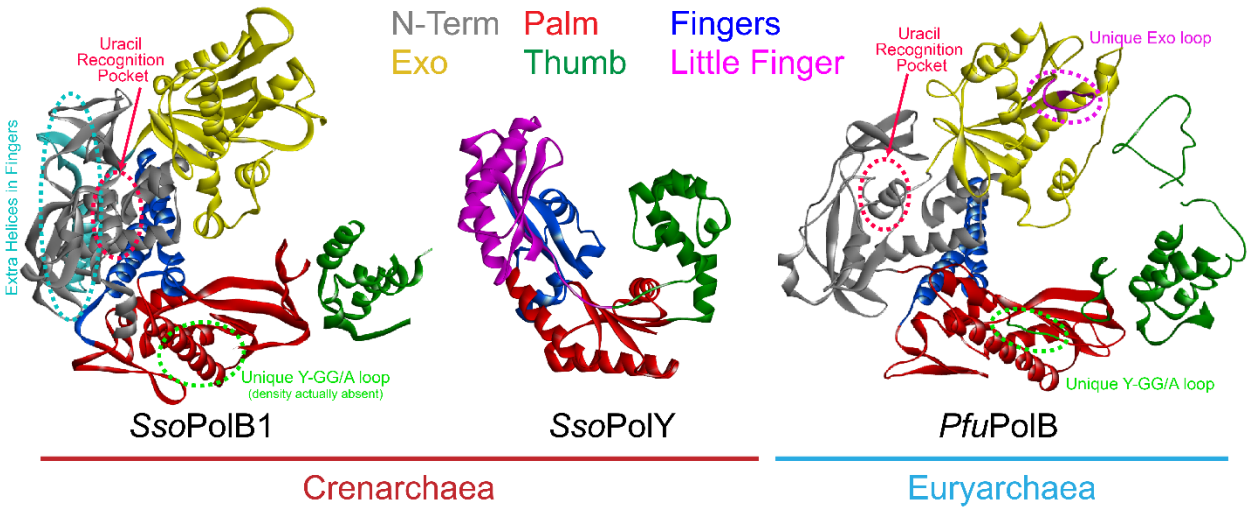

Figure 1.3: Structures of Archaeal DNA Polymerases
Structures of crenarchaeal, *Sso*PolB1 (PDB: 1S5J), *Sso*PolY (PDB: 1JX4), and euryarchaeal *Pfu*PolB (2JGU) DNA polymerases highlighting conserved N-terminal (grey), exonuclease (yellow), palm (red), thumb (green), fingers (blue), and little finger (pink) domains. The extra α-helices in the fingers of *Sso*PolB1 are highlighted in cyan; the unique Y-GG/A loop is highlighted in green; the unique exonuclease (Exo) loop is highlighted in pink; and the uracil recognition pocket is circled in red.

Crenarchaeal PolB2 is not as well characterized and has been postulated to be inactive based on bioinformatic analysis of unconserved active site residues [87]. PolB2 has high sequence conservation with PolB1, and it is thought that duplication of PolB2 gave rise to PolB1. Intriguingly, expression of *Sso*PolB2 is upregulated in response to UV exposure prompting many to hypothesize a role in bypassing cylobutane thymidine dimers.[49, 88, 89] Recently, *Sso*PolB2 has

been shown to have some basic polymerase activity, but it is the least active of the four *Sso* polymerases (**Figure 1.3**) and actually lacks the *in vitro* ability to bypass thymine dimers [(90)]. Rather, PolB2 was able to bypass uracil, hypoxanthine, and 8-oxoguanine. The binding affinity of PolB2 to DNA is weak compared to PolB1 and limits both the polymerase and exonuclease activities. It is speculated that PolB2 participates either in oxidative DNA lesion bypass or in short patch repair of UV-induced DNA damage after excision of the damaged bases, and additional protein interactions may be required to form stable complexes on DNA for efficient activity.

Bioinformatic analysis suggests that crenarchaeal PolB3 and its homolog from Euryarchaea, PolB, are actually the original Archaeal polymerases [(91)]. Further studies indicate PolB3 may have evolved into the inactive polymerase or exonuclease domain found near the C-terminus of eukaryotic ortholog pol ε [(92)]. In PolB3, the highly conserved active site YxDTD motif, which is generally responsible for the coordination of the two active site Mg^{2+} ions for catalysis, has diverged significantly. While it had been previously shown that both aspartic acid residues in this motif were required for polymerase activity [(93, 94)], *Sso*PolB3 has been found to be moderately active despite having a mutated motif (LAN-D) [(83, 90)]. As a consequence, the polymerase activity and DNA binding ability of PolB3 are surprisingly low, and similar to PolB2. The kinetics and fidelity of PolB3 are moderate placing it squarely between values for replication or repair polymerases (**Figure 1.4**). Although the exact metabolic role of PolB3 has not yet been uncovered, it can bypass cyclobutane dimers *in vitro* more efficiently than any of the other polymerases in *Sso* including PolY, indicating a potential role in UV-induced damage repair [(90)].

The number, conservation, and biochemistry of B-family polymerases in Crenarchaea present the possibility that they are utilized similarly to those of eukaryotes [(91, 95)], with PolB1 acting as the leading strand replicase, and either PolB2 or PolB3 as the lagging strand replicase. The fidelities of B-family polymerases are generally greater than Y-family members providing for highly accurate and robust synthesis on the leading and lagging strands. The remaining polymerase(s) (B2 and/or B3) would have a more specialized role in DNA damage repair, potentially complimenting or providing redundancy to the function of the Y-family polymerase. The combination of specificities, fidelities, kinetics, and lesion bypass abilities of the four DNA

polymerases in *Sso* encompass a broad range of complimentary activities for efficient replication and repair (**Figure 1.3**).

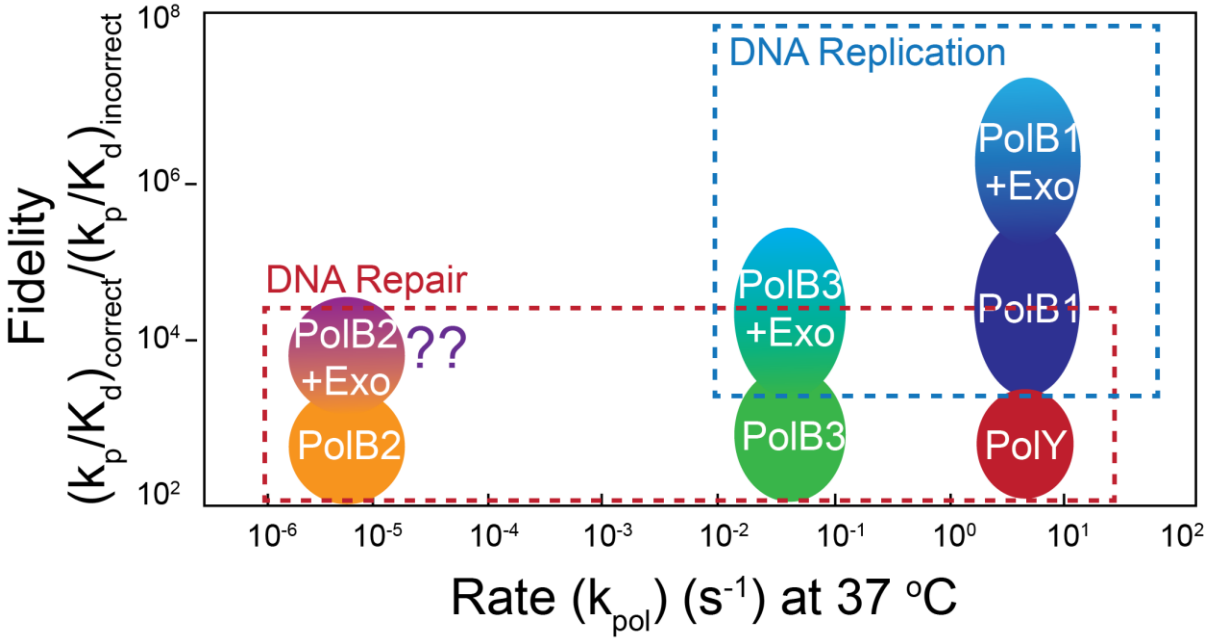

Figure 1.4: Polymerase Kinetics

Representation of the kinetics and fidelity of all four DNA polymerases in *Sso*. The fidelities for both the polymerase and exonuclease domains are shown. Highlighted are regions required for efficient DNA replication or DNA repair calculated from the total genome size (2.99 Mb) [(96)], number of origins of replication (3) [(97)], and S-phase time (1.5 hours) of *Sso* [(98)].

1.4.2 Euryarchaeal B-Family DNA Replication Polymerases

In Euryarchaea, there is typically only a single chromosomally encoded PolB. *Pyrococcus furiosus* (*Pfu*) and *Thermococcus gorgonarius* (*Tgo*) PolB have been characterized extensively and are commonly used in PCR applications due to their robust accurate activities and high thermostabilities [(99, 100)]. Many euryarchaeal PolB polymerases contain inteins that splice together and form the catalytic polymerase active site [(101)]. However, the resulting amino acid sequence is similar between crenarchael and euryarchaeal PolBs. The crystal structure of euryarchaeal B-family polymerases shows a right hand conformation with only slight differences in the loop regions compared to crenarchaeal PolB. One unique loop structure was revealed within the exonuclease domain responsible for regulating the polymerase and nuclease activities of these

polymerases **(Figure 1.3)** [82, 102]. This exonuclease loop is not observed in structures of B-family polymerases of other organisms like RB69; and appears to be unique to euryarchaeal PolB. Mutation of the exonuclease loop results in a conformational change in the editing-cleft caused by altered interactions between the loop and the thumb domain decreasing exonuclease activity and making the polymerase more amenable for PCR reactions[103]. Control and regulation of the polymerase and nuclease activities is important for the accurate and efficient replication necessary for maintenance of the archaeal genome. While in Crenarchaea, PolB1 is thought to perform both leading and lagging strand replication, euryarchaeal PolB functions on only the leading strand during chromosomal replication [104].

1.4.3 **Archaeal Y-Family Lesion Bypass Polymerases**

Archaeal Y-family polymerases are found primarily in Crenarchaea but are not universally conserved throughout the phyla and are proposed to only be present in those organisms exposed to UV light [5]. Interestingly, Y-family polymerases do not share sequence identity to any of the other polymerase families (A, B, C, D, X) and also lack the 3'-5' exonuclease domain present in the archaeal B- and D-families [105]. Despite these differences, the structure of PolY is similar to that of polymerases in the A- and B-families, possessing the usual palm, fingers, and thumb subdomains (**Figure 1.3**). However in addition to the usual domains, PolY possesses an additional "little finger" subdomain and linker, primarily important for DNA binding. Archaeal Y-family polymerases have served as models for understanding lesion bypass mechanisms and specificities as related to the eukaryotic orthologs of the same family: Pol η, pol ι, and pol κ.

As has been observed in bacteria and eukaryotes, archaeal Y-family polymerases have a much more specialized role in the maintenance of the archaeal genome. Y-family polymerases have error rates 100 to 1000-fold higher than B-family polymerases (**Figure 1.4**) [106]. This is due not only to the lack of a proofreading exonuclease domain but also to a larger, more accommodating active site which allows for binding of incoming nucleotides in additional orientations, prevented by steric clashes with residues in the active sites of polymerases in other high fidelity polymerase families [107]. Multiple dNTP orientations in the active site allow for

potential base pairing with a damaged template base and the concurrent bypass of these sites of damage. The Y-family polymerases from *Sso*PolY (Dpo4) and *Sulfolobus acidocaldarius* (*Sac*Dbh) are two of the best characterized polymerase enzymes and have been found to bypass a large number and variety of DNA lesions including: abasic [108, 109], (deoxyguanosin-8-yl)-1-aminopyrene [110], benzo[*a*]pyrene diol epoxide[111], 8-oxoguanine [112, 113], methylguanine and benzlguanine [90] and thymine dimers [114, 115]. Active site metal ion composition has also been shown to be important in determining which lesions can be bypassed by Y-family polymerases. While typically Mg^{2+} is the metal cofactor most associated with nucleotide binding and incorporation, it has been observed that when replaced by Mn^{2+}, *Sso*PolY exhibits increased catalytic efficiency yet reduced fidelity, with an ability to efficiently bypass otherwise unfavorable substrates such as abasic sites and cyclopyrimidine dimers [116].

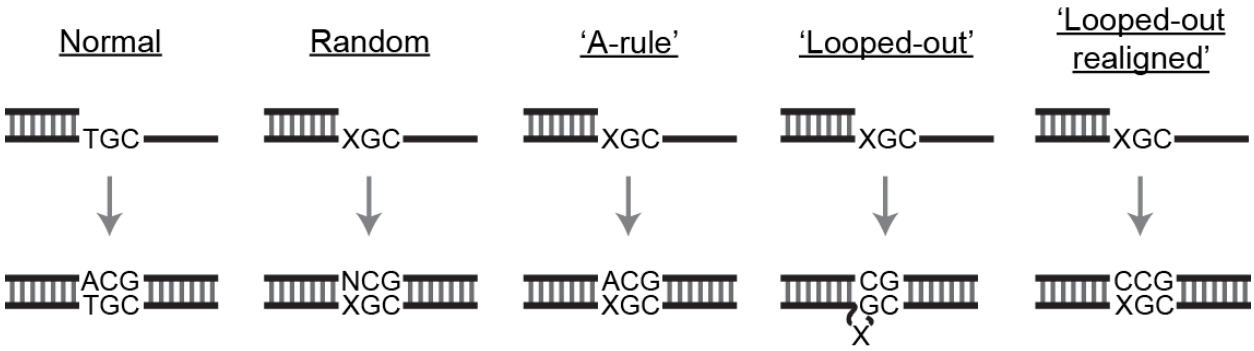

Figure 1.5: Lesion Bypass Mechanisms for Archaeal Y-family DNA Polymerases
Random incorporation includes partial base pairing to the template strand for preferential incorporation of nucleotides dependent on the lesion type. The 'A-rule' is utilized primarily when no templating base is available and preferentially incorporates adenine over the other three bases. The 'looped-out' mechanism utilizes base pairing interactions at the +1 site of the template strand while excluding the lesion and results in a -1 frameshift. The looped-out mechanism can also realign to avoid the frameshift albeit with much less frequency.

Y-family polymerases are able to bypass lesions through error free and error prone means (**Figure 1.5**). For example, *Sso*PolY is able to correctly incorporate cytosine across from the aminofluorine adduct of guanine, however base deletions or substitutions occur directly after the lesion [117]. When bypassing an abasic site, *Sso*PolY is known to employ either the "A-rule" [118], where an adenosine is added opposite a noninstructional template lesion, or a template slippage loop out mechanism where the template lesion is looped out and replication continues opposite the next base resulting in a -1 frameshift [119, 120]. Y-family polymerases are also known to be able to

induce deletions of a single base through a template slippage mechanism [120]. While *Sso*PolY is able to bypass most lesions, the ability to bypass cyclopyrimidine dimers is limited and instead speculated to be performed by the B-family polymerase, *Sso*PolB3 (Dpo3) [90].

In addition to the lesion bypass properties observed from Y-family polymerases, Archaeal B-family polymerases are able to detect uracil in the downstream DNA sequence [121]. The presence of uracil in DNA usually arises due to the deamination of cytosine, however as a result of uracil base pairing to thymine, this deamination results in a transversion to a C-G base pair after replication. A uracil recognition pocket was identified in the N-terminal region of *Tgo*PolB [100] and *Sso*PolB1 [71] that stalls the polymerase four bases from the primer template junction (**Figure 1.3**). It is noteworthy that this uracil binding pocket is not present in eukaryotic B-family polymerases, including those with high homology to archaeal B-family polymerases. As a result, it is speculated that the uracil read-ahead function serves as a means to recognize DNA damage prior to replication in organisms with incomplete base excision repair (BER) or nucleotide excision repair (NER) pathways.

1.4.4 **Archaeal DNA Polymerase Holoenzymes**

DNA polymerases by themselves are traditionally not very processive and require complexation with their respective clamps to replicate long stretches of DNA without dissociating. In Archaea, the proliferating cell nuclear antigen (PCNA) clamp is loaded onto DNA by the replication factor-C (RFC) clamp-loader in an ATP dependent manner to facilitate recruitment of the DNA polymerase to the holoenzyme complex (**Table 1.3**). This minimal DNA polymerase holoenzyme complex will be active on both the leading and lagging strands during replication as well as participate in lesion bypass mechanisms of exchange at DNA damage sites.

Table 1.3: Replication Holoenzyme Components

System	Polymerase	Clamp	Clamp Loader
T4 Bacteriophage	gp43	gp45	gp44/62
Escherichia coli	Pol III	B-clamp	Gamma Complex ($\delta`\gamma_3\delta$)
Sulfolobus solfataricus	PolB1	PCNA123	RFC
Human	Polε (leading strand) / Polδ (lagging strand)	PCNA	RFC

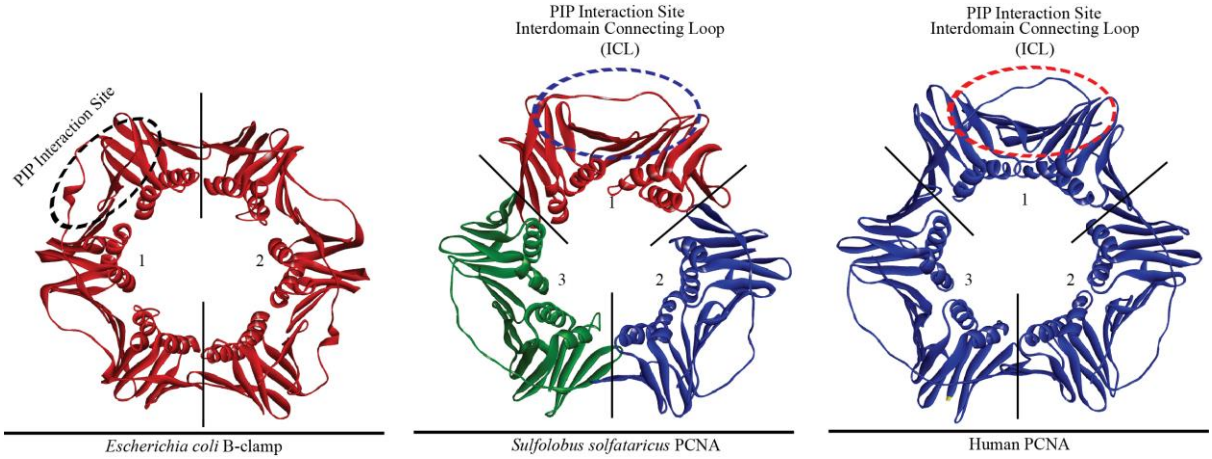

Figure 1.6: Replication Sliding Clamps
A) Structures of three sliding clamps, the homodimeric B-clamp from E. coli (PDB ID: 3D1E, left, red), the heterotrimeric PCNA from *Sulfolobus solfatiaricus* (PDB ID: 2HIK, middle, PCNA1 red, PCNA2 blue, PCNA3 green), and the homotrimeric PCNA from humans (PDB ID: 1W60, right, blue). Each sliding clamp has an interaction site indicated on the first monomer units, where the PCNA Interacting Peptide, from a variety of enzymes from each respective organism are able to interact.

B-family polymerases from both Crenarchaea and Euryarchaea have been found to interact with their processivity clamps through a motif called the PCNA interacting peptide (PIP) box [122, 123]. This motif has a consensus sequence of Qxxhxxaa, where x is any amino acid, h is a hydrophobic residue, and a is an aromatic residue [124], and binds to a region on the clamp called the interdomain connecting loop (ICL) (**Figure 1.6**). PCNA loading on DNA allows for binding of the polymerase and formation of a replicative holoenzyme similar to those seen in both prokaryotes and eukaryotes. The association of PCNA with PolB is thought to result in a highly processive complex that limits dissociation and allows synthesis of greater than 10 kb products in a single binding event. The structure of euryarchaeal (*Pfu*) DNA polymerase

holoenzyme has provided significant insight into the holoenzyme assembly mechanism and conformational changes required for both polymerization, editing, and switching (**Figure 1.7 A**) [125-127]. *Pfu*PolB was found to possess an additional site of contact with PCNA (standby), proposed to be important for pivoting between the editing (locked-down) and polymerization (tethered) modes. This flexibility provided through multiple interactions between PCNA and the polymerase allows for uninterrupted and dynamic, error-free DNA synthesis and may also be important for polymerase switching during replication.

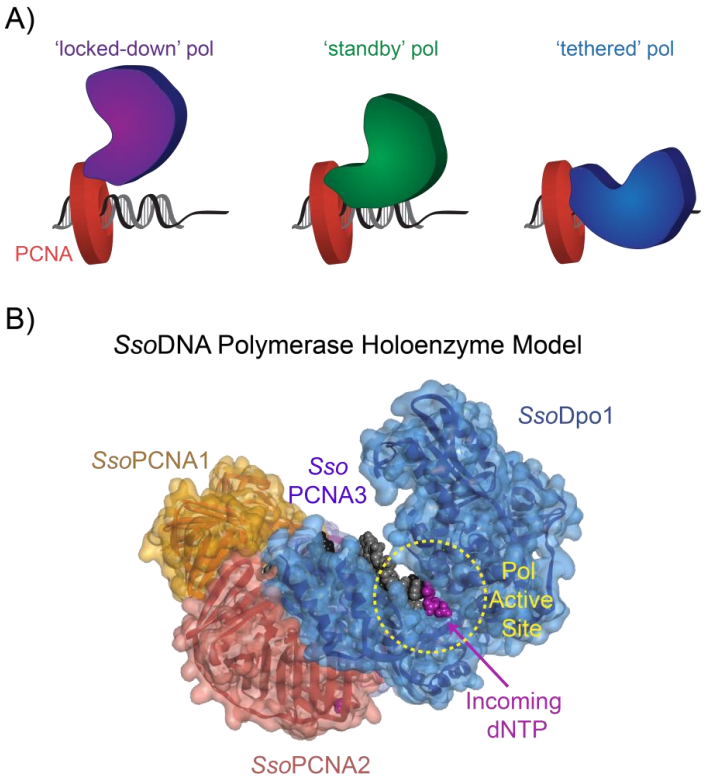

Figure 1.7: Replication Holoenzyme Model
A) Complexation of the DNA polymerase with the PCNA clamp can occur in different conformational state for assembly or activation of exonuclease or polymerase activities. B) DNA polymerase holoenzyme model from *Sso* showing the specific interaction of *Sso*PolB1 (blue) with *Sso*PCNA2 (red) built from specific detected interactions of PCNA123 and *Sso*PolB1 (PDB 1s5J) simulating the tethered complex. The polymerase active site is highlighted with the incoming dNTP base pairing to the primer template junction prior to catalysis.

Unlike the euryarchaeal homotrimeric PCNA, the crenarchaeal PCNA is a heterotrimeric complex comprised of three separate proteins (PCNA1, 2 and 3). PolB1 from *Sulfolobus*

solfataricus has been found to interact specifically with PCNA2 subunit within the heterotrimer to increase processivity [(128)] (**Figure 1.5**). Using specific contact points and measured distances between the *Sso*PCNA123 and *Sso*PolB1, we have created a DNA polymerase holoenzyme model to highlight interactions in the polymerization mode (**Figure 1.8 B**).[2] By having three separate proteins, crenarchaeal PCNA123 can also specifically interact with additional proteins, such as flap endonuclease (PCNA 1) and DNA ligase (PCNA3) in close proximity to the polymerase to efficiently process Okazaki fragments in a 'tool-belt' fashion [(129-131)]. The retention of additional DNA replication accessory factors as well as multiple copies of DNA polymerases in high local concentration at the replication fork as coordinated by PCNA provides for uninterrupted DNA synthesis ability.

Lesion bypass polymerases from the Y-family are also known to interact with the crenarchaeal PCNA1 subunit [(132)]. Much like the B-family polymerases, those of the Y-family exhibit increased processivity and replication rates in the presence of the clamp [(133, 134)]. Although much is known about the mechanism of lesion bypass for these Y-family DNA polymerases, the influence of PCNA on this activity is not known. PolY from euryarchaeal *Methanosarcina acetivorans* is unique among Y-family pols as when it is complexed with PCNA, it can synthesize extremely long products, greater than 7.2 kilobases.[(135)] Typically mutagenic lesion bypass polymerases are not able to synthesize such long products presumably due to the effect their low fidelities would have on the genome. Therefore, molecular access to PCNA must be regulated.

The DNA binding specificity for all DNA polymerases is primarily afforded by the 3'OH on the primer strand but also includes significant contacts with both the dsDNA and the ssDNA template. When multiple DNA polymerases are present in a single organism with similar DNA substrate specificities, a question arises as to how polymerase binding to DNA is regulated to ensure accurate DNA replication and efficient DNA repair. Regulation of polymerase binding and access to DNA in the cell utilizes multiple biophysical strategies including: kinetics, thermodynamics, transcriptional and translational regulation, interactions with accessory proteins, and oligomer formation.

[2] As further detailed in chapter 4

1.4.5 **Oligomeric DNA Polymerases and Complexes**

In *E. coli,* three DNA polymerase III cores are coordinated within the replisome by the clamp-loader complex [(136)]. Two of the three polymerase cores are proposed to be involved in formation of alternating Okazaki fragments while the other consistently synthesizes DNA on the leading strand. Other polymerases including T4 gp43 [(137)], and Klenow [(138)], have been found to interact with DNA in a dimeric state. In Archaea, *Sso*PolB1 can assemble into a unique trimeric complex to increase both replication rate and processivity of the enzyme [(78)]. Trimeric *Sso*PolB1 is observed at temperatures ranging from 10 to 70 ºC where processivity values increase with temperature and routinely exceed 1000 bases [(139)]. As discuss above, DNA polymerases are generally nonprocessive with synthesis of only 20 bases before dissociation from the template and require interactions with their respective clamps to achieve extremely large processivity values. As such, we have suggested that the large processivity value for trimeric *Sso*PolB1 is a consequence of direct interactions between subunits, effectively encircling the DNA template akin to the structural role of the clamp proteins (**Figure 1.8 A**). Similarly, the Y-family polymerase, *Sso*PolY, also forms oligomeric complexes on DNA in a concentration dependent manner as highlighted in a variety of crystal structures (**Figure 1.8 B**). The function of oligomeric PolY complexes is not known and no known enzymatic enhancement has been noted, but this interaction may be used to keep high concentrations of polymerases at the replication fork.

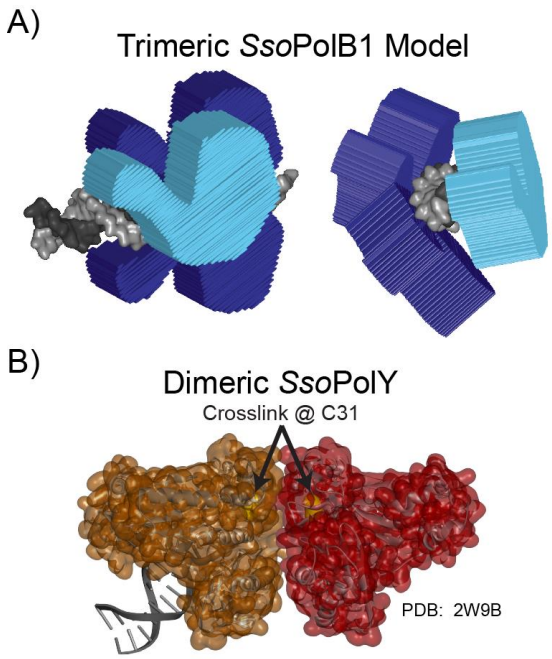

Figure 1.8: Oligomeric Polymerase Models
A) Model of the trimeric *Sso*PolB1 polymerase bound to DNA. The encircled conformation is proposed based on binding and footprinting on a small primer-template DNA substrate. B) Crystal structure (PDB: 2W9B) of dimeric *Sso*PolY consistent with chemical crosslinking at cysteine 31.

In all, these results suggest that polymerase action may be more complicated than previously thought, utilizing both intimately and loosely bound polymerase molecules in the replisome. In T4 and T7, DNA polymerase molecules can exchange freely at the site of catalysis during replication [(140, 141)]. This 'dynamic polymerase processivity', along with the variety of different possible homo and hetero oligomeric complexes that can form between *Sso*PolB1 and *Sso*PolY highlight the possibility that the archaeal cell utilizes these complexes in a variety of yet unknown genomic maintenance functions. The regulation of oligomeric polymerase complex formation may be controlled through subtle changes in equilibria at the site of action to afford specific genome maintenance functions.

1.4.6 **Polymerase Participation in DNA Repair**

Archaea maintain a level of genomic stability equivalent to or slightly better than other microorganisms. This is somewhat surprising due to the environments that many of these organisms thrive in where oxidation and deamination would be common. Therefore, Archaea must possess very robust mechanisms by which DNA damage is repaired [(142)]. In bacteria and

eukaryotes, DNA is typically repaired through several means including error prone lesion bypass, BER, NER, and mismatch repair. B-family polymerases contain exonuclease domains and would shuttle between incorporation and excision events at sites of DNA damage but may be able to bypass certain oxidative and UV induced damages [(90)]. Most Crenarchaea also possess Y-family polymerases capable of performing the error prone lesion bypass processes in spite of DNA damage, however this ability may not be essential as knockouts of PolY are unaffected by DNA damaging agents [(143)].

The observed interactions between the polymerases and differing subunits of PCNA has led to the proposal that both B-family and Y-family polymerases can be retained simultaneously for dynamic polymerization in the presence of lesions [(144, 145)]. If the replicative polymerase encounters a DNA damage site, the polymerases are hypothesized to switch, allowing the Y-family polymerase to bypass the damage site while maintaining PolB within the holoenzyme. After the lesion has been successfully bypassed, the B-family polymerase can return, reestablishing accurate and normal DNA synthesis. Of course, this would require that multiple polymerases are intimately associated in and around the replisome. Polymerase switching has been observed between the replicative polymerase (PolIII) and a Y-family repair polymerase (PolV) in *E. coli*. Where it was found that binding of the regulatory subunit of PolV, termed UmuD' to the *E. coli* processivity clamp resulted in release of the PolIII catalytic subunit, which is thought to facilitate polymerase exchange.[(146)] It has also been observed that direct interactions between PolIII and PolV, inhibit PolIII from interacting with ssDNA, which would also promote replication by PolV.[(147)] In addition to its interactions with the replicative polymerase, the UmuD regulatory subunit is also known to interact and inhibit the -1 frameshit mutagenesis of *E. coli* Pol IV. (UmuD and RecA modulate the mutagenic potential of the Y-Family Polymerase DinB). Some evidence has been presented that similar interactions are also found in Archaea. For example in *Sulfolobus solfataricus,* a direct interaction between the replication (*Sso*PolB1) and lesion bypass (*Sso*PolY) polymerases have also been detected highlighting another contact point for polymerase exchange,[(148)] however, an enzymatic function for this interaction has not been determined. The interaction between a Y-family polymerase with one from the B-famly is not unique to Archaea, as this has been observed with Eukaryotic pols Rev1 (Y-family) and Pol ζ (B-family). This Eukaryotic complex differs from the archaeal PolB1/PolY complex in that both Eukaryotic polymerases involved are repair specific.

While only PolY is a repair polymerase with PolB1 being the primary replicative polymerase in Archaea.

As the error prone polymerases are not universally conserved, DNA repair in Archaea must include alternative mechanisms. Traditionally, BER and NER pathways would fulfill this role, but many archaea are missing many of the proteins homologs to either the eukaryotic or bacterial versions making identification difficult [5]. Therefore, it is still not understood how Archaea maintain stable genomes even in spite of intense environmental stress, but it is certain that polymerases in Archaea will have both specific and redundant roles in repair processes.

1.5 CONCLUSION

Despite the increasing amount of information available about the workings of the replication processes a number of knowledge gaps exist. One such gap revolves around the dynamics of multiple B-family DNA polymerases. While the eukaryotic replication system is complex and expression of these enzymes is often difficult, crenarchaeal organisms have been found to possess three easily expressed B-family polymerases. Through sequence homology, these enzymes have been identified as ancestral forms of those present in Eukaryotes. The homology in conjunction with the ease by which these polymerases may be manipulated in the laboratory setting have resulted in Archaea serving as an ideal model for understanding the interplay between multiple B-family polymerases and their respective complexes formed in the replication process.

The similarities between the eukaryotic and archaeal systems extend beyond their polymerases. From a homologous clamp (PCNA), clamp loader (RFC), MCM helicase, and primase (PriSL); the archaeal forms of these enzymes have been found to possess striking, sequence, structural, and functional homology to those from eukaryotes. The regulatory complexity through posttranslational modification of a variety of replication components of the eukaryotic replication system makes studying these enzymes and their respective protein complexes a difficult task. In Archaea however, despite the enzymatic similarities, the overall replication system is simpler, more similar to those found in bacteria with some proteins also having homology to the bacterial system as well. As a result of this organizational simplicity, and

the enzymatic similarities to their eukaryotic counterparts, the archaeal system has proven to be a valuable model system for understanding a variety of aspects of DNA replication.

2.0 KINETICS AND FIDELITY OF POLYMERIZATION BY DNA POLYMERASE III FROM *SULFOLOBUS SOLFATARICUS*[3]

2.1 SUMMARY

We have biochemically and kinetically characterized the polymerase and exonuclease activities of the third B-family polymerase (PolB3) from the hyperthermophilic Crenarchaeon, *Sulfolobus solfataricus* (*Sso*). We have established through mutagenesis that despite weak sequence conservation; the polymerase and exonuclease active sites are functionally conserved in *Sso*PolB3. Using presteady-state kinetics, we can measure the fidelity of nucleotide incorporation by *Sso*PolB3 from the polymerase active site alone to be 10^3 to 10^4 at 37 °C. A functional exonuclease proofreading active site will increase fidelity by at least 10^2 making *Sso*PolB3 comparable to other DNA polymerases in this family. Additionally, *Sso*PolB3's exonuclease activity is modulated by temperature, where a loss in promiscuous degradation activity can be attributed to a reorganization of the exonuclease domain when bound to primer template DNA at high temperatures. Unexpectedly, the DNA binding affinity is weak compared with other DNA polymerases of this family. A comparison of the fidelities, polymerization kinetics, and associated functional exonuclease domain with those previously reported for other *Sso* polymerases (*Sso*PolB1 and *Sso*PolY) illustrates that *Sso*PolB3 is a potential player in the proper maintenance of the archaeal genome.

[3] Reprinted (adapted) with permission from **Bauer, R.J**., Begley M.T., and Trakselis, M.A. (2012) Kinetics and fidelity of polymerization by DNA polymerase III from *Sulfolobus solfataricus, Biochemistry,* 51, 1996-2007.

2.2 INTRODUCTION

Over the past 20 years, many additional DNA polymerases have been discovered within the genome of most organisms. This raises the question of how multiple DNA polymerases are regulated with regards to their individual functions for the maintenance of the organism's genetic material. DNA polymerases have been divided into six main families (A, B, C, D, X, and Y) [149, 150]. It is clear that B-family DNA polymerases provide the bulk of DNA synthesis during replication, and that X and Y-family DNA polymerases only act under special circumstances in various DNA repair pathways [151]. In addition to the twelve other DNA polymerases in humans, there are three B-family DNA polymerases that act both in the initiation and elongation phases of DNA replication [152].

DNA polymerases from the B-family are generally robust and accurate enzymes with inherent nucleotide specificities augmented further by exonuclease proofreading domains that give nucleotide fidelities greater than 10^8 , or one error every 10^8 bases incorporated [72]. They become processive for >10,000 bases after complexation with their respective processivity factors or clamps [73]. The leading (ε) and lagging (δ) strand polymerases [153] as well as the pol-α primase complex [154] are the three B-family polymerases found in humans. There are few significant mechanistic differences in enzymatic activities between ε and δ, except for their strand specificities which are not fully understood [155]. Pol-α primase, on the other hand, is able to synthesize short oligoribonucleotide primers that can be extended further through incorporation of deoxyribonucleotides on both strands to initiate replication elongation [55, 156].

The DNA processing enzymes in Archaea have been shown to be more similar to those of eukaryotes than bacteria and serve as a simplified model for understanding more complex eukaryotic activities [157-160]. Of the two main phyla in Archaea, euryarchaea have both B-family and D-family (unique to this archaeal phyla) DNA polymerases [161], whereas crenarchaea have B-family and Y-family DNA polymerases [162, 163]. Crenarchaea have a more conserved arsenal of eukaryotic-like DNA polymerases; however the metal binding domain of eukaryotic polymerases (ε & δ) may have instead evolved from the euryarchaeal D-family polymerases.[92] The Crenarchaeon, *Sulfolobus solfataricus* (*Sso*), has within its genome three B-family polymerases

(*Sso*PolB1, *Sso*PolB2, and *Sso*PolB3); similar in number to the main analogous DNA polymerases (α, δ, and ε) found in humans. Both the proposed DNA replication polymerase, *Sso*PolB1, and the lesion bypass polymerase, *Sso*PolY, have been well characterized with regards to their nucleotide incorporation mechanism [79, 164], fidelities[75, 165], and structures [71, 105]. *Sso*PolB2 and *Sso*PolB3, have been identified by sequence homologies [95, 166], and until very recently had no biochemical characterization of activities [90].

Here, we have characterized the mechanism and kinetics of polymerization, exonuclease proofreading, and DNA binding activities of the third B-family DNA polymerase from *Sulfolobus solfataricus*, *Sso*PolB3. We have identified and mutated conserved amino acids in both the polymerization and exonuclease domains to confirm conservation and quantify their respective activities. Surprisingly and unlike other DNA polymerases, *Sso*PolB3 binds weakly to DNA requiring higher concentrations of enzyme for efficient nucleotide incorporation. This weak binding can be attributed to a mutation in the universally conserved Pol I motif. We have also quantified the selectivity of nucleotide incorporation for all 16 possible combinations into undamaged DNA templates using presteady-state kinetics. Circular dichroism analyses suggest that *Sso*PolB3 is a stable enzyme with a T_m > 94 °C, although the thermostability of the specific exonuclease domain may be regulated by substrate binding and temperature. The nucleotide incorporation rates, fidelity values, and exonuclease results are compared to the more thoroughly characterized *Sso* DNA polymerases (*Sso*PolB1 and *Sso*PolY) to gain a better understanding of the diversity of DNA polymerase functions in the cell.

2.3 MATERIALS AND METHODS

2.3.1 Materials

Oligonucleotide substrates were purchased from Integrated DNA Technologies (IDT, Coralville, IA) and are listed in Table 2.1. DNA strands over 28 nucleotides were gel-purified utilizing denaturing acrylamide gel electrophoresis [167]. Radioactive ATP [γ-^{32}P] was purchased

from MP Biomedicals (Solon, OH). Optikinase (USB, Cleveland, OH) was used for 5'-end labeling of DNA substrates according to manufacturer protocols. Radiolabeled primers were added to cold complementary template strands at a ratio of 1:1.2 to ensure proper annealing. Annealing was performed by heating the sample to 95 °C for five minutes, followed by slowly cooling to room temperature for at least two hours. Commercial enzymes were from NEB (Ipswich, MA). All other chemicals were analytical grade or better.

Table 2.1: DNA Primers

DNA Substrates	Sequence (5'-3')
***Sso*PolB3 For**	5'-CACCCATATGATTAAGGATTTCTTTATATTAG
***Sso*PolB3 For**	5'-CTCGAGTTTCTTCTTAGAAGCTCCAAATAAG
D226A For	5'-GGAGATTCGTTGACTACATATTAAATTATGCTCCTG ATATAATATTTGTATATGATTCA
D226A Rev	5'-TGAATCATATACAAATATTATATCAGGAGCATAATT TAATATGTAGTCAACGAATCTCC
D228A For	5'-CGTTGACTACATATTAAATTATGATCCTGCTATAAT ATTTGTATATGATTCAGATCTCC
D228A Rev	5'-GGAGATCTGAATCATATACAAATATTATAGCAGGAT CATAATTTAATATGTAGTCAACG
D234A For	5'-TAAATTATGATCCTGATATAATATTTGTATATGCTA GCGATCTCCTTCCCTGGAAATATA
D234A Rev	5'-ATAATTTCCAGGGAAGGAGATCGCTAGCATATACAA ATATTATATCAGGATCATAATTTA
D236A For	5'-CCTGATATAATATTTGTATATATGATTCAGCGCTCC TTCCCTGGAAATATATTACAGAAA
D236A Rev	5'-GGACTATATTATAAACATATATACTAAGTCGCGAGG AAGGGACCTTTATATAATGTCTTT
D234A/D236A For	5'-GATATAATATTTGTATATGCTAGCGCGCTCCTTCCC TGGAAATATATTACAG
D234A/D236A Rev	5'-CTGTAATATATTTCCAGGGAAGGAGCGCGCTAGCAT ATACAAATATTATATC
D424A For	5'-ATTATTCAACCAAAAGTTGGTATCTATACAGCTGTT TATGTTCTTGATATATCTTCAGTT
D424A Rev	5'-ACCTGAAGATATATCAAGAACATAAACAGCTGTATA GATACCAACTTTTGGTTGAATAAT
D542A For	5'-AGGTTTAGATGTGATTTTAGCTAATGCATTATTAAT ATTTGTGACAGGCGGATCTAGAG

2.3.2 *Sso*PolB3 Protein Purification

*Sso*PolB3 was amplified from *Sulfolobus solfataricus* P2 genomic DNA (ATCC #35092) with Pfx50 polymerase (Invitrogen, Carlsbad, CA). The gene was initially subcloned into pGEM-T (Promega, Madison, WI), and then ligated into pET30a (EMD Chemicals, Gibbstown, NJ) using the restriction sites *NdeI* and *XhoI* included in the primer sequences **(Table 2.1)** to allow for expression of a C-terminal 6X His tag. The DNA polymerase (D424A, D542A, and D424A/D542A) and exonuclease (D226A, D228A, D234A, D236A) mutant constructs were created using a standard QuikChange protocol (Agilent, Santa Clara, CA) with KAPA HiFi DNA polymerase (KAPA Biosystems, Woburn, MA). BL21(DE3) Rosetta 2 cells containing the various pET30a- *Sso*PolB3 constructs were grown at 37 °C, and protein expression was autoinduced as described.[168] Cell pellets were resuspended in 50 mM sodium phosphate buffer (pH 7.0), 50 mM NaCl, and 5 mM β-mercaptoethanol. The cells were lysed by the addition of lysozyme and sonicated. After centrifugation, the supernatant was heat treated at 70 °C for 20 minutes to precipitate host proteins and centrifuged again. The supernatant containing *Sso*PolB3 was purified using a Ni^{2+} column (Thermo Fisher, Waltham, MA) and eluted with a step gradient of 500 mM imidazole.

Table 2.2: DNA Substrates Used for Enzymatic Assays

DNA Substrates	Sequence (5'-3')
ssDNA	5'-GCTACTCTCGCTCAGCGTACCATAGCAG
ptDNA	5'-GCTACTCTCGCTCAGCGTACCATAGCAG 3'-GATGAGAGCGAGTCGCATGGTATCGTCTACGGCCA GCCCCACCCTTCGCATCCCTCTCCAC
dsDNA	5'-GCTACTCTCGCTCAGCGTACCATAGCAG 3'-CGATGAGAGCGAGTCGCATGGTATCGTC
Cy3DNA	5'-Cy3CACCTCTCCCTACGCTTCCCACCCCGACCGGCA TCTGCTATGGTACGCTGAGCGAGAGTAGC
Long ptDNA	5'-GCTACTCTCGCTCAGCGTACCATAGCAGATGCCGG TCGGGGTGGGTGGG 3'-CGATGAGAGCGAGTCGCATGGTATCGTCTACGGCC AGCCCCACCCTTCGCATCCCTCTCCAC
Hairpin	┌TCGCCGGCCCGGG-3' TTGCGGCCGGGCCCTTTTTTTTTT-5'
Template A	5'-CACCCCCTGGCTAGGCCG 3'-GTGGGGGACCGATCCGGCATTAGTCCAAC

Table 2.2: DNA Substrates Used for Enzymatic Assays Continued

DNA Substrates	Sequence (5'-3')
Template C	5'-CACCCCCTGGCTAGGCCG3'- GTGGGGGACCGATCCGGCCTTAGTCCAAC
Template G	5'-CACCCCCTGGCTAGGCCG 3'-GTGGGGGACCGATCCGGCGTTAGTCCAAC
Template(T)G	5'-CACCCCCTGGCTAGGCCA 3'-GTGGGGGACCGATCCGGTGTTAGTCCAAC
Template T	5'-CACCCCCTGGCTAGGCCG 3'-GTGGGGGACCGATCCGGCTATAGTCCAAC

Further purification was performed using an ATKA Prime FPLC with HiTrap DEAE and Heparin columns (GE Healthcare, Piscataway, NJ) and elution with a linear gradient to 1 M NaCl. Separation of a major degradation product can be performed using a pH gradient from 8.5 to 7.9 and a MonoQ column (GE Healthcare). Final cleanup and sizing was performed with a Superdex 200 26/60 (GE Healthcare). The extinction coefficient for *Sso*PolB3 was determined to be 117,893 $M^{-1}cm^{-1}$ *(169)*. Typical yields of purified protein were greater than 3 mg/L of cells.

2.3.3 **Polymerase Activity Assays**

Standard assays were performed in polymerization buffer [20 mM Tris-acetate (pH 7.5), 100 mM potassium acetate, and 10 mM magnesium acetate] containing 36 nM primer template DNA (ptDNA), and various concentrations of *Sso*PolB3 as indicated. Prior to initiation by addition of dNTPs, the reaction components were incubated for five minutes at the reaction temperature. Experiments were conducted at temperatures, polymerase concentrations, dNTP concentrations, and times as indicated in each figure legend. Reactions were terminated by the addition of an equal volume of a formamide quench (100 mM EDTA, 0.1% SDS, 79% formamide). To examine the products for short templates, denaturing gels [20% acrylamide, 8 M urea, and TBE buffer (45 mM Tris-borate, 1 mM EDTA)] were used. Phosphor screens were then exposed to the gels for a minimum of 4 hours, imaged by a Storm 820 Phosphorimager (GE Healthcare), and quantified using ImageQuant software (v. 5.0).

2.3.4 **Divalent Cation Optimization**

Optimization of divalent cations was performed in polymerase activity assay reaction conditions as detailed above, however, the concentration of divalent metal, M^{2+} (Mg^{2+} or Mn^{2+}), was varied. Reactions were quenched and analyzed as above for standard polymerase reactions. Data obtained from M^{2+} titration reactions were fit to a Michaelis-Menten equation with a cooperativity (*n*) parameter:

$$[product] = \frac{V_{max}[M^{2+}]^n}{{K_m}^n + [M^{2+}]^n} \quad (2.1)$$

where V_{max} is the maximal rate, K_M is the Michaelis constant, and $[M^{2+}]$ is the concentration of the divalent cation included in the reaction.

For those reactions where inhibition was observed at higher concentrations of M^{2+}, an inhibition reaction equation was used instead:

$$[product] = \frac{V_{max}[M^{2+}]}{K_m + ([M^{2+}]\left(1 + \frac{[M^{2+}]}{K_i}\right))} \quad (2.2)$$

where K_i is the inhibition constant.

2.3.5 **Polymerase Fidelity**

Fidelity assays were performed as detailed above for polymerase reactions, however each pre-incubated reaction contained 9.6 nM DNA, 2 μM *Sso*PolB3 (D236A) and was initiated with varying concentrations of dNTPs. Samples were removed and placed 1:1 into quench at time points as indicated in each figure legend. The time course of product formation was fit to a single exponential equation for each concentration of dNTP:

$$[product] = A(1 - e^{(-k_{obs}t)}) \quad (2.3)$$

where *A* represents the reaction amplitude, k_{obs} is the observed polymerase rate, and *t* is time in seconds.

The observed rates extracted from the time courses of product formation for each dNTP concentration were then plotted against their respective *[dNTP]* and fit to a hyperbolic equation:

$$k_{obs} = \frac{k_p[dNTP]}{([dNTP]+K_d)} \tag{2.4}$$

where k_p is the maximum rate of dNTP incorporation and K_d is the dissociation constant for the incoming nucleotide.

2.3.6 **Fluorescent Anisotropy DNA Binding Assays**

Anisotropy assays were performed in polymerization buffer, in the absence of dNTPs with 1 nM ssDNA or ptDNA, where a Cy3 fluorescent label was placed on the 5' end of the single strand or template strand respectively, and varying concentrations of *Sso*PolB3 (D236A) as depicted. Anisotropy values were obtained using a Fluoromax-3 fluorimeter with automated polarizers (HORIBA Jobin Yvon – Edison, NJ.) Cy3 were excited at 550 nm during 1 second integration times and data points represent an average of five consecutive readings. The anisotropy values reported are the average and standard error from three independent titrations. The absolute fluorescence emission (565 nm) was unchanged during the course of the titration, eliminating the possibility that *Sso*PolB3 binds directly to Cy3. The fluorescence anisotropy (*r*) was calculated using the following equation:

$$r = \frac{I_{VV}-GI_{VH}}{I_{VV}+2I_{VH}} \tag{2.5}$$

where *I* is the polarization intensity and the subscripts, *V* and *H*, represent vertical or horizontal polarized light, respectively. *G* is a correction factor for any differences in intensity of horizontally and vertically polarized light and is calculated automatically by the included FluorEssence software (v2.5.2.0).

The change in anisotropy was fit to a single binding equation:

$$r = \frac{A[Dpo3]}{K_d + [Dpo3]} \tag{2.6}$$

where *A* is the reaction amplitude, and K_d is the dissociation constant for the interaction between *Sso*PolB3 and DNA.

2.3.7 Exonuclease Assays

Standard exonuclease assays were performed in polymerization reaction buffer containing 18 nM ptDNA and 2 μM *Sso*PolB3. Prior to initiation by addition of DNA, the reaction components were incubated for five minutes at 55 °C, unless otherwise indicated. Experiments were performed for times as indicated in each figure legend. Reactions were quenched and analyzed as described for polymerase reactions.

2.3.8 Circular Dichroism (CD) Denaturing Measurements

Circular dichroism (CD) experiments to monitor conformational changes of either polymerase alone or bound to DNA were performed using a DSM 17 (Olis Inc., Bogart, GA) using a 1 mm path length cell. The experiments were assembled either in the presence or absence of DNA hairpin (2 μM) and *Sso*PolB3 (4 μM). The molar ellipticity (Θ) at 222 nm was monitored over a temperature range from 20 to 95 °C in 2 °C intervals controlled by a peltier. The spectra from at least three separate scans were averaged and analyzed as described [(170)].

2.3.9 Homology Modeling and Alignment

Local and global sequence alignments were performed using ClustalW2 analysis (http://www.ncbi.nlm.nih.gov/blast/bl2seq/wblast2.cgi). The homology model of *Sso*PolB3 was created by threading the global alignment of *Sso*PolB3 with *Sso*PolB1 onto the structure of *Sso*PolB1 (PDB ID: 1S5J)[71] using SWISS-MODEL [171]. The DNA and incoming nucleotide were modeled into the active site of the homology model of *Sso*PolB3 by aligning the polymerase active site of the RB69 gp43/DNA/dTTP ternary structure (PDB ID: 1IG9) [172] with the homology model of *Sso*PolB3 using PyMol (http://www.pmol.org).

2.4 RESULTS

2.4.1 Conditions for Optimal Polymerase Activity of *Sso*PolB3

After purifying wild-type (WT) *Sso*PolB3 to homogeneity **(Figure 2.1 A)**, we characterized the buffer conditions required for maximal polymerase activity in 100 mM NaCl at 60 °C. Purification with a gel-filtration column for size selection was required for maximal polymerase activity, although no significant shift in molecule size was noted in the chromatogram. Neither HEPES nor Tris buffers nor varying pH over a limited physiological range (6.0 - 8.5) yielded a significant change in the polymerase activity of *Sso*PolB3 **(Figure 2.2 A)**. Maximal activity was observed with 20 mM Tris between pH (7 - 8.5), and so, pH 7.5 was used in all subsequent reactions. A comparison of the polymerization ability in our buffer compared with that used previously [90] showed no significant difference in the rate of incorporation (data not shown).

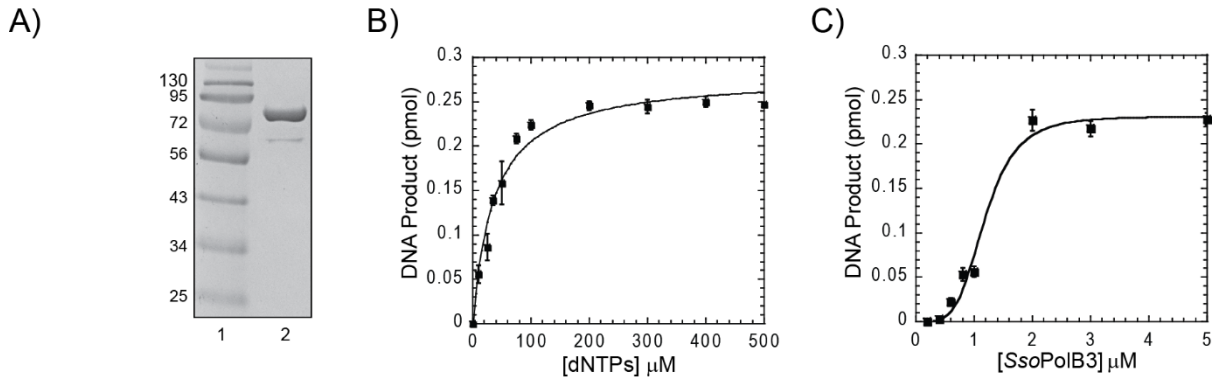

Figure 2.1: Optimization of Buffer Conditions
A) Purified *Sso*PolB3 on a Coomassie-stained sodium dodecyl sulfate−polyacrylamide gel electrophoresis gel: lane 1, protein markers; lane 2, *Sso*PolB3 (88 kDa). B) Optimization of dNTP concentrations on total DNA product produced by 2 μM *Sso*PolB3 on ptDNA in Tris (pH 7.5) and 10 mM Mg^{2+} at 70 °C. The K_M for dNTPs (36 ± 5 μM) was determined from the average of three independent experiments fit to eq 1. C) Effect of *Sso*PolB3 concentration on the total amount of DNA product produced using a long ptDNA template. Reactions were performed in Tris (pH 7.5), 200 μM dNTPs, and 10 mM Mg^{2+} at 70 °C for 10 min. The apparent dissociation constant (K_d') for *Sso*PolB3 activity (1.2 ± 0.1 μM) was determined from the average of three independent experiments fit to Equation 2.1. The cooperativitiy parameter (n) was equal to 4.4 ± 1.1.

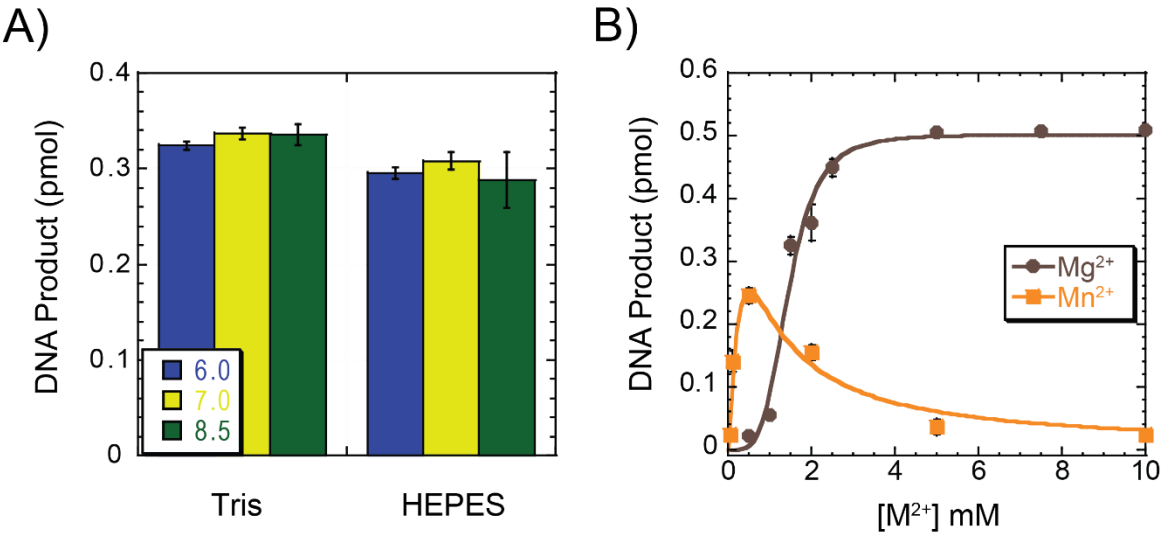

Figure 2.2: Further Optimization of Buffer Conditions
A) Optimization of reaction buffer (Tris or HEPES) and the effect of pH on total DNA produced by 2 μM *Sso*PolB3 from ptDNA in a 10 minute reaction at 60 °C with 200 μM dNTPs and 10 mM Mg^{2+}. B) Optimization divalent metal (M^{2+}) concentration on the total DNA product produced from long ptDNA by 2 μM *Sso*PolB3 in Tris buffer (pH = 7.5) and 200 μM dNTPs at 70 °C. The K_M for Mg^{2+} (1.43 ± 0.08 mM) was determined from a fit to Equation 2.1, and the K_M for Mn^{2+} (0.24 ± 0.15 mM) was determined from a fit to the inhibition Equation 2.2.

The importance of divalent cations in the nucleotide incorporation process has been well characterized, where the quantity of product extension is known to be dependent on metal concentration [(173)]. We performed polymerase reactions while varying the concentration of Mg^{2+} **(Figure 2.2 B)** and fit the data to Equation 2.1 with an observed K_M of 1.43 ± 0.08 mM. Identical experiments with Mn^{2+} showed an inhibition at concentrations greater than 0.5 mM. Based on these results, we chose to include 10 mM Mg^{2+} in the reaction buffer. Similarly, the optimal concentration of dNTPs was monitored **(Figure 2.1 B)**, where the K_d for incoming nucleotides was determined to be 36 ± 5 μM. 200 μM dNTPs were included in all subsequent polymerase reactions unless indicated otherwise. As a note, the exonuclease activity present in WT *Sso*PolB3 reduced the detected amount of fully extended product slightly from the theoretical maximum.

Having established appropriate reaction buffer conditions, we titrated *Sso*PolB3 to determine the optimal concentration for maximal activity **(Figure 2.1 C)**. Interestingly, very low activity levels were observed until a reaction concentration of 750 nM was reached. The data required a cooperativity coefficient for an appropriate fit to extract the apparent dissociation constant (K_d') equal to 1.2 ± 0.1 μM. The sigmoidal shape of the curve indicates that the concentration of the polymerase is critical for binding and associated activity. Further kinetic assays were performed at 2 μM *Sso*PolB3 determined to provide for maximal activity unless indicated otherwise.

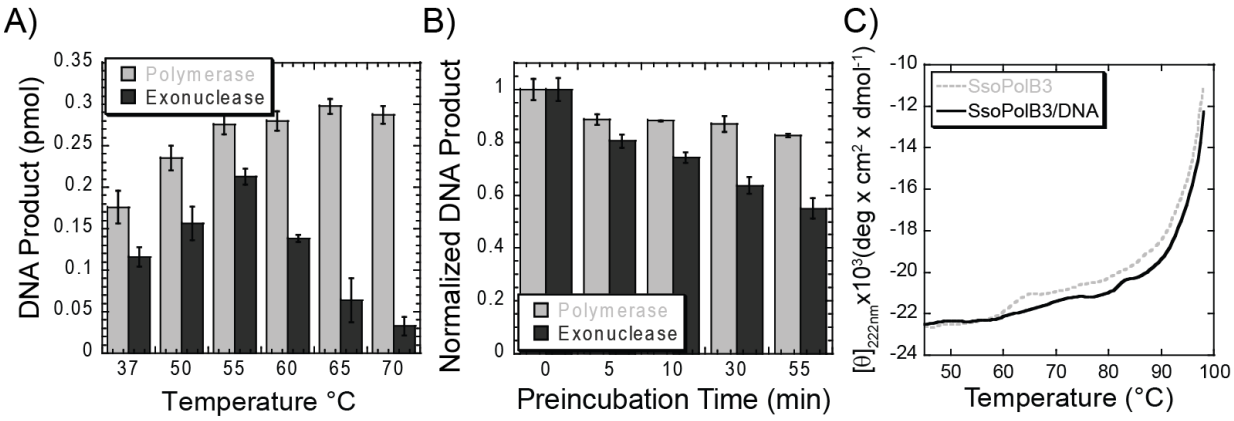

Figure 2.3: Temperature Dependence
A) Temperature dependence of 2 μM *Sso*PolB3 (WT) in 50 mM Tris (pH 7.5), 10 mM Mg^{2+}, and 200 μM dNTPs on polymerase (gray) and exonuclease (black) activities on ptDNA (36 nM) in a 10 min reaction. The reported values and errors are the average of three independent experiments. B) Thermostability of 2 μM *Sso*PolB3 (WT) after preincubation at 70 °C for the indicated time points. Quantification of product formation for polymerase activity (gray) after the addition of dNTPs and exonuclease activity (black) after the addition of ptDNA, in a 10 min reaction at 70 °C (polymerase activity) or 55 °C (exonuclease activity). The error bars represent the standard error from at least three independent experiments. C) Thermal melting of *Sso*PolB3 alone (gray dashed line) or bound (black solid line) to hairpin DNA monitored by circular dichroism at 222 nm (2 °C increments).

2.4.2 **Thermostability of *Sso*PolB3**

The optimal reaction temperature was determined by examining total product synthesized from ptDNA at temperatures varying from 37 °C to 70 °C in a 10 minute reaction **(Figure 2.3 A)**. We observed maximal polymerase product formation at 65 °C. Reactions in the absence of dNTPs monitored the exonuclease activity and were maximal at 55 °C and decreased as temperature was increased further. The purification protocol included a 70 °C incubation step which typically eliminates any background nuclease activity. The exonuclease activity of any contaminating nucleases from *E. coli* should be maximal around 37 °C and decrease at temperatures greater than 45 °C. The parallel increases in both polymerase and exonuclease activities from 37 °C to 55 °C is evidence that the observed exonuclease activity is intrinsic to the polymerase.

Although the polymerization activity of *Sso*PolB3 is maximal at temperatures greater than 65 °C, in order to assay the thermostability of the *Sso*PolB3 protein structure, we preincubated the

wild-type polymerase at 70 °C for various times and then initiated the reaction by the addition of dNTPs or DNA to monitor polymerase or exonuclease activity, respectively **(Figure 2.3 B)**. Extension to full length product from primer template was used to evaluate any loss in polymerization activity. Even after incubation at 70 °C for 55 minutes, the loss in DNA polymerase activity was minimal. The reduction in exonuclease activity was slightly greater, but 55% of the activity remained after the 55 minute high temperature incubation period.

To get a more direct measure of protein structure thermostability, we used circular dichroism (CD) to monitor the change in molar ellipticity at 222 nm as a function of temperature in the absence and presence of hairpin DNA **(Figure 2.3 C)**. The protein structure of *Sso*PolB3 is highly thermostable with an estimated melting temperature (T_m) greater than 94 °C. The data could not be quantified accurately because the maximum of the denatured curve was not apparent at 100 °C. We also note a small but reproducible unfolding event that occurs at 63 °C. This may be localized unfolding of a small thermally unstable domain within *Sso*PolB3. In the presence of ptDNA, the T_m for *Sso*PolB3 shifts slightly higher (~96 °C) and the local unfolding event at 63 °C disappears.

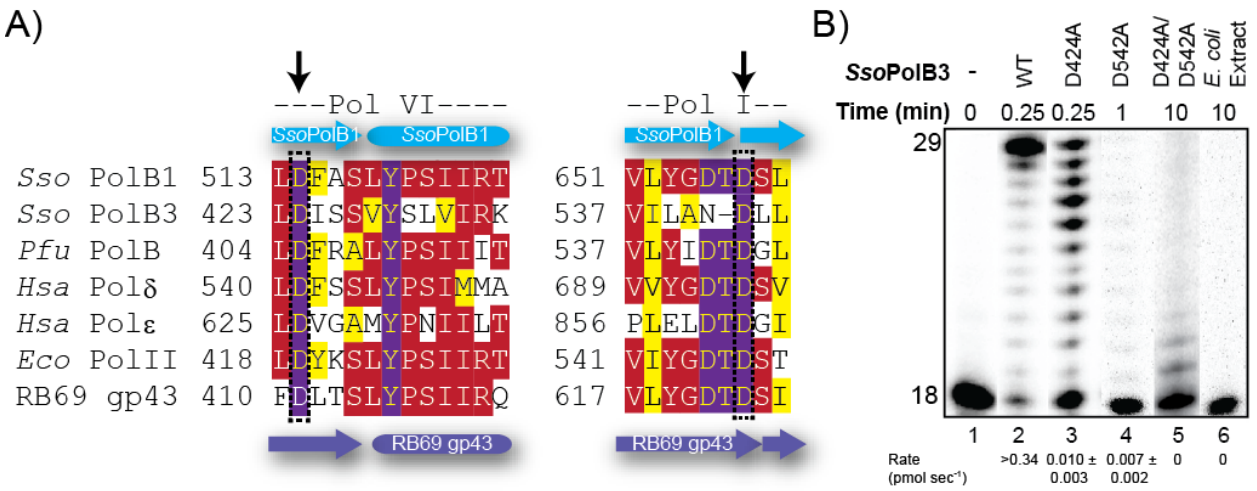

Figure 2.4: Confirming *Sso*PolB3 Active Site Conservation
A) Amino acid alignment of DNA polymerase domains VI and I using CLUSTAL W2 (http://www.ebi.ac.uk/Tools/clustalw2) for common members within the B-family of DNA replication polymerases. Slightly (yellow), mostly (red), and absolutely (purple) conserved residues are denoted. The secondary structure elements are derived from the crystal structure of *Sso*PolB1 (cyan) (PDB entry 1S5J) or RB69 gp43 (purple) (PDB entry 1CLQ). Species are identified with three-letter codes: *Sso*, *S. solfataricus*; *Pfu*, *Pyrococcus furiosus*; *Hsa*, *Homo sapiens*; *Eco*, *E. coli*. Arrows denote the residues in *Sso*PolB3 that were mutated and constitute the active site aspartates. B) Effect of *Sso*PolB3 single (D424A or D542A) or double (D424A/D542A) mutants on the extension of template (T)G at 60 °C for the indicated times under optimal buffer conditions. The average rates in picomoles per second from multiple independent experiments are listed below the corresponding lanes of the gel.

2.4.3 Conserved Mutations in the Polymerase Active Site Disrupt Activity

There is a conserved aspartic acid residue (D424) within the polymerase six (Pol VI) domain and a single aspartic acid (D542) within the polymerase one (Pol I) domain of *Sso*PolB3 **(Figure 2.4 A)**. It has been previously shown that mutation of the conserved active site aspartates in homologous DNA polymerases abolishes nucleotide incorporation ability *(93, 94, 174, 175)*. Interestingly, *Sso*PolB3 lacks the first aspartate in the highly conserved DTD motif in Pol I domain **(Figure 2.4 A)** known to be important in coordinating Mg^{2+} and contributing to translocation *(93)*. To determine if the polymerase active site of *Sso*PolB3 is functionally conserved in in the absence of a conserved Pol I domain, we constructed three mutants; two single (D424A, D542A) and one double (D424A/D542A). We then examined the polymerase activity of the mutants compared to

WT *Sso*PolB3 at 60 °C **(Figure 2.4 B)**. The polymerase activity for synthesis of full length products for the D424A mutant was reduced more than 30-fold from WT
(0.010 ± 0.003 vs. 0.34 pmol•sec^{-1}, respectively), while the D542A mutant was reduced more than 50-fold (0.007 ± 0.002 pmol•sec^{-1}). The activity of the double mutant (D424A/D542A) was reduced to just above background levels and required much longer times to detect any product.

2.4.4 **Conserved Mutations in the Exonuclease Active Site Disrupt Activity**

The exonuclease domain of polymerases can be organized into three motifs (Exo I, Exo II, and Exo III). Aspartates within each domain have been implicated in the proofreading function in different polymerases. *Sso*PolB3 has a conserved aspartate (D172) in the exonuclease I domain shown to be important for *E. coli* Pol II [176] and pol ε [177], but mutation to alanine had no effect on the exonuclease activity (data not shown). Examination of the exonuclease II motif (Exo II) showed no universally conserved aspartate or glutamate [78, 178, 179] for *Sso*PolB3 but contained four potential catalytic aspartates **(Figure 2.5 A)**. We individually mutated each aspartate (D226A, D228A, D234A, and D236A) in Exo II and examined their effect on the exonuclease activity levels on three DNA substrates (ssDNA, ptDNA, dsDNA). As proof that D236 is involved in proofreading, the D236A mutant incorporates nucleotides fully to the end of the template unlike WT which stops one base prior to the end (-1) in this time frame **(Figure 2.5 B)**. D236A had the lowest exonuclease activity and therefore greatest perturbation **(Figure 2.5 C & 2.5 D)** of the four mutants. A double mutant D234A/D236A had no further reduction in exonuclease activity over the D236A single mutant (data not shown). The rate for the exonuclease product formation for WT was 0.031 ± 0.001 pmol•sec^{-1}, while the rate for D236A was reduced approximately seven-fold to 0.0046 ± 0.0003 pmol•sec^{-1}, implicating this aspartate in the proofreading mechanism **(Figure 2.5 E)**.

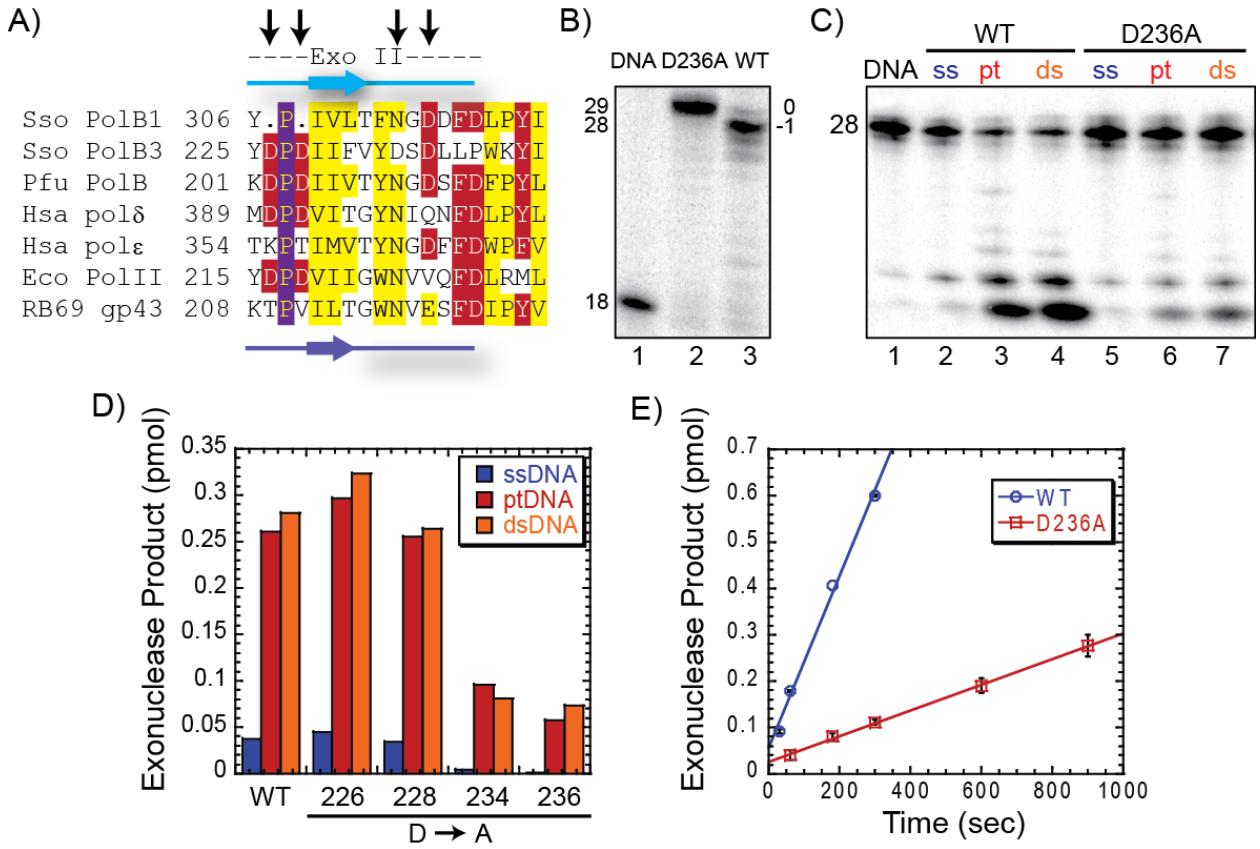

Figure 2.5: Analysis of *Sso*PolB3 Exonuclease Activity

A) Amino acid alignment of exonuclease domain II using CLUSTAL W2 (http://www.ebi.ac.uk/Tools/clustalw2) for common members within the B-family of DNA replication polymerases. Slightly (yellow), mostly (red), and absolutely (purple) conserved residues are denoted. The secondary structure elements are derived from the crystal structure of *Sso*PolB1 (cyan) (PDB entry 1S5J) or RB69 gp43 (purple) (PDB entry 1CLQ). Species are identified with three-letter codes: *Sso, S. solfataricus*; *Pfu, P. furiosus*; *Hsa, H. sapiens*; *Eco, E. coli*. Arrows denote the residues in *Sso*PolB3 that were mutated. B) Polymerase reactions comparing formation of the full-length product from WT and D236A *Sso*PolB3 on template T at 70 °C for 3 min, showing major products (29 base, blunt, 0) or (28 base, recessed, −1) for D236A or WT *Sso*PolB3, respectively. C) Exonuclease experiment with single-stranded (ssDNA), primer−template (ptDNA), and double-stranded (dsDNA) DNA for both WT and D236A *Sso*PolB3 at 55 °C for 10 min. D) Quantification of exonuclease cleavage products for WT *Sso*PolB3 and each prospective exonuclease mutant (D226A, D228A, D234A, and D236A), on all three DNA conformations [ssDNA (blue), ptDNA (red), and dsDNA (orange)] at 55 °C for 10 min. E) Quantification of the steady-state rate of exonuclease products produced from ptDNA by WT (0.031 ± 0.001 pmol•sec^{-1}) or D236A (0.0046 ± 0.0003 pmol•sec^{-1}) *Sso*PolB3 from at least two independent experiments. The error bars represent the standard error of the reaction.

2.4.5 **DNA Binding Affinity of *Sso*PolB3 Monitored through Fluorescence Anisotropy**

DNA binding of B-family polymerases is typically robust, and shows a preference for ptDNA over ssDNA [(78)]. To determine if the relatively high concentrations of *Sso*PolB3 required for activity are a result of a weak binding affinity, we measured the DNA binding properties using fluorescence anisotropy. Fluorescence anisotropy measures the molecular rotational diffusion rates of molecules, where a decrease in these rates using fluorescently labeled DNA occurs upon formation of a protein DNA complex.

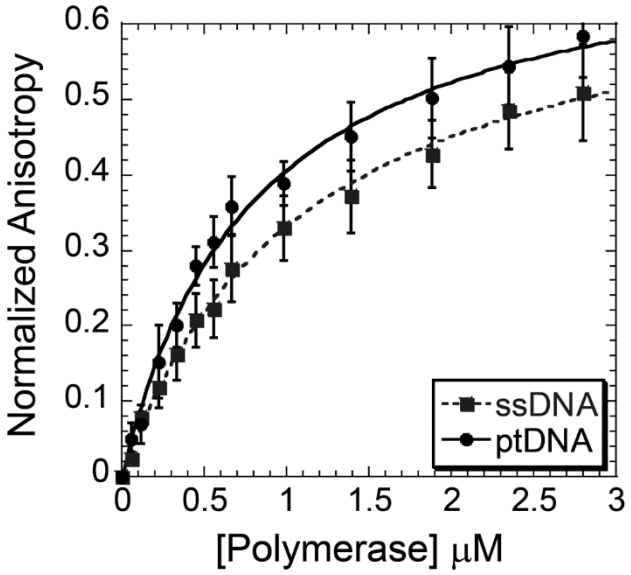

Figure 2.6: DNA Binding Affinity
Change in fluorescence anisotropy upon binding of *Sso*PolB3 (D236A) to either Cy3-labeled ssDNA (Cy3DNA) (gray dashed line) or ptDNA (black solid line). Data points were fit to Equation 2.4 to extract a K_d of binding for ssDNA (1.10 ± 0.08 μM) and ptDNA (0.81 ± 0.06 μM). The error bars represent the standard error from at least three independent experiments.

The resulting increase in anisotropy (r) can be plotted to determine the binding coefficient (K_d). Both ssDNA and ptDNA were used as the substrate with a fluorescent dye, Cy3, located at the 5' end of the template or single strand. Anisotropy values were measured as *Sso*PolB3 concentration was increased. The K_d for the interaction between *Sso*PolB3 and ssDNA was 1.10 ± 0.08 μM, while the K_d for the interaction between ptDNA was tighter at 0.81 ± 0.06 μM **(Figure 2.6).**

2.4.6 **Correct Nucleotide Specificity**

We analyzed the presteady-state dNTP incorporation rate of the *Sso*PolB3 exonuclease mutant (D236A) for correctly paired nucleotides across from all four different template bases. These reactions could be performed accurately by hand at 37 °C due to a decreased rate of synthesis at lower temperatures. Previously, Suo and coworkers established that fidelity reactions with *Sso*PolB1 and *Sso*PolY performed at lower temperatures did not have significantly different values than those performed at higher temperatures.[(75)]

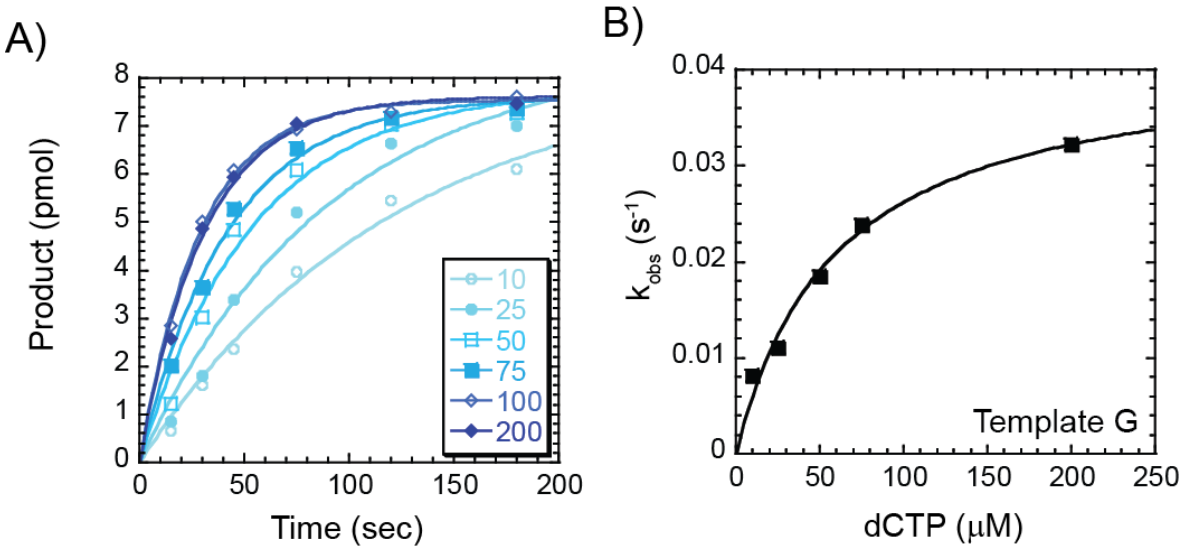

Figure 2.7: Correct Nucleotide Incorporation
Concentration dependence of the pre-steady-state rate of correct nucleotide incorporation. A) A preincubated solution containing 2 μM *Sso*PolB3 and template G (9.6 nM) was mixed with increasing concentrations of dCTP (from 10 to 200 μM) for the indicated time points. The data were fit to Equation 2.3 to determine the single-exponential rate (k_{obs}). B) k_{obs} values were plotted as a function of dCTP concentration and fit with Equation 2.4 to yield k_p (0.045 ± 0.008 s^{-1}) and K_d (61 ± 26 μM).

Single turnover reactions were performed where the enzyme concentration (2 μM) was held well above the DNA concentration (9.6 nM) as required based on the affinities and activities measured above. The quantified products for different concentrations of dCTP incorporated onto Template G were plotted as a function of the reaction times to obtain the apparent rate constants (k_{obs}) according to Equation 2.3 **(Figure 2.7 A)**.

These single-turnover rates were plotted as a function of the concentration of dCTP and fit to Equation 2.4 to yield the second order polymerization rate (k_p), 0.045 ± 0.007 sec^{-1} and dissociation constant for dCTP (K_d), 61 ± 25 μM **(Figure 2.7 B & Table 2.1)**. The measure of substrate specificity (k_p/K_d) was calculated to be 7.4 x 10^{-3} $\mu M^{-1}sec^{-1}$. If *Sso*PolB3 is able to bind nucleotides nonspecifically in the absence of DNA, high concentrations of enzyme could affect the K_d value measured if the concentration of enzyme was similar in magnitude. In our experiments, a large excess of enzyme was required to promote DNA binding, but this concentration is still at least 5 to 100 times less than the experimental concentration of dCTP.

Table 2.3: Pre-Steady State PolB3 Kinetic Parameters

dNTP	k_p (sec^{-1})[1]	K_d (mM)[1]	k_p/K_d (μM^{-1} sec^{-1})	Misincorporation Frequency[2]
Template A				
dATP	0.0010 ± 0.0002	0.23 ± 0.02	4.5 x 10^{-6}	6.7 x 10^{-3}
dCTP	0.0016 ± 0.0002	2.0 ± 0.6	7.9 x 10^{-7}	1.2 x 10^{-3}
dGTP	0.0017 ± 0.0004	1.7 ± 1.1	9.6 x 10^{-7}	1.5 x 10^{-3}
dTTP	0.038 ± 0.002	0.057 ± 0.008	6.6 x 10^{-4}	
Template C				
dATP	0.00065 ± 0.00005	0.74 ± 0.20	8.9 x 10^{-7}	3.0 x 10^{-4}
dCTP[3]	-	-	-	-
dGTP	0.069 ± 0.005	0.024 ± 0.007	2.9 x 10^{-3}	
dTTP	0.0013 ± 0.0001	0.43 ± 0.16	3.1 x 10^{-6}	1.1 x 10^{-3}
Template G				
dATP	0.0025 ± 0.0005	1.9 ± 0.9	1.3 x 10^{-6}	1.9 x 10^{-3}
dCTP	0.045 ± 0.008	0.061 ± 0.025	7.4 x 10^{-4}	
dGTP[4]	0.0011 ± 0.0001	0.056 ± 0.017	2.0 x 10^{-5}	2.8 x 10^{-2}
dTTP	0.0016 ± 0.0001	0.30 ± 0.08	5.3 x 10^{-6}	7.6 x 10^{-3}
Template (T)G				
dGTP	0.0021 ± 0.0002	0.69 ± 0.20	3.1 x 10^{-6}	4.4 x 10^{-3}
Template T				
dATP	0.12 ± 0.01	0.018 ± 0.006	6.8 x 10^{-3}	
dCTP	0.0009 ± 0.0001	0.79 ± 0.34	1.1 x 10^{-6}	1.6 x 10^{-4}
dGTP[5]	0.0025 ± 0.0001	0.41 ± 0.03	6.0 x 10^{-6}	8.7 x 10^{-4}
dTTP	0.0015 ± 0.0001	0.39 ± 0.08	3.7 x 10^{-6}	5.4 x 10^{-4}

[1]Calculated from the fit to Equation 2.4 of the second order plot. [2]Calculated as $(k_p/K_d)_{incorrect}/(k_p/K_d)_{correct}$. [3]Was not incorporated appreciably above background and unable to quantify. [4]Inhibition at [dGTP] > 1mM. [5]Inhibition at [dGTP] > 2 mM.

Single turnover experiments for other correct nucleotide incorporations (dTTP on Template A, dGTP on Template C, and dATP on Template T) were also performed similarly **(Figure 2.8, Figure 2.10)**. The kinetic parameters (k_p, K_d, and k_p/K_d) are reported in **Table 2.3**. Interesting observations from this analysis includes incorporation of dATP on Template T was roughly three-fold faster (0.12 ± 0.01 sec^{-1} vs. 0.038 ± 0.002 sec^{-1}) than the reverse incorporation (dTTP on Template A). Also, the K_d for binding dATP was three-fold tighter than for dCTP or dTTP on their respective correctly base paired templates.

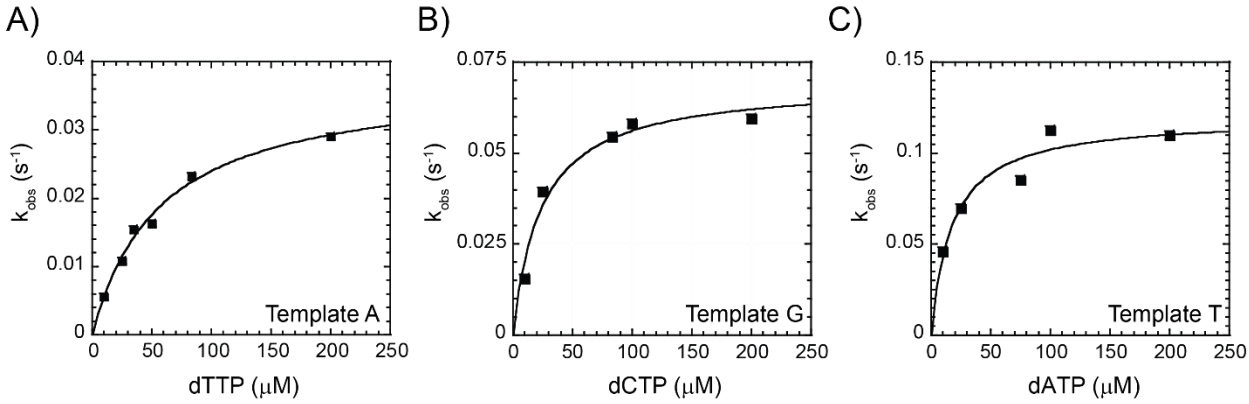

Figure 2.8: k_p Determination
Concentration dependence of the pre-steady state rate of correct nucleotide incorporation. A preincubated solution containing 2 μM *Sso*PolB3 and 9.6 nM A) Template A, B) Template G and C) Template C was mixed with increasing concentrations of the complementary nucleotide. The k_{obs} values were plotted as a function of each dNTP concentration and fit with Equation 2.4 to yield the k_p and K_d parameters reported in Table 2.1.

2.4.7 **Incorrect Nucleotide Specificity**

Presteady-state incorporation rates for incorrect nucleotides opposite all four templates were also analyzed similarly as described above. As an example, single nucleotide misincorporation of dTTP at various concentrations onto template T is shown in **Figure 2.9 A** to obtain k_{obs}. These observed rates were plotted against the dTTP concentration and fit to Equation 2.4 to give k_p (0.0015 ± 0.0001 s^{-1}), K_d (0.39 ± 0.08 mM), and k_p/K_d (3.7 x 10^{-6} $\mu M^{-1}s^{-1}$) values **(Figure 2.9 B, Figure 2.10 and Table 2.3)**. Misincorporation of dTTP on Template T was roughly 100-fold slower and with a 20-fold weaker K_d than for correct incorporation of dATP. This results in a misincorporation frequency for incorrect dNTPs of 5.4 x 10^{-4} **(Table 2.3)** or 1 error every

2000 bases with polymerase active site selection alone. In some cases, inhibition was noted at high concentrations of incorrect nucleotides. Incorporation of dGTP on Template T was inhibited at concentrations greater than 2 mM, and dGTP incorporation on Template G was inhibited at concentrations greater than 1 mM. Nucleotide selection seems to be the most discriminative for Template C and Template T provided by a concomitant decrease in both the polymerization rate and affinities.

For the most part, incorrect nucleotide incorporations are 20-100 times slower than for correct incorporations with K_d values 4-30 times weaker **(Figure 2.10, Table 2.3)**. One exception seems to be that the K_d of dGTP and dCTP are identical on Template G. The 40-fold slower rate of incorporation for dGTP on that template is the only factor that provides for the selectivity in this case, leading to a weaker fidelity value of 2.77 x 10^{-2}.

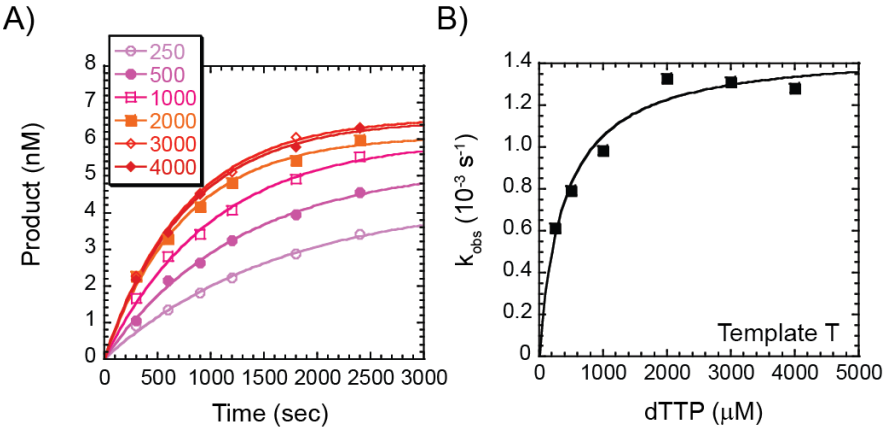

Figure 2.9: Incorrect Nucleotide Incorporation Concentration dependence of the pre-steady-state rate of incorrect nucleotide incorporation. A) A preincubated solution containing 2 μM *Sso*PolB3 and template T (9.6 nM) was mixed with increasing concentrations of dTTP (from 250 μM to 4 mM) for the indicated time points. The data were fit to Equation 2.3 to determine the single-exponential rate (kobs). B) k_{obs} values were plotted as a function of dTTP concentration and fit with Equation 2.4 to yield k_p (0.0015 ± 0.0001 sec^{-1}) and K_d (0.39 ± 0.08 mM).

For Template G, the preceding base (-1) in the template is cytosine which allows for the possibility that the strong binding of dGTP on Template G noted above is the result of a looping mechanism that base pairs the incoming nucleotide at the -1 position in the template. To test this, we changed the -1 base in the template strand to T to create Template (T)G. When single nucleotide misincorporation assays were performed with dGTP on this template, there was a significant increase in the K_d to 0.69 ± 0.20 mM **(Table 2.4)**. This resulted in a decrease in k_p/K_d (3.1 x 10^{-6} μM^{-1} s^{-1}) and misincorporation frequency (4.4 x 10^{-3}) more consistent with the rest of **Table 2.3**.

Except for dGTP on Template G, the error frequencies for *Sso*PolB3 range from 10^{-3} to 10^{-4} and are in line with other polymerases in this family [180, 181].

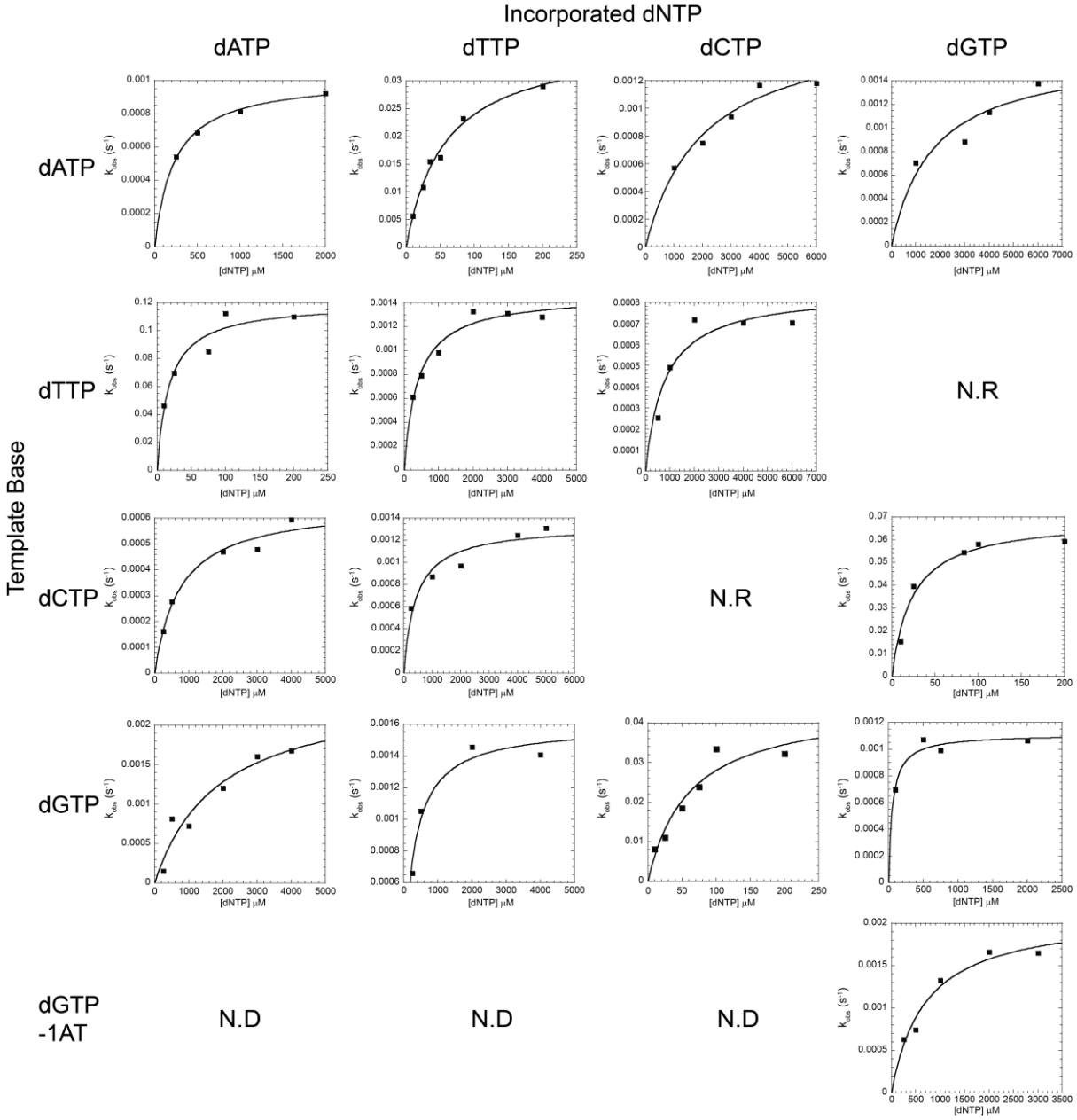

Figure 2.10: Determination of Single Nucleotide Incorporation Rate
K_{obs} values determined through time course replication experiments were plotted against the concentrations the reactions were performed at and fit using Equation 2.4 to determine k_p. All k_p values are recorded in **Table 2.3**. N.R – no reaction, N.D. – experiment was not performed.

Table 2.4: Pre-Steady State PolB3 Kinetic Parameters

Polymerase	Fidelity $(k_p/K_d)_{correct}/(k_p/K_d)_{incorrect}$	K_d Difference $(K_d)_{incorrect}/(K_d)_{correct}$	k_p difference $(k_p)_{correct}/(k_p)_{incorrect}$
*Sso*PolB3[1]	1.5 x 10^2 to 6.3 x 10^3	4 to 45	17 to 140
*Sso*PolB1[2]	1.6 x 10^3 to 2.9 x 10^5	110 to 920	4 to 580
*Sso*PolY[3]	3.1 x 10^2 to 6.7 x 10^3	1 to 18	99 to 1600

[1]At 37 °C (This work). [2]At 37 °C *(75)*; data does not include the fidelity contribution from the 3-5'exonuclease activity. [3]At 37 °C. *(165)*

2.5 DISCUSSION

We have biochemically characterized both the DNA polymerization and exonuclease activities of the third B-family DNA polymerase in *Sulfolobus solfataricus* and verified that it is an active enzyme. Although *Sso*PolB3 is characterized as a B-family DNA polymerase, the Pol I motif in the active site is not absolutely conserved prompting speculation that it may be inactive .*(87)* *Sso*PolB3 was proposed to have evolved thorough a gene duplication event *(95)*, which eventually became the precursor for the human DNA polymerase ε implicated in leading strand DNA replication in eukaryotes.*(92, 153)* In order to better understand the role of *Sso*PolB3 in chromosomal maintenance in Archaea, we investigated the polymerase and exonuclease activities, fidelity, and thermostability of this polymerase. *Sso*PolB3 is an accurate B-family DNA polymerase whose fidelity is increased further with the inclusion of an active exonuclease domain. *Sso*PolB3 has high thermostability that is increased slightly in the presence of DNA. Surprisingly, *Sso*PolB3 binds DNA weakly compared with other B-family polymerases *(75, 78)* and the exonuclease and polymerase activities are maximal at different temperatures. While preparing this manuscript, a recent report has also characterized the *in vitro* activity of *Sso*PolB3 *(90)*, and although there are some similarities such as weak DNA binding, we have measured significant differences in the kinetic and thermodynamic parameters as well as verified and compared the importance of the catalytic residues in the polymerase and exonuclease active sites. In spite of the nonconserved active site motifs, *Sso*PolB3 has been confirmed to be a B-family DNA polymerase with enzymatic activities that allow participation in coupled DNA replication or repair activities in Archaea. The

roles and activities of multiple DNA polymerases in this organism provide a model for understanding and characterizing DNA polymerase specificities in higher organisms. Nonconserved Polymerase Motifs Reduce DNA Binding and Enzymatic Activity

Although *Sso*PolB3 is considered to be a B-family DNA polymerase, the most conserved Pol I domain contained in all DNA polymerases is mutated. This conserved YGDTD sequence is used to coordinate Mg^{2+} where the tyrosine and both aspartates are thought to be essential for polymerase activity.[93, 94, 182] In *Sso*PolB3, the homologous sequence is LAN-D, where rather than a pair of aspartic acids residues coordinating Mg^{2+} and contributing to translocation, a single aspartic acid residue is important for the catalytic activity. Crystal structures for RB69 gp43 [172] and yeast pol δ [183] highlight the importance of the second aspartate (Pol I) in metal coordination and catalysis and is consistent with a similar role for D542 in *Sso*PolB3.

Conversely, the first aspartate in the Pol I motif is generally orientated away and towards the minor groove at the site of insertion.[184, 185] Although this first aspartate is conserved, the actual role of this residue is elusive. Mutation of the first aspartate (Pol I) in Phi29 DNA polymerase disrupted the translocation step between catalysis steps and resulted in lower processivity, possibly representing a looser grip on DNA.[186] Interestingly, high concentrations of *Sso*PolB3 (in excess of 750 nM) were required for stable binding and efficient DNA extension as also noted previously [90] and could be the consequence of the missing first aspartate. Mutation of the homologous first aspartate in human polymerase α required Mn^{2+} to restore the wild-type activity.[94] Our metal dependent studies for *Sso*PolB3 may actually be similar in that at concentrations less than 1 mM metal, Mn^{2+} provides the optimal activity. At higher concentrations, Mn^{2+} is inhibitory and Mg^{2+} provides for optimal activity similar to the D1002N mutant of human pol α.[94]

The other catalytic aspartate contained in the Pol VI motif and known to be involved in Mg^{2+} coordination is conserved in *Sso*PolB3 (D424) but residues adjacent to this residue have also been shown to affect catalysis. Previous work by Kennedy *et al*. implicated a conserved ALY motif within the Pol VI domain of the *Pyrococcus furiosus* B-family polymerase in a stacking interaction with the ribose of the incoming nucleotide.[187] A408S and L409V mutations in *Pfu*Pol both result in a decrease in catalytic efficiency (k_{cat}/K_M). It seems that increased side chain volume interacting at the back of the incoming nucleotide negatively affect catalysis and fidelity. The

homologous wild-type sequence in *Sso*PolB3 is 427-SVY and may also contribute to *Sso*PolB3's slower incorporation rates and reduced fidelity.

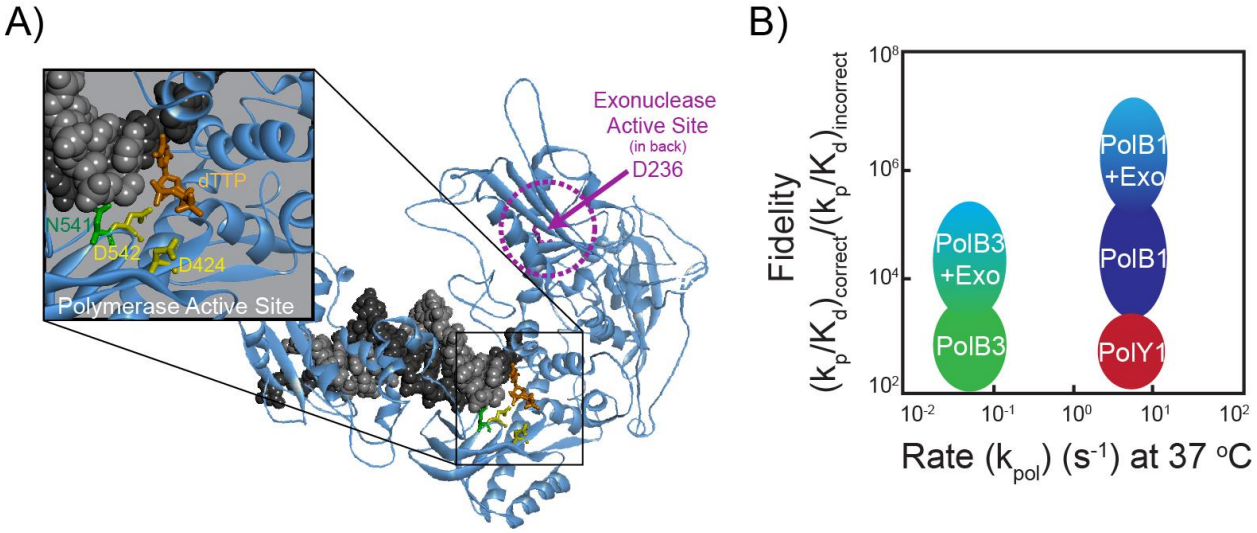

Figure 2.11: PolB3 Homology Model
A) Homology model of the ternary complex of *Sso*PolB3 bound to DNA (black and gray) with incoming dTTP (orange) highlighting the aspartates in the polymerase (D424 and D542, yellow) and exonuclease (D236, pink) active sites. N541 (green) is also shown oriented toward the minor groove of the dsDNA template. B) Graphical representation of the fidelity [(k_p/K_d)correct/(k_p/K_d)incorrect] as a function of the rate (k_{pol}) comparing *Sso*PolB1, *Sso*PolB3, and *Sso*PolY.

To highlight the two active site aspartates primarily responsible for metal binding and catalysis, we created a ternary homology model of *Sso*PolB3 bound to DNA with an incoming dTTP **(Figure 2.11 A)**. In this model, it is clear that D424 and D542 are orientated properly for binding metals in the active site required for catalysis and incoming dNTP stabilization. Interestingly, N541 seems to adopt a similar conformational position as the first aspartate in the Pol I motif of other polymerases. The absence of a negative charge at this position in *Sso*PolB3 would disrupt native interactions with Mg^{2+} and the DNA template possibly explaining the reduced affinity of binding.

2.5.1 *Sso*PolB3 has Moderate Polymerase Activity

We have shown through detailed kinetic analysis that the catalytic activity of *Sso*PolB3 is moderate, although the rate of nucleotide incorporation is significantly faster than previously published [(90)]. During the purification of *Sso*PolB3, it became clear that inclusion of a gel filtration column for size selection and cleanup was required for maximal activity. A comparison of the reaction conditions used in our study with those from the previous report [(90)] noted no significant differences in extension rates using our purified protein. Polymerization reactions for *Sso*PolB3 at 37 ^{o}C or 50 ^{o}C converted more than 50-70% of the substrate to full length product in 10 minutes **(Figure 2.3 A)** compared with little full length product formed at these temperatures in a 30 minute reaction previously [(90)]. The kinetic rate constants are difficult to compare between the studies, because we used presteady-state analysis monitoring the fastest rate of single nucleotide incorporation for *Sso*PolB3, while the previous study used steady-state analysis. Presteady-state analysis has been shown to be more accurate for measuring the kinetic and thermodynamic basis for fidelity of nucleotide incorporation [(188)]. Moreover, we have verified that *Sso*PolB3 has an active exonuclease proofreading domain which would make steady-state analysis of polymerase fidelity with the wild-type enzyme difficult.

The fidelities of nucleotide incorporation for the *Sso*PolB3 polymerase active site alone are generally $10^2 – 10^3$. One exception where the fidelity is less occurs when the incoming base is incorporated based on complementarity to the preceding -1 template base (dGTP on Template G). In this case, incorporation would require destabilization of the terminal base pair and looping out of the last base in the primer strand. Incorporation would then proceed opposite the -1 base in the template. An analogous looping out mechanism has been noted previously for *Sso*PolY [(108, 119)], although the looped-out base occurs in the template strand instead, in favor of nucleotide incorporation opposite the +1 position. We can rule out a similar mechanism for *Sso*PolB3 as incorporation dATP in Templates G (where the +1 base is T) has the weakest K_d value of the group.

In general, the presteady-state kinetics of *Sso*PolB3 are reduced compared with the other two well-characterized DNA polymerase (*Sso*PolB1 and *Sso*PolY) in *Sso* (**Table 2.4).** We compared the nucleotide binding, kinetic incorporation rate, and the fidelity differences of

*Sso*PolB3 with *Sso*PolB1 and *Sso*PolY. *Sso*PolB3 possesses nucleotide selectivity (K_d difference) values more similar to the Y-family DNA polymerase, *Sso*PolY. The ratio of the maximal rate of incorporation (k_p) for correct versus incorrect nucleotides for *Sso*PolB3 is more similar to the selectivity provided by *Sso*PolB1, although the absolute rate of catalysis is roughly 100-fold slower. Therefore, the fidelity of *Sso*PolB1 is primarily driven by a reduced rate of incorporation for incorrect nucleotides rather than selectivity in nucleotide binding. The fidelity values for *Sso*PolB3 are comparable to those for *Sso*PolY but less than *Sso*PolB1 **(Table 2.2)**. The exonuclease domain contained within *Sso*PolB3 will increase the fidelity value further; approaching that required for accurate DNA synthesis making this polymerase more accurate than *Sso*PolY **(Figure 2.11 B)**.

2.5.2 Variable Thermostabilities of the Polymerase and Exonuclease Domains of *Sso*PolB3

Interestingly, the temperatures in which the polymerase and exonuclease activities are maximal are different. The maximal exonuclease activity occurs at 55 °C which is below the physiological temperature while the maximal polymerase activity occurs above 65 °C. The thermostability of the entire *Sso*PolB3 structure is high with a T_M of > 94 °C which is increased slightly in the presence of DNA. This is in direct contrast to a previous report which showed that preincubation for 20 minutes at 60 °C completely abolished activity [90]. Conversely, we can show that preincubation at 70 °C for 55 minutes only minimally reduces polymerase activity and the exonuclease domain retains more than half the original activity. Thermostabilites for *Sso*PolB1 and *Sso*PolY have been measured previously [115, 189] and are similar to that found for *Sso*PolB3.

Looking closely at the CD spectra, we have noticed a reproducible but slight deviation around 63 °C suggesting that a local reversible unfolding event may be possible. This spectral change is not observed when DNA is included in the experiment suggesting that a more stable protein complex exists in the presence of DNA, possibly representing the closed conformation. Based on the decrease in promiscuous exonuclease activity above 55 °C and the CD spectra change

at 63 °C, we conclude that the exonuclease domain is stabilized in a proofreading conformation in the presence of DNA at high temperatures.

When dNTPs are included, the role of the exonuclease activity is to increase the fidelity by monitoring correct base incorporations. Clearly, there is a cycle between nucleotide incorporation and exonuclease proofreading that occurs with the wild-type enzyme similar to other B-family DNA polymerases. The exonuclease activity is controlled by kinetics of the forward rate constant for nucleotide incorporation. When dNTPs are absent or in low abundance, the kinetic rate of incorporation is low and causes the slightly slower exonuclease rate to proceed instead. For *Sso*PolB3, the exonuclease activity is somewhat temperature dependent. The change in the CD spectrum coupled with slower kinetics at higher temperatures suggest that the DNA binding specificity (ssDNA or ptDNA) may be modulated by temperature. This may also help explain the lower exonuclease activity on ssDNA versus ptDNA at higher temperature in spite of somewhat similar affinities. Even so, the recognition or proofreading of misincorporated bases opposite damaged templates (hypoxanthine, 8-oxoG, and cyclobutane dimers) may be less restrictive in some cases dependent on the geometry as *Sso*PolB3 has been shown recently to be able to bypass these lesions [(90)].

2.5.3 **Role of Multiple B-family DNA polymerases in Archaea**

The DNA replication system from *Sulfolobus* is now an even more enticing model system with the discovery that there are multiple active B-family DNA polymerases along with a single Y-family lesion bypass polymerase. This is similar to other organisms which have multiple DNA replication polymerases at the replication fork [(136, 153)]. The measured *in vitro* activity of *Sso*PolB3 is absolutely slower than the proposed DNA replication polymerase, *Sso*PolB1 **(Figure 2.10 B)**. Therefore, it seems that *Sso*PolB1 will provide the major replicative activity during replication. Of course, we cannot rule out an increase in activity for *Sso*PolB3 with additional accessory factors *in vivo*. The included active exonuclease proofreading domain of *Sso*PolB3 would suggest that it has a role in faithful DNA replication and not necessarily repair or lesion bypass. Of course, genetic knockouts of this polymerase could provide some further information on the proposed role in genomic maintenance.

DNA binding and recognition of the DNA template will be difficult for *Sso*PolB3 due to its weaker affinity. We have shown previously that *Sso*PolB1 can form a trimeric complex at a similar concentration range [(78)]. It was noted recently, that the protein expression levels of *Sso*PolB3 are similar to *Sso*PolB1 and much greater than *Sso*PolY [(90)], suggesting that the cellular concentrations and thermodynamics may favor formation of a *Sso*PolB3/DNA complex. Therefore, the local concentrations of polymerases around the replication fork will strongly influence associations.

Based on the enzymatic properties described here, *Sso*PolB3 could be involved in initiating DNA replication, extension of Okazaki fragments on the lagging strand [(190)], or in a more directed role of synthesis across specific lesions [(90)]. The initiation of DNA replication after RNA priming is performed by DNA polymerase α in humans. There is no direct homolog in Archaea and the polymerase responsible for extending the RNA primer to initiate DNA replication has not been identified [(48)]. The measured *in vitro* synthesis rate of *Sso*PolB3 extrapolated at 75 °C is roughly 150 s^{-1}, based on the rate increase measured with temperature for *Sso*PolB1.[(75)] This is slightly faster than required (92 sec^{-1}) for bidirectional synthesis of the leading strand at three origins [(97)] on the *Sso* genome (2.99 x 10^6 bases) [(96)] over a 90 minute S-phase [(98)]. It is equally possible that synthesis of the short 100-150 base Okazaki fragments [(191)] could be performed by *Sso*PolB3 in parallel to provide the necessary speed for genomic replication. Probably just as likely though, *Sso*PolB3 could be confined to a specialized role in DNA repair, although with the identification of an active exonuclease domain, the specific lesions that are processed remain to be determined. Identification of interacting protein partners with *Sso*PolB3 may be able to better reveal a potential role for this polymerase *in vivo*. Clearly, there are multiple kinetic and thermodynamic association events that occur with DNA in an organism with multiple DNA polymerases. The regulation of each DNA polymerase's individual activity will be dynamically controlled by cellular concentrations and interactions with other accessory proteins that direct binding along with their individual kinetics to maintain the genome.

2.6 CONCLUSION

This chapter details the first ever full kinetic examination of a B-Family Pol3, from an archaeal organism. We were able to purify this enzyme to homogeneity, generating a more active enzyme after employment of a gel filtration chromatography step. Despite previous evidence based on sequence homology indicating the enzyme would lack activity, we were able to quantify both polymerase and exonuclease activity for *Sso*PolB3 and illustrate which residues are important for metal coordination through mutagenesis. We also examined the fidelity of the polymerase domain for single nucleotide incorporation across from both correct and incorrect template bases. The resulting data illustrates that the polymerase active site on its own has intermediate fidelity, however, fidelity will be increased with the active exonuclease domain. The activity of the nuclease domain was observed to be temperature dependent, and we hypothesize this dependence is resultant from a structural change, which is supported by the change observed in the thermal melting experiments over a similar temperature range. This research is an important advancement in our understanding of the involvement of multiple B-family polymerases in the crenarchaeal system. The high homology of the B-family DNA polymerases between Archaea and Eukaryotes allows for an extrapolation of function between these two domains of life.

3.0 ASSEMBLY AND DISTRIBUTIVE ACTION OF AN ARCHAEAL DNA POLYMERASE HOLOENZYME[4]

3.1 SUMMARY

The assembly and enzymatic ability of the replication DNA polymerase holoenzyme from *Sulfolobus solfataricus* (*Sso*) was investigated using presteady-state FRET assays coupled with functional and structural studies. Kinetic experiments reveal that ATP binding to RFC is sufficient for loading the heterotrimeric PCNA123 clamp onto DNA which includes a rate-limiting conformational rearrangement of the complex. ATP hydrolysis is required for favorable recruitment and interactions with the replication polymerase (PolB1) that most likely include clamp closing and RFC dissociation. Surprisingly, the assembled holoenzyme complex synthesizes DNA distributively and with low processivity, unlike most other well-characterized DNA polymerase holoenzyme complexes. We show that PolB1 repeatedly disengages from the DNA template, leaving PCNA123 behind. Interactions with a newly identified C-terminal PCNA interacting (PIP) motif on PolB1 specifically with PCNA2 is required for holoenzyme formation and continuous re-recruitment during synthesis. The extended tail-like structure of the C-terminal PIP motif in PolB1 is revealed alone and when bound to DNA using small angle X-ray scattering (SAXS) allowing us to develop a model for the holoenzyme complex. This is the first detailed kinetic description of clamp loading and holoenzyme assembly in Crenarchaea and has revealed a novel mode for dynamic processivity that occurs by a polymerase exchange mechanism. This work has important implications for processive DNA replication synthesis and also suggests a potential mechanism for polymerase switching to bypass lesions.

[4] The bulk of this chapter is derived from **Bauer, R.J.**, Wolff, I. D., Zuo, X., Lin, H.-K. and Trakselis, M. A. (2013). Assembly and Distributive Action of an Archaeal DNA Polymerase Holoenzyme. *Journal of Molecular Biology "DNA replication and Genomic Instability – Replicaon Theory",* 425, 4820-4836.

3.2 INTRODUCTION

The DNA replication process is complex and multifaceted, involving the interplay of a variety of proteins in order to faithfully duplicate an organism's genome. The process needs to be performed both quickly and with a high degree of specificity such that it is completed accurately within a single cell cycle. DNA polymerases alone are known to synthesize DNA strands somewhat distributively, incorporating a small number of nucleotides into the primer strand before dissociating. As a result, DNA polymerases by themselves are unable to replicate DNA with the necessary speed to complete synthesis of the genome. Therefore, replicative DNA polymerases form holoenzyme complexes with cognate sliding clamp proteins that encircle the DNA template to limit dissociation of the polymerase, and allow for stimulated repeated synthesis or high processivity of replication.

In the bacteria, the sliding clamp (β-clamp) is a homodimeric complex, while in eukaryotes, the proliferating cell nuclear antigen (PCNA) clamp is a homotrimeric complex, but both adopt overall structural and functional homology.[192, 193] In solution, these sliding clamps are typically closed and require the action of an ATP-dependent clamp-loader complex to open and load the clamp onto and around DNA.[194-197] The clamp-loading reaction is a complex multistep kinetic process that has been extensively characterized in bacteriophage T4[198-200], bacteria[194, 201-203], yeast[204-206], and human[207] systems. The core bacterial clamp-loader γ-complex is composed of three copies of the γ subunit (truncated product from *dnaX*) and one of each δ and δ' ($\gamma_3\delta\delta'$). Within the clamp-loader complex, the γ-subunit can be replaced with the τ-subunit, the full length product of *dnaX*, to interact with and retain multiple DNA polymerases at the replication fork.[136] Both γ and τ are members of the AAA^+ family of ATPases that utilize the binding and hydrolysis energy of ATP to coordinate conformational changes within macromolecular complexes.[208, 209] ATP binding to the clamp-loader is sufficient to open the beta clamp,[210, 211] while ATP hydrolysis is required for release of β onto DNA.[212, 213] The energy from hydrolysis imparts conformational changes within the β-clamp to open and close the ring for loading onto DNA as well as recruit the DNA polymerase III (Pol III) to form the holoenzyme. Pol III is known to dissociate from the

DNA template but maintains contact with the τ-subunit in the clamp-loader for repeated loading and synthesis during replication especially on the lagging strand.[136, 214]

In the eukaryotic system, replication factor C (RFC) is comprised of one large (RFC1) and four different small subunits (RFC2-5) which form a heteropentameric clamp-loading complex.[215] The mechanism of loading PCNA and coupled ATP binding and hydrolysis is mostly conserved with that of the bacterial system.[197] Both eukaryotic RFC1-5[216] and the bacterial γ-complex[217] adopt a spiral conformation that is proposed to not only open the clamp but also closely matches the pitch of the DNA duplex allowing for binding of DNA on the interior of the clamp-loader suggesting a mechanism for clamp loading.[218] Upon closure of the PCNA ring, the polymerase can interact with the clamp while RFC dissociates, resulting in the formation of the polymerase holoenzyme. Many proteins (including the DNA polymerase) that interact with PCNA do so through a conserved PIP (PCNA interacting peptide) motif that binds to a hydrophobic pocket on PCNA.[124, 219, 220] Analogous interaction motifs with the *E. coli* and T4 clamps have also been described and are known to act similarly.[221-223]

The archaeal clamp-loaders are more similar to the eukaryotic complexes with one large (RFCL) but four identical small subunits (RFCS) making up the heteropentameric complex. The global structure of the archaeal PCNA complexes are conserved, but organisms in the Euryarchaea phyla have homotrimeric PCNAs while those in the Crenarchaea phyla, including *Sulfolobus solfataricus* (*Sso*), have a heterotrimeric PCNA with three different subunits (PCNA123).[128] Requirements for ATP in the euryarcheaon, *Achaeoglobus fulgidus*, RFC clamp-loading mechanism seems to be conserved with other systems, with ATP binding sufficient for clamp loading and hydrolysis required for release of PCNA and formation of the DNA-PCNA-polymerase holoenzyme complex.[224, 225] Electron microscopy images of the euryarchaeon, *Pyrococcus furiosus*, clamp and clamp-loader system has captured both a closed and open PCNA complex on DNA prior to ATP hydrolysis by RFC.[226, 227] Although the clamp-loading mechanism in Archaea is not as well studied as in other organisms and not at all in the Crenarchaea phyla, it is clear that at least certain aspects of the clamp-loading pathway are conserved in this domain of organisms as well.

Formation of DNA polymerase holoenzyme complexes are evolutionarily conserved in all domains of life and are shown to drastically increase the processivity of DNA polymerases, with

processivity values for the *E. coli* pol III holoenzyme having a lower limit of 50 kilobases.[228] However, the human polymerase (pol δ) holoenzyme has been shown to function distributively and with extremely low processivity.[229] This may be due in part to pol δ acting as the eukaryotic lagging strand replicase, where high processivity is not required for Okazaki fragment extension.[155] Alternatively, it may be that dissociation of RFC after pol δ has securely bound to a loaded PCNA restricts re-recruitment of the polymerase.[207] Conversely in *S. cerevisiae*, the pol δ holoenzyme is shown to be highly processive (>5 kb), despite playing a similar discontinuous role on the lagging strand.[230]

In this work, we detail the assembly of the DNA replication polymerase holoenzyme from the crenarchaeon, *Sulfolobus solfataricus*. Using both activity assays and presteady-state fluorescence, we reveal the preferred pathway for assembly of the holoenzyme. ATP binding to RFC is required for PCNA123 loading, but efficient recruitment of the polymerase (PolB1) requires ATP hydrolysis. We identified a critical C-terminal PIP motif in PolB1 that is essential for maintaining interactions specifically with the PCNA2 subunit. Small-angle X-ray scattering was used to visualize this elusive C-terminal motif not seen in the crystal structure and highlights the binding conformation on the DNA template. Surprisingly, the assembled DNA polymerase holoenzyme is not processive and instead requires the C-terminal PIP motif for continuous recruitment of PolB1 to PCNA2 for distributive and dynamic processivity of synthesis.

3.3 MATERIALS AND METHODS

3.3.1 Materials

Oligonucleotide substrates and primers were purchased from Integrated DNA Technologies (IDT, Coralville, IA) and are listed in **Table 3.1**. [γ-^{32}P]-ATP was purchased from Perkin Elmer (Waltham, MA). Optikinase (Affymetrix, Santa Clara, CA) was used for 5′-end labeling of DNA substrates according to manufacturer's protocols. M13mp18 ssDNA template was purchased from Affymetrix. Radiolabeled primers were added to cold complementary template

strands at a ratio of 1:1.2, heated to 95 °C for 5 min, and cooled to room temperature over at least two hours to ensure proper annealing. All other commercial enzymes were from NEB (Ipswich, MA). Alexa488 and Alexa594-maleimides are from Life Technologies (Grand Island, NY). All other chemicals were analytical grade or better.

Table 3.1: DNA Sequences

DNA Primers	Sequence (5'-3')
PCNA1For	CACCATGTTTAAGATTGTTTACCCTAATGC
PCNA1Rev	CTATAACCTTGGCGCTATCCAAAAGATC
PCNA2For	ATTACATATGATGAAAGCTAAGGTAATTG
PCNA2Rev	ATTACTCGAGGTCTGCCCTTGGTGCAATGTA
PCNA3For	ATTACATATGATATATCTTAAATCTTTTG
PCNA3Rev	ATTACTCGAGTCAAACTTTTGGAGCTAATAAATAAG
RFCSLFor	CAGACATATGAGCACGAAGGTCGAAGAAATAC
RFCSLRev	TAATCTCGAGTCAAGATTTAGATATGGAACTAAGATAC
PCNA1(S191C) OE1	CTAAAGGAACTTTGTATAGATACATCG
PCNA1(S191C) OE2	CGATGTATCTATACAAAGTTCCTTTAG
PCNA2(S92C) OE1	CGTTAATACTATGCTCGAACGAATC
PCNA2(S92C) OE2	GATTCATTCGAGCATAGTATTAACG
PCNA3(S48C) OE1	AAAGTTTAAGCAAGACAGCGTAGAGTTAGTCGCG
PCNA3(S48C) OE2	CGCGACTAACTCTACGCAGTCTTGCTTAAACTTT
PolB1 (S740C) QC1	GAGGTAAAGGAGCTAATGATATGCATAAACTCGCCAAACGATG
PolB1 (S740C) QC2	CATCGTTTGGCGAGTTTATGCATATCATTAGCTCCTTTACCTC
PolB1 (C67S) QC1	GATTATGATGGTAAGAAAGGTAAGGCTGTCGCGAAGCTATTCG ATAAAGAAACTCAAAAG
PolB1 (C67S) QC2	CTTTTGAGTTTCTTTATCGAATAGCTTCGCGACAGCCTTACCTTT CTTACCATCATAATC
PolB1 (D514A) QC1	TGGAATATTCTTTAACATAACTGTTTTAGCTTTTGCATCACTATA TCCTTCAATAATTA
PolB1 (D514A) QC2	TAATTATTGAAGGATATAGTGATGCAAAAGCTAAAACAGTTATGT TAAAGAATATTCCA
PolB1 (D657A) QC1	AACTCTATTATACGGTGATACTGCTTCTTTATTCCTCCTTAATCCTC
PolB1 (D657A) QC2	GAGGATTAAGGAGGAATAAAGAAGCAGTATCACCGTATAATACAG TT
PolB1 (FF873/874AA) QC1	TTTATTGAAGCAATAGGATTAGACAAGGCAGCTGATACTTAAGGA TCCGAATTCGAGCTC
PolB1 (FF873/874AA) QC2	GAGCTCGAATTCGGATCCTTAAGTATCAGCTGCCTTGTCTAATCCT ATTGCTTCAATAAA
PolB1 (F8A) QC1	AGCGGGTTTAGATGAAGGAATATCAGCTAGCGTAAGTTGCTTAGT CATTATGTATATC
PolB1 (F8A) QC2	GATATACATAATGACTAAGCAACTTACGCTAGCTGATATTCCTTCA TCTAAACCCGCT
M13mp18 primer	CCGGAAACCAGGCAAAGCGCCATTCG
31mer template	TATCTTCTATGGCACGCGGCGAGAGCACAGC(A488)

Table 3.1: DNA Sequences Continued

DNA Primers	Sequence (5'-3')
14mer primer	GCTGTGCTCTCGCC
66mer template	CACCTCTCCCTACGCTTCCCACCCACCCCGACCGGCATCTGCTATG GTACGCTGAGCGAGAGTAGC
Hairpin primer/template	TTTTTTTTTTCCCGGGCCGGCGTTTCGCCGGCCCGGG
Cy5 hairpin	(Cy5)TTTTTTTTTTCCCGGGCCGGCGTTTCGCCGGCCCGGG

3.3.2 Cloning and Purification of *Sso* PolB1 Mutants

Exonuclease deficient PolB1 (D231A/D318A) was purified as described previously, indicated as wild-type (polymerase activity), and used in all assays unless stated otherwise.[(78)] PolB1 (D231A/D318A/C67S/S740C) for fluorescent labelling was created using a standard QuickChange protocol (Agilent, Santa Clara, CA) using two sets of QuickChange primers from pET30-PolB1 (D231A/D318A) and KAPA HiFi DNA polymerase (KAPA Biosystems, Woburn, MA). PCNA interacting peptide (PIP) mutants: PolB1 N-ter PIP$^-$ (D231A/D318A/F8A); C-ter PIP$^-$ (D231A/D318A/F873A/F874A); and C-ter PIP$^-$ C740 (D231A/D318A/C67S/S740C/F873A/F874A) as well as catalytically deficient PolB1 (D231A/D318A/D514A/D657A) and catalytically deficient and C-term PIP$^-$ (D231A/D318A/D514A/D657A/F873A/F874A) were created similarly using the QuickChange protocol (**Table 3.2**). DNA sequences were verified by the Genomics and Proteomics Core Laboratories at the University of Pittsburgh. Expression and purification of all mutants were performed identical to wild-type.

Table 3.2: Labels, Mutations, Phenotypes and Binding Affinities of PolB1 Mutants

PolB1	Mutations	Phenotype	K_d (μM)[1]
WT	D231A/D318A	Exonuclease deficient	0.22 ± 0.01
C740	D231A/D318A/ C67S/S740C	Exonuclease deficient Free Cys at 740	N/D[2]
N-ter PIP$^-$	D231A/D318A/ F8A	Exonuclease deficient Candidate N-ter PIP mutation	N/D[2]
C-ter PIP$^-$	D231A/D318A/ F873A/F874A	Exonuclease deficient Candidate C-ter PIP mutation	0.32 ± 0.05
Cat$^-$	D231A/D318A/ D514A/D657A	Exonuclease deficient Polymerase deficient	N/D[2]
Cat$^-$ C-ter PIP$^-$	D231A/D318A/ D514A/D657A/ F873A/F874A	Exonuclease deficient Polymerase deficient Candidate C-ter PIP mutation	N/D[2]
C-ter PIP$^-$ C740	D231A/D318A/ F873A/F874A/ C67S/S740C	Exonuclease deficient Candidate C-ter PIP mutation Free Cys at 740	N/D[2]

[1]Determined from fluorescence anisotropy binding to Cy5 hairpin DNA. [2]N/D – not determined

3.3.3 **Cloning and Purification of RFC**

The operon containing both RFC-small (*Sso*0768) and RFC-large (*Sso*0769) was amplified from genomic *S. solfataricus* P2 DNA and inserted into pET30a using the *NdeI* and *XhoI* restriction sites. BL21(DE3) Rosetta 2 cells containing the pET30a-RFCSL construct were grown at 37 °C, and protein expression was autoinduced as described previously.[(168)] Cell pellets were resuspended in 20 mM HEPES buffer (pH 7.0), 75 mM NaCl, and 5 mM β-mercaptoethanol. The cells were lysed by the addition of lysozyme and sonicated. After centrifugation, the supernatant was heat treated at 70 °C for 20 min and centrifuged again. The supernatant containing the complex of RFC-S and RFC-L was purified using an ATKA Prime FPLC system with HiTrap MonoQ and heparin columns (GE Healthcare, Piscataway, NJ) and elution with a linear gradient to 1 M NaCl. Final cleanup and sizing were performed with a Superdex 200 26/60 column (GE Healthcare) to select for RFC-S and RFC-L in a 4:1 ratio.

3.3.4 Cloning and Purification of PCNA Subunits

PCNA1 (*Sso*0397), PCNA2 (*Sso*1047), and PCNA3 (*Sso*0405) were separately amplified from genomic *S. solfataricus* P2 DNA. Cysteine mutants of each PCNA subunit (PCNA1-S191C; PCNA2-S91C; PCNA3- S48C) required for fluorescent labelling were cloned using a standard overlap extension protocol. PCNA1 was inserted into pDEST-14 using Gateway technology (Invitrogen) according to manufacturer's directions. PCNA2 and PCNA3 were separately cloned into pET30a using *NdeI* and *XhoI*. Expression and purification of individual PCNA subunits proceeded as described above with a 70 °C heat treatment, heparin column, and gel filtration size selection.

Heterotrimeric PCNA123 or combination of individual mutants used for fluorescent labelling were selected using a 6X His-tag included on PCNA1. Equal molar amounts of each PCNA were combined, applied to a Ni^{2+} column (Thermo Fisher, Waltham, MA), and eluted with a step gradient of 500 mM imidazole. Final selection and sizing of the heterotrimeric wild-type or mutant PCNA123 complexes were performed with a Superdex 200 26/60 column. Analytical gel filtration was performed using a Superdex 10/30 column injecting 5 pmol PCNA with vitamin B12 as an internal standard.

3.3.5 Polymerase Reaction Conditions

Standard assays were performed in reaction buffer [20 mM Tris-acetate (pH 7.5), 100 mM potassium acetate, and 10 mM magnesium acetate] containing 18 nM primed M13mp18 DNA (ptDNA) unless otherwise indicated. . Standard reaction conditions included 0.2 μM PolB1, 2 μM PCNA123, 0.4 μM RFC-SL, and 0.2 mM ATP, and were used unless otherwise indicated. Prior to initiation, the reaction components were incubated for 5 minutes at reaction temperature before addition of 0.2 mM dNTPs. Reactions were terminated by the addition of an equal volume of a basic quench (300 mM NaOH, 6 mM EDTA, 18% w/v Ficol 400, 0.15% w/v bromocresol green, and 0.25% w/v xylene cylanol). Products were separated on alkaline 0.8% agarose gels, and dried for 30 minutes under vacuum. Phosphor screens were then exposed to the gels for a minimum of

4 hours, imaged with a Storm 820 Phosphorimager (GE Healthcare), and quantified using ImageQuant version 5.0.

Processivity assays included 3 mg/mL salmon sperm DNA (spDNA) (Invitrogen) as a trap in all reactions added simultaneously with dNTPs to initiate the reaction. To analyze shorter DNA products, reactions were terminated by the addition of an equal volume of a formamide quench (100 mM EDTA, 0.1% SDS, and 79% formamide) and separated using denaturing gels [20% acrylamide, 8 M urea, and TBE buffer (45 mM Tris-borate and 1 mM EDTA)].

Dilution reactions were setup and initiated as described for polymerase reactions. After 15 seconds a 1:8 dilution was performed by adding 210 μL to the initial 30 μL reaction volume diluting only the proteins as indicated in the figure legend, all other reaction components were held at constant concentrations as determined in reaction optimization experiments. Reactions were quenched and imaged as described above. Product length was determined by creating a standard curve of DNA ladder length versus the distance traveled to extrapolate the sizes of the products created for each condition using ImageQuant.

3.3.6 ATPase Experiments

ATPase reactions were incubated at 60 c for five minutes and initiated by addition of ATP. Optimal reaction conditions included reaction buffer, 0.2 mM ATP, 0.2 μM cold 28mer/66mer ptDNA (if present), 0.2 μM RFC, 0.2 mM PolB1 (If present) and 0.2 μM PCNA123 (if present) totaling 30 μL per reaction. Samples were quenched at 15, 30, and 45 min after initiation into equal volumes of 0.7 M formic acid. 0.5 μL of quenched reaction was spotted on Analtech Cellulose PEI-F, allowed to dry, resolved in 0.6 M potassium phosphate (pH 3.5) buffer, phosphorimaged and analyzed as described previously.[(231)]

3.3.7 Protein Fluorescent Labeling

PolB1 and PCNA subunits were labelled at a single accessible cysteine residue as indicated with either Alexa488-maleimide or Alexa 594-maleimide. Proteins were dialyzed into labelling

buffer (50 mM HEPES, pH = 7.2, 100 mM NaCl) before adding dye in a 3-5 fold molar excess. Reactions were allowed to proceed for two hours at room temperature before quenching with 3 mM β-mercaptoethanol (BME). Label proteins were separated from free dye using a 1 mL G-25 column (GE Healthsciences), gel filtration chromatography Superdex-200 (GE Healthsciences), and/or extensive dialysis in labelling buffer. Labelling efficiencies were calculated from a ratio of concentrations (dye:protein) using the extinction coefficients and were determined to be essentially one in all cases.

3.3.8 **Steady-State Fluorescence Spectroscopy**

Steady-state fluorescence spectroscopy was performed using a FluoroMax-3 spectrofluorimeter (HORIBA Jobin Yvon) thermostated to 23 °C. Various PCNA subunits labeled with Alexa 488 at 50 nM were titrated with increasing concentrations of PolB1 as indicated in the figure legends. The excitation wavelength was 485 nm and the emission was monitored from 505 to 650 nm. The slits were adjusted accordingly between 3 and 8 nm to keep the spectrum within range. The quenching at 519 nm normalized to the donor only intensity (ν) was plotted as a function of PolB1 concentration and fit to the following equation:

$$\nu = \frac{\Delta F \times [P]}{K_d + [P]} \tag{3.1}$$

where ΔF is the change in fluorescence amplitude, [P] is the protein concentration, and K_d is the dissociation constant calculated by using KaleidaGraph ver. 3.52 (Synergy Software). Fluorescence anisotropy was used to measure binding to a Cy5 labelled DNA hairpin as described previously and fit to Equation 3.1.[83, 139]

3.3.9 **Presteady-State Fluorescence Spectroscopy**

Stopped-flow fluorescence experiments were performed on an Applied Photophysics (Leatherhead, UK) SX.20MV in fluorescence mode equipped with a temperature controlled water bath chamber at 22, 37, or 60 °C. Individually labelled PCNA subunits, PolB1, or primer template DNA at 0.5-6 μM were mixed as described in the Figure legends. Template DNA (31 mer) was labelled at the 5' end with Alexa 488 by IDT (Coraville, IA). Primers of 14 or 21 bases were complementary to the 5' end of the template and placed the 3'OH at different positions. The samples were excited at 485 nm, and a 590 nm cutoff filter was used to collect 4,000 oversampled data points detecting only Alexa 594 emission. The excitation path length was 3 mm. At least eight traces were averaged for each experiment. The observed averaged traces were fit to one, two, or three exponentials using the supplied software. Kinetic simulations were performed and optimized at each step using KinTekSim (Kintek Corp.) and Berkeley Madonna (University of California, Berkeley) as described previously.*(139, 198, 232)*

3.3.10 **SAXS Experiment and Data Analysis**

Solution small-angle x-ray scattering (SAXS) experiments were performed at beamline 12ID-B of Advanced Photon Sources (APS) at Argonne National Laboratory. The wavelength, λ, of x-ray radiation was set as 0.866 Å. Scattered x-ray intensities were measured using a Pilatus 2M detector (DECTRIS Ltd). The sample-to-detector distance was set as 3.6 m and the detecting range of momentum transfer,

$$q = 4\pi \sin\frac{\theta}{\lambda} \tag{3.2}$$

where 2θ (the scattering angle) at such setting was 0.006-0.53 $Å^{-1}$. To reduce the radiation damage, a flow cell made of a cylindrical quartz capillary with a diameter of 1.5 mm and a wall of 10 μm was used and the exposure time was set to 1 second. In order to obtain good signal-to-noise ratios, twenty images were taken for each sample and buffer. The two-dimensional scattering images were converted to one-dimensional SAXS curves through azimuthally averaging after solid

angle correction and then normalizing with the intensity of the transmitted x-ray beam, using the software package developed at beamline 12ID-B. The radii of gyration, R_g, was determined from the Guinier equation:

$$\ln[I(q)] = \ln[I(q=0)] - \frac{1}{3}q^2 R_g^2 \quad (3.3)$$

Three dimensional molecular envelopes were calculated from SAXS data up to q of 0.52 $Å^{-1}$, using both programs of GASBOR[(233)] and DAMMIN.[(234)] Twenty runs were performed for each calculation. The DAMMIN results were further averaged using program DAMAVER[(235)] and the calculation convergences were excellent for both PolB1 and PolB1/DNA indicated by a score of normalized spatial discrepancy (NSD) less than 0.7. The GASBOR results were not further averaged because the dummy residues in GASBOR result would lose their representations during averaging. Nevertheless, those individual GASBOR results were topologically similar.

3.4 RESULTS

3.4.1 Optimization of *Sso* Holoenzyme Components Necessary for Rapid DNA Synthesis

After purifying PolB1, PCNA123, and RFC to homogeneity, we optimized the solution conditions for maximal replication efficiency. Maximal product formation (both length and amount) occurred when the concentration of RFC used was greater than 0.1 μM **(Figure 3.1, lane 2)** and PCNA123 greater than 0.75 μM **(Figure 3.1, lane 11**). The concentration of ATP (0.2 mM) used was determined systematically from the ATPase data below. All subsequent reactions involving the full replication holoenzyme were performed using 0.2 μM PolB1, 0.4 μM RFC, 2 μM PCNA123, and 0.2 mM ATP unless indicated otherwise.

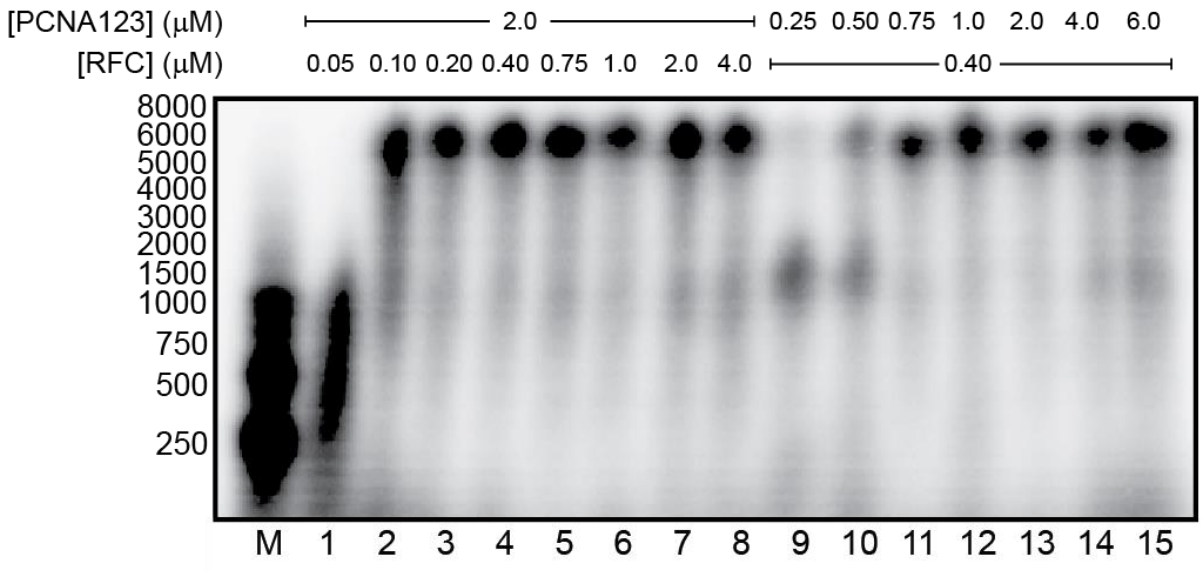

Figure 3.1: Holoenzyme Concentration Optimization
Optimization of PCNA123 and RFC concentrations for efficient product formation by PolB1 (0.2 μM) at 60 °C separated on a 0.8% agarose gel. Lanes 1-8 are titrations of RFC (0.05 μM to 4 μM) with constant 2 μM PCNA123. Lanes 9-15 are titrations of PCNA123 (0.25 μM to 6 μM) with constant 0.4 μM RFC.

After establishing the optimal concentrations for efficient synthesis with the holoenzyme complex, we compared the effect of accessory proteins on the PolB1 extension rate **(Figure 3.2)**. Because PolB1 is known to bind DNA as a monomer or trimer dependent on concentration,[(139)] we used concentrations of 0.2 μM PolB1 to limit contributions of trimer and primarily assess the monomer extension rate. The nucleotide incorporation rate of the polymerase alone at 60 °C is 8.1 ± 0.5 nt sec^{-1}. Addition of either RFC or PCNA123 individually stimulated the rate of extension 2-3 fold. A small amount of full-length product was seen with PCNA123 even in the absence of RFC suggesting that a fraction of PCNA123 can load independently. The rate and product formation was maximally stimulated upon inclusion of both PCNA123 and RFC to form of the complete holoenzyme to 66 ± 8 nt sec^{-1}, ~8-fold higher than the rate of the polymerase alone.

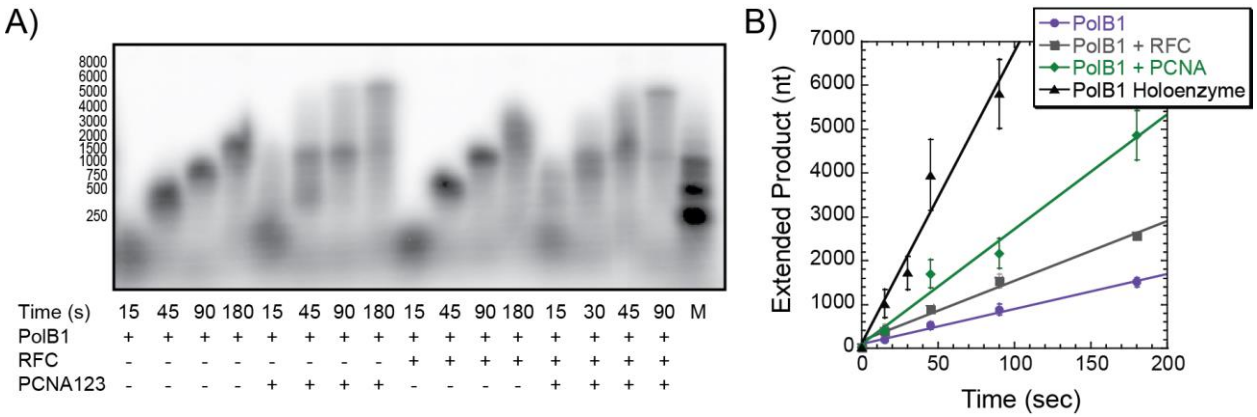

Figure 3.2: Polymerase Extension Rates

A) Time course of optimized PolB1, +/- PCNA123, +/-RFC concentrations replicating primed M13 at 60 °C separated on an alkaline agarose gel. B) Quantification of rates for PolB1 alone (-●-) (8.1 ± 0.5 nt•sec^{-1}), PolB1/PCNA123 (-■-) (26 ± 2 nt•sec^{-1}), PolB1/RFC (-♦-) (14 ± 1 nt•sec^{-1}), and PolB1 Holoenzyme (-▲-) (66 ± 8 nt•sec^{-1}).

Clamp loader proteins are members of the AAA^{+} family of ATPases and have the intrinsic ability to hydrolyze ATP to load clamps onto DNA. Similar to other archaeal clamp loader complexes, [225, 236] the *Sso*RFC complex contains four small subunits and one large subunit as isolated by gel filtration chromatography. We investigated the ATPase activity of RFC in the presence of DNA polymerase holoenzyme components.

Table 3.3: RFC ATPase Rate during Holoenzyme Assembly

Sso Holoenzyme Proteins	Rate (pmol min^{-1})[1]
RFC	8.6 ± 0.9
RFC/DNA	23.6 ± 3.0
RFC/PolB1	8.2 ± 0.4
RFC/PCNA123	12.4 ± 1.2
RFC/DNA/PolB1	28.3 ± 0.4
RFC/DNA/PCNA123	30.2 ± 1.0
RFC/PCNA123/PolB1	7.6 ± 0.1
RFC/DNA/PCNA123/PolB1	28.2 ± 0.8

Individual PCNA Subunits	Rate (pmol min^{-1})[1]
RFC + PCNA1	6.2 ± 0.8
RFC + PCNA2	3.7 ± 0.4
RFC + PCNA3	6.6 ± 0.9

[1] Calculated from a linear fit of ATPase data during a time course.

We first measured the ATP hydrolysis rate of RFC alone (0.2 μM) with increasing concentrations of ATP. The K_m was determined to be 14 ± 6 μM with a V_{max} of 43 ± 3 pmol•min^{-1}•μM^{-1} at 60 °C. We then examined the ATPase activity of RFC in the presence of other holoenzyme components **(Table 3.3** and **Figure 3.3)**. Stimulation in the overall ATP hydrolysis rate was observed upon addition of PCNA123 (12.4 ± 1.2 pmol•min^{-1}) and DNA (23.6 ± 3.0 pmol•min^{-1}) over that of RFC alone (8.6 ± 0.9 pmol•min^{-1}). RFC is maximally stimulated with both PCNA123 and DNA are included (30.2 ± 1.0 pmol•min^{-1}). No significant change in RFC's ATP hydrolysis is noted when only PolB1 is added.

Additional experiments were performed examining the effect of the individual subunits of PCNA (1, 2, or 3) on the ATP hydrolysis rate of RFC or extension products from primed M13. Gel filtration chromatography shows that PCNA1 forms a homotrimer, while PCNA2 is primarily monomer **(Figure 3.4)**.

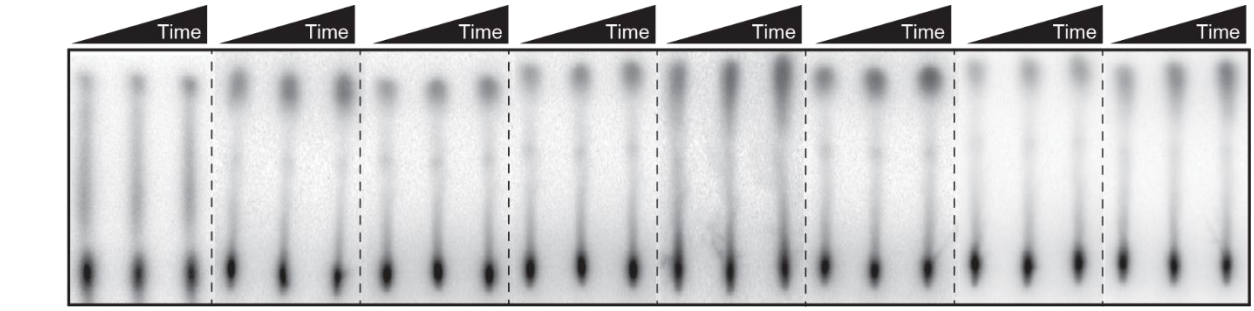

Figure 3.3: RFC ATPase Reaction TLC Plates
Hydrolysis of α-P^{32}-ATP by RFC (0.2 μM) at 15, 30 and 45 minutes separated on PEI-cellulose TLC plates as described in **Materials and Methods**. Shown are examples of an individual reaction for each condition as the replication holoenzyme is formed. Reactions include PolB1 (0.2 μM), PCNA123 (0.2 μM), and DNA (0.2 μM) if indicated. All reactions were performed at 60 °C. Dashed lines indicated separate TLC plates.

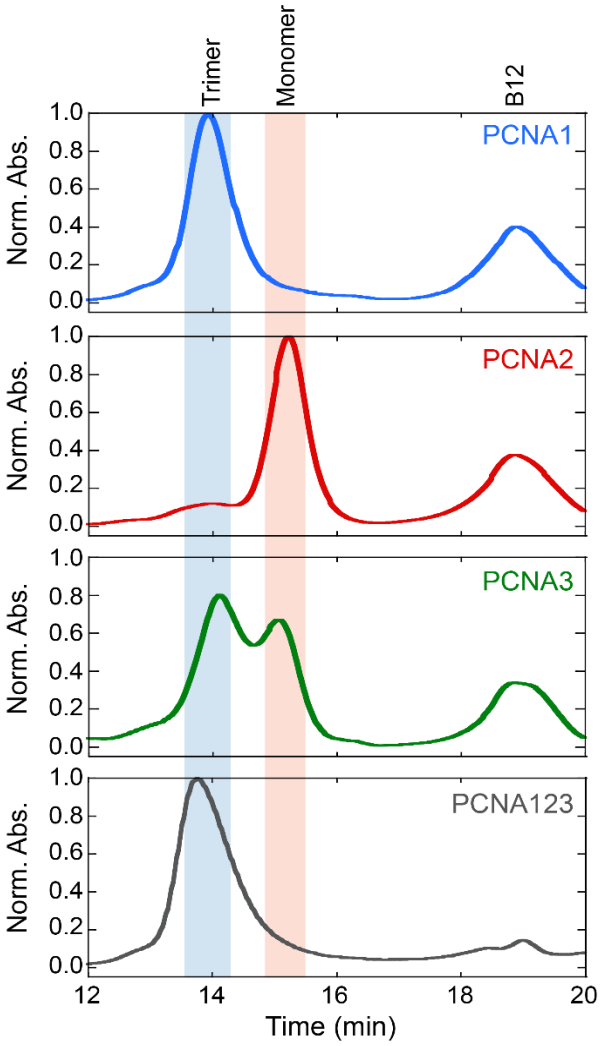

Figure 3.4: Analytical Gel Filtration on PCNA Gel filtration profile of 50 μM PCNA1, PCNA2, PCNA3, and PCNA123. Relative positions of monomer (shaded red) and trimer (shaded blue) are indicated by rectangular regions. Vitamin B12 was used as an internal standard in all experiments to account for drift in the elution profile.

PCNA3 is a mix between monomer and trimer suggesting a weaker equilibrium for the trimer. It noteworthy that unlike PCNA123, all three of the individual subunits resulted in a decrease in the rate of RFC's ATP hydrolysis **(Table 3.3)**, perhaps due to the formation of nonproductive complexes or to inhibit loading of alternative oligomeric forms of the clamp. Extension experiments showed a small but significant increase in product length when either PCNA2 or PCNA3 were used, but significantly smaller than with the entire PCNA123 heterotrimeric complex was included **(Figure 3.5)**.

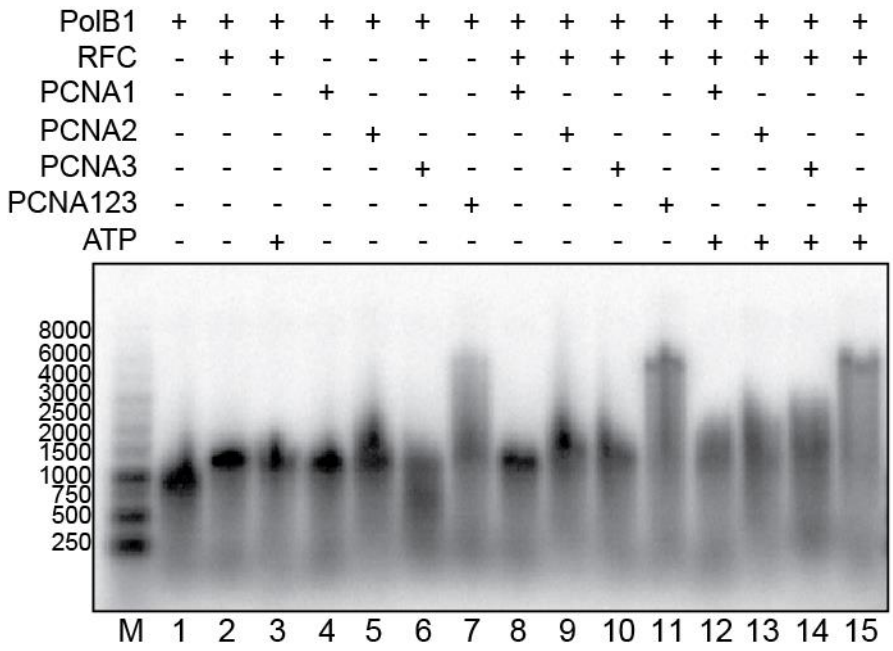

Figure 3.5: PCNA123 Assembly and Holoenzyme Efficacy
Effect of individual subunits of PCNA on formation of the PolB1 (0.2 μM) replication holoenzyme. The concentration of each PCNA subunit was 2 μM, RFC was 0.4 μM, and ATP was 0.2 mM as indicated. All reactions were performed at 60 °C and quenched after 4 minutes.

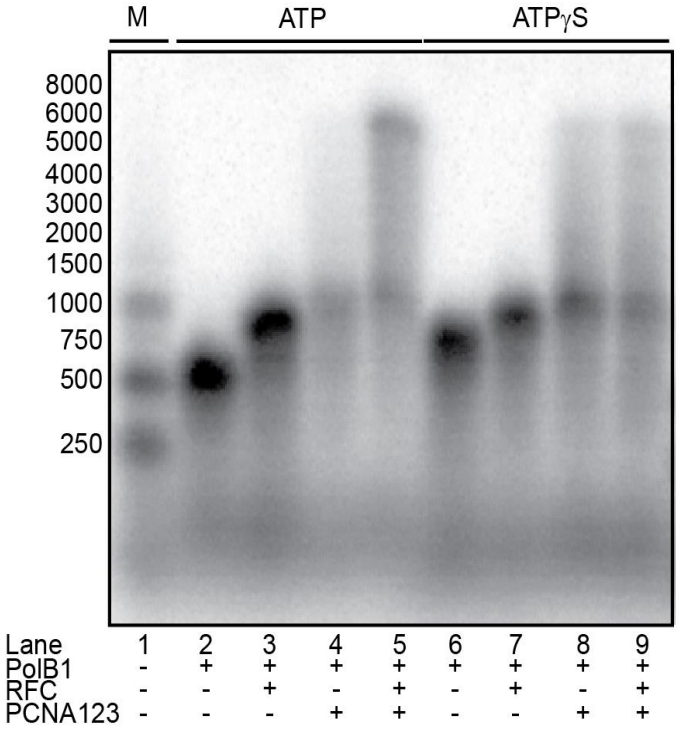

Figure 3.6: ATP and Holoenzyme Formation
Requirements for ATP hydrolysis on formation and kinetics of the *Sso* PolB1 holoenzyme. The concentrations of holoenzyme components were: PolB1 (0.2 μM), PCNA (2 μM), RFC (0.4 μM), and ATP/ATPγS (0.2 mM). Reactions were at 60 °C for 2 minutes before quenching.

Inclusion of ATPγS instead of ATP with the holoenzyme gives long but less abundant products similar to when PCNA123 is included in the absence of RFC **(Figure 3.6)**. These experiments confirm that ATP hydrolysis is needed for efficient holoenzyme formation and function. The less abundant longer products with either PCNA123 alone or RFC/ATPγS suggest that small amounts of PCNA123 can assemble on DNA and interact with PolB1 inefficiently in the absence of RFC or its associated ATPase activity.

3.4.2 The *Sso* DNA Polymerase Holoenzyme Has Low Processivity of Nucleotide Incorporation

Despite the increase in kinetic rate associated with formation of the PolB1 holoenzyme, it has limited processivity of nucleotide incorporation. Processivity is defined as the probability of a polymerase incorporating another nucleotide or dissociating from the template.[237] When salmon sperm DNA trap (spDNA) is added simultaneously with dNTPs to initiate the reaction, any polymerase that dissociates will bind the unlabeled trap, no longer contributing to the reaction. spDNA consists of sheared DNA (~ 2000 bp) with blunt, 3' and 5' overhangs and will readily bind polymerases that have dissociated from the ^{32}P labelled template.[78] In these processivity reactions, there is a slight increase in product length with increasing temperature **(Figure 3.7 A, even lanes)**, but no significant products greater than 200 bases are noted. This observed increase in product length is most likely associated with a faster rate of catalysis compared with a similar off-rate from DNA as described previously.[139]

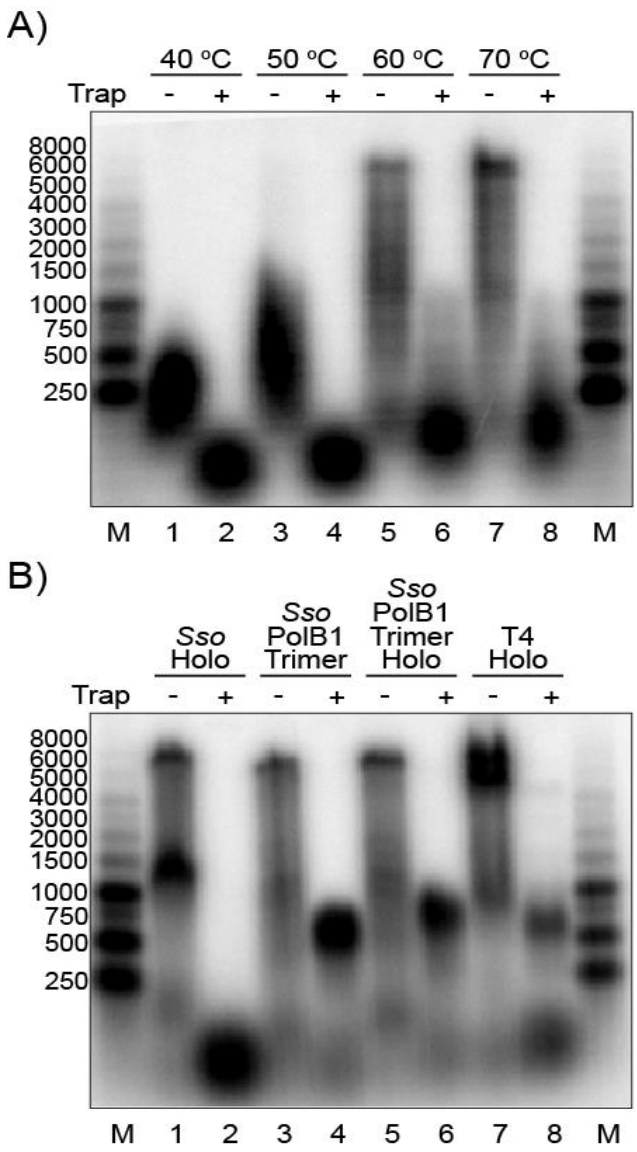

Figure 3.7: Comparison of Processivity and Replication Products

A) Effect of temperature on both replication activity and processivity of the *Sso* replication holoenzyme (0.2 μM PolB1, 0.4 μM RFC, and 2 μM PCNA123) on a primed M13mp18 template, and separated on a 0.8% agarose gel. Odd numbered lanes in the absence of trap monitor the replication rate and were quenched after reacting for 2 minutes. Even numbered lanes include spDNA trap to monitor processivity were quenched after 6 minutes. B) Comparison of replication and processivity for the *Sso* holoenzyme including 0.2 μM PolB1 (*Sso* Holo), 2 μM PolB1 only (*Sso* PolB1 Trimer), *Sso* holoenzyme including 2 μM PolB1 (*Sso* PolB1 Trimer Holo), and the T4 replication holoenzyme (T4 Holo; 0.24 μM gp43, 0.24 μM gp45, 0.24 μM gp44/62). All *Sso* reactions were performed at 60 °C, T4 reactions were performed at 37 °C. Processivity reactions were quenched after 6 minutes; *Sso* replication assays were quenched after 2 minutes; and T4 replication was quenched after 1 minute.

Examination of the shorter products from the processivity reactions were also analyzed using a denaturing acrylamide gel for better separation **(Figure 3.8, lanes 1-5)**. PolB1 alone has a maximal processivity of 25-30 bases consistent with previous results.[78] Addition of PCNA123 increases the processivity but with minimal longer products highlighting the need for RFC in formation of the holoenzyme. Inclusion of both PCNA123 and RFC has the greatest effect on the amount of longer products. We then compared the processivity of the monomeric PolB1 holoenzyme with other polymerase systems including trimeric PolB1[78] and the well characterized T4 DNA polymerase holoenzyme **(Figure 3.7 B)**. The PolB1 trimer with or without accessory factors (PCNA123 and RFC) has a processivity of ~1000 bases consistent with previous results.[78,

[139] The T4 DNA polymerase holoenzyme also produced the majority of products around 1000 bases with a smear of longer products up to the length of the M13 template verifying its high processivity.[238] Therefore, it seems that the *Sso* DNA polymerase holoenzyme acts more distributively than other replication systems including the homotrimer of PolB1.

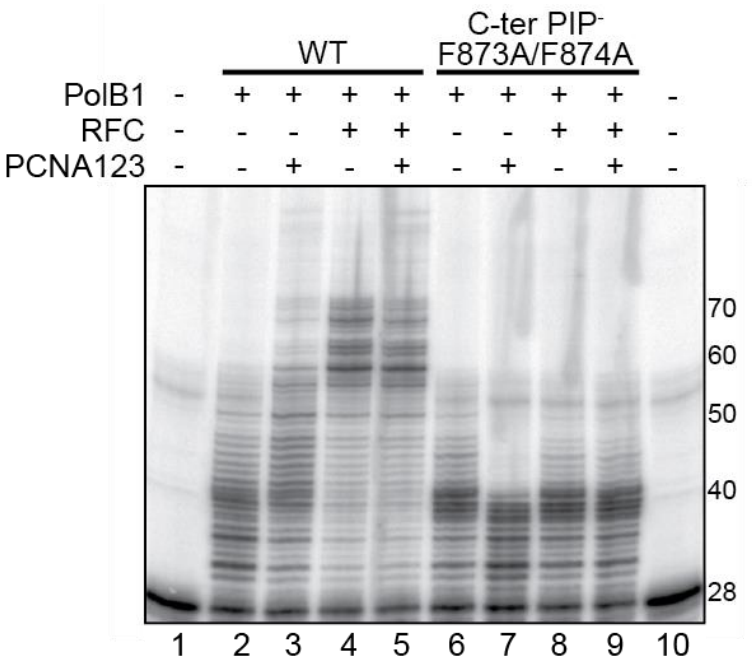

Figure 3.8: Holoenzyme Processivity
Processivity of PolB1 WT (Lanes 2-5) and C-ter PIP- (F873A/F874A) (Lanes 6-9) monitored as the replication holoenzyme is assembled. Reactions were performed at 60 °C, initiated with dNTPs and 3 mg/mL spDNA, quenched after 6 minutes and separated on a 20% acrylamide gel.

When using spDNA as a trap, any dissociated holoenzyme components will be bound preventing further interactions with the ^{32}P-labeled substrate. In order to determine the individual contributions to processivity for each of the holoenzyme components, we instead performed dilution experiments **(Figure 3.9)**. 8-fold dilution of the entire *Sso* holoenzyme (PolB1, RFC, and PCNA123) after 15 seconds resulted in a severe reduction in DNA length similar to that seen with the spDNA trap above. Dilution of RFC and PCNA123 reduced the total overall products but only slightly reduced the absolute length of the product distributions. Instead, dilution of both PCNA123 and PolB1 had the most significant effect on product length, similar to the result when the entire holoenzyme is diluted. Dilution of RFC and PolB1 had a modest effect reducing the total amount of product as well as shifting the distribution peak towards smaller lengths. In all, dilution of the *Sso* holoenzyme verifies that this complex has limited processivity, and that PCNA123 and PolB1 have the most significant role in maintaining repeated DNA synthesis.

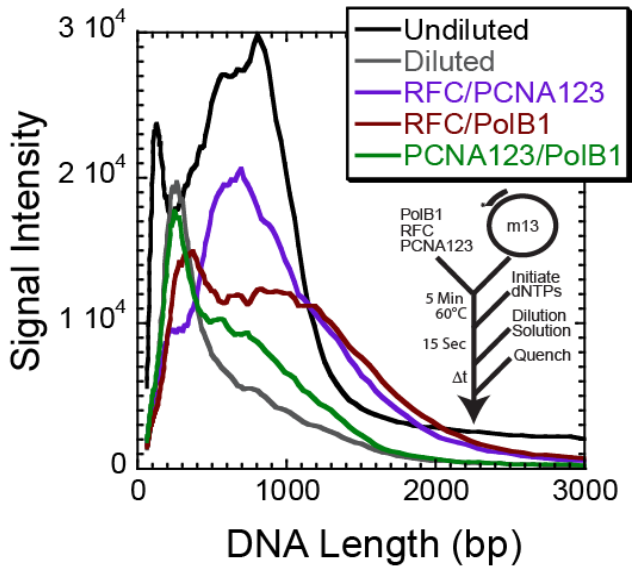

Figure 3.9: Holoenzyme Dilution
Sso DNA polymerase holoenzyme dilution experiments were performed as outlined in the reaction scheme and described in **Materials and Methods**. Either the entire holoenzyme (grey), RFC/PCNA123 (purple), RFC/PolB1 (brown), or PCNA123/PolB1 (green) were diluted 8-fold and the intensity as a function product length was quantified and compared to an undiluted reaction (black).

3.4.3 **Monitoring Assembly of the *Sso* DNA Polymerase Holoenzyme by Presteady-State FRET**

In order to understand the individual steps for loading and assembly of the *Sso* holoenzyme on DNA, we utilized presteady-state stopped-flow fluorescence resonance energy transfer (FRET) experiments. Individual subunits of PCNA (1, 2, or 3) or PolB1 were mutated to contain single solvent accessible cysteines for labeling with donor (Alexa 488) or acceptor maleimide dyes (Alexa 594). Individual PCNA subunits have no native cysteines and allowed us to mutate them at specific sites (PCNA1-S191C; PCNA2-S92C; PCNA3-S48C) for optimal dye placement.

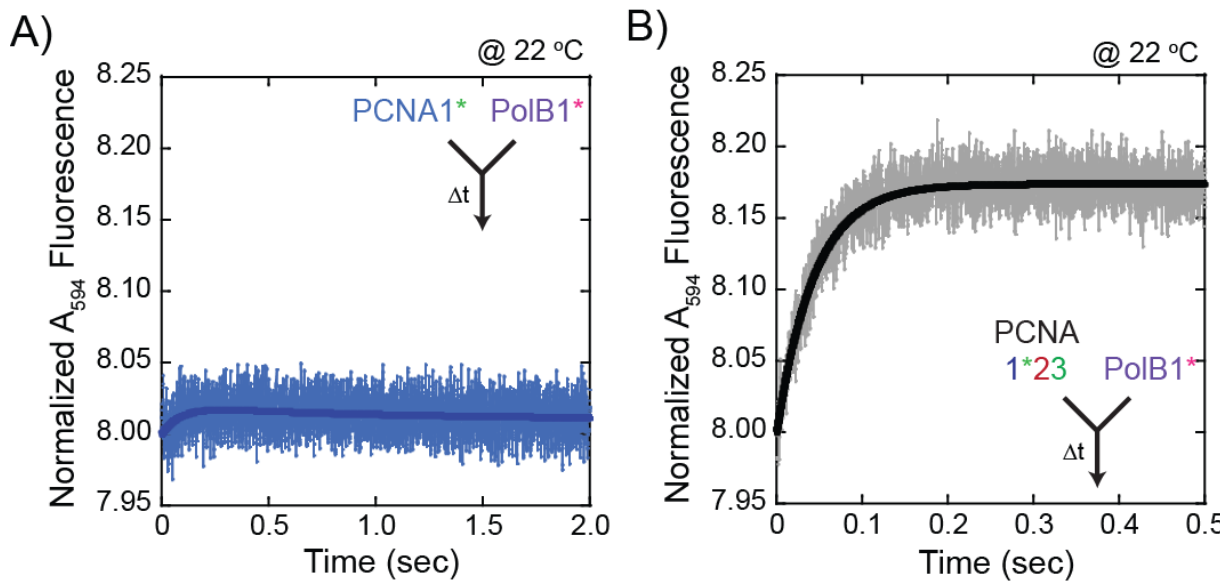

Figure 3.10: PCNA PolB1 Presteady-State FRET
Presteady-state stopped-flow FRET traces and exponential fits showing PCNA binding specificity for PolB1 at room temperature. A) $PCNA1^{488}$ (3 μM) versus $PolB1^{594}$ (3 μM) were fit to a double exponential with rates of k_1 = 12.8 ± 2.2 and 0.98 ± 0.18 sec^{-1}. B) $PCNA1^{488}23$ (3 μM) versus $PolB1^{594}$ (3 μM) was fit to a single exponential rate of k_1 = 22.9 ± 1.4 sec^{-1}. Asterisks note the labeled subunit (green – $Alexa_{488}$; pink – $Alexa_{594}$). Fluorescence traces were normalized to 8.0 for a more direct comparison.

PolB1 has a single solvent accessible cysteine residue that was mutated to serine (C61S) in favor of moving the labelling position (S740C) closer to the C-terminus. All mutated and labeled proteins showed appropriate gel filtration profiles and near wild-type activities (data not shown). DNA was labeled at the 3' end of the template strand and annealed to a primer with lengths of 14 or 21 bases. Holoenzyme formation was limited with the shorter primer-template (14/31mer); so, all further experiments were performed with the longer primer-template (21/31mer).

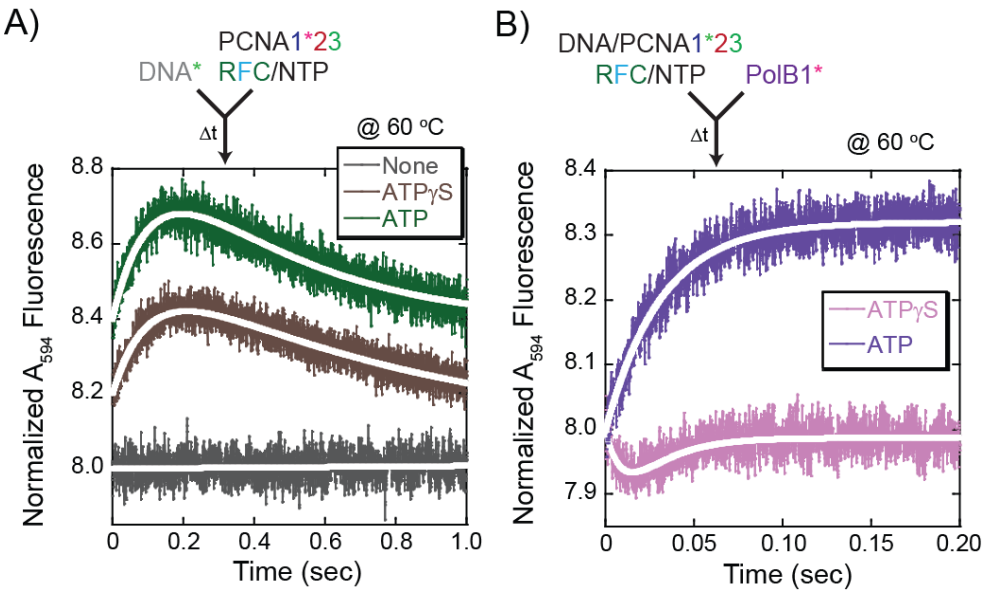

Figure 3.11: PCNA RFC PolB1 with DNA Presteady-State FRET
Presteady-state stopped-flow FRET traces and exponential fits following assembly of the *Sso* DNA polymerase holoenzyme. A) RFC (3 μM) dependent PCNA123 (3 μM) loading onto DNA (3 μM) in the absence (grey) and presence of 1 mM ATP (green) or ATPγS (brown) at 60 °C. Loading efficiency is stimulated with either ATP or ATPγS and fitting of the data to a double exponential (white) gives k_1 = 9.1 ± 1.0 and k_2 = 2.4 ± 0.7 and k_1 = 10.1 ± 1.1 and k_2 = 1.2 ± 0.6 sec^{-1} respectively. Fluorescence traces were normalized to 8.0 (none), 8.2 (ATPγS) and 8.4 (ATP) for a more direct comparison. B) Assembly of PolB1 (3 μM) onto a preloaded PCNA123/DNA/RFC (3 μM) complex to form the holoenzyme and its dependence on ATP (purple) or ATPγS (pink). With ATPγS, the data fits to a double exponential with rates of k_1 = 100 ± 40 and k_2 = 49 ± 10 sec^{-1}. With ATP, the data fits with rates of k_1 = 468 ± 15 and k_2 = 20 ± 1 sec^{-1}. Asterisks note the labeled subunit (green – $Alexa_{488}$; pink – $Alexa_{594}$). Fluorescence traces were normalized to 8.0 for a more direct comparison.

PolB1 was previously shown to interact primarily with PCNA2 and not PCNA1.[(128)] Stopped-flow FRET experiments were used to verify the specificity of PolB1 with individual PCNA subunits or the heterotrimer. When donor and acceptor labelled $PCNA1^{488}$ and $PolB1^{594}$, respectively, were rapidly mixed, little fluorescence change was noted verifying no significant interaction **(Figure 3.10 A)**. However, when donor-labelled $PCNA1^{488}$ was included within the $PCNA1^{488}23$ heterotrimer, an interaction with PolB1 was observed with a single exponential increase in acceptor fluorescence **(Figure 3.10 B)**. Changing the concentration of enzymes by half or 2-fold did not significantly affect the observed rate but did increase the fluorescence intensity indicating that we are monitoring a first-order conformational step after association. All further

experiments utilized a PCNA1^{488}23 labeled heterotrimeric clamp to minimize contributions of PCNA2 or PCNA3 binding to PolB1 individually.

Next, we investigated the requirements for PCNA123 loading onto DNA at 60 ˚C. No significant signal was noted for DNA^{488} (3 μM) versus PCNA1^{594}23 (3 μM) alone (data not shown)**.** When RFC was included in the absence of nucleotide, again no significant interaction between DNA^{488} and PCNA1^{594}23 and was noted (**Figure 3.11 A**). Instead, when either ATP or ATPγS (1 mM) was included with RFC, there was a similar and significant change in fluorescence corresponding to two exponentials and associated with clamp loading. Observed rates were similar for ATPγS (k_1 = 10.1 ± 1.1 sec^{-1} and k_2 = 1.2 ± 0.6 sec^{-1}) or ATP (k_1 = 9.1 ± 1.0 sec^{-1} and k_2 = 2.4 ± 0.7 sec^{-1}). Doubling the concentration of enzyme (6 μM) did not change the observed rates but did increase the fluorescence intensity slightly (data not shown) suggesting that PCNA123 was quantitatively converted to a new conformational state on DNA and confirming that both observed steps are first-order. The similarity in the fluorescent signals (both rate and intensity) indicate that ATP binding and not hydrolysis is required for clamp loading.

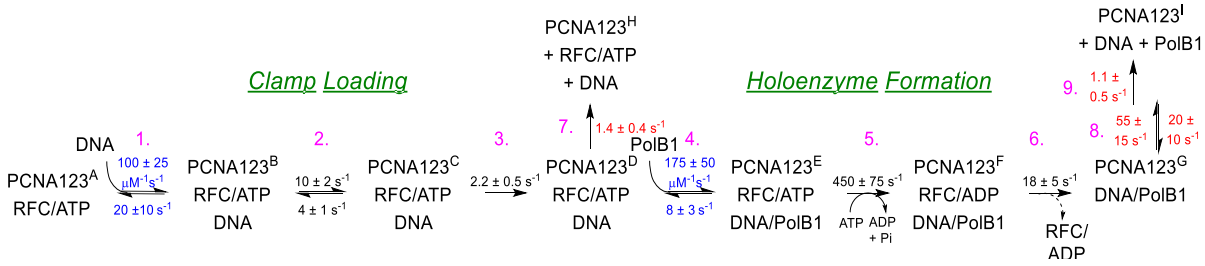

Figure 3.12: *Sso*Holoenzyme Assembly Pathway
Shows the minimal kinetic assembly pathway for formation of the *Sso* DNA polymerase holoenzyme. Observed rates from the presteady-state experiments were individually and globally simulated as described in **Materials and Methods**. Bimolecular rate constants (blue) were fit and then simulated from the fits to amplitude change in intensity when stopped flow experiments were performed at difference concentrations. Disassembly of complexes and associated rates are in red. Superscripts designate individual complexes and numbers represent individual kinetic steps.

Conformational states A-D and I were successfully fit using the Scheme in **Figure 3.12**. Since the initial binding event was not observed by fluorescence, step 1 was added to the mechanism. A second order fit of the observed amplitudes in the stopped flow FRET experiments as a function of concentration estimated the K_d for PCNA123/RFC/ATP to DNA of ~0.25 μM which is similar to current or previously determined values. The individual forward and reverse rate constants were then simulated in step 1 **(Figure 3.12)**. The off-rates of the PCNA1^{594}23 from DNA^{488} in the absence and presence of RFC/ATP was measured directly by rapidly mixing with 0.5 mg/ml spDNA trap **(Figure 3.13 A)**. The observed off-rate was 20-fold greater when RFC/ATP was absent (28 ± 3 sec^{-1}) than when it was present (1.5 ± 0.1 sec^{-1}) suggesting more productive and stable clamp loading in the presence of RFC/ATP **(Figure 3.13 B-C)**.

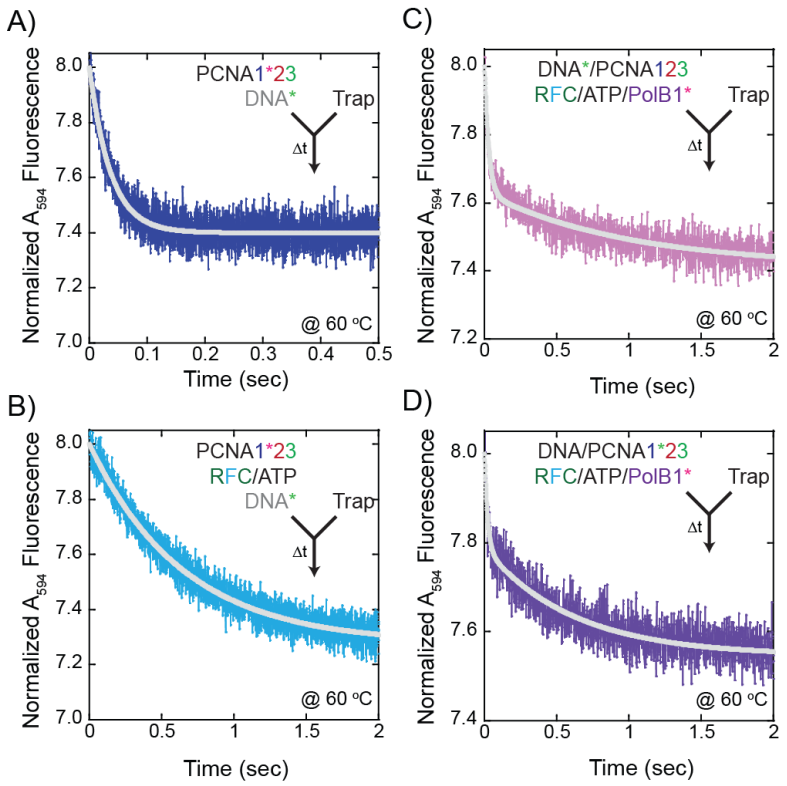

Figure 3.13: Holoenzyme Off Rates

Presteady-state stopped-flow FRET traces and exponential fits monitoring off-rates of proteins within the *Sso* DNA polymerase holoenzyme from DNA. A) PCNA1^{594}23 (3 μM) from DNA^{488} (3 μM) (blue) had an observed single exponential decrease of 28 ± 3 sec^{-1}. B) PCNA1^{594}23/RFC/ATP (3 μM) from DNA^{488} (3 μM) had an observed exponential decrease of 1.5 ± 0.1 sec^{-1}. Dissociation of the PolB1 holoenzyme (3 μM) was monitored from two different positions and fit best to two exponential decays. C) Holoenzyme labelled at DNA$_{488}$/PolB1^{594} had exponential decreases of 49 ± 4 sec^{-1} and 1.6 ± 0.1 sec^{-1}. D) Holoenzyme labelled at PCNA1^{488}23/PolB1^{594} had exponential decreases of 35 ± 2 sec^{-1} and 1.0 ± 0.1. All protein and DNA concentrations were 3 μM, trap concentration was 0.5 mg/mL, and experiments were performed at 60 °C. Asterisks note the labeled subunit (green – Alexa$_{488}$; pink – Alexa$_{594}$). Fluorescence traces were normalized to 8.0 for a more direct comparison.

The simulated first-order rate constants for steps 2, 3, and 7 were also close to the observed rates in all cases but were varied systematically to determine the experimental error for these steps in the mechanism **(Figure 3.12)**. Inclusion of a reverse rate constant at step 2 was beneficial but at step 3 decreased the quality of the simulation.

Finally, we monitored the association of PolB1^{594} to a preloaded DNA/PCNA1^{488}23/RFC complex at 60 ˚C **(Figure 3.11 B)**. Here ATP and not ATPγS is required for the association of PolB1. With ATPγS, there is a small change in the fluorescence that does not seem to correlate with productive polymerase association. Instead when ATP is utilized, there is a faster more significant change in fluorescence with observed first order rates of 468 ± 15 and 20 ± 1 sec^{-1}. Doubling the PolB1^{594} concentration did not change the observed rates significantly but did increase the fluorescence intensity (data not shown). Therefore, the absolute requirement for ATP hydrolysis occurs after the bimolecular PolB1 association (step 4 not observed). We propose that ATP hydrolysis by RFC is required for either chaperoning PolB1 with PCNA123 to form the holoenzyme, associated with a conformational change allowing RFC to dissociate and PolB1 to bind, or clamp closing.

We simulated the observed rate constants for each step associated with PolB1 recruitment, binding, and dissociation (Steps 4, 5, 6, 8 and 9 in **Figure 3.12**). A K_d of ~50 nM was estimated from a second order plot of the amplitude as a function of concentration and is similar to those seen for DNA binding previously and PCNA123 interactions described below. The off-rates for the holoenzyme from DNA were tested using labels detecting FRET between PolB1 and either PCNA123 or DNA **(Figure 3.13 C and 3.13 D)**. In both cases, the data fit to two exponentials with similar values of 49 ± 4 sec^{-1} and 1.6 ± 0.1 or 35 ± 2 sec^{-1} and 1.0 ± 0.1 sec^{-1}, respectively. Interestingly, dissociation of the holoenzyme (Steps 8 and 9 in **Figure 3.12**) proceeds through two steps for separation of PCNA123 and PolB1 from each other and DNA. Because of the similar rates when both PCNA123 and DNA are labelled as the donor, the first step is most likely a rearrangement of the holoenzyme complex on DNA before complete dissociation in the second step. The individual rate constants were systematically varied to determine the experimental error associated with the goodness of fit and in most cases were similar to the observed rated constants measured directly from stopped-flow FRET. Inclusion of a reverse rate constant at either steps 5 or 6 decreased the quality of the simulation, but was tolerated at step 8.

3.4.4 **Identification of a C-terminal PIP Motif in *Sso*PolB1 That is Required to Maintain the Holoenzyme During Synthesis.**

Previously, a region at the N-terminus of PolB1 (4 QLTLFDI) was suggested as a candidate PCNA interacting peptide (PIP) motif.[(128)] As most other candidate PIP motifs in DNA polymerases are instead located at the C-terminus, we searched for and identified a second candidate PIP motif at the C-terminus of PolB1 (867 TMSIDSFF). To test the functional interaction between PCNA123 and the two candidate PIP mutants of PolB1, we performed both kinetic and processivity assays. Binding to DNA measured by fluorescence anisotropy was not significantly different for the C-term PIP$^-$ mutant compared to wild-type PolB1 (**Table 3.2**). Surprisingly, mutation of the N-terminal (F8A) or C-terminal (F873A/F874A) PIP site resulted in a slight decrease in polymerase rate compared to wild-type (**Figure 3.14 A**). More interestingly, inclusion of RFC/PCNA123 with PolB1 N-term PIP$^-$ (F8A) stimulated the replication rate, while with PolB1 (C-term PIP$^-$), there was no stimulation. Processivity experiments also showed no enhancement when RFC/PCNA123 was included with PolB1 (C-term PIP$^-$) compared to wild-type (**Figure 3.8**). These results verify that mutation of the C-term PIP site and not the candidate N-term PIP site in PolB1 abrogates the interaction with PCNA2 and eliminates any stimulation in the extension rate or processivity.

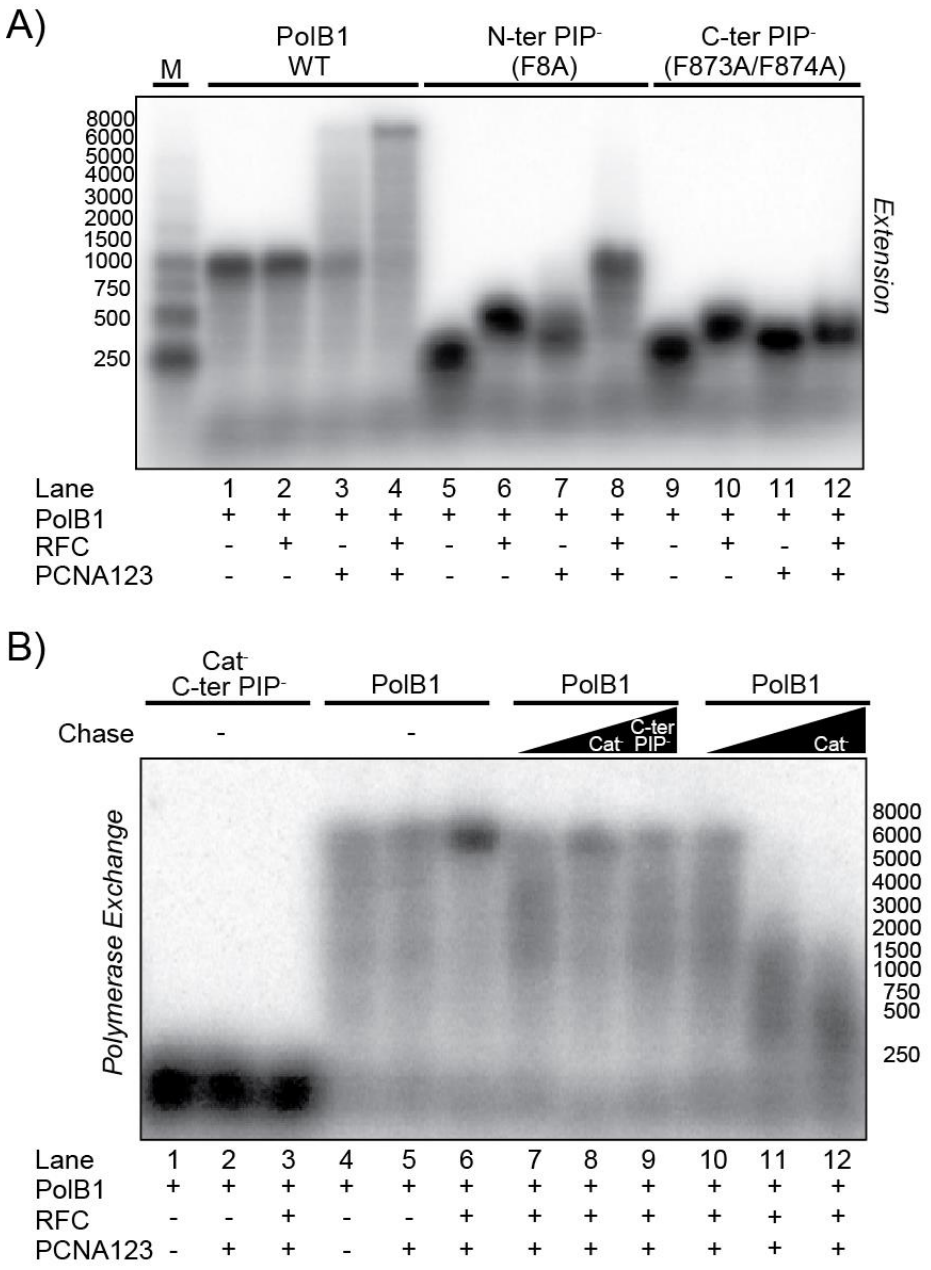

Figure 3.14: PolB1 PIP- Mutants

Effect of PIP mutants on PolB1 replication kinetics and exchange during synthesis. A) Comparison of the effects of formation of the PolB1 replication holoenzyme with the two potential PIP mutants (N-ter - F8A and C-ter - F873A/F874A) on replication extension. Reaction conditions were 0.2 μM PolB1 or mutants, 0.4 μM RFC, 2 μM PCNA123, 0.2 mM ATP were also included as indicated. All reactions were performed at 60 °C, quenched after 2 minutes and separated on a 0.8% agarose gel. B) Polymerase chase experiment showing the importance of the C-ter PolB1 PIP interaction with PCNA2 in maintaining efficient synthesis. Experiments were preincubated with PolB1 and primed M13 template for five minutes at 60 °C before addition of dNTPs and or

various concentrations of a polymerase chase. Experiments were quenched after 4 minutes. Catalytically deficient (Cat^-) or catalytically deficient and C-terminal PIP deficient PolB1 (Cat^- C-ter PIP^-) were added as a chase at concentrations from 0.2 to 1 μM. Lane 1-3 show the disruption of polymerase activity for the Cat^- C-ter PIP^- PolB1 mutant. Lanes 4-6 show wild-type extension reactions for PolB1. Lanes 7-9 show near wild-type extension when Cat^- C-ter PIP^- PolB1 was added as the chase. Lanes 10-12 show a shutdown in extension with increasing concentration of Cat^- PolB1.

Steady-state and presteady-state experiments were used to determine the importance of the C-terminal PIP motif of PolB1 for binding PCNA123. Titration of either PolB1 wild-type or C-term PIP^- (F873A/F874A) labelled with Alexa594 into 50 nM PCNA1, PCNA2, or PCNA3 labelled with Alexa 488 show donor quenching consistent with FRET that could be fit to Equation 3.1. (**Figure 3.15 A-C**). Wild-type PolB1 show the tightest interaction with PCNA2 (0.13 ± 0.01 μM) followed by PCNA3 (0.28 ± 0.01 μM) with little affinity for PCNA1 (1.0 ± 0.1 μM). On the other hand, PolB1 (C-term PIP^-) showed similar binding to PCNA1 (1.0 ± 0.1 μM) (**Figure 3.15 A**) and PCNA3 (0.25 ± 0.01 μM) (**Figure 3.15 C**), but had significantly reduced affinity for PCNA2 (0.96 ± 0.01 μM) (**Figure 3.15 B**) compared to wild-type. Stopped flow FRET experiments using the same labelled proteins showed similar trends with little difference in observed first-order rates between wild-type PolB1 and PolB1 (C-term PIP^-) for PCNA1 or PCNA3 (**Figure 3.15 D&F**). Conversely, experiments with PolB1 (C-term PIP^-) and PCNA2 eliminated the first fast exponential step leaving only a single observed rate similar in magnitude to the second exponential with wild-type PolB1/PCNA2 (**Figure 3.15 E**) or that seen with PCNA123 above (**Figure 3.11 B**).

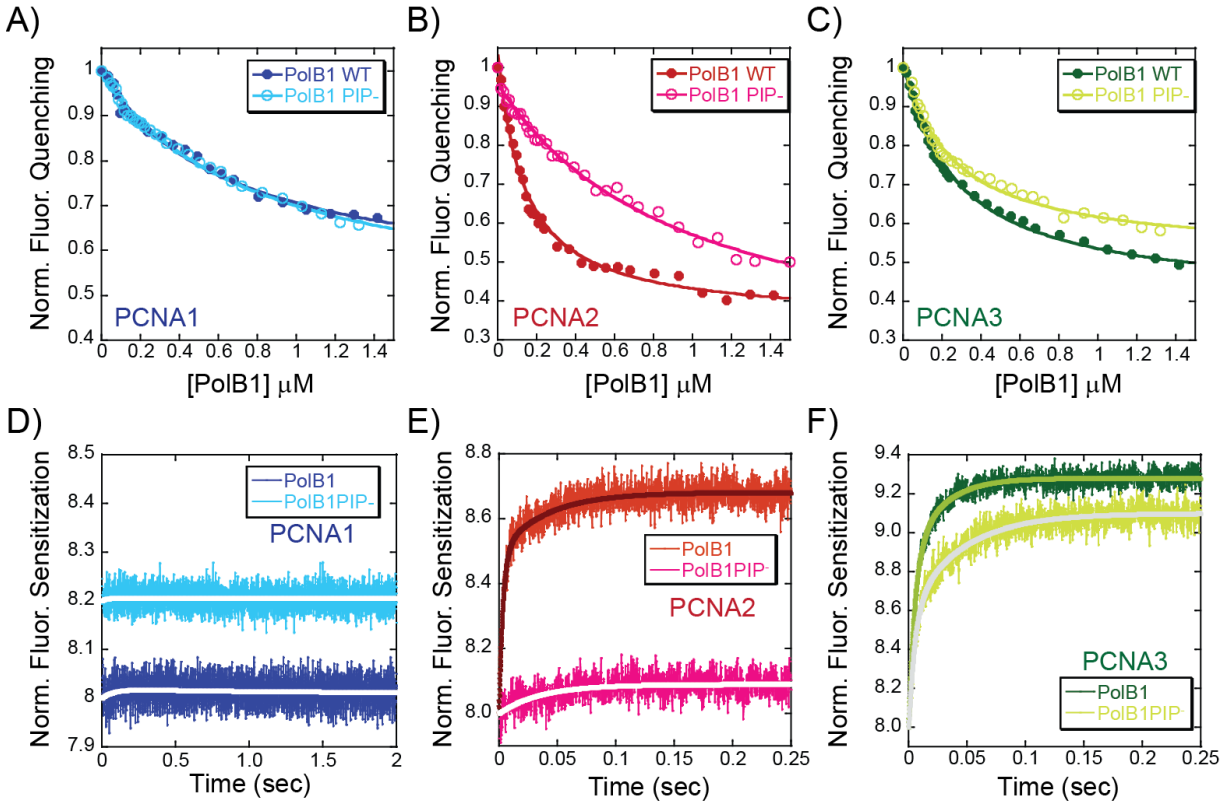

Figure 3.15: Presteady-State FRET between PCNA and PolB1 PIP Mutant
Specificity of PolB1 C-ter PIP motif for PCNA2 determined by fluorescence. Steady-state FRET quenching of a titration of PolB1 (-●-) or PolB1 C-term PIP$^-$ (-○-) labelled at S740C with Alexa594 into 50 nM: A) PCNA1-S191C (blue/cyan), B) PCNA2-S92C (red/pink), or C) PCNA3 S48C (dark green/ light green) labelled with Alexa488. Data was fit to Equation 3.1 to determine a K_d of binding for wild-type PolB1 with PCNA1 (1.0 ± 0.1 μM), PCNA2 (0.13 ± 0.01 μM), or PCNA3 (0.28 ± 0.01 μM) or for the C-term PIP$^-$ mutant of PolB1 binding to PCNA1 (1.0 ± 0.1 μM), PCNA2 (0.96 ± 0.01 μM), or PCNA3 (0.25 ± 0.01 μM). Analogous presteady-state FRET experiments monitoring the fluorescence sensitization above 590 nm and exponential fits for D) PCNA1 interacting with PolB1 (blue) (k_1 = 13 ± 10 sec^{-1} and k_2 = 1.0 ± 0.9 sec^{-1}) or PolB1 C-term PIP$^-$ (cyan) (k_1 = 20 ± 15 s^{-1}), E) PCNA2 interacting with PolB1 (red) (k_1 = 303 ± 17 sec^{-1} and k_2 = 25 ± 1 sec^{-1}) or PolB1PIP$^-$ (pink) (k_1 = 28 ± 2 sec^{-1}), or F) PCNA3 interacting with PolB1 (dark green) (k_1 = 190 ± 8 sec^{-1} and k_2 = 39 ± 2 sec^{-1}) or PolB1 C-term PIP$^-$ (light green) (k_1 = 185 ± 12 sec^{-1} and k_2 = 23 ± 1 sec^{-1}). Data and fits for PCNA1 and PolB1 or PolB1PIP$^-$ were normalized to 8.0 and 8.2, respectively, to visualize data. All others were normalized to 8.0.

Polymerase chase experiments were also performed to determine whether the C-terminal PIP motif was required for the exchange of polymerases within the holoenzyme complex during active synthesis explaining the low processivity values. (**Figure 3.14 B**). Titration of a catalytically

inactive PolB1 (Cat^-) that contained a native C-terminal PIP site shut down synthesis in a concentration dependent manor. Instead, when a mutant of PolB1 that had both an active site mutation and C-terminal PIP mutation (Cat^-/C-term PIP^-) was added as a chase, no significant change in product formation was detected. Therefore, exchange of polymerases within the holoenzyme during synthesis is mediated by contacts between the C-terminal PIP sites and PCNA2.

3.4.5 C-terminal PIP motif in *Sso*PolB1 is Visualized Using Small Angle X-ray Scattering (SAXS)

Both candidate PIP locations are absent from the crystal structure of PolB1, and therefore it is impossible to model interactions with PCNA123 to form the basis of a holoenzyme model.[(71)] Thus, we utilized small angle X-ray scattering (SAXS) to determine the solution structure of PolB1 alone and bound to 31 base hairpin primer-template DNA (10 base duplex region, 10 ssDNA region, and a 3 base loop) (**Figure 3.16 A-B and Figure 3.17**). The samples were measured at a series of concentrations, i.e., 1, 2 and 5 mg/ml, and undesired interactions among the protein molecules due to concentration and other factors were corrected before further analysis. The radii of gyration, R_g, for PolB1 and PolB1/DNA were 36 and 41 Å, respectively, determined from Equation 3.3.

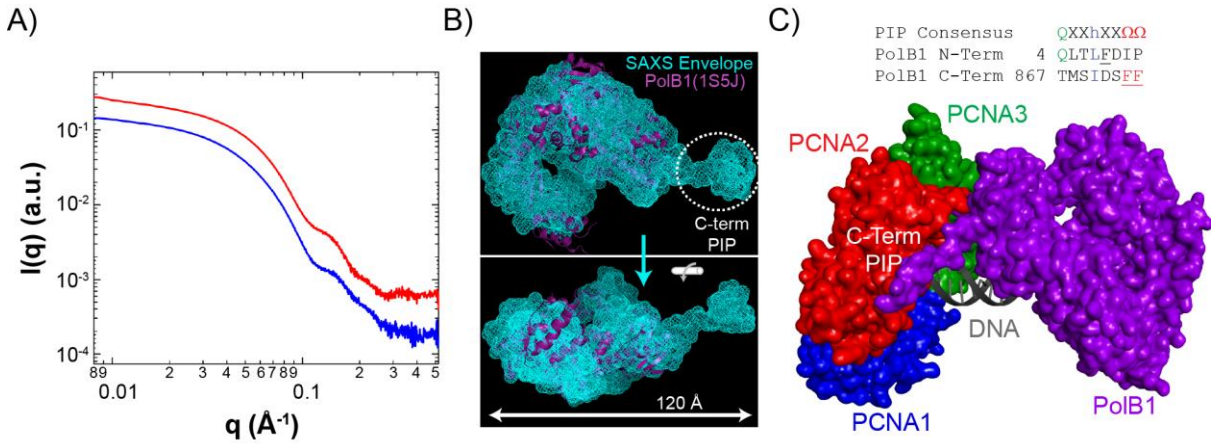

Figure 3.16: Small Angle X-Ray Scattering Analysis of PolB1
Visualization of the PolB1 C-terminal PIP motif using small angle a-ray scattering (SAXS) and modelled within the holoenzyme complex. A) Solution SAXS data for PolB1 (red) and PolB1/DNA (blue) collected in Tris buffer. The curves were vertically offset for clarity. B) Two views of the superimposition of the crystal structure (purple, in carton mode) and a representative SAXS envelope (cyan, in mess mode) calculated with program GASBOR. The figures were generated using Pymol.[(235)] C) PIP consensus motif (h –hydrophobic, Ω – aromatic) aligned with the previously identified N-terminal sequence[(128)] and the C-terminal sequence from *Sso*PolB1. Underlined residues were mutated in this study. Shows a model of the *Sso* DNA polymerase holoenzyme highlighting specific interactions of the C-terminal PIP domain with the interdomain connecting loop (ICL) of PCNA2 as well as adjacent interactions with PCNA3 modelled from the *Pfu* cocrystal structure of *Pfu*PolB1-PCNA (PDBID: 3A2F) and *Sso*PCNA123 (PDBID: 2IX2). Primer-template DNA was modelled in the active site from analogous interactions with the RB69 polymerase-DNA structure (PDBID: 1IG9).

Three dimensional molecular envelopes were calculated from SAXS data up to *q* of 0.52 Å^{-1}, for PolB1 using both programs of GASBOR[(233)] and DAMMIN[(234)] and for PolB1/DNA using DAMMIN. Both programs reconstruct the three dimensional molecular shape or envelope from the one-dimensional SAXS data. DAMMIN is a general program for biomacromolecules, while GASBOR was designed for proteins and uses real parameters, such as averaged form factor of amino acids and the number of residues in the protein under study, therefore often generates better results for protein-alone samples. The D_{max}, the largest dimension of the molecule indicated by the pair distance distribution function, P(r), (**Figure 3.17 A**) that was derived from the SAXS data program using GNOM[(239)], for PolB1 alone was 120 Å. The representative SAXS envelope for

PolB1 alone is overlaid and fit with the available crystal structure (PDB: 1S5J) and is displayed in **Figure 3.16 B**. For PolB1 alone, there is an obvious additional mass in the SAXS envelope that does not overlap with the X-ray crystal structure. The SAXS molecular envelope corresponding to the C-terminal region of PolB1 is also enlarged when primer-template hairpin DNA was added showing additional scattering from the dsDNA region (**Figure 3.17 B)**. The primer template DNA does not change the overall D_{max} significantly, consistent with the binding site size for PolB1 determined previously.[78] This extended tail region is consistent with the C-terminus density (including the C-term PIP motif) missing from the X-ray structure.

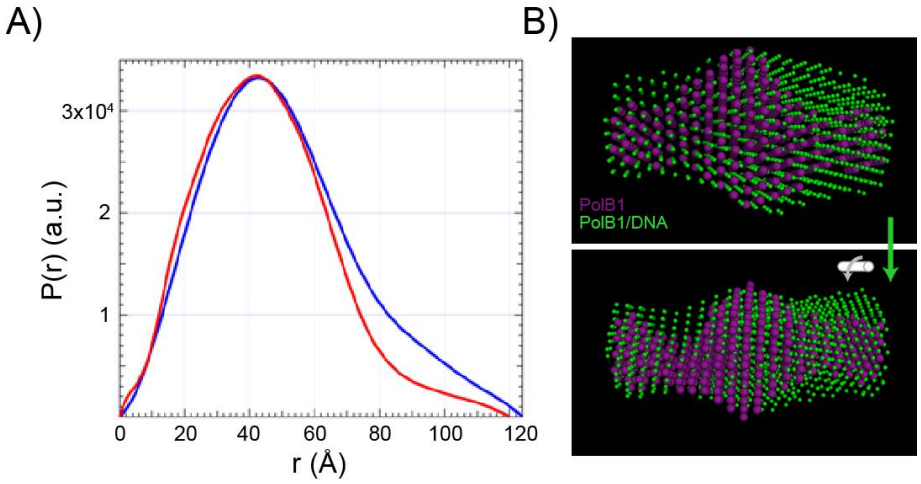

Figure 3.17: SAXS Distance Distribution of PolB1
A) The pair distance distribution functions, P(r), of PolB1 (red) and PolB1/DNA (blue) derived from the SAXS data in **Figure 3.16 A** using program GNOM. The largest dimension of a molecule, Dmax, is given at P(r = D_{max}) = 0. B) Two views of the superimposition of the SAXS molecular envelopes of PolB1 (purple) and PolB1/DNA (green). Both envelopes were an average of 20 independent DAMMIN calculations. The envelopes were displayed in sphere mode using Pymol and the sphere radii were set at different scales for a better comparison.

3.5 DISCUSSION

With the aid of their processivity clamps, DNA replication polymerases are known to form tight complexes on DNA, reducing their off-rates and contributing to repeated nucleotide additions. This repetitive and rapid synthesis is postulated to occur primarily on the leading strand so that a single DNA polymerase holoenzyme can do the bulk of the elongation. This ability also occurs on the lagging strand but may be restricted only by the length of Okazaki fragments. Although most DNA polymerase holoenzymes (i.e. T4, T7, *E. coli*, yeast) have been shown to have high processivities *in vitro*[230, 240-242], others have been found to be less processive (*i.e.* human pol δ).[229] The mechanism of classical processivity has also been challenged recently with the observation that DNA polymerases can exchange within replisomes during synthesis to maintain successive incorporations or bypass lesions through dynamic exchange events.[131, 140, 141, 144] Although the stepwise mechanism of clamp loading and DNA polymerase holoenzyme assembly has been studied in great detail for a number of other model replication systems[194, 205, 207, 212, 243-247], it has not been characterized thoroughly in archaeal organisms. In this study, we detail the assembly of the DNA polymerase holoenzyme from the crenarchaeon, *Sulfolobus solfataricus*, using site specific fluorescence labelling strategies and show biochemically that it acts distributively and that repeated synthesis is maintained through specific interactions with the C-terminal PIP motif of PolB1 and PCNA2. Clamp loading requires ATP binding to the clamp-loader which is hydrolyzed upon leaving DNA with simultaneous recruitment of PolB1 to form the holoenzyme. Implications for dynamic DNA polymerase processivity, holoenzyme formation, and polymerase exchange are discussed in relation to other well characterized systems.

3.5.1 *Sso* Clamp Loading Requires ATP Binding but not Hydrolysis

Similar to previous studies,[128, 134] we have verified that the heterotrimer of PCNA123 is required for maximal kinetics of nucleotide incorporation by PolB1. Although both PCNA1 and PCNA3 may form oligomeric species on their own at high concentrations, they do not seem to interact with nor contribute to increased kinetics for RFC or PolB1. The steady-state ATP

hydrolysis rate of RFC is only stimulated in the presence of PCNA123 or DNA associated with repeated cycles of clamp loading on DNA.

When presteady-state FRET experiments were performed with either ATP or ATPγS to monitor clamp loading, there was no significant difference in the rates or amplitudes indicating that ATP binding is solely required for initial interactions with DNA. The biphasic nature of these fluorescence changes also suggests that the two first order steps are conformationally similar to those shown for human PCNA loading.[207] Because our assay monitors only interactions between holoenzyme components and not clamp opening/closing directly, it is not clear if ATP hydrolysis is required for clamp closing. Previous work studying clamp loading in euryarchaeal organisms showed that ATP hydrolysis is required both for closing of the PCNA clamp and release of RFC leaving the PCNA/DNA complex[224, 226] and is also consistent with our work here on crenarchaeal clamp loading. In fact, ATP binding by the clamp-loader seems to be sufficient for placing an open clamp on DNA in most well characterized systems including T4[245], *E. coli*[203, 211], yeast[244, 246, 247], and human,[207] while hydrolysis is required for closing of the clamp and/or dissociation of the clamp-loader from the protein-DNA complex.

3.5.2 *Sso* PolB1 Holoenzyme Formation Requires ATP Hydrolysis

Upon addition of PolB1, there is a requirement for ATP hydrolysis by RFC for formation of the holoenzyme detected in the stopped flow assembly and kinetic incorporation experiments. ATP hydrolysis corresponds with conformational changes in either RFC, PCNA123, or both noted in step 5 of our holoenzyme assembly scheme (**Figure 3.12**). Although we do not directly measure clamp closing in these assays, we interpret these results as being consistent with other studies which have shown that clamp closing is required for stable association on DNA and favorable interactions with the polymerase.[198, 202, 203, 207, 212, 245, 247] We can also not visualize the fate of RFC after clamp loading and holoenzyme formation. In general, ATP hydrolysis also facilitates clamp-loader dissociation with other replication systems.[206, 207, 248] At this point, we speculate that RFC will dissociate in step 6 (**Figure 3.12**) to allow binding of PolB1 to the closed form of the clamp on DNA. This step was considered to be irreversible in our simulations, consistent with RFC

dissociation. Stimulation of the ATPase rate of RFC was most notable with DNA suggesting repeated dissociation and cycling from the DNA template. The ATPase rate was also not reduced when PolB1 was added signifying unstable holoenzyme complexes on DNA and repeated assembly. This differs from the T4 holoenzyme system where the ATPase rate was shut down when the polymerase was included.[249] Alternatively, this may also indicate that RFC dissociates during step 8 (**Figure 3.12**) allowing for a rearrangement of holoenzyme on DNA. Future studies will be required to monitor the opening and closing of PCNA123 throughout the assembly pathway as well as determine if and when RFC dissociates from the holoenzyme complex.

3.5.3 The *Sso* DNA Polymerase Holoenzyme Synthesizes DNA Distributively

Although most *in vitro* characterized DNA replication polymerase holoenzymes are considered to have high processivity, surprisingly, the assembled *Sso* holoenzyme has very low processivity which is only slightly stimulated over polymerase alone. In fact, the processivity of the *Sso* holoenzyme is much less than the homotrimeric *Sso* DNA polymerase in the absence of PCNA that we have characterized previously.[78, 139] The only other DNA replication polymerase holoenzyme system shown to act distributively and with low processivity is human pol δ[229]. The assembled *Sso* DNA replication polymerase holoenzyme appears to synthesize DNA distributively by exchanging polymerases through the clamp bound to DNA during synthesis. This exchange process is mediated by direct interactions between the C-terminal PIP motif in PolB1 and PCNA2.

Processivity was directly measured using two complementary assays: trapping and dilution. In the trapping experiments, a large excess of DNA is added to bind and sequester all DNA binding proteins from participating further in the reaction. Dilution experiments on the other hand, can more directly parse individual contributions to processivity by changing the concentrations/equilibria of individual components. Both PCNA123 and PolB1 were most sensitive to dilution and resulted in significantly shorter products than undiluted. Again, the dissociation of PolB1 from the template and/or PCNA123 is prevalent leading to low processivity for the *Sso* holoenzyme. Off-rate experiments of the holoenzyme from DNA are also informative and show two separate exponential decays (steps 8 & 9, **Figure 3.12**). We were able to measure

these decays using FRET from both PolB1 to DNA or PCNA123 and show values that are correlative suggesting multiple conformational transitions involved in complete dissociation. At either of those dynamic states, PolB1 can be efficiently removed by a DNA trap or increased by dilution to halt synthesis.

The stimulation of nucleotide incorporation/kinetics of DNA polymerases by their accessory factors are often errantly correlated with increased processivity. In those scenarios, it is speculated that the dissociation step (k_{diss}) is reduced when the clamp is complexed with the polymerase effectively allowing for more repetitive incorporation events (k_{cat}) in the timeframe before dissociation. Although this argument is absolutely valid for some systems, it does not explain the seemingly contradictory increased kinetics and low processivity for the *Sso* holoenzyme with PCNA123. The processivity increase (<100bases) is not sufficient to account for the 8-fold increase in synthesis rate over polymerase alone.

PolB1 has been shown previously to interact with itself and form a homotrimeric complex on DNA.[78, 139] At the concentrations and temperatures used within this report, the oligomeric state of PolB1 will be greater than 95% monomer, but it does not preclude transient interactions with itself. As additional molecules of PolB1 have also been shown to increase the kinetic rate of nucleotide incorporation, this association may be stimulated in the presence of PCNA123 retaining additional polymerases in molecular proximity to the holoenzyme. Alternatively, PolB1 may act distributively by transiently or completely dissociating from the template during synthesis even in the presence of PCNA123. Dissociation can occur directly at the polymerase active site or during shuttling between polymerase and exonuclease active sites potentially breaking contacts with PCNA123. Multiple binding sites on PCNA123 for PolB1 may also allow for transient dissociation from the template that can be trapped or alternatively reassociate for continued synthesis. This may be especially important for retaining the lesion bypass polymerase within the holoenzyme through specific interactions with PCNA1.[132]

3.5.4 C-terminal PIP Motif in PolB1 is Required for Interactions with PCNA123 and to Maintain Processive Replication

Based on the cumulative results showing a specific interaction of PCNA2 with the C-terminal PIP motif of PolB1 and PCNA3 with PolB1, we created a model of the *Sso* DNA polymerase holoenzyme (**Figure 3.16 C**). Available crystal structure data for individual *Sso* proteins,[71, 250, 251] a cocrystal structure of the homologous *Pfu*PCNA-PolB1, SAXS data highlighting the C-terminus of PolB1, and the functional data described here were integrated to form the basis of the model. The crystal structure of *Sso*PolB1 is incomplete, most notably missing the N and C-termini.[71] The visualization of extra density in SAXS molecular envelope compared with the X-tray structure is consistent with the C-terminus of PolB1 and was essential in correlating the C-terminal PIP motif, instead of the purported N-terminal PIP motif[128], with interactions with PCNA2. Moreover, this extended region in PolB1 is similar in structure to other C-terminal tail PIP motifs of other DNA polymerases. This PolB1 PIP site interaction with PCNA2 has only subtle differences in the binding pocket compared with either PCNA1 or PCNA3[252] but still provides for explicit discrimination in binding that is not fully understood.

Importantly, the C-terminal PIP motif in PolB1 was absolutely required for holoenzyme formation. Most notably, the steady-state and stopped flow experiments show both reduced affinity and association rates to PCNA2 specifically when the PIP site was mutated. Although no specific interaction was detected with PCNA1, PCNA3 had an intermediate affinity for PolB1 that does not occur at the PIP site. The cocrystal structure of *Pfu*PCNA-PolB identified a conserved negatively charged residue that interacts with specific residues in the thumb domain of *Pfu*PolB.[125, 126] Although this structure traps the complex in an inactive state, this "switch-hook" region is implicated in regulating conformation changes between proteins during polymerization and exonuclease proofreading. The arrangement of PCNA3 within the PCNA123 structure as well as within our holoenzyme model places this analogous switch-hook region within PCNA3.

More significantly, the C-terminal PIP site in PolB1 is implicated in active polymerase exchange as indicated by a shutdown in synthesis by a catalytically deficient polymerase only when a native PIP binding site is available. Therefore, we conclude that PolB1 is actively

exchanging during synthesis and that this exchange is occurring through polymerase PIP interactions with PCNA2. In addition to PolB1 exchange within the holoenzyme during DNA replication, this dynamic polymerase exchange mechanism may be employed with PolY as well, allowing for replacement of PolB1 at lesion sites encountered during replication though specific contacts with PCNA123.

3.6 CONCLUSION

We have shown that the *Sso*PolB1 holoenzyme from *Sso* is an inherently distributive enzyme complex. The assembly of the holoenzyme complex is a multistep process requiring ATP binding for clamp loading and ATP hydrolysis for PolB1 recruitment. Although PCNA123 increases the processivity of PolB1 slightly, it does not have the same intrinsic stimulation seen in other well characterized holoenzyme systems. The significant increase in the rate of synthesis observed when PCNA123 and RFC are included can be attributed to a repeated more rapid recruitment of PolB1 to the DNA template than when PCNA123 is not present. Therefore, synthesis by the *Sso* holoenzyme proceeds by successive nucleotide additions that are modestly increased by PCNA123 during a single binding event. After which, destabilization of PolB1 from the holoenzyme leaves PCNA123 behind for rapid recruitment of another molecule of PolB1 to the DNA through specific PIP interactions with PCNA2. This mode of synthesis is dynamic and provides a mechanism for polymerase exchange during DNA replication.

4.0 EXCHANGE OF POLYMERASE SUBUNITS IN ARCHAEAL DNA REPLICATION COMPLEXES

4.1 SUMMARY

In this chapter, we have examined the exchange of polymerase subunits within DNA replication complexes from *Sulfolobus solfataricus (Sso)*. We have found that subunits of the trimeric *Sso*PolB1 complex are able to exchange with those free in solution while the complex is actively replicating on DNA. We have also confirmed that a similar homooligomeric complex is able to form in solution, in the absence of DNA for the *Sulfolobus solfataricus* Y-family DNA polymerase (*Sso*PolY). We detail the evidence for a polymerase-polymerase interaction between the replication polymerase *Sso*PolB1 and the repair polymerase *Sso*PolY within the context of the replication holoenzyme. The presence of *Sso*PolY with and without a functional PCNA interaction site was found to decrease replication rate of the holoenzyme, implicating the change in replication rate on the interaction between the polymerases. Finally, we describe the creation of a mutant *Sso*PolB1 designed to inhibit its interaction with *Sso*PolY.

4.2 INTRODUCTION

DNA replication is an essential process in all forms of life, allowing for the propagation of genomic information to newly created cells and organisms. Replication is performed through the delicate interplay of a variety of enzymes and accessory proteins which together synthesize DNA in a 5'-3' direction on each parental template strand. Efficient DNA replication relies on both precise and uninterrupted DNA synthesis at the replication fork. As such, DNA replication polymerases form complexes with a variety of accessory factors to coordinate accurate synthesis in a discontinuous fashion on both the leading and lagging strands. These heteroprotein replication

holoenzymes (HE) are composed of a polymerase, a processivity factor (clamp) and a clamp-loader.

A DNA polymerases' processivity is defined by the average number of nucleotides which can be added to the growing DNA strand in a single binding event.[140, 253, 254] Formation of DNA polymerase holoenzyme complexes are evolutionarily conserved in all domains of life and are shown in many cases to drastically increase the processivity of DNA polymerases. For example, the processivity value for the *E. coli* pol III holoenzyme has a lower limit of 50 kilobases.[228] However, both the human polymerase (pol δ), and *Sulfolobus solfataricus* (archaeal) replication holoenzymes have been shown to replicate distributively and with extremely low processivity, while still maintaining the fast replication rates necessary for genomic propagation.[229, 255] We have shown that the low processivity for the *Sso* replication HE is due to rapid dissociation and re-recruitment of the polymerase to PCNA. This polymerization processes where the kinetic rate of synthesis is stimulated while the processivity values remains small is termed "dynamic processivity."[255]

In the event that the replication HE comes in contact with a damaged base it is unable to bypass due to the presence of the 3'-5' exonuclease error checking domain, the HE will pause.[256] The pausing event requires the recruitment of specialized repair polymerases with more open active sites, able to perform nucleotide incorporation across from the site of damage, to bypass the damage site and allow replication to resume.[115, 119] For this process to happen, an exchange event between the replication and repair polymerase must occur on the DNA template. Polymerase exchange has been explored in a variety of organisms in both the eukaryotic (humans, *Saccharomyces cerevisiae*) and bacterial (*Escherichia coli*) domains. In the eukaryotic system, upon stalling of the replication holoenzyme at a site of damage, a mono-ubiquitination event occurs on PCNA. This posttranslational modification signals for the recruitment of the DNA repair polymerases ζ (B-family) and Rev1 (Y-family).[257, 258] These two polymerases have been observed to form a complex, which stimulates the bypass abilities of pol ζ.[257] PCNA mono ubiquitination was thought to be necessary in the eukaryotic system to prevent recruitment of these more error prone polymerases when DNA damage was not present, however the accumulation of mutations on undamaged templates due to replication by pol ζ has been unexpectedly identified in

Saccharomyces cerevisiae. This implies that the formation of a polymerase-polymerase complex between ζ and REV1 occurs outside the DNA damage response system.[220, 259]

In *E. coli*, two separate polymerase exchange mechanisms have been proposed, mediated by interactions between the polymerases and the dimeric β-clamp. One model is referred to as the tool belt model, where two different polymerases are bound to the β-clamp simultaneously, through interaction with the binding site of a separate monomer.[260] In a separate model, switching between *E. coli* repair polymerase Pol IV and replication polymerase Pol III, shows that Pol IV is able to replace Pol III at a single binding site, through interactions with the rim of the β-clamp.[145, 261] Additionally, an interaction between Pol III and the regulatory subunit from the repair polymerase Pol V ($UmuD_2$), has been identified.[146, 147] This interaction has an inhibitory effect on Pol III's interaction with ssDNA, leading to its dissociation from the DNA template. As a result, this Pol III-Pol V interaction serves as a primitive damage checkpoint, and allows for error prone translesion synthesis by the repair polymerase. In the archaeon, *Sulfolobus solfataricus*, a physical interaction between the B-family polymerase PolB1 and Y-family polymerase PolY has been reported,[148] but currently there are no enzymatic effects noted for this interaction. Further contacts between polymerases are reported for the trimeric form of the PolB1 enzyme, which possesses stimulated replication rates similar to the holoenzyme, and increased processivity.[128, 255] In this chapter, we describe polymerase exchange events in the context of the *Sso*PolB1 replication holoenzyme as well as within the *Sso*PolB1 homotrimer. We also detail an enzymatic effect for interaction of *Sso*PolB1 and *Sso*PolY in the replication holoenzyme.

4.3 MATERIALS AND METHODS

4.3.1 Materials

Oligonucleotide substrates and primers were purchased from Integrated DNA Technologies (IDT, Coralville, IA) and are listed in **Table 4.1**. [γ-^{32}P]-ATP was purchased from Perkin Elmer (Waltham, MA). Optikinase (Affymetrix, Santa Clara, CA) was used for 5′-end

labeling of DNA substrates according to manufacturer's protocols. M13mp18 ssDNA template was purchased from Affymetrix. Radiolabeled primers were added to cold complementary template strands at a ratio of 1:1.2, heated to 95 °C for 5 min, and cooled to room temperature over at least two hours to ensure proper annealing. All other commercial enzymes were from NEB (Ipswich, MA).

4.3.2 **Cloning and Purification of *Sso*PolB1 Mutants**

Exonuclease deficient PolB1 (D231A/D318A) was purified as described previously, indicated as wild-type (polymerase activity), and used in all assays unless stated otherwise.[(78)] Mutant PolB1 interaction deficient enzymes (D501K, E550K, and D501K/E550K, **Table 4.2**) were created using a standard QuickChange protocol (Agilent, Santa Clara, CA) using two sets of QuickChange primers (**Table 4.1**) from pET30-PolB1 (D231A/D318A) and KAPA HiFi DNA polymerase (KAPA Biosystems, Woburn, MA).

Table 4.1: DNA Sequences

DNA Name	Sequence (5'-3')
PolB1 E550K FWD	5'-CCCTATGAAGTAAAGGATGAGACCGGTAAGGTGCTA CATATAGTTTGC
PolB1 E550K REV	5'-CATGCAAACTATATGTAGCACCTTACCGGTCTCATCCT TTACTTCATAGGG
PolB1 E501K FWD	5'-GAAAAGGATATAAAGGCGCAGTAGTTATAAAACCAC CTGCTGGAATA
PolB1 E501K REV	5'-TATTCCAGCAGGTGGTTTTATAACTACTGCGCCTTTAT ATCCTTTTC
PolY1 F349A/F350A FWD	5'-TTTATTGAAGCAATAGGATTAGACAAGGCAGCTGATA CTTAAGGATCCGAATTCGAGCTC
PolY1 F349A/F350A REV	5'-GAGCTCGAATTCGGATCCTTAAGTATCAGCTGCCTTG TCTAATCCTATTGCTTCAATAAA
PolY1 D105A/E106A FWD	5'-GAGAAGATCGAGATTGCAAGTATAGCTGCAGCTTATC TTGATATCTCAGACAAAG
PolY1 D105A/E106A REV	5'-CTTTGTCTGAGATATCAAGATAAGCTGCAGCTATACTT GCAATCTCGATCTTCTC
M13mp18 Primer	5'-CCGGAAACCAGGCAAAGCGCCATTCG
Hairpin DNA	5'-TTTTTTTTTTCCCGGGCCGGCGTTTCGCCGGCCCGGG

4.3.3 **Cloning and Purification of *Sso*PolY Mutants**

Mutant PolY1 enzymes (F349A/F350A (PIP-), D105A/E106A (Cat-), D105A/E106A/F349A/F350A (Cat-/PIP-) were created using a standard QuickChange protocol (Agilent, Santa Clara, CA) using two sets of QuickChange primers (**Table 4.1**) from pET30-PolY1 and KAPA HiFi DNA polymerase (KAPA Biosystems, Woburn, MA). The enzymes were auto-induced as described previously.[(168)] Cell pellets were resuspended in 20 mM sodium phosphate buffer (pH 7.0), 75 mM NaCl, and 5 mM β-mercaptoethanol 100 mM EDTA. The cells were lysed by the addition of lysozyme and sonicated. After centrifugation, the supernatant was heat treated at 70 °C for 20 min and centrifuged again. The supernatant containing PolY was purified using an ATKA Prime FPLC system with HiTrap MonoQ and heparin columns (GE Healthcare, Piscataway, NJ) and elution with a linear gradient to 1 M NaCl. Proteins were subsequently bound to hydroxyl appetite and eluted with 500 mM sodium phosphate. Final cleanup and sizing were performed with a Superdex 200 26/60 column (GE Healthcare), PolY was stored in 20 mM Hepes pH 7.5 100 mM NaCl 5 mM BME and 10% Glycerol.

4.3.4 **Purification of Replication Holoenzyme Components**

Both replication factor C (RFC) and the proliferating cell nuclear antigen complex (PCNA123) were expressed and purified as described previously (Chapter 3).[(255)]

4.3.5 **Polymerase Reaction Conditions**

Standard assays were performed in polymerase reaction buffer [20 mM Tris-acetate (pH 7.5), 100 mM potassium acetate, and 10 mM magnesium acetate] containing 18 nM primed M13mp18 DNA (ptDNA) unless otherwise indicated. Holoenzyme reaction conditions included 0.2 μM PolB1, 2 μM PCNA123, 0.4 μM RFC-SL, and 0.2 mM ATP. Prior to initiation, the reaction components were incubated for 5 minutes at reaction temperature before addition of 0.2 mM dNTPs. Trimeric polymerase replication assays were performed in reactions containing 1.5 mM

PolB1 and initiated by the addition of 0.1 mM dNTPs. Processivity assays were initiated by the addition of 0.1 mM dNTPs and 3 uL salmon sperm DNA as a trap.

Reactions were terminated by the addition of an equal volume of a basic quench (300 mM NaOH, 6 mM EDTA, 18% w/v Ficol 400, 0.15% w/v bromocresol green, and 0.25% w/v xylene cylanol). Products were separated on alkaline 0.8% agarose gels, and dried for 30 minutes under vacuum. Phosphor screens were then exposed to the gels for a minimum of 4 hours, imaged with a Storm 820 Phosphorimager (GE Healthcare), and quantified using ImageQuant version 5.0.

4.3.6 Electrophoretic Mobility Shift Assays (EMSAs)

EMSAs were performed in 10 μL volumes where the total polymerase concentration was maintained at a 1.5 μM while varying individual concentrations of WT and Cat- PolB1. The reactions were performed in EMSA complex buffer (10 mM Bis-Tris pH 7.0, 40 mM Tricine, 150 mM NaCl, 10 mM Mg(OAc), and 4% glycerol) in the presence of 4 nM 5'-P^{32}-labeled Hairpin DNA (Table 4.1). Reactions were incubated at room temperature for 30 minutes and separated on 6% Bis-Tris-Tricine gels. Phosphor screens were then exposed to the gels for a minimum of 4 hours, and imaged and quantified as above.

4.3.7 Bis-Tris Tricine Coomassie-G250 Native-PAGE

15, 30 and 45 μM PolY1 were electrophoresed using a Bis-Tris Native Gel Systems(Invitrogen) in 1X Native Page Sample Buffer (40 mM Bis-Tris, 10 μL 6M HCl, 0.1 g glycerol, 50 mM NaCl and 40 μg ponceau. The pH is 7.2) Samples were separated on 8% Bis-Tris-Tricine gels containing 5% glycerol, and run according to the manufacturer's protocol. The native gel separations were performed at three separate temperatures 5 °C, 22 °C and 50 °C.

4.3.8 Protein-Protein Docking

Protein-protein docking models were used to predict residues involved in the binding interaction between *Sso*PolB1 and *Sso*PolY using ClusPro 2.0 [262]. The structures used for these models were crystal structures for *Sso*PolB1 (PDBID: 1S5J) and *Sso*PolY (PDBID: 1K1Q). Protein complexes were predicted by docking *Sso*PolB1 with *Sso*PolY. The top 10 results were analyzed and compared.

4.4 RESULTS

4.4.1 Inclusion of Cat- *Sso*PolB1 in the *Sso*PolB1 Trimer Shuts Down DNA Replication

In previous studies, we showed that a trimeric PolB1 complex formed as polymerase concentration was increased, resulting in a fully trimeric polymerase on DNA when total polymerase concentration was equal to or greater than 1.5 μM [78]. In order to further understand the mechanism of action of this trimeric complex, we examined the enzymatic effect of subunit replacement with a catalytically inactive polymerase within the trimer. Reactions were assembled containing various ratios of catalytically active (WT PolB1) and inactive (Cat- PolB1) polymerase, while holding the total concentrations at 1.5 μM (**Figure 4.1 A**). As the overall concentration of the catalytically inactive polymerase (Cat-) was increased, there was a decrease in both replication rate and processivity (**Figure 4.1 B**). The product length decreases linearly as the concentration of Cat- is increased, but interestingly, the processivity value is maintained at ~1200 bp until a 1:0.7 of WT:Cat- PolB1 is exceeded (**Figure 4.1 A&B**). We confirmed by EMSA that the trimeric form of the mixed polymerase complexes bind DNA equal to that of wild type (**Figure 4.1 C**)

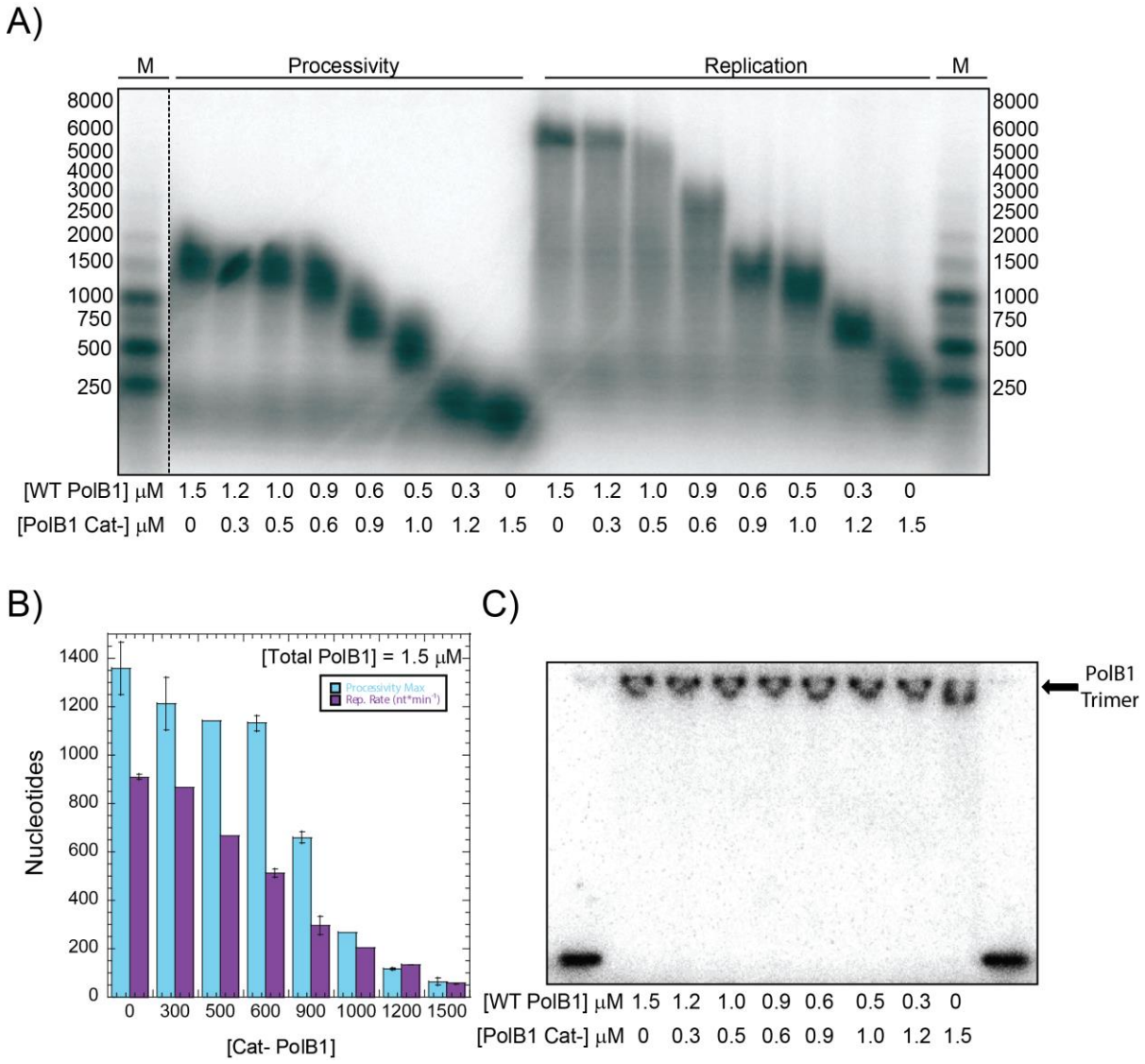

Figure 4.1: Incorporation of Cat- Subunits in the Trimeric SsoPolB1 Complex
A) Replication and processivity assays examining the effect of changing the ratio of WT vs. Cat- *Sso*PolB1 while total polymerase concentration is held at 1.5 mM. All reactions were quenched after 6 minutes. B) Quantification of Replication rate (nt•min^{-1}) and maximal polymerase processivity as the ratio of Cat- is increased. C) EMSA illustrating that the trimeric polymerase complex is maintained with the concentrations of WT and mutants of *Sso*PolB1 used in this experiment.

4.4.2 **The Subunits of the Trimeric PolB1 Dynamically Exchange During Replication.**

Having established the presence of catalytically inactive polymerase subunits in the *Sso*PolB1 trimer reduces the replication rate, we wanted to determine whether exchange could occur between polymerases free in solution and those contained within the trimeric complex during replication. To test this, we performed two sets of time course experiments. In the first set, the trimeric *Sso*PolB1complex was pre-assembled with increasing concentrations of a catalytically inactive polymerase (**Figure 4.2 A**). This experiment will test the initial kinetics of mixed WT:Cat- trimeric complexes. In the second set, replication assays were initiated and then chased, after 15 seconds of reaction time with increasing concentrations of the catalytically inactive polymerase (**Figure 4.3 A**). Here, we will test exchange of polymerase subunits during active replication.

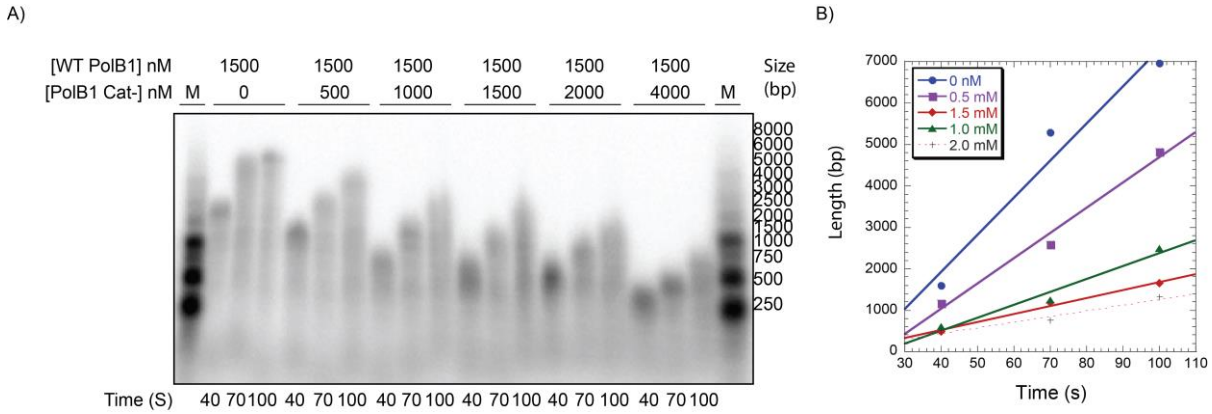

Figure 4.2: Subunits of the Trimeric PolB1 Complex Freely Exchange with Those in Solution: Pre-incubation
A) Pre mixed replication assay where increasing concentrations of *Sso*PolB1 Cat- were titrated into trimeric (1.5 μM) concentrations of WT PolB1. B) Plot of maximal produced product length for pre-mixed reactions vs time.

Rates were determined by plotting the maximal product length versus time for both the premixed reaction (**Figure 4.2 B**) and *Sso*PolB1 Cat- chase experiment. We saw a similar decrease in the replication rate observed in both cases as the concentration of the catalytically inactive polymerase was increased (**Figure 4.3 B**), indicating that the subunits of the trimer can rapidly exchange with those polymerases free in solution during the processive replication process.

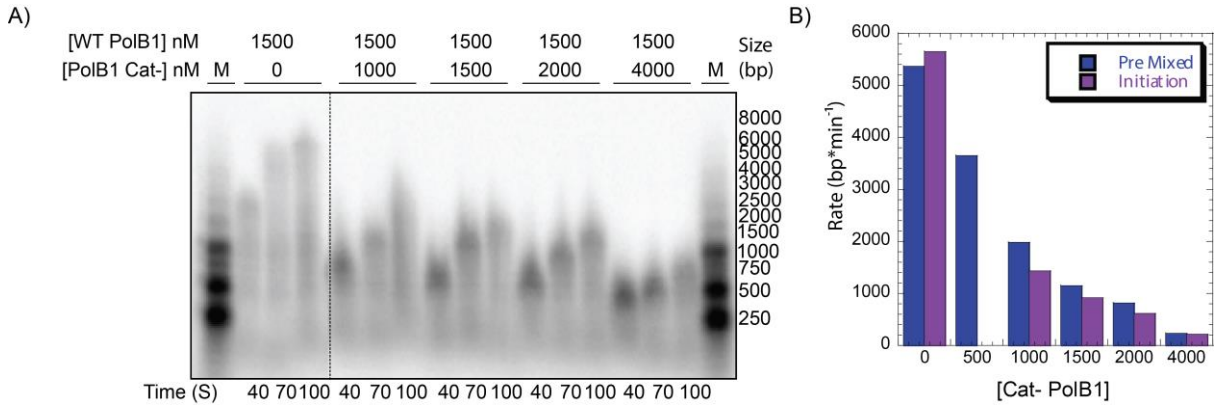

Figure 4.3: Subunits of the Trimeric PolB1 Complex Freely Exchange with Those in Solution: Polymerase Chase
A) Replication assay where increasing concentrations of Cat- PolB1 were titrated into trimeric (1.5 μM) concentrations of WT PolB1 15 seconds after the reaction had been initiated with dNTPs. B) Replication rates observed for each concentration of Cat- PolB1 titrated for both pre-mixed and pre-initiated reactions.

There is a notable difference between the rate reported in **Figure 4.1 B** to what is shown in **Figure 4.3 B.** The value shown in **Figure 4.1 B** is the average rate as observed over a six minute reaction and saturates as the M13 template (7.2 kb) is completely replicated. At concentrations of 1.5 and 1.2 μM WT *Sso*PolB1 over six minutes, this results in a replication rate that is slower than what is shown later in **Figure 4.3 B** at earlier time points. Therefore, the rate shown in **Figure 4.3 B** is more accurate for the trimeric enzyme (1.5 μM) covering a shorter timeframe that includes the linear extension rate.

4.4.3 *Sso*PolY Forms Native Oligomers in Solution without DNA

Previously, the Trakselis laboratory observed evidence for the formation of a *Sso*PolY oligomeric complex by isotermal titration calorimetry (ITC) and chemical crosslinking studies.[(139)] This result was seen both in the presence and absence of DNA. Due to *Sso*PolY's highly positive exterior charge, it difficult to resolve the native solution state of the polymerase using standard native gel electrophoresis protocols. In order to confirm the solution oligomeric state of *Sso*PolY, native blue PAGE gels were employed and electrophoresed at various temperatures in the absence

of DNA. The various temperatures were used to confirm the stability of the solution state SsoPolY complex. The advantage of native blue PAGE over standard native gel protocols is the use of Coomassie G-250 in the gel running buffer. Coomassie-G250 is a highly negatively charged dye, however unlike standard denaturing surfactants like SDS which bind to the peptide backbone, Coomassie-G250 only interacts electrostatically with positively charged surface residues. As a result, Coomassie-G250 bound proteins retain their natural globular state, but possess a highly negative surface charge, allowing for efficient separation of their native solution state through traditional electrophoresis.

We observed for *Sso*PolY that while the polymerase is predominantly monomeric, as the concentration is increased, formation of two higher order oligomeric complexes are observed (**Figure 4.4 A**). At the lowest temperature (4 °C), the oligomer is primarily tetrameric. As temperature is increased, the proportion of the tetramer decreases leaving additional monomeric polymerase (22 °C). Finally, the tetramer further dissociates into monomer and dimer (50 °C) (**Figure 4.4 B**). This data validates the ITC experiments and provides further information regarding the complex equilibria that exists in solution as a function of temperature.

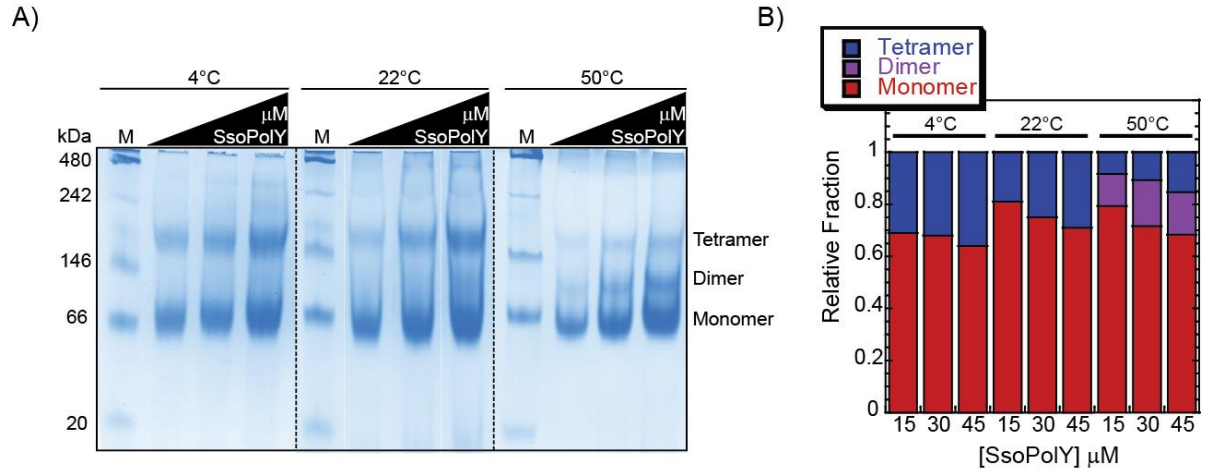

Figure 4.4: *Sso*PolY Blue-Native Gels

A) Native polyacrylamide gels titrating increasing concentrations of *Sso*PolY to examine the oligomeric state in solution of the polymerase in the absence of DNA. Proteins are drawn into the gel and stained through interaction with Coomassie-G250 dye. The polymerase oligomeric state is indicated for each of the temperatures examined (4 °C, 22 °C and 50 °C). B) Quantification of the relative abundance of monomer, dimer and tetramer for each concentration and temperature.

4.4.4 *Sso*PolY Inhibits the *Sso*PolB1 Replication HE through Contacts with Both PCNA123 and *Sso*PolB1

Previously, we described how the *Sso* replicative holoenzyme achieves high rates of replication through a process of rapid polymerase re-recruitment, rather than processive single enzyme synthesis.[255] This mechanism may also allow for the rapid exchange of the *Sso*PolB1 replication polymerase stalled at sites of DNA damage with a lesion bypass polymerase, *Sso*PolY. Experiments were designed where the *Sso*PolB1 replication HE was titrated with increasing concentrations of either *Sso*PolY, *Sso*PolY Cat-, or *Sso*PolY Cat- PIP- (**Figure 4.5 A**). The PIP- mutation in *Sso*PolY disrupts its ability to interact with PCNA2. The synthesis rate was reduced in the presence of the slower *Sso*PolY and further reduced when the catalytically

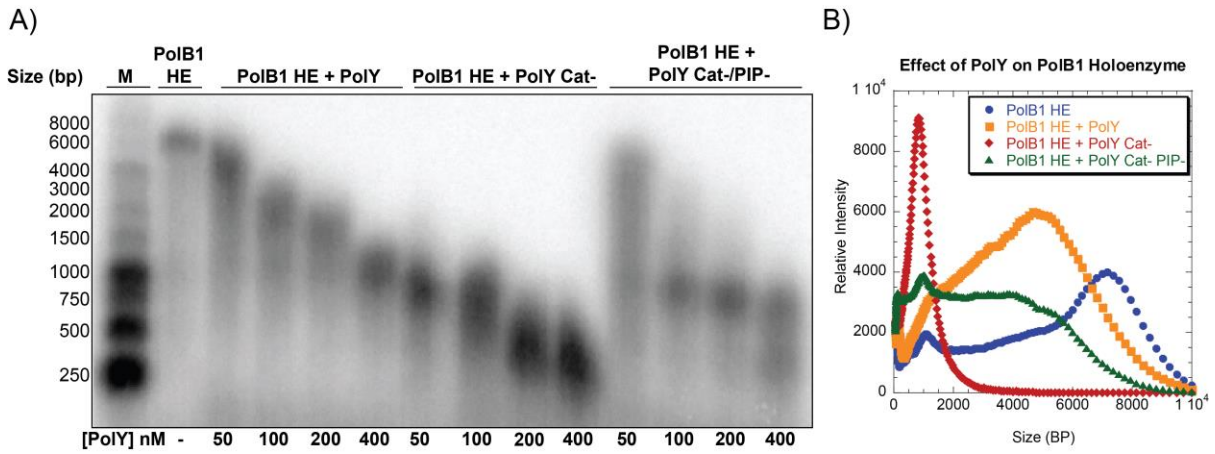

Figure 4.5: Effect of *Sso*PolY on the *Sso*PolB1 Replication Holoenzyme

A) Replication assay examining the effect of three different *Sso*PolY enzymes (Wild Type, Cat- and Cat-/PIP-) on the replication rate of the *Sso*PolB1 replication holoenzyme. B) Lane profiles from A) for each of the different reaction types. For reactions including *Sso*PolY, the 50 nM lane was plotted.

inactive *Sso*PolY was added. As can be seen in **Figure 4.5 B,** the predominant product size shifts from 7250 bp for the HE (blue) to ~5000 bp for the HE + PolY (orange) to ~1000 bp for the HE + PolY Cat- (red). However, when the catalytically inactive *Sso*PolY (Cat-PIP-) also lacking the ability to interact with PCNA was added (green), replication was not inhibited until higher concentrations of the polymerase were titrated. This indicates that *Sso*PolY is able to replace *Sso*PolB1 in the holoenzyme through contacts with PCNA, but that importantly, there are also

contacts between *Sso*PolB1 and *Sso*PolY, as the *Sso*PolY Cat- PIP- is still able to inhibit holoenzyme synthesis rate despite being unable to make contact with PCNA.

4.4.5 Model of Potential Contacts between *Sso*PolB1 and *Sso*PolY

Using the crystal structure of *Pyrococcus furiosus* PolB bound to a PCNA subunit, *Sso*PolB1 was overlaid and modeled onto this structure. *Sso*PolY was then added based on known contacts at the PIP site of PCNA1[(132)] (**Figure 4.6 A**). Charged residues on the surface of *Sso*PolB1 were then identified as potential interacting sites with *Sso*PolY within the context of the holoenzyme. Next, a protein docking program was utilized to assist in the prediction of potential interacting residues between the two polymerases, and residues D501 and E550 were identified (**Figure 4.6 B**). These mutant (D501K and E550K and D501K/E550K) *Sso*PolB1 enzymes were expressed and purified (**Figure 4.6 C**), however the D501K mutation resulted in truncation of *Sso*PolB1 during the recombinant expression process in *Escherichia coli* with an observed molecular weight of 57.98 kDa.

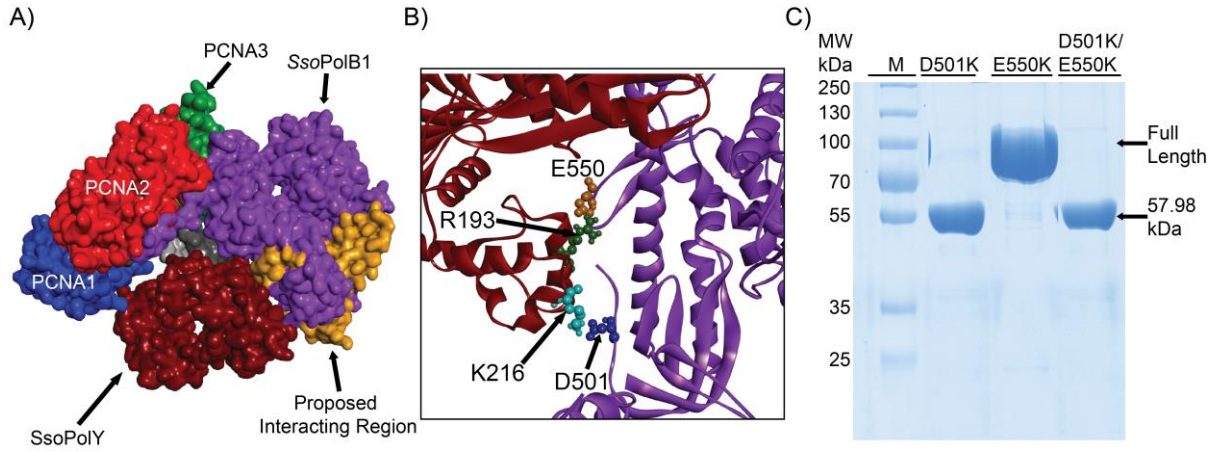

Figure 4.6: Electrostatic Mutations to Affect Polymerase Polymerase Interactions and Docking Model

A) Model of *Sso* replication supraholoenzyme, containing both *Sso*PolB1 and *Sso*PolY, modelled from the *Pfu* cocrystal structure of *Pfu*PolB1-PCNA (PDBID: 3A2F) and *Sso*PCNA123 (PDBID: 2IX2). Primer-template DNA was modelled in the active site from analogous interactions with the RB69 polymerase-DNA structure (PDBID: 1IG9), and *Sso*PolY (PDBID: 3FDS). B) Residues involved in the interaction between *Sso*PolB1 and *Sso*PolY as predicted by a docking model. Interacting negatively charged *Sso*PolB1 residues D501 (dark blue) and E550 (yellow), and positively charged *Sso*PolY residues R193 (green) and K216 (light blue) are shown. C) SDS PAGE gel of the purification of the *Sso*PolB1 mutants. All proteins are prepared to over 99% purity, however the D501K mutation resulted in the formation of a truncated protein product.

Current experimental data indicates that the E550K alone does not disrupt the interaction between *Sso*PolY and *Sso*PolB1 (**Figure 4.7**) as both holoenzyme complexes are inhibited in the presence of increasing concentrations of *Sso*PolY Cat-/PIP-, therefore future mutation will be needed to determine the binding interface for *Sso*PolB1 and *Sso*PolY.

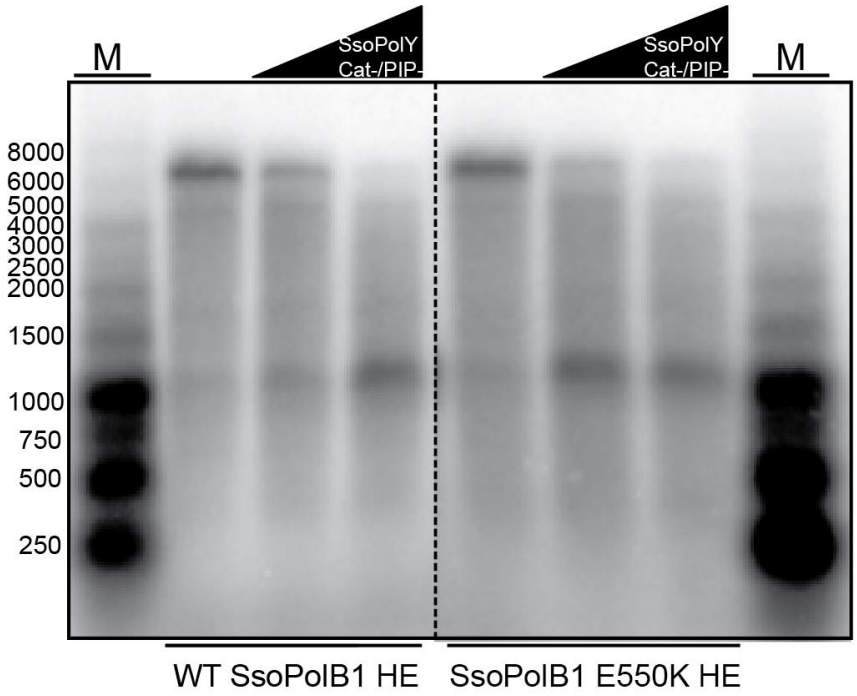

Figure 4.7: *Sso*PolB1 E550K Mutant is Inhibited by *Sso*PolY

Replication reaction where increasing concentrations of *Sso*PolY Cat-/PIP- were titrated into either the WT *Sso*PolB1 HE, or *Sso*PolB1 E550K HE. Polymerases were premixed and allowed to react for 2 minutes at 60 °C.

4.5 DISCUSSION

During replication, when the replicative holoenzyme encounters a damage site on DNA, it pauses, unable to extend past. In order for replication to resume, a Y-family DNA lesion bypass polymerase must be recruited, and an exchange event between the replication and repair polymerase occurs. A variety of different exchange processes have been observed in several model replication systems with no real conclusion on the mechanism of the process.[141, 144, 147, 263, 264] There have been many studies characterizing the function of *Sulfolobus solfataricus* PolB1 and PolY, and their respective interactions with PCNA, however little is known about the polymerase switching mechanisms between them.[78, 84, 115, 120, 132, 148, 255] Here, we have biochemically characterized exchange events occurring within both the *Sso*PolB1 trimer as well as the *Sso*PolB1 replication HE complex. There is recent evidence that eukaryotic DNA polymerases have evolved from their archaeal predecessors [1, 92] and therefore, contacts described here may provide clues into this complex exchange process in higher organisms as well.

4.5.1 **Trimeric *Sso*PolB1 Complex**

Previous work from the Trakselis lab has detailed the formation of a trimeric polymerase complex at polymerase concentrations 1.5 μM or greater. [78] The formation of this complex was observed to increase both the replication rate and the processivity of the polymerase. We hypothesized that this complex replicated along DNA in a "revolver" fashion, with the DNA rapidly dissociating from one polymerase active site and re-binding to another with the trimeric complex explaining the increase in processivity. To examine this exchange process, we began by examining the kinetics of the complex while varying the ratio of active versus inactive polymerases. We observed that an increasing ratio of catalytically inactive PolB1 reduces both the replication rate and also the processivity of the trimeric complex, consistent with the revolver model. If the DNA remained bound to only a single polymerase subunit within the trimeric complex, there would be a wider distribution of product sizes, rather than the majority of the DNA being elongated a similar length as is observed (**Figure 4.1 A**). Moreover, the processivity remains high until the concentration of Cat- exceeds WT. When there are statistically more WT subunits than Cat-, exchange within the trimer can occur giving higher processivity values. Once the Cat- concentration is greater than WT, exchange within the trimer is more futile leading to lower processivity values. This experimental set supports our hypothesis, where the increased processivity is due to rapid re-association of the DNA to different subunits within the trimeric DNA complex.

We also illustrated that rapid exchange of polymerase units free in solution occurs with those within the trimeric complex (**Figure 4.3 B**), which better explains the lag period for the effect of *Sso*PolB1 Cat- on processivity observed in **Figure 4.1 A&B**. If the trimeric complexes are stable and unable to rapidly exchange subunits, there would be a greater distribution of trimeric complexes containing only one, two, or three subunits of *Sso*PolB1 Cat-. As a result, we would see a wider distribution of product length in the processivity reactions, as additional Cat- subunits would inhibit replication rate. The increased inhibition from complexes containing the Cat- subunits would allow for fewer successive nucleotide incorporations prior to complex dissociation from the template. Instead, we observe production of DNA products of a uniform length, indicating

that the trimeric complex polymerase composition is homogenous, only possible with a rapidly exchanging population of monomer units.

4.5.2 *Sso*PolY also Forms an Oligomeric Complex in Solution

Previously, we have shown by ITC and EMSA experiments that in addition to the observed *Sso*PolB1 trimer, there also exists a *Sso*PolY oligomer on DNA[(139)]. Native-Blue PAGE experiments visualized the formation of both a dimeric and tetrameric complexes of *Sso*PolY alone which change as a function of temperature. In particular at high temperatures, the tetrameric species is reduced in favor of the dimeric complex indicating that this is the preferred state at *Sulfolobus* physiological growth temperatures. *Sso*PolY has also been observed to display increased processivity at higher reaction concentrations.[(139)] These findings, along with the previously identified *Sso*PolB1 trimeric complex illustrate the possibility that the equilibrium distribution of polymerase complexes is a complex but common theme controlling enzymatic activity in archaeal replication and repair. These oligomers generally allow for a faster rate of synthesis due to the increased processivity associated with more stable binding to DNA than the monomeric species. It is interesting that the DNA damage repair *Sso*PolY forms a dimeric complex with increased processivity, as processive synthesis is not required for the lesion bypass processes by Y-family polymerases. Thus, it is possible that the oligomeric *Sso*PolY complex plays further genomic maintenance roles in *Sulfolobus*; one where processive DNA synthesis is necessary.

4.5.3 *Sso*PolY Inhibits the Replication Rate of the *Sso*PolB1 Replication Holoenzyme

In Chapter 3, we identified that the *Sso* replication holoenzyme does not possess the high processivity that is expected from replication HE complexes. Rather, it attains stimulated replication rates, through the rapid dissociation and re-association of the replicative *Sso*PolB1 polymerase, in a process we refer to as “dynamic processivity”.[(83)] The rapid dissociation of the polymerase from this complex, allowed us to hypothesize that dynamic processivity may also

account for exchange from the replication *Sso*PolB1 polymerase to the repair *Sso*PolY polymerase. The *Sso*PolY Cat-/PIP, mutant is both catalytically inactive and unable to interact with PCNA due to mutations in its PIP box. Addition of this construct at low concentrations had minimal effect on the replication rate, as expected due to its inability to interact with PCNA. However, at higher concentrations, there was a reduced rate of synthesis producing a maximally sized ~750 nt product in the 2 minute experimental reaction time. This indicates that *Sso*PolY is still able to bind within the HE complex, and this interaction is likely mediated by contacts between the two polymerases. Such an interaction has been previously observed using a GST pull-down assay between *Sso*PolY and *Sso*PolB1 truncations and isolated the interacting region to within residues 481-617 from *Sso*PolB1[(148)].

In order to identify potential candidates for surface residues on *Sso*PolB1 which mediate this polymerase-polymerase interaction we utilized two methods. The first method was overlaying of the crystal structures of polymerases bound to DNA (**Figure 4.6 A**), and identifying charged residues on each in the regions where these polymerases would make contact with in the previously identified binding region (481-617). In our supraholoenzyme model, *Sso*PolB1 D510 and E550 residues are in close proximity to positively charged surface residues, K216 and R193, in *Sso*PolY allowing for possible salt bridge binding stabilization. The D501K mutation resulted in the creation of a protease sensitive site allowing for cleavage of the polymerase and purification of a truncated product. This was, similar in size to products detected previously by limited proteolysis used to map the general structure[(265)] (**Figure 4.6 C**). The *Sso*PolB1 E550K mutant was tested for any further decrease in processivity in the presence of *Sso*PolY, however, the resultant product formation was identical for the WT *Sso*PolB1 enzyme (**Figure 4.7**). It is possible that either there are other important electrostatic contacts between the polymerases, or that the interaction is more hydrophobic in nature.

4.6 FUTURE DIRECTIONS

The experiments detailed throughout this chapter, were predominantly preliminary in nature, illustrating a number of intriguing enzymatic effects resultant from the exchange of

polymerases at the site of replication from the context of both the replication holoenzyme and oligomeric polymerase complexes. As such, there are a variety of directions which can be explored to better clarify the presented data and aid in the understanding of polymerase exchange mechanisms in *Sulfolobus solfataricus*.

4.6.1 Subunit exchange in oligomeric polymerase complexes

We have identified that during active replication, polymerase subunits free in solution can exchange with those in a trimeric *Sso*PolB1 complex. We have also determined that in solution, *Sso*PolY formation of a dimeric complex is increasingly preferred over the tetramer as temperatures are increased verifying previous ITC experiments[(139)]. Therefore, *Sso*PolY is expected to be predominantly dimeric under standard 60 °C replication reaction conditions as well as at physiological conditions of thermophilic archaea. Previously, Pisani *et al*. detected a direct interaction between *Sso*PolB1 and *Sso*PolY, which is separate from their respective ternary complexes with DNA and PCNA[(148)]. It would be interesting to explore whether subunits can exchange between the *Sso*PolY oligomer with *Sso*PolB1, and also between the *Sso*PolB1 trimer and *Sso*PolY. Preliminary data examining the effect of either *Sso*PolB1 Cat- or *Sso*PolY Cat- on the processivity of a trimeric *Sso*PolB1 complex, shows a decrease in processivity when a PolB1 Cat- chase is employed. However, no major change in processivity is observed upon the addition of *Sso*PolY Cat-, (**Figure 4.8**) even at high polymerase concentrations (8 μM).

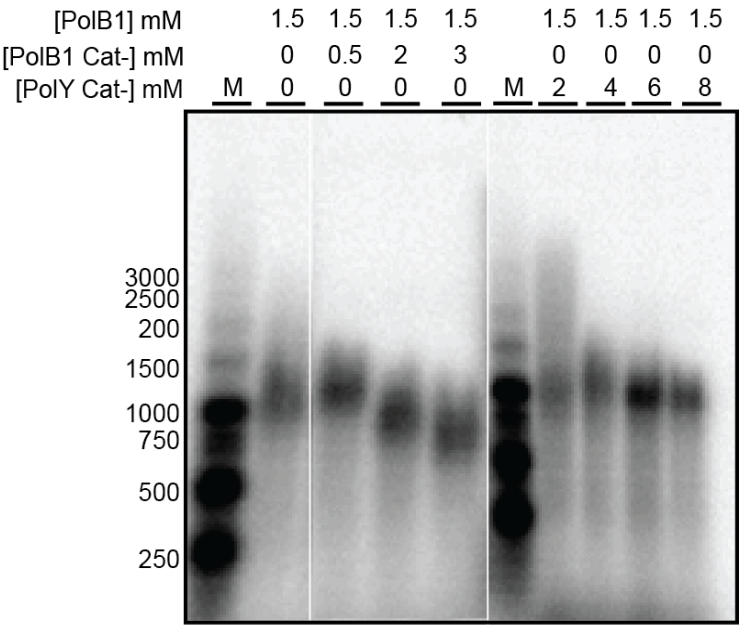

Figure 4.8: Effect of *Sso*PolY on *Sso*PolB1 Trimer Processivity Processivity assay examining the effect of both *Sso*PolB1 Cat- and *Sso*PolY Cat- on a trimeric *Sso*PolB1 complex processivity.

These results indicate that either *Sso*PolY cannot join the *Sso*PolB1 trimer, or it has no effect on the processivity. One caveat to this experiment is *Sso*PolY forms an oligomeric complex on its own, especially at higher concentrations (**Figure 4.4 A&B**), and this complex formation may inhibit it from exchange with *Sso*PolB1 subunits. Additional experimentation will be necessary to confirm this result, looking more closely at lower concentrations of *Sso*PolY where formation of the oligomer is less favored. Additionally, the effects of titrating *Sso*PolY Cat- on the overall replication rate of the *Sso*PolB1 HE should be performed, as it is possible that formation of an oligomeric complex including the Y-family Pol would not reduce the processivity but may affect the kinetics. Validating the formation and functional kinetics of *Sso*PolB1/PolY hetero oligomeric complexes would, not only be a unique finding, but also implicate the use of these complexes by *Sulfolobus solfataricus* in various replication or repair processing stages unlike what has been observed in any other replication system. Moreover, this work could provide valuable insight and relevance to transient polymerase complexes that have recently been detected in other organisms.

4.6.2 **The Polymerase-Polymerase Interaction Site and Formation of Trimeric *Sso*PolB1**

We hypothesized that the site on the surface of *Sso*PolB1 which allows for the interaction with *Sso*PolY also plays a role in the formation of the trimeric *Sso*PolB1 complex. We tested the ability of the *Sso*PolB1 E550K mutation to form a trimeric complex, by examining the replication rate of the polymerase as its concentration is titrated (**Figure 4.9**). Based on the extension rate as a function of polymerase concentrations, the E550K mutation is similar to the WT enzyme. This serves as confirmation that the E550 is either not a critical residue for these polymerase-polymerase interactions, or that additional contacts are involved.

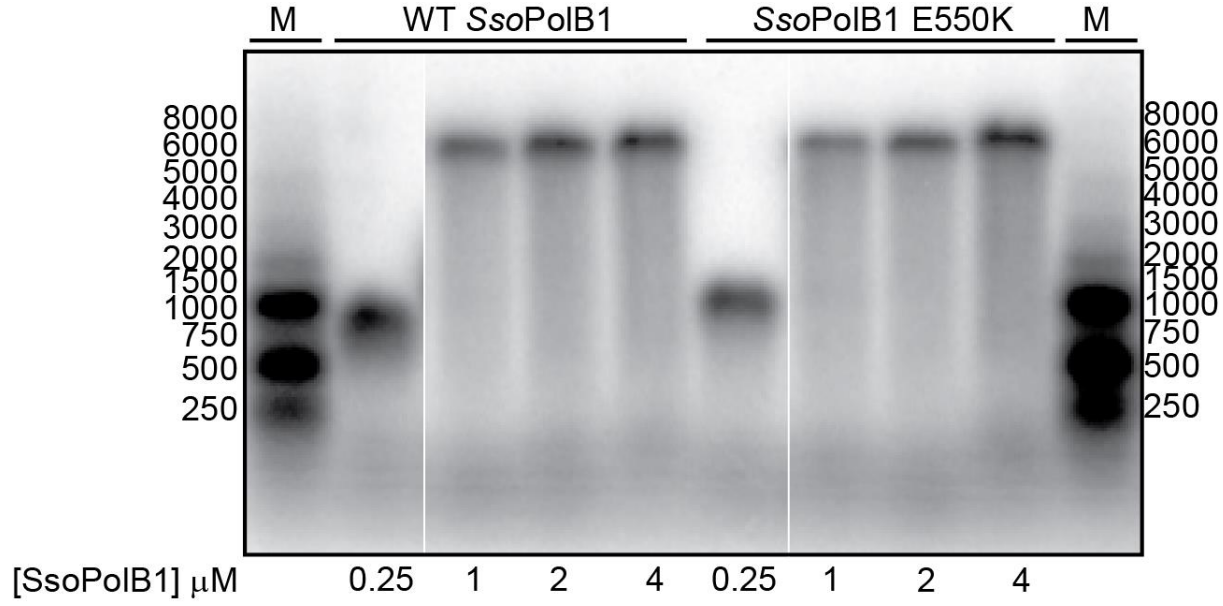

Figure 4.9: Formation of Trimeric *Sso*PolB1
Replication assay examining formation of the trimeric *Sso*PolB1 (0.25 μM – 4 μM) complex both for the wild type enzyme (WT) and also for the E550K putative polymerase-polymerase interaction disruption mutation. Reactions were performed at 60 °C and quenched after two minutes.

4.6.3 **Characterization of the Strength of the Binding Interaction between *Sso*PolB1 and *Sso*PolY**

Fluorescence anisotropy could be used to examine the binding interaction between polymerases, in both the presence and absence of a short DNA substrate, in order to determine the

whether formation of a ternary complex is observed. This would entail the N-terminal labeling of *Sso*PolY with a flourophore and a titration of *Sso*PolB1 as well as any available *Sso*PolB1 polymerase-polymerase interaction deficient mutants (*e.g.* E550K). Identification and quantification of the strength of this interaction would implicate a *Sso*PolB1/PolY complex either within a stable replisome complex. Alternatively, a strong interaction between *Sso*PolB1 and PolY may be involved in different repair processes such as gap filling, where a more stable complex would be necessary. A weaker more transient interaction may implicate the *Sso*PolB1/PolY complex in a lesion bypass processing role.

4.6.4 **Creation of *Sso*PolB1 Δ533-559 and *Sso*PolY I62K Mutants**

Mutation of the individual D550 residue was not sufficient to disrupt the enzymatic effect of *Sso*PolY on the *Sso*PolB1 replication holoenzyme. The D550 residue is located on an exterior loop structure (residues 533-559) which was predicted to be the binding site for the interaction between the two polymerases. The previous mutations were designed for a potential electrostatic interaction. Instead, the interaction between polymerases may be primarily hydrophobic. In support of this, the *Sso*PolB1 (533-559) loop contains a hydrophobic patch which was identified from a docking model where the I62 residue from *Sso*PolY is seen to interact with I535 and I554 from *Sso*PolB1 (**Figure 4.10**). To test for a hydrophobic interaction, a loop deletion mutant (D533-559) of *Sso*PolB1 would disrupt interactions between *Sso*PolB1 and *Sso*PolY. Alternatively, mutation of *Sso*PolY (I62) or *Sso*PolB1 (I554 or I535) to a non-hydrophobic residue such as lysine may also aide in testing the importance of this potential hydrophobic interaction site between replication and lesion bypass polymerases in *Sulfolobus*.

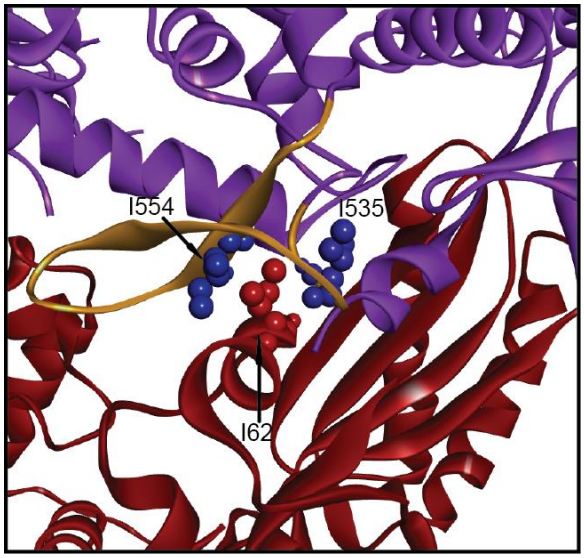

Figure 4.10: Hydrophobic Mutations to Affect Polymerase-Polymerase Interactions

Docking model structure showing *Sso*PolB1 (purple) with proposed loop deletion is shown (residues 534-559, yellow) also labeled are hydrophobic residues (I535 and I554, blue) and *Sso*PolY (maroon) hydrophobic residue (I62, red). These residues may play a role in the interaction between these two enzymes.

5.0 NOVEL INTERACTION OF THE BACTERIAL-LIKE DNAG PRIMASE WITH THE MCM HELICASE IN ARCHAEA[5]

5.1 SUMMARY

DNA priming and unwinding activities are coupled within bacterial primosome complexes to initiate synthesis on the lagging strand during DNA replication. Archaeal organisms contain conserved primase genes homologous to both the bacterial-DnaG and archaeo-eukaryotic primase (AEP) families. The inclusion of multiple DNA primases within a whole domain of organisms complicates the assignment of the metabolic roles of each. In support of a functional bacterial-like DnaG primase participating in archaeal DNA replication, we have detected an interaction of *Sulfolobus solfataricus* DnaG (*Sso*DnaG) with the replicative *Sso*MCM helicase on DNA. The interaction site has been mapped to the N-terminal tier of *Sso*MCM analogous to bacterial primosome complexes. Mutagenesis within the metal binding site of *Sso*DnaG verifies a functional homology with bacterial DnaG that perturbs priming activity and DNA binding. The complex of *Sso*DnaG with *Sso*MCM stimulates the ATPase activity of *Sso*MCM but leaves the priming activity of *Sso*DnaG unchanged. Competition for binding DNA between *Sso*DnaG and *Sso*MCM can reduce the unwinding ability. Fluorescent gel shift experiments were used to quantify the binding of the ternary *Sso*MCM-DNA-*Sso*DnaG complex. This direct interaction of a bacterial-like primase with a eukaryotic-like helicase suggests that formation of a unique but homologous archaeal primosome complex is possible but may require other components to stimulate activities. Identification of this archaeal primosome complex broadly impacts evolutionary relationships of DNA replication.

[5]The bulk of the material for this chapter is taken from **Bauer, R. J.***, Graham, B.W.* and Trakselis, M. A. (2013). Novel interaction of the bacterial-Like DnaG Primase with the MCM helicase in archaea. *Journal of Molecular Biology,* 425, 1259-1273. *Both Bauer and Graham are co-first authors, although we worked together on the majority of the research, I was primarily responsible for the construction of DnaG mutations enzymes and yeast two-hybrid constructs, DNA priming assays, fluorescence anisotropy, and GST pulldowns.

5.2 INTRODUCTION

DNA replication is a highly coordinated, yet dynamic, process that includes assemblies of multiprotein complexes to form the active replisome. After separation of the duplex DNA at an origin of replication by the concerted efforts of the DNA helicase and its accessory proteins, DNA replication begins with the *de novo* synthesis of an RNA primer by the DNA primase. Primer synthesis occurs at defined initiation sites on the single-stranded DNA (ssDNA) template both to initiate leading strand synthesis and repeatedly for each Okazaki fragment on the lagging strand. DNA primases are thought to exist within protein subcomplexes to both control and coordinate activities at the replication fork in all domains of life.

Two separate DNA primase families exist: one group (DnaG family) contains all the primases from bacteria and their phages, while the other group consists of archaeo-eukaryotic primases (AEP family).[16, 266] The eukaryotic primase is a four subunit complex comprised of a small catalytic subunit (p48) and a large regulatory subunit (p58) that modulates binding and activity. These subunits are almost always found in complex with two other proteins, DNA polymerase α (p180) and polymerase B (p68), to form the polymerase α-primase complex (pol-prim).[53] This complex can synthesize RNA primers initially with minimal template specificity[54] and can then extend them by incorporating dNTPs by pol α and pol B. Eukaryotic primases may control primer length (7-10 bases) through p58 regulation of binding to the ssDNA template that directs RNA synthesis by closing a hinge between p49/p58 subunits.[55, 56] The handoff of RNA primers larger than 7 nucleotides from p58 to pol α occurs by direct handoff within the complex for further extension into hybrid RNA-DNA products.[57, 58] The clamp loader complex (RFC) plays an important role in displacing polα after roughly 30 nucleotides for replacement with a more processive DNA polymerase holoenzyme complex that includes PCNA and either pol δ or pol ε.[59, 60]

AEP primases from Archaea contain only two of the four subunits of the pol α primosome (small catalytic, PriS, and large regulator PriL, subunits) and have been characterized in *Pyrococcus*[61, 62], *Thermococcus kodakaraensis*[63], and *Sulfolobus solfataricus* (*Sso*).[64-66] In addition to RNA primer synthesis ranging from 2-500 nucleotides, these primases have

surprisingly novel and unregulated DNA synthesis abilities producing oligonucleotide products greater than 7 kilobases. Temperature and slight differences in the affinity of NTP or dNTP may direct function towards RNA or DNA synthesis, respectively. An indirect link between PriSL and the MCM helicase is thought to be mediated by GINS23 to coordinate priming and unwinding activities in Archaea.[67] The DNA replication homology between Archaea and Eukaryotes would predict that like other functional homologs, PriSL will fulfill the DNA priming role in Archaea as well.[5, 68]

The bacterial DnaG primase has three domains: the N-terminal Zn^{2+} binding domain, the catalytic domain (TOPRIM), and the C-terminal helicase binding domain. TOPRIM (TOpoisomerase-PRIMase) is a signature motif in DnaG-type primases, topoisomerase, and other nucleases that encompasses an acidic metal binding active site required for catalysis.[16, 19] Binding to DNA is generally weak and transient but occurs along an elusive positively charged region adjacent to the active site that orientates the DNA template.[20] The C-terminal domain of *Escherichia coli* DnaG (*Ec*DnaG) is associated with the N-terminus of the DnaB helicase (*Ec*DnaB) to form the bacterial primosome complex that increases both priming and helicase activities.[21-24] This primase-helicase interaction and orientation has been seen in a variety of other bacterial and phage organisms[25-29] and is required for synthesis of primers on the lagging strand. Primers synthesized by *Ec*DnaG are typically 11 nucleotides but can range from 2-14.[34] The mechanism of RNA synthesis as well as the protein interactions of *Ec*DnaG have been well studied.[18, 20, 35-44] Primer length is controlled through coordination of the two subunits of bacterial DnaG with the Zn^{2+} binding domain to regulate DNA template binding.[20, 23, 40, 45] The influence *Ec*DnaG and *Ec*DnaB have on each other's activities is only just starting to be revealed.

Interestingly, Archaea also contain within their genome a homolog to the bacterial-like DnaG primase.[16] We have found that archaeal *Sso*DnaG has a conserved and essential active site glutamate required for synthesis of primarily 13mer RNA products.[48] In support of priming activity, *Sso*DnaG is able to *de novo* synthesize RNA primers with greater efficiency than archaeal *Sso*PriSL. To date, there have been no reported interactions of archaeal *Sso*DnaG with any other members of the replisome. Instead, *Sso*DnaG is found as a structural component within the archaeal exosome, albeit with no associated enzymatic activity.[267] The exosome complex is

required for the degradation of RNA and is actually contrary to the DNA priming or synthesis function of the primase.

To support a possible role for *Sso*DnaG in archaeal DNA replication, we have detected and verified a specific interaction with the *Sso*MCM helicase responsible for separation of duplex DNA ahead of the replication fork. The interaction site has been mapped to the N-terminal domain of the *Sso*MCM helicase analogous to other primase-helicase interactions found in bacteria. The priming activity of *Sso*DnaG is unaffected by this interaction, the unwinding ability of *Sso*MCM is inhibited, and the ATPase activity of *Sso*MCM is stimulated. Active site mutations in *Sso*DnaG verify conservation of acidic metal binding residues required for priming and DNA binding and are used to highlight *Sso*DnaG's interaction with both DNA and *Sso*MCM. DNA unwinding, ATPase, and fluorescent electrophoretic mobility shift assays (EMSA) suggest that *Sso*DnaG binds to a *Sso*MCM-DNA complex forming a ternary conformation. This work has broad evolutionary consequences for RNA priming in Archaea and suggests that formation of an analogous bacterial-like primosome complex may also be important for coordinating activities at the replication fork in Archaea.

5.3 MATERIALS AND METHODS

5.3.1 Materials

Oligonucleotide substrates (sequences are in **Tables 5.1** & **5.2**) were purchased from IDT (Coralville, IA) and gel purified.[(167)] Fluorescent HPLC purified DNA was from IDT. All radiochemicals were purchased from MP Biochemicals (Santa Ana, CA) or Perkin Elmer (Waltham, MA). Cy5 succinimidyl ester was from Invitrogen (Carlsbad, CA). Commercial enzymes were from NEB (Ipswich, MA). All other chemicals were analytical grade or better.

Table 5.1: DNA Sequences

DNA Primers	Sequence (5'-3')
DnaG D179A FWD	5'-ATTTAATAATAGTAGAAGGAAGAGCTGCAGTAATAAA TCTACTCAGATATGGCTAC
DnaG D179A REV	5'-GTAGCCATATCTGAGTAGATTTATTACTGCAGCTCTTC CTTCTACTATTATTAAAT
DnaG D220A FWD	5'-GACAGTAATAGCGTTTTTAGCCGGTGACCACGGTG GAGA
DnaG D220A REV	5'-TCTCCACCGTGGTCACCGGCTAAAAACGCTATTACTGTC
DnaG D222A FWD	5'-GCGTTTTTAGACGGAGCCCACGGTGGAGATCTG
DnaG D222A REV	5'-CAGATCTCCACCGTGGGCTCCGTCTAAAAACGC
DnaG RemoveStop F	5'-CCGATATTATTTCTTCTGTCGAGCACCACCACCAC
DnaG RemoveStop R	5'-GTGGTGGTGGTGTCGACAGAAGAAATAATATCGG
DnaG GST For	5'-CACCCATATGAGCTTCCAAATGAAATATGATATAAGG
DnaG GST Rev	5'-ATTACTCGAGAGAAGAAATAATATCGGTAAATGTC
DnaG pGADT7 For	5'-ACGTCGACCCCGGGATGAGCTTCCAAATGAAATATG ATAT
DnaG pGADT7 Rev	5'-ATTACTCGAGAGAAGAAATAATATCGGTAAATGTC
MCM FWD	5'-ATTAGGATCCATGGAAATTCCTAGTAAACAGATTGAC
MCM 106 FWD	5'-TTTGGATCCATTAATGGGTAAACTAATAACTATTG ATGG
MCM 267 FWD	5'-TTTGGATCCATTAATAAAGTATTAGATGAGGTAATC ATCTC
MCM 267 REVStop	5'-ATTACTCGAGCTATTTTTGTGAAACTTCTATACTAC
MCM 612 REVStop	5'-ATTACTCGAGCTAATCTATATCTATTTTTCCACTTTCC
MCM pGBKT7 For	5'-ATTAGGATCCATGGAAATTCCTAGTAAACAGATTGAC
MCM pGBKT7 Rev	5'-ATAGATGTCGACCTAGACTTTTTTGTAACATTC

Table 5.2: DNA Substrates

DNA[1]	**Sequence[2,3]**
ssDNA (5'Cy5)	5'-5GCTACTCTCGCTCAGCGTACCATAGCAG
3'-tail-30 nt	5'-CACCTCTCCCTACGCTTCCCACCCACCCCGACCGGCATCTGCTAT GGTACGCTGAGCGAGAGTAGC
5'-tail-30 nt	5'-CGATGAGAGCGAGTCGCATGGTATCGTCTAGCCGGTCGGGGTGG GTGGGAAGCGTAGGGAGAGGTG
3'-tail-30 nt (5'Cy3)	5'-3CACCTCTCCCTACGCTTCCCACCCACCCCGACCGGCATCTGCTA TGGTACGCTGAGCGAGAGTAGC
5'-tail-0 nt	5'-GCCGGTCGGGGTGGGTGGGAAGCGTAGGGAGAGGTG

[1]nt – nucleotides; [2]Modifications are underlined; [3]3 – Cy3, 5 - Cy5

5.3.2 **Protein Purifications**

The *Sso*DnaG gene was PCR amplified from pET30a-*Sso*DnaG[48] and cloned into pGEX-6P2 using *SmaI* and *XhoI* restriction sites included in the primer sequences. Active site mutant constructs (pET30-*Sso*DnaG-D179A, D220A, and D222A) with and without a 6X His-tag were created using a standard QuikChange protocol (Agilent, Santa Clara, CA) with KAPA HiFi DNA polymerase (KAPA Biosystems, Woburn, MA). Wild-type and His-tagged *Sso*DnaG constructs and *Sso*PriSL were expressed and purified as described previously.[48] Overexpressed GST-*Sso*DnaG was purified using a HiTrap Glutathione Sepharose Column (GE Healthsciences) and a Superdex 26/60 gel filtration column. GST-*Sso*DnaG was stored in binding buffer (10 mM Na_2PO_4, 1.8 mM K_2HPO_4, 140 mM NaCl, 2.7 mM KCl pH 7.3, and 10% glycerol).

Full length *Sso*MCM was purified as previously described using 70 °C heat treatment, MonoQ, heparin, and gel filtration columns to isolate the hexameric species.[15] Truncated forms of *Sso*MCM with included stop codons (1-267, 106-612, 267-612, and 1-612) were cloned into pET30a using *NdeI* and *XhoI* restriction sites eliminating any affinity tags. Truncated proteins were expressed using an auto-induction protocol at 37 °C[168] and purified similarly to wild-type.

*Ec*DnaB was autoinduced using pET11b-DnaB in BL21DE3 Rosetta 2 cells[168] and purified essentially as described previously.[268, 269] Briefly, *Ec*DnaB was purified using an ammonium sulfate precipitation and MonoQ and Heparin columns with 0.5 M NaCl gradient elution. Positive fractions were pooled and stored in *Ec*DnaB storage buffer (20% glycerol, 0.1 mM EDTA, 5 µM ATP, 5 mM $MgCl_2$, 20 mM Tris-Cl pH 8.0, 50 mM NaCl, and 2 mM DTT). The *Ec*DnaB concentration was determined with UV-Vis using an extinction coefficient of 29,870 M^{-1} cm^{-1}. All protein preparations were verified to have no significant background DNA contamination by UV (260/280 ratio < 0.9) and direct labeling with ^{32}P-γ-ATP in a polynucleotide kinase reaction.

5.3.3 **Fluorescent Protein Labeling**

Both *Sso*DnaG and *Sso*MCM constructs were labeled at the N-terminus with Cy5-succinimidyl ester in labeling buffer (50 mM Hepes pH 6.8, 100 mM NaCl, 5 mM β-

mercaptoethanol, and 10% glycerol) as described previously.[232, 270] The lower pKa of the N-terminus compared to lysine residues preferentially labels at this location under these conditions. Proteins were reacted with three molar excess of dye for 30 minutes at room temperature. Excess fluorophore was removed through extensive dialysis in labeling buffer. The labeling efficiency was determined by UV-Vis spectroscopy.

5.3.4 **Yeast Two-Hybrid Assay**

To generate the yeast two-hybrid plasmids, *Sso*MCM was cloned into *SalI* and *NdeI* sites of pGBKT7 (Clontech) and *Sso*DnaG was cloned into the *XhoI* and *NdeI* sites of pGADT7 (Clontech). The yeast strain PJ69-4A (*MATa leu2-3,112 ura3-52 trp1-901 his3-200 gal4Δ gal80Δ GAL2-ADE2 lys2::GAL1-HIS3 Met2::GAL7-LacZ*) was transformed with the appropriate plasmids (see figure legends) according to the manufacturer instructions using the lithium acetate procedure (Clontech Matchmaker manual). Liquid cultures were grown overnight in media lacking tryptophan and leucine. The cells were serial diluted and spotted on either SD/-Trp/-Leu or SD/-Trp/-Leu/-His medium and incubated at 30 °C for 2-3 days.

5.3.5 **GST Pulldown Assays**

20 µM GST-*Sso*DnaG was incubated at room temperature in the presence of 30 µM *Sso*MCM for 30 minutes. The sample was then immobilized on 200 µL Glutathione Sepharose 4B resin (GE Healthsciences) washed with 200 µL GST binding buffer (10 mM Na_2PO_4, 1.8 mM K_2HPO_4, 140 mM NaCl, 2.7 mM KCl pH 7.3), centrifuged for 10 seconds at 6,000 X g, washing was repeated at least seven times. Proteins were eluted with 600 µL GST elution buffer (50 mM Tris pH 8.0, 10 mM reduced glutathione). Eluted samples were concentrated, separated using 8 or 10 % SDS-PAGE gels, and stained with Coomassie. Fluorescent GST-pulldown SDS-PAGE gels were performed similarly and then imaged using a Typhoon phosphorimager (GE Healthsciences).

5.3.6 **DNA Priming Assays**

Priming reactions with or without *Sso*MCM were performed in primase reaction buffer (50 mM Tris, pH 8.5, 1 mM $MnSO_4$, 100 mM NaCl, and 0.2 mM NTPs, including 0.025 μCi/μl [α-^{32}P]GTP) as described previously.[48] The concentration of *Sso*MCM is indicated in each figure legend and either 4 nM M13 ssDNA, 200 nM forked, 200 nM 3'-tail, or 200 3'-tail-30 nt ssDNA at 70 °C was used as the template. Forked DNA is 3'-tail-30 nt annealed to 5'-tail-30 nt; 3'-tail is 3'-tail-30 nt annealed to 5'-tail-0 nt (Supplementary Table S2) as previously described.[15] Aliquots of the priming reaction were quenched in an equal volume of stop solution (88% formamide, 10 mM EDTA, and 1 mg/ml bromophenol blue) at times as indicated in each figure legend. The ^{32}P-labeled RNA primers were then resolved on a 20% denaturing polyacrylamide gel, phosphorimaged using a Storm 820 (GE Healthsciences), and quantified with ImageQuant software (version 5.0) to calculate reaction rates.

5.3.7 **DNA Unwinding Assays**

*Sso*MCM helicase unwinding reactions with and without *Sso*DnaG or *Sso*PriSL (concentrations indicated in the figure legends) were performed as described previously using 15 nM ^{32}P-labelled forked DNA.[15] Briefly, reactions were incubated at 60 °C for 5 min and initiated upon addition of either *Sso*MCM, *Sso*MCM and *Sso*DnaG, or ATP. Reactions were quenched with an equal volume (1.6% w/v SDS, 50% v/v glycerol, 0.1% w/v bromophenol blue, 100 mM EDTA pH 8.0 and 150 nM trap ssDNA complementary to the unlabeled strand), and then stored on ice until loading. ^{32}P-DNA products were separated on denaturing acrylamide gels and analyzed as described above.

*Ec*DnaB unwinding reactions were performed with 4.2 μM *Ec*DnaB (monomer) with and without *Sso*DnaG and incubated with 15 nM ^{32}P-labelled forked DNA in assembly buffer (50 mM Hepes pH 7.6, 100 mM NaCl, 0.2 mg/mL BSA, 5 mM BME, 10 mM $Mg(OAc)_2$, and 100 nM AMP-PNP) at 37 ºC for five minutes to assemble hexameric *Ec*DnaB on DNA. *Ec*DnaB unwinding

reactions were initiated with 2 mM ATP, quenched after 10 minutes, and processed as described above.

5.3.8 ATPase Assays

ATPase reactions were incubated at 60 ºC for five minutes and initiated upon addition of ATP. Reaction conditions were determined empirically by titrating ATP, DNA, and *Sso*DnaG concentrations while keeping *Sso*MCM constant at 4.2 μM (700 nM hexamer). Optimal reaction conditions included helicase buffer, 2.0 mM ATP, 1 μM cold forked DNA (if present), 4.2 μM *Sso*MCM and 0.7 μM *Sso*DnaG (if present) totaling 20 μL per reaction. Samples were quenched at 5, 10, and 15 min after initiation into equal volumes of 0.7 M formic acid. 0.8 μL of quenched reaction was spotted on Analtech Cellulose PEI F, allowed to dry, resolved in 0.6 M potassium phosphate (pH 3.5) buffer, and then phosphorimaged to calculate ATPase rates. P-values were calculated comparing the different conditions for ATPase experiments using a Student's *t*-test in Excel. A *p*-value of <0.05 was considered statistically significant.

5.3.9 Homology Modeling of the *Sso*DnaG Core Domain

Local and global sequence alignments were performed using ClustalW2 analysis (http://www.ncbi.nlm.nih.gov/blast/bl2seq/wblast2.cgi). The homology model of *Sso*DnaG was created by threading the global alignment of *Sso*DnaG with *Ec*DnaG onto the structure of *Ec*DnaG (PDB ID: 3B39)[20] using SWISS-MODEL[171] and overlayed and represented using PyMol (http://www.pmol.org).

5.3.10 Anisotropy DNA Binding Assays

Anisotropy assays were performed in *Sso*DnaG reaction buffer with 4 nM 28mer ssDNA (5'Cy5) and titrating *Sso*DnaG (WT, D179A, D220A, or D222A) as indicated. Anisotropy values

were obtained and quantified as detailed previously.[83] The change in anisotropy was fit to a single binding equation:

$$r = \frac{A \times [P]}{K_d + [P]} \quad (5.1)$$

where *A* is the amplitude, *P* is the concentration of *Sso*DnaG, and K_d is the dissociation constant, or a cooperative binding equation:

$$r = \frac{A \times [P]^n}{K_d{}^n + [P]^n} \quad (5.2)$$

where *n* is the hill coefficient.

5.3.11 **Electrophoretic Mobility Shift Assays**

EMSAs were performed in 10 μL volumes by the stepwise addition of 100 nM 66mer ssDNA (3'-tail-30 nt (5'Cy3)), *Sso*MCM (as specified) and 200 nM Cy5 labeled *Sso*DnaG (if present). Reactions were incubated at 60 ºC for 10 minutes to promote native thermodynamic complex formation and resolved on 5% native polyacrylamide gels (in 1X TBE). The gels were imaged using a Typhoon phosphorimager and the Cy3 and Cy5 intensities were quantified using ImageQuant. The Cy5-*Sso*DnaG volume was corrected for background Cy3-DNA intensities and plotted versus *Sso*MCM concentration to determine the K_d of the ternary complex according to Equation 1, where *P* is the concentration of *Sso*MCM.

5.4 RESULTS

5.4.1 Detection and Verification of a Direct *Sso*MCM-*Sso*DnaG Interaction

After screening for interacting *Sso* replication proteins with *Sso*DnaG using a yeast two-hybrid approach, we found that the *Sso*MCM helicase allows for growth on selective plates. In this experiment, *Sso*MCM is the bait constrained with the DNA binding domain within pGBKT7. *Sso*DnaG was cloned into pGADT7 containing the activation domain and acts as the prey. As observed in **Figure 5.1 A**, growth on selective media (SD/-Trp/-Leu/-His) is only allowed when both *Sso*MCM and *Sso*DnaG are included. Empty vectors or strains containing only single baits or preys (*Sso*MCM or *Sso*DnaG) showed no background growth on SD/-Trp/-Leu/-His but grew as expected on media (SD/-Trp/-Leu) selecting for plasmids alone.

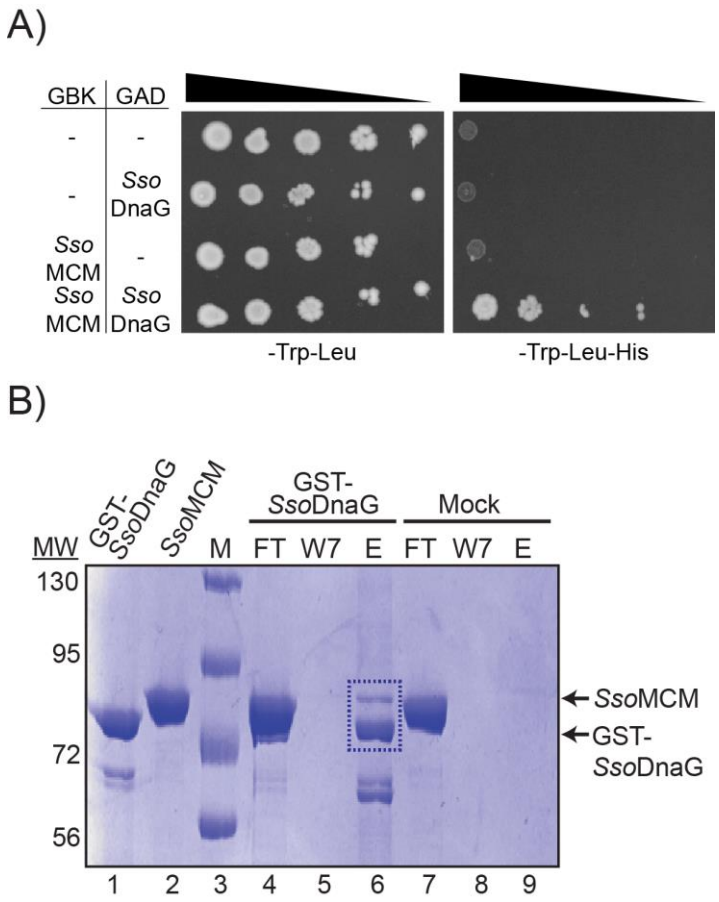

Figure 5.1: Physical Interaction between Full Length *Sso*MCM and *Sso*DnaG.
A) Yeast two-hybrid analysis of the *Sso*DnaG and *Sso*MCM interaction. *Sso*MCM was cloned into the GAL4 DNA binding domain vector, pGBKT7 (GBK), and *Sso*DnaG was cloned into GAL4 activation domain vector, pGADT7 (GAD). Cultures were serial diluted on either SD/-Trp/-Leu or SD/-Trp/-Leu/-His media. B) Coomassie stained SDS-PAGE gel showing purified proteins**,** GST-*Sso*DnaG (lane 1), *Sso*MCM (lane 2) and molecular weight markers (lane 3). GST pull down with (lanes 4-6) or without (lanes 7-9) immobilized *Sso*DnaG. *Sso*MCM flow through (FT, lanes 4 & 7), seventh wash (W7, lanes 5 and 8), and elution with glutathione (E, lanes 6 & 9). Interaction between GST-*Sso*DnaG and *Sso*MCM is seen in lane 6 outlined in a box.

In order to verify the yeast two-hybrid interaction between *Sso*MCM and *Sso*DnaG, we performed a GST-pulldown assay. Using an immobilized GST-tagged-*Sso*DnaG construct, we are able to verify that *Sso*MCM specifically interacts with *Sso*DnaG **(Figure 5.1 B)**. After addition and flow through of *Sso*MCM, the column was washed seven times, before eluting with glutathione. The difference in molecular weight between GST-tagged-*Sso*DnaG (73 kDa) and untagged *Sso*MCM (78 kDa) is not large, but *Sso*MCM can be clearly seen above GST-*Sso*DnaG in lane 6. Mock pull downs in the absence of GST-*Sso*DnaG show no background *Sso*MCM binding (lane 9).

5.4.2 **Effect of *Sso*MCM-*Sso*DnaG Interaction on Priming and Unwinding Activities**

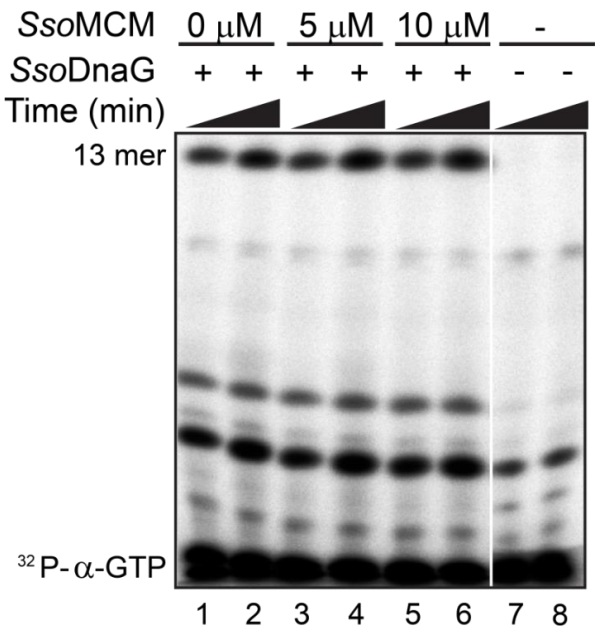

Figure 5.2: Effect of *Sso*MCM on *Sso*DnaG Primer Synthesis
*Sso*MCM does not significantly increase RNA primer synthesis by *Sso*DnaG. RNA primer synthesis by 1.3 μM *Sso*DnaG on M13 single strand DNA substrate at 60 °C showing 13mer and shorter products from ^{32}P-α-GTP as a function of *Sso*MCM concentration. Times are 30 and 60 minutes. Lanes 7-8 are no enzyme controls.

In order to determine if the interaction of *Sso*MCM influences the priming activity of *Sso*DnaG, we performed priming assays in the presence of *Sso*MCM **(Figure 5.2 A)**. No significant effect on *Sso*DnaG's priming rate on M13 was observed with *Sso*MCM concentrations up to 20 μM **(Figure 5.2, and data not shown)**. The priming rate of *Sso*DnaG was 17.0 ± 1.0 pmol•min^{-1} in the absence of *Sso*MCM and 16.5 ± 0.4 pmol•min^{-1} in the presence of 10 μM *Sso*MCM. We note that the priming rates observed in these experiments were roughly 10-fold higher per unit enzyme than we reported previously[(48)] and attribute this to purification of a more active unaggregated enzyme. Additional priming experiments were performed on short DNA templates (forked, 3'-tail, and ssDNA) with similar results, illustrating that even with substrates traditionally utilized for *Sso*MCM binding and unwinding experiments, no further stimulation of priming activity was observed **(Figure 5.3)**.

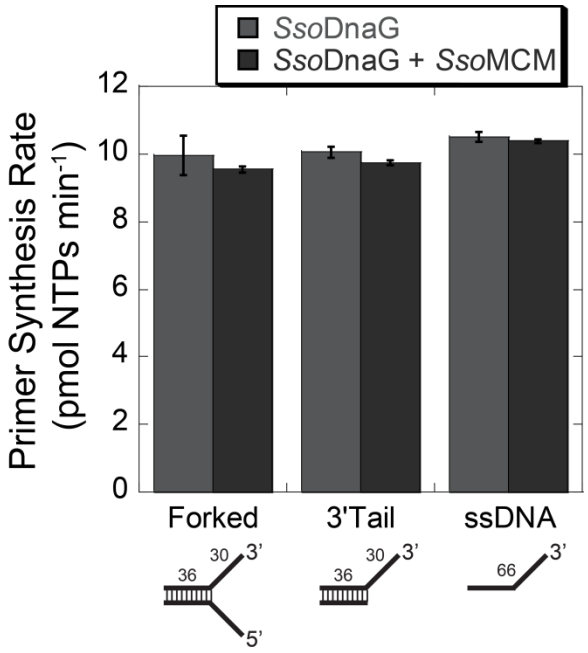

Figure 5.3: Effect of MCM on *Sso*DnaG Primer Synthesis Rate

*Sso*DnaG priming reactions were performed in the presence and absence of 3.2 μM *Sso*MCM (533 nM hexamer) on forked, 3'-tail and ssDNA. The plot quantifies the formation of RNA primer products by the *Sso*DnaG on these DNA templates. Error bars are the standard error for each reaction.

To test the effect of *Sso*DnaG on the unwinding activity of *Sso*MCM, we monitored the *in vitro* unwinding activity of a forked DNA substrate. 4.2 μM *Sso*MCM (700 nM *Sso*MCM hexamer) was tested for unwinding in the absence and presence of 700 nM *Sso*DnaG. The presence of *Sso*DnaG inhibits *Sso*MCM unwinding 6-fold **(Figure 5.4 A-B)**. Experiments were initiated by addition of *Sso*MCM, but other order of addition experiments where ATP or primase/ATP was added to initiate showed no difference (data not shown). Importantly, inclusion of the other archaeal primase (up to 4.2 μM) from *Sulfolobus*, *Sso*PriSL, had no effect on unwinding as the unwinding rate is identical to *Sso*MCM alone and similar to that reported previously.[67] The K_d of *Sso*PriSL binding to DNA[271] is estimated to be larger than for *Sso*DnaG, but in these experiments, both primases are well above their individual K_d values. Therefore, a specific interaction between *Sso*MCM and *Sso*DnaG on DNA is responsible for the unwinding inhibition whereas no effect is seen from the purported *Sso*PriSL primase.

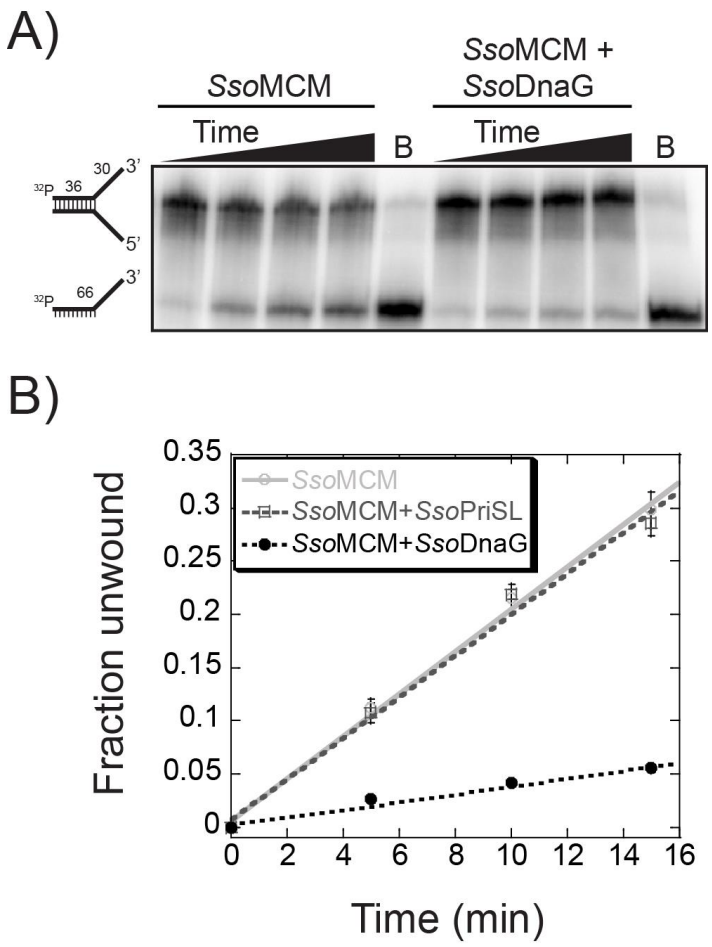

Figure 5.4: Inhibition of *Sso*MCM DNA Unwinding Upon Interaction with *Sso*DnaG.
A) Representative DNA unwinding assay and denaturing acrylamide gel for 4.2 μM *Sso*MCM (700 nM hexamer) alone and in the presence of 0.7 μM *Sso*DnaG monitoring unwinding of 15 nM forked DNA. B stands for boiled only DNA samples. B) Kinetics of DNA unwinding as a function of time for 4.2 μM *Sso*MCM alone (-o-) or in the presence of 0.7 μM *Sso*PriSL (-□-) or 0.7 μM *Sso*DnaG (-●-) at 60 °C. Error bars represent the standard error from at least three independent unwinding experiments.

The ATPase activity of hexameric helicases is generally stimulated upon binding DNA to activate unwinding or translocation.[232, 272] ATPase experiments were used to monitor any effect on ATP hydrolysis by *Sso*MCM when *Sso*DnaG was included. Titrations were performed to determine the optimal concentrations of ATP, *Sso*DnaG, and DNA in the ATPase assays **(Figure 5.5)**. Increasing concentration of ATP increased the ATPase rate for *Sso*MCM before leveling off above 2 mM. The *Sso*MCM ATPase rates at DNA concentrations above 1 μM were fairly consistent. Interestingly, when *Sso*DnaG was titrated up to 1 μM in the reaction, there was stimulation in *Sso*MCM's ATPase rate, while at higher *Sso*DnaG concentrations the ATPase rate of *Sso*MCM returned to basal levels.

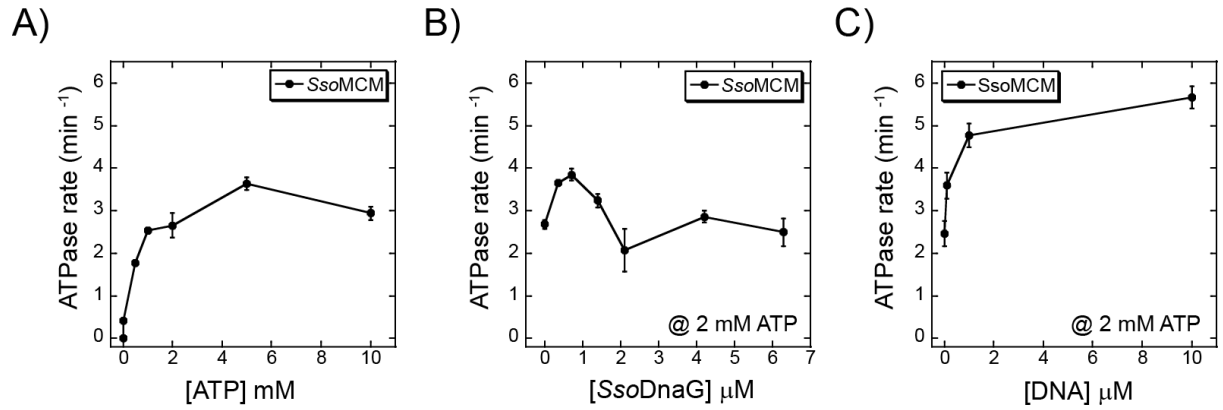

Figure 5.5: ATPase Activity of *Sso*MCM
ATPase as a function of A) ATP, B) *Sso*DnaG, and C) forked DNA concentration. ATPase activity of 4.2 μM *Sso*MCM was measured at 60 ºC. Multiple time points were averaged to calculate the number of ATP molecules hydrolyzed per minute per MCM monomer. The error bars represent the standard error from at least three independent experiments.

Under optimal reaction conditions, 4.2 μM *Sso*MCM (700 nM hexamer) alone has an ATPase rate of 217 ± 17 pmols min $^{-1}$ **(Figure 5.6 and Figure 5.7)**. Inclusion of 0.7 μM *Sso*DnaG significantly stimulated the ATPase activity of *Sso*MCM alone 1.5-fold (326 ± 17 pmol•min $^{-1}$). Addition of 1 μM forked DNA to *Sso*MCM stimulated the ATPase activity almost 2-fold (414 ± 28 pmol•min $^{-1}$) consistent with previous results.[8, 232] The addition of DNA with *Sso*DnaG/*Sso*MCM had no further stimulatory effect (327 ± 22 pmol•min $^{-1}$) over *Sso*DnaG-*Sso*MCM alone and is significantly less than for *Sso*MCM-DNA. ATPase experiments with *Sso*DnaG alone or with DNA had only background levels of hydrolysis.

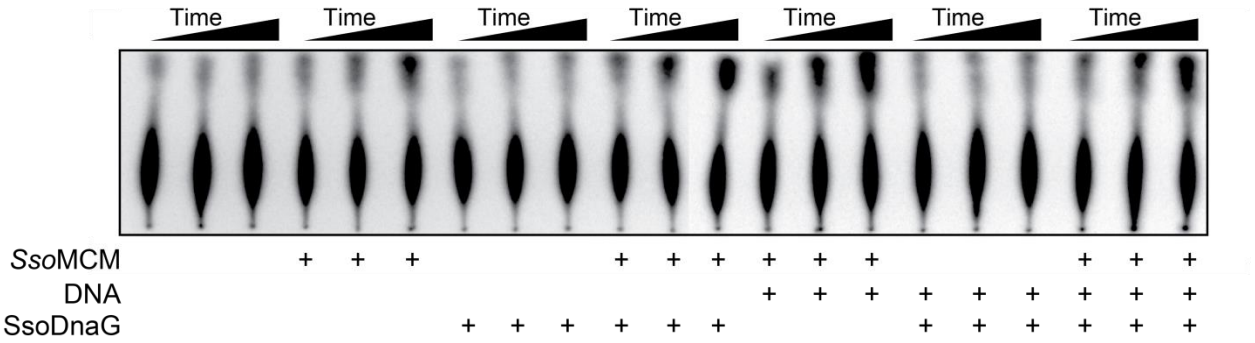

Figure 5.6: Example *Sso*MCM ATPase TLC plate.
Representative raw data from TLC separated ATPase assay at 60 °C. Quantification of the rate of ATP hydrolysis as a function of time (5, 10, and 15 minutes) is shown in Figure 5.7.

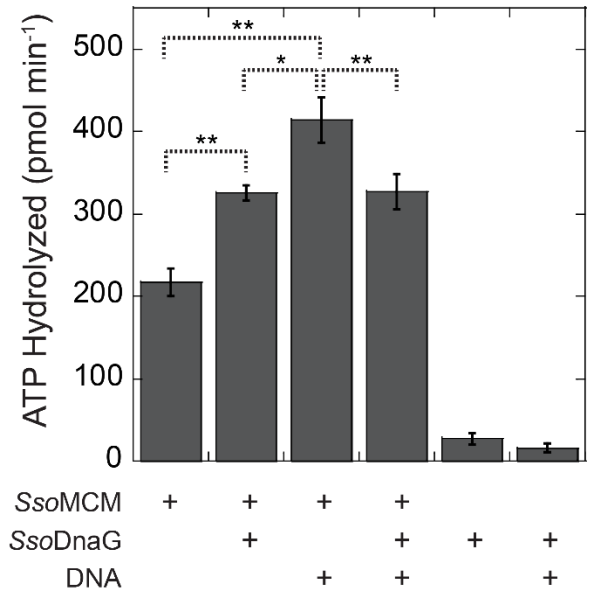

Figure 5.7: *Sso*DnaG Stimulates ATPase Activity of *Sso*MCM.
ATPase activity of *Sso*MCM without and with *Sso*DnaG measured at 60 ºC in the absence and presence of DNA. 4.2 μM *Sso*MCM (700 nM hexamer), 700 nM *Sso*DnaG and 1 μM forked DNA were used. DNA stimulated ATPase activity of *Sso*MCM 1.9-fold. In the absence of DNA, *Sso*DnaG stimulated the ATPase activity of *Sso*MCM 1.5-fold. However, the presence of DNA did not stimulate the ATPase activity of *Sso*MCM further in the presence of *Sso*DnaG. As a control, *Sso*DnaG alone and in the presence of DNA is shown to have no ATPase activity above background. P-values: * = $p < 0.05$; ** = $p < 0.01$. Error bars represent the standard error for each reaction.

5.4.3 Characterization of the Conserved Acidic Active Site Mutants from *Sso*DnaG

Previously, we have shown that the mutation of a conserved glutamate (E175Q) abolished the priming activity of *Sso*DnaG.[48] The core TOPRIM domain of *Sso*DnaG also includes other conserved acidic aspartates (D179, D220, and D222) that are proposed to define metal binding in the active site. Mutation of these homologous aspartates in *Ec*DnaG resulted in catalytically inactive enzymes with decreased metal binding affinities.[273, 274]

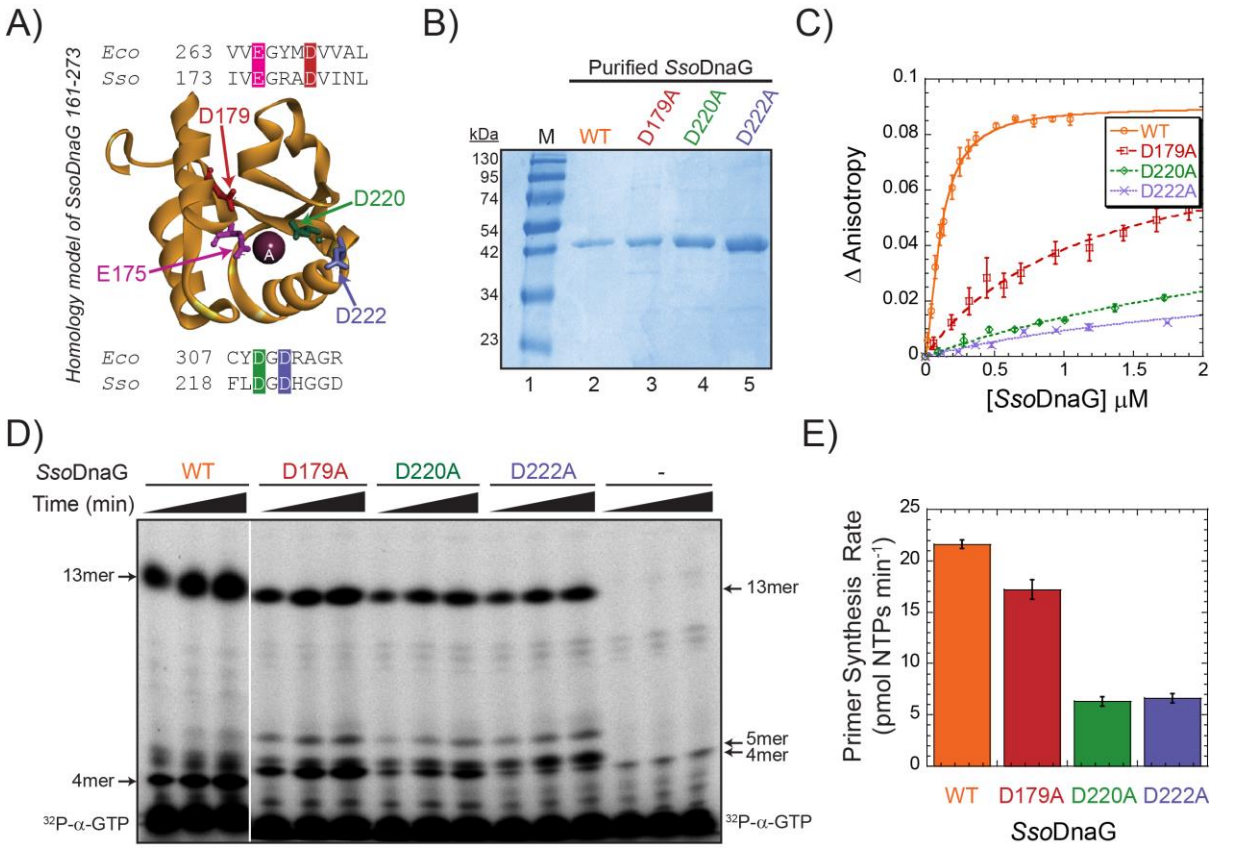

Figure 5.8: Conserved *Sso*DnaG Active Site Residues Disrupt DNA Binding and Priming Activity

A) Homology model of the TOPRIM domain of *Sso*DnaG (residues 161-273) highlighting conserved catalytic E175 (pink) and proposed metal binding residues D179 (red), D220 (green), and D222 (purple). The divalent metal A is positioned from alignment with the *Ec*DnaG structure (PDB: 3B39). B) Coomassie stained SDS-PAGE gel showing wild-type (WT) and mutant forms of *Sso*DnaG. C) Fluorescence anisotropy DNA binding experiments of each *Sso*DnaG construct to a 28 mer ssDNA (5'Cy5). The dissociation constant (K_d) for wild-type *Sso*DnaG (WT, orange -o-) binding was obtained from a fit to Equation 2 and is 0.11 ± 0.01 μM with a Hill coefficient of 1.5 ± 0.1, while the K_d for *Sso*DnaG-D179A (red -□-) was obtained from a fit to Equation 5.1 and is 1.2 ± 0.1 μM. The K_ds for D220A (green -◊-) and D222A (purple -x-) are much larger and not quantifiable over the concentration range tested (0.05 - 9 μM). D) DNA priming assays were separated on a 20% denaturing acrylamide gel and phosphorimaged showing primarily 13mer, 4mer, and dimer products synthesized from ^{32}P-α-GTP and E) quantified. The error bars represent the standard error from at least three separate experiments.

A homology model of the core domain of *Sso*DnaG was created by threading the alignment onto the crystal structure of the TOPRIM domain of *Ec*DnaG (PDB: 3B39) and illustrates these conserved acidic residues **(Figure 5.8 A)**. We individually mutated *Sso*DnaG D179A, D220A, and

D222A and purified the mutant recombinant proteins **(Figure 5.8 B)**. The DNA binding ability of each of these mutants to 28mer ssDNA (5'Cy5) template was determined using fluorescence anisotropy. The D179A mutant had a 10-fold reduction in ssDNA binding affinity (K_d) for DNA (1.2 ± 0.1 µM) compared to wild-type *Sso*DnaG (0.10 ± 0.01 µM) **(Figure 5.8 C)**. The K_d values for the D220A and D222A mutants are significantly larger than for D179A but cannot be calculated accurately with the experimental concentration range used (0.05 – 9 µM) as high concentrations of *Sso*DnaG promote aggregation rendering the enzyme inactive.

The priming ability of *Sso*DnaG-D179A (17.2 ± 1.0 pmol min^{-1}) was not significantly affected compared to wild-type (21.6 ± 0.5 pmol min^{-1}), but mutations at D220A (6.3 ± 0.5 pmol min^{-1}) and D222A (6.6 ± 0.5 pmol min^{-1}) had a 3-fold reduction in priming activity **(Figure 5.8 D-E)**. The composition of primers generally consists of two major products, a 13mer and a tetramer. However, the primer product distribution differs for D222A, where the amount of tetramer (4mer) is drastically reduced in favor of formation of a pentamer (5mer) product **(Figure 5.8 D)**.

5.4.4 Direct Interactions of *Sso*DnaG with both DNA and *Sso*MCM Inhibit Unwinding

To further test the mechanism of *Sso*MCM unwinding inhibition by *Sso*DnaG, we titrated the *Sso*DnaG mutants in unwinding reactions. Wild-type or the three metal binding mutants of *Sso*DnaG (D179A, D220A and D222A) were preincubated with radiolabeled forked DNA for 5 min at 60 ºC and then *Sso*MCM was added to initiate the reaction **(Figure 5.9)**.

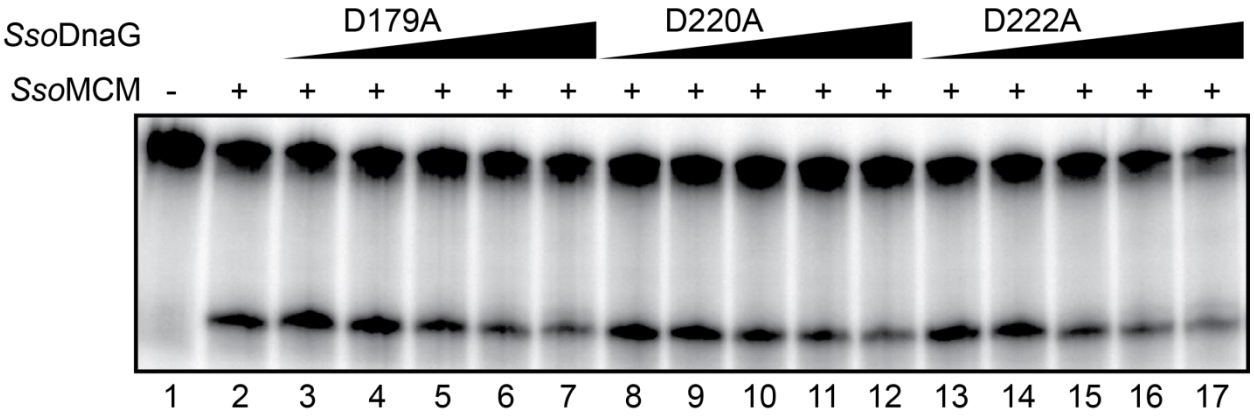

Figure 5.9: Effect of *Sso*DnaG Active Site Mutants on *Sso*MCM
Representative DNA unwinding assay on a denaturing acrylamide gel for 700 nM *Sso*MCM hexamer alone and in the presence of *Sso*DnaG mutants (350 nM, 700 nM, 2.1 µM, 4.2 µM and 6.3 µM for each set). Reactions are performed with 15 nM forked DNA at 60 ºC for 15 minutes.

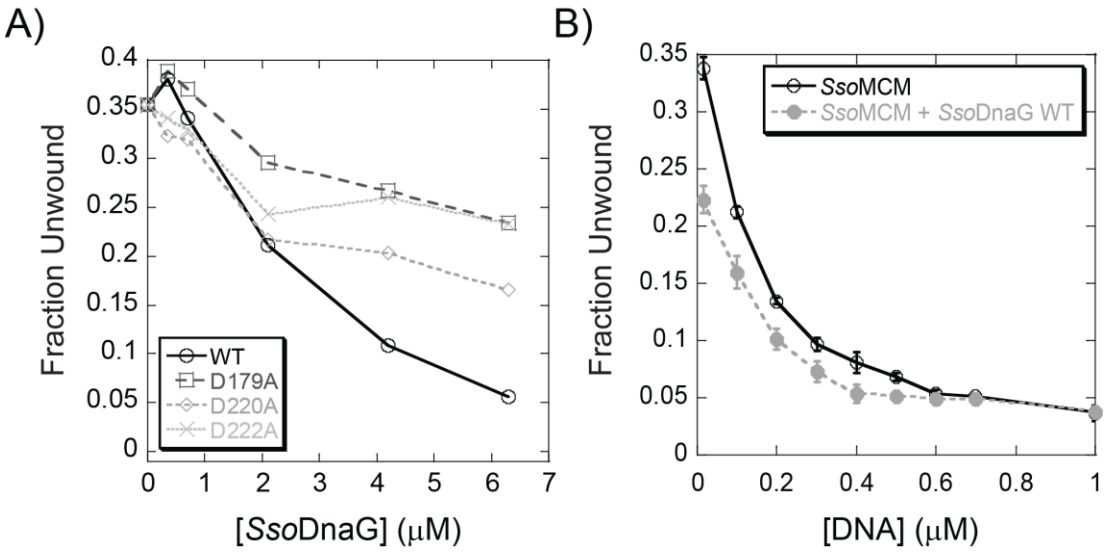

Figure 5.10: *Sso*MCM unwinding activity as function of increasing *Sso*DnaG or forked DNA concentrations.
A) Fraction unwound of forked DNA by *Sso*MCM hexamer (700 nM) as a function of *Sso*DnaG concentration at 60 °C for 15 min. The concentration dependence inhibition by wild-type (WT, -o-), D179A (-□-), D220A (-◊-), or D222A (-x-) *Sso*DnaG are shown. Error bars represent the standard error from at least three independent unwinding experiments. B) DNA titration of *Sso*MCM hexamer (700 nM) unwinding in the absence and presence of *Sso*DnaG (4.2 µM). Fraction unwound of forked DNA by *Sso*MCM in the absence (-o-) and presence (-●-) of *Sso*DnaG at 60 °C for 15 min. Error bars represent the standard error from at least three independent unwinding experiments.

In all cases, increasing concentrations of *Sso*DnaG inhibited *Sso*MCM unwinding, but the trends were different for the DNA binding mutants **(Figure 5.10 A)**. *Sso*DnaG concentrations less than 1 µM show little or no inhibition of *Sso*MCM. Unwinding inhibition is strongest at or above 2 µM where the *Sso*MCM: *Sso*DnaG ratio is 2:1. To show specificity, little to no unwinding inhibition by *Sso*DnaG was seen with the *Ec*DnaB helicase compared to *Sso*MCM **(Figure 5.11)**.

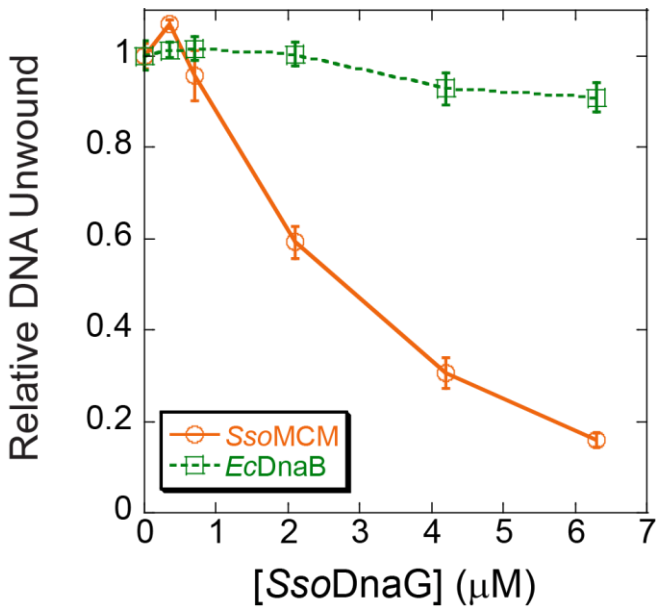

Figure 5.11: *Sso*MCM Helicase Activity is Only Reduced by *Sso*DnaG not EcDnaG
*Sso*MCM (orange, -o-) or *Ec*DnaB (green, -□-) unwinding activity as function of increasing *Sso*DnaG concentration. Relative fraction unwound of forked DNA by 700 nM *Sso*MCM hexamer (@ 60 °C) as in Figure 5.10 A or 700 nM *Ec*DnaB hexamer (@ 37 °C) for 15 minutes for *Sso*MCM and 10 minutes for *Ec*DnaB as a function of *Sso*DnaG concentration.

Interestingly, each of the aspartate mutants of *Sso*DnaG has less of an inhibitory effect on MCM unwinding than wild-type. At 4 μM where *Sso*DnaG:*Sso*MCM is essentially 1:1, the mutants inhibit 2-fold, while wild-type *Sso*DnaG inhibits 4-fold. We also tested the effect of increasing the DNA concentration on unwinding of *Sso*MCM in the absence and presence of equal molar amounts of *Sso*DnaG **(Figure 5.10 B)**. For these experiments, *Sso*MCM and *Sso*DnaG were added simultaneously to initiate the unwinding reaction. At the lowest concentration of forked DNA, there is a significant reduction in the fraction unwound. As the DNA concentration increases towards 700 nM, where there is equal molar *Sso*MCM hexamer:DNA, there is a reduction in *Sso*DnaG's ability to inhibit unwinding consistent with competition of *Sso*MCM and *Sso*DnaG for binding DNA. The individual binding affinities (K_d) for hexameric *Sso*MCM is 4-fold lower (26 nM)[15] than for *Sso*DnaG **(Figure 5.8)**. Therefore, at low DNA concentrations, *Sso*MCM binding to DNA will be favored followed by secondary binding of *Sso*DnaG to the *Sso*MCM-DNA complex. At higher DNA concentrations, the equilibrium of the *Sso*MCM-DNA-*Sso*DnaG ternary complex will rearrange in favor of individual binding of each enzyme to DNA.

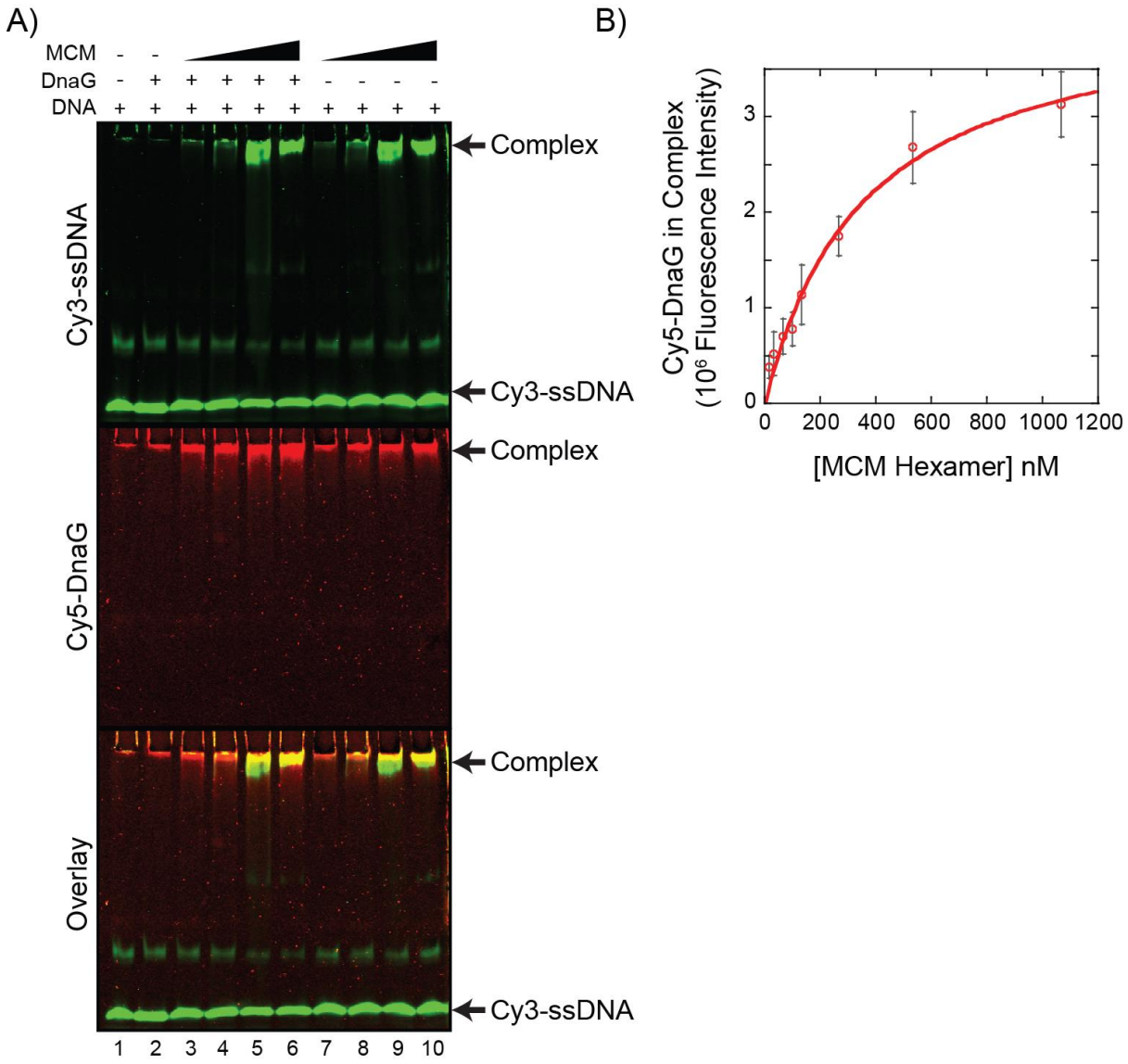

Figure 5.12: Fluorescent EMSA
Fluorescent EMSA demonstrating the ternary complex (TC) of *Sso*MCM-ssDNA-*Sso*DnaG. A) Separate channels of a fluorescent EMSA showing signals for 100 nM 66mer 3'-tail-30 nt (5'Cy3) ssDNA, 200 nM Cy5-DnaG, and the overlay for a titration of *Sso*MCM (16-1066 nM hexamer) (lanes 3-10). Lane 1 is Cy3-ssDNA alone and lane 2 is *Sso*DnaG and Cy3-ssDNA. B) A plot of the Cy5-*Sso*DnaG intensity contained in the complex band versus *Sso*MCM hexamer concentration. A fit of the data to Equation 5.1 gives a K_d of 360 ± 60 nM. Error bars represent the standard error from at least three independent EMSA experiments.

In order to clearly identify the presence of a stable ternary complex, fluorescent EMSA experiments were used to show and quantify binding of *Sso*DnaG to *Sso*MCM-DNA **(Figure 5.12 A)**. Unlabeled *Sso*MCM was titrated into a constant amount of 3'-tail-30 nt (5'Cy3) ssDNA (100 nM) in the presence and absence of N-terminally Cy5-labeled *Sso*DnaG (200 nM). Cy5-*Sso*DnaG in the absence of *Sso*MCM does not significantly form a stable complex with DNA **(Figure 5.12 A, lane 2)**. Titration of *Sso*MCM promotes the ternary complex formation as indicated by an increase in the Cy5-*Sso*DnaG signal towards the top of the gel **(Figure 5.12 A, lanes 3-5)**. Notably, the concentration of Cy5-*Sso*DnaG does not change across the gel; rather, it becomes more concentrated near the top of the gel only as *Sso*MCM is titrated. *Sso*DnaG alone does not efficiently enter the gel under these experimental conditions nor does it form a stable complex with DNA at these concentrations.[48] At the higher concentrations of *Sso*MCM (especially lanes 3-5), there is a significant amount of ternary complex formed presumably by sequestering *Sso*DnaG within the complex for entry into the gel. Importantly, titration of unlabeled *Sso*MCM to Cy3-labeled ssDNA is required before *Sso*DnaG is able to bind and form the ternary complex. When *Sso*DnaG is absent in the reaction, binding of *Sso*MCM to DNA shifts the ssDNA towards the top of the gel similarly to form a binary complex **(Figure 5.13 B, lanes 3-10)**. The molecular weight of a binary *Sso*MCM-DNA complex alone is ~500 kDa and cannot be resolved from larger ternary complexes that include *Sso*DnaG. Background Cy5 fluorescence intensity due to overlapping excitation spectra in Cy3 only lanes was subtracted from the Cy3-Cy5 lanes from parallel reactions **(Figure 5.13)**.

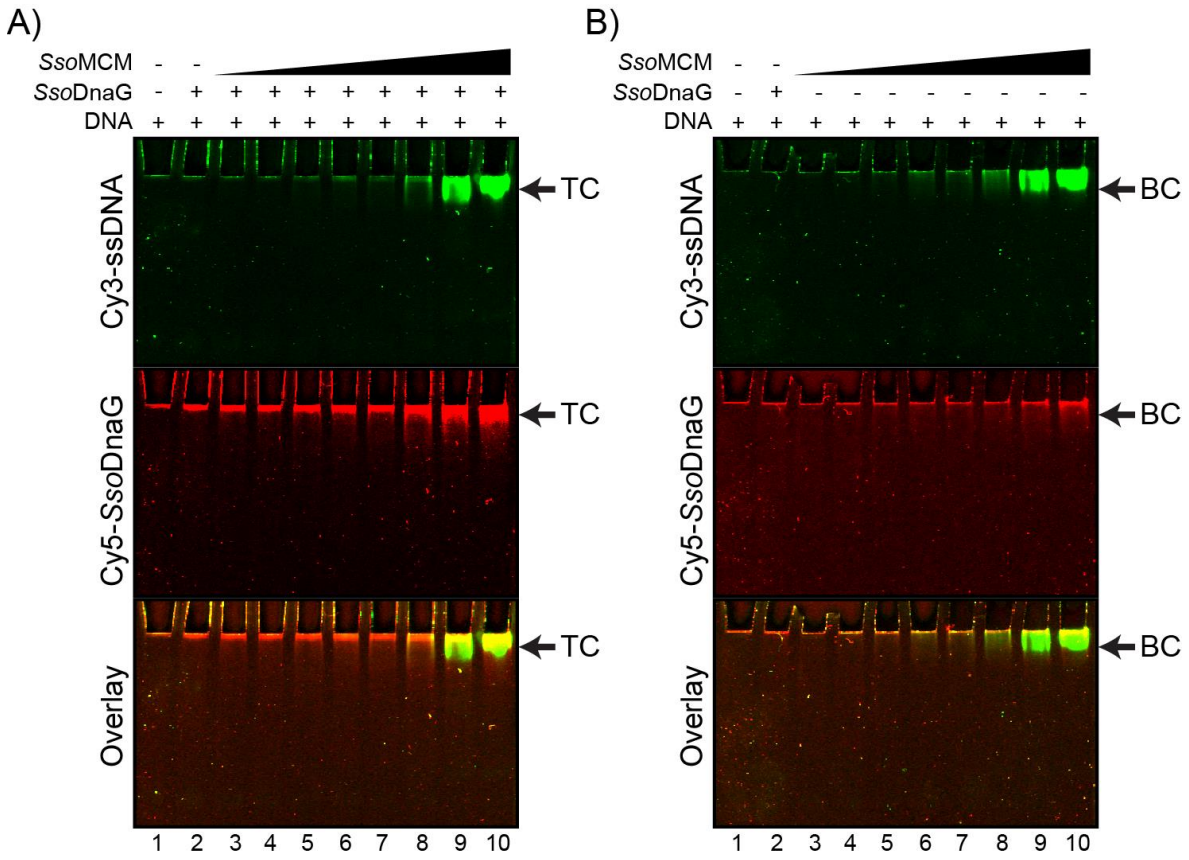

Figure 5.13: DnaG MCM DNA Ternary Complex
Fluorescent EMSA demonstrating the A) ternary complex (TC) of *Sso*MCM-ssDNA-*Sso*DnaG or B) the binary complex (BC) of *Sso*MCM-ssDNA in the presence and absence of *Sso*DnaG, respectively. Separate channels of a fluorescent EMSA showing signals for 100 nM 66mer 3'-tail-30 nt (5'Cy3) ssDNA, 0 or 200 nM Cy5-DnaG, and a titration of unlabeled *Sso*MCM (16-1066 nM hexamer). A Cy5-DnaG-DNA complex (lane 2) does not stably form alone at these concentrations. Only upon increasing MCM concentrations (lanes 3-10) does the Cy5 signal (from constant DnaG concentration) appear near the top of the gel. Free unbound Cy3-DNA was electrophoresed off of this particular gel to highlight BC and TC.

A plot of the Cy5-*Sso*DnaG fluorescence intensity in the complex band towards the top of the gel averaged from at least three independent reactions gives an apparent K_d of 360 ± 60 nM for the *Sso*MCM-DNA-*Sso*DnaG ternary complex **(Figure 5.12 B)**. This value is estimated to be at least an order of magnitude lower than a *Sso*MCM-*Sso*DnaG binary complex in the absence of DNA isolated in the GST pulldown assays above and data not shown. More important than absolute quantification, these results show that binding of *Sso*DnaG is dependent on both the presence of *Sso*MCM and DNA to form a ternary complex.

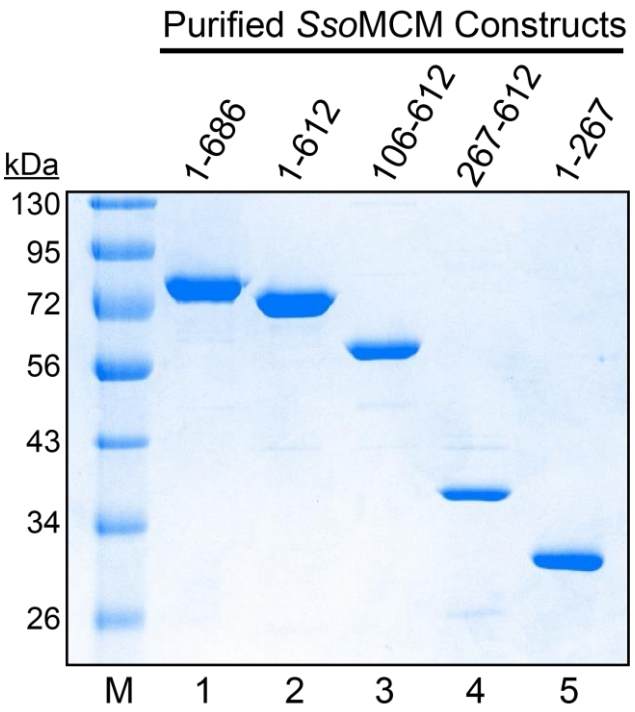

Figure 5.14: Purification of *Sso*MCM Truncation Constructs
Coomasie stained SDS-PAGE gel of *Sso*MCM constructs. Shown are purified full length untagged *Sso*MCM (1-686) and truncation (1-612, 106-612, 267-612, and 1-267) proteins.

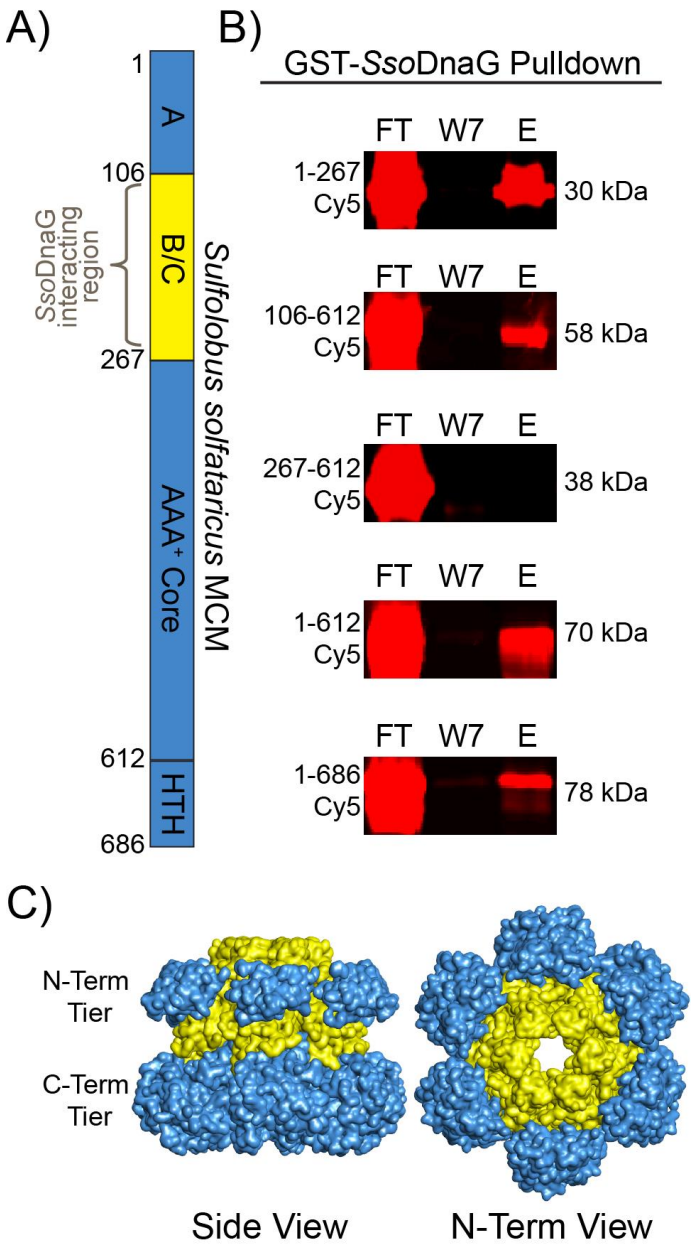

Figure 5.15: Fluorescent Pulldown Assay
Binding of *Sso*DnaG to *Sso*MCM is localized to the N-terminal B/C domain. A) Schematic of the protein sequence of *Sso*MCM mapped for *Sso*DnaG binding identifying individual domains. B) Fluorescent GST-*Sso*DnaG pulldown assays showing binding of N-terminal Cy5-labeled domains of *Sso*MCM (amino acids 1-267, 106-612, 267-612, 1-612, and full length 1-686). Shown are fluorescent images of specific regions of SDS-PAGE gels of *Sso*MCM domain flow through (FT), the seventh wash (W7), and elution (E) with glutathione. C) *Sso*MCM hexamer model (PDBID: 3F9V) highlighting the *Sso*DnaG interacting region (amino acids 106-267) in yellow.

The truncated *Sso*MCM constructs had oligomeric states generally consistent with His-tagged versions previously published[8] with 267-612 in a monomer-dimer state and 1-612 and 106-612 as hexamers (data not shown). The only subtle difference is that 1-267 is either a dimer-trimer instead of monomer-dimer[8] as identified by gel filtration (data not shown), but this is likely a concentration dependent effect. Each *Sso*MCM construct was labeled specifically with Cy5 at the N-terminus, and the ratios of *Sso*MCM:Cy5 were essentially 1:1 in all cases. GST-*Sso*DnaG

was incubated with various Cy5-labeled *Sso*MCM truncation constructs and immobilized to a glutathione sepharose column. After extensive washing, we observed an interaction between *Sso*DnaG and all *Sso*MCM constructs except 267-612 after elution with glutathione **(Figure 5.15)**. Mock experiments in the absence of GST-*Sso*DnaG showed no significant background *Sso*MCM binding for any construct **(Figure 5.16)**. Because both 1-267 and 106-612 showed an interaction with GST-*Sso*DnaG, we can confine the interaction site to the B/C domain of *Sso*MCM (residues 106-266). Mapping residues 106-266 onto the hexameric model of the crystal structure of *Sso*MCM [9] identified the extreme N-terminal tier as the most probable *Sso*DnaG interaction site **(Figure 5.15 C, yellow)**.

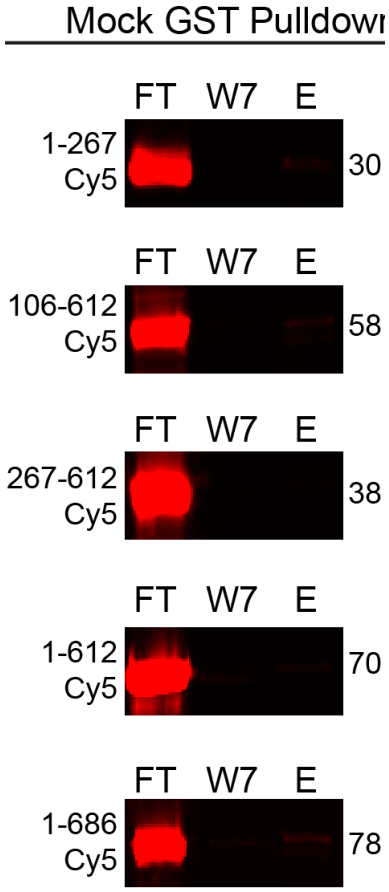

Figure 5.16: Mock Pulldowns
Mock fluorescent pulldown assays with GST resin and N-terminal Cy5-labeled domains of *Sso*MCM (amino acids 1-267, 106-612, 267-612, 1-612, and full length 1-686). Shown are fluorescent images of specific regions of SDS-PAGE gels of *Sso*MCM domain flow through (FT), the seventh wash (W7), and elution (E) with glutathione. No significant background binding of any Cy5-labelled MCM construct is noted.

5.5 DISCUSSION

The DNA replisome is a large dynamic assembly of multiple proteins required for efficient synthesis on the leading and lagging strands. The interactions and coordination of protein subunits and complexes within the bacterial replisome have been well characterized structurally and biochemically. The eukaryotic replisome is much more complex adding an additional dimension of regulation to DNA replication. Therefore, the archaeal DNA replisome is quickly becoming an appropriate core model for the more complex eukaryotic replisome, but it suffers from incomplete evolutionary linearity. For example, DNA priming in Archaea is complicated by the fact both bacterial (DnaG) and eukaryotic-type (PriSL) primases are conserved throughout this domain with similar *in vitro* priming activities.[48] Here, we report the surprising result that the bacterial-like DnaG primase from *Sulfolobus solfataricus* (*Sso*DnaG) physically interacts with the eukaryotic-like *Sso*MCM helicase forming a ternary complex on DNA. The site of interaction at the N-terminus of *Sso*MCM is analogous to primosome complexes from bacteria and phage. Conserved acidic active site mutants of *Sso*DnaG (D220A and D222A) show decreased binding affinity to ssDNA as well as decreased priming activity verifying functional homology to bacterial *Ec*DnaG. The unwinding activity of *Sso*MCM is inhibited in the presence of *Sso*DnaG by probable restriction of the *Sso*MCM conformation or disruption of the interaction with the DNA strands. Characterization of this unique primosome-like complex supports a role for the *Sso*DnaG primase in archaeal DNA replication as well as provides important evolutionary links between bacterial and eukaryotic DNA replication mechanisms.

The interaction between the DnaG primase and DnaB helicase constitutes the bacterial primosome and is a well characterized subcomplex within the replisome.[275, 276] After separation of bacterial genomic DNA, the lagging strand passes through the central channel of the DnaB helicase before encountering the DnaG primase for RNA primer synthesis.[27] DNA priming on the lagging strand of eukaryotes is not as well characterized but is thought to be coupled to polymerase ε through interaction with the GINS complex.[277, 278] Although a direct primase-MCM interaction has never been detected in Archaea, there is precedent from a single gene from the bacterium, *Bacillus cereus*, which encodes an MCM helicase with a putative DNA primase domain at the N-terminus.[279, 280] Interestingly, direct interactions between the eukaryotic primase (pol-

prim) and SV40 Large T antigen (a functional MCM homolog) are known to be required for efficient primer synthesis most likely by orientating pol-prim in a proper orientation for catalysis and increased binding affinity.[25, 281]

5.5.1 Archaea DNA Primase Dichotomy

Archaeal organisms are the only domain of organisms that contain two purported DNA primases: a eukaryotic-like PriSL and a bacterial-like DnaG. Archaeal *Sso*PriSL is known to interact with the *Sso*GINS complex involved in helicase complex regulation, assembly, and function but has no effect on priming or unwinding activity.[67] Instead it is hypothesized that *Sso*GINS acts as a molecular bridge between *Sso*MCM and *Sso*PriSL coupling but not increasing activities. The clamp-loader, *Sso*RFC, is also found to interact with *Sso*PriSL, but its presence inhibited full length primer formation by competing *Sso*PriSL off of the DNA template.[271] Interaction of *Sso*PriSL with either *Sso*GINS or *Sso*RFC could support a role in primer hand-off on the lagging strand but may also be consistent with trailing the *Sso*MCM helicase complex on the leading strand and behaving more like a DNA polymerase than a primase under certain conditions. In addition to ribonucleotide synthesis ability, archaeal PriSL has robust deoxynucleotide synthesis activity leading to long template dependent and independent DNA products.[61, 63, 64] Phylogenetic analysis has revealed that archaeal PriSL may have evolved from a common ancestor of the B-family DNA polymerase,[266] but continued evolution into eukaryotes resulted in DNA polymerase X-family members known for terminal transferase (TdT) activity and participation in double strand break (DSB) repair.[69, 282] Analogously, *Sso*PriSL by itself has been shown to have promiscuous TdT activity[64] that facilitates discontinuous polymerization across multiple templates mimicking DSB repair.[65] *Sso*PriSL also interacts with Rad50 which is involved in double strand break repair[283] and is upregulated slightly in the presence of UV damage.[49] Although PriSL is suggested to be the DNA primase in Archaea, the experimental evidence is actually more consistent with a DNA polymerase repair role.[65, 284]

Unfortunately, experimental results on the role of archaeal DnaG are also conflicting. Previously, *Sso*DnaG was found to interact with the exosome, but definition of a functional role is hampered by no detectable associated enzymatic activity.[267, 285] The exosome is a large

multisubunit complex responsible for degradation and turnover of nascent mRNA transcripts and has exactly the opposite activity of a DNA primase. *Sso*DnaG has been found to exist in at least two different populations in both soluble and membrane bound states in the archaeal cell.[286-288] Interestingly, DNA replication in Archaea was also recently found to be localized at the same peripheral membrane location.[289] It is possible that the oligomeric state of *Sso*DnaG or interactions with other proteins modulate its activity to more than one location and metabolic process in Archaea.

On the other hand, the *in vitro* enzymatic primase ability of archaeal *Sso*DnaG is clear. *Sso*DnaG synthesizes discrete RNA primers of 13 nucleotides in length as well as smaller dimer and tetramer products selecting against deoxyribonucleotides.[48] Moreover, the core TOPRIM active site of DnaG is conserved between Bacteria and Archaea. In addition to the essential glutamate involved in chemistry of primer synthesis,[48] we have now characterized additional proposed metal binding aspartates that when mutated mimic the phenotypes of *Ec*DnaG mutants.[19, 40, 273, 274] Interestingly, only E175Q abolished priming activity,[48] while D220A and D222A only reduce priming. *Sso*DnaG also has a relatively high affinity to bind ssDNA even though it lacks the N-terminal zinc binding domain (ZBD) found in *Ec*DnaG. The metal binding aspartate dyad mutants (D220A or D222A) in particular decreased the binding affinity of DNA to unmeasurable values. In *E. coli*, the homologous residues (D309/D311) have recently been verified to coordinate metals A and B, respectively, required for nucleotide binding and catalysis.[19] Mutation of *Sso*DnaG D179A reduced DNA binding to micromolar affinity but did not significantly affect priming under the conditions tested. The homologous aspartate (D269) in *Ec*DnaG seems to coordinate a third metal C only upon nucleotide binding.[19] Therefore, it seems that for *Sso*DnaG, coordination of metals A and B by E175, D220, and D222 disrupts binding of catalytic metal A, reducing DNA binding and priming activity; while coordination of metal C by D179 has much less of an inhibitory effect. The cumulative mutagenesis results for *Sso*DnaG are strikingly similar to *Ec*DnaG and suggest a high degree of conserved structural and functional features of priming between the archaeal and bacterial TOPRIM domains.

5.5.2 Architecture of a Potential Archaeal Primosome Complex

After validating that archaeal *Sso*DnaG interacts with *Sso*MCM using yeast two hybrid assays, pull down assays, and EMSAs, we mapped the interacting region to the extreme N-terminal tier of *Sso*MCM. Interestingly, this interaction site is analogous to interactions and orientations found in bacterial and phage primase-helicase complexes.[27, 275, 290] Importantly, *Sso*DnaG stimulates the basal ATPase activity of *Sso*MCM suggesting that their interaction promotes the arrangement of the hexamer into a more active state. By separately monitoring, ssDNA, *Sso*DnaG, and *Sso*MCM using fluorescent EMSA experiments, we can now verify that a ternary primosome complex exists with reasonable affinity. The interaction of *Sso*MCM and *Sso*DnaG without DNA is much weaker and is similar to interactions between DnaG and DnaB in *E. coli*.[29] Therefore, stable ternary complex formation is dependent on interactions of *Sso*DnaG with both DNA and *Sso*MCM.

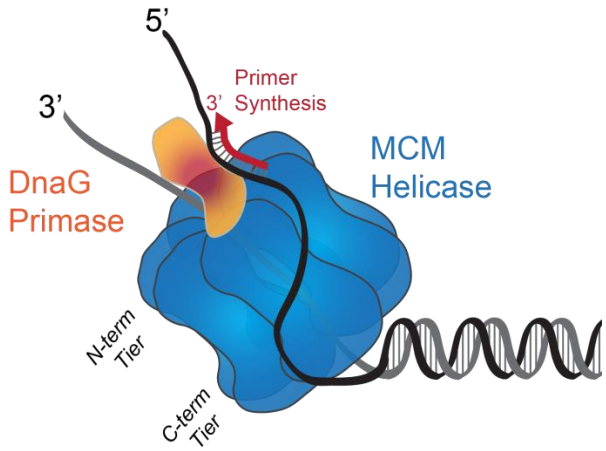

Figure 5.17: Primosome Model
Model of a proposed archaeal DnaG–MCM primosome complex on DNA. MCM (blue) encircles the 3′-strand placing the C-terminal tier towards the duplex region and the N-terminal tier towards the 3′-end. The excluded 5′-strand interactions are on the exterior surface of the MCM helicase in the SEW model. DnaG (orange) interacts at the extreme N-terminal tier of MCM poised to synthesize RNA primers on the lagging strand.

We have previously suggested that *Sso*DnaG minimally forms a dimer on DNA but also has the tendency to aggregate at high concentrations.[48] Bacterial DnaG also has the propensity to self-associate but only when bound to DnaB as a mechanism to control primer length.[23, 291] Because *Sso*MCM (267-612) had a significant monomer population and showed no detectable interaction with *Sso*DnaG, it is also possible that *Sso*DnaG interacts minimally with a dimer of

*Sso*MCM. Nevertheless, the interaction of *Sso*DnaG is also seen with *Sso*MCM (1-267) consistent with N-terminal tier binding. The stoichiometry of bacterial or phage helicase to primase subunits varies from 1:1 to 6:1.[21, 24, 27, 31-33] The absolute ratio of *Sso*MCM to *Sso*DnaG will require further future experiments, but in our model **(Figure 5.17)**, newly separated and excluded DNA will interact with the external surface of *Sso*MCM in the steric exclusion and wrapping (SEW) unwinding model[15] before being handed off to the interacting *Sso*DnaG primase. Interactions of the lagging strand template on the external surface of *Sso*MCM will provide the flexibility needed for coupled unwinding and priming activities.[292] Our unwinding experiments in the presence of *Sso*DnaG and associated mutants would suggest *Sso*MCM is rendered in an inactive conformation for unwinding possibly by disrupting the *Sso*MCM interaction with the 5'-tail known to be important for unwinding in the SEW mechanism.[15] Alternatively, *Sso*DnaG may alter the conformation of the *Sso*MCM hexamer and its interactions with the encircled 3' DNA strand inhibiting unwinding and preventing further stimulation of the ATPase rate. Because the priming activity is unaffected, the binding of DNA to *Sso*DnaG is unaffected. It may be that additional factors are required for formation of an optimal primosome conformation required for efficient coupled priming and unwinding activities.

Formation of the bacterial primosome increases both the priming and unwinding activities of DnaG and DnaB, respectively.[22, 24, 29] We were unable to see stimulation in either primer synthesis or DNA unwinding when *Sso*DnaG and *Sso*MCM were included together, but the ATPase activity of *Sso*MCM was stimulated in the presence of *Sso*DnaG. Analogously, *Sso*PriSL priming inhibition was also seen upon interaction with *Sso*RFC with increased *Sso*RFC ATPase activity.[271] Unlike *Ec*DnaG, *Sso*DnaG has a relatively high DNA binding ability by itself and may not require interactions with the helicase to increase catalytic priming ability through recruitment to the template. Increased ATPase activity of *Sso*MCM suggests that *Sso*DnaG interacts specifically and causes a conformational change within the hexamer to stimulate the hydrolysis activity. This conformation is different than a *Sso*MCM-DNA complex as further simulation in ATPase activity was not seen when forked DNA is added suggesting that *Sso*MCM is interacting with DNA in an incompetent state.

The inactive *Sso*MCM-DNA-*Sso*DnaG ternary complex can be controlled by equilibria processes. Unwinding inhibition was strongest at or above stoichiometric concentrations of

*Sso*DnaG or when DNA is limiting. When the conserved acidic *Sso*DnaG active site residues were mutated, the inhibitory effect on DNA unwinding was reduced. Because the *Sso*DnaG aspartate mutants also show reduced DNA binding affinity, we suspect that unwinding inhibition is caused through interaction with both DNA and *Sso*MCM. The EMSA experiments show that *Sso*DnaG is assembled on the *Sso*MCM-DNA template, but the ATPase assays reflect that although *Sso*MCM is arranged in a more competent ATP hydrolysis state, its unwinding activity is compromised. Larger DNA templates or interactions with other pre-replication proteins may be required to load and arrange *Sso*MCM in an active unwinding complex in the presence of *Sso*DnaG.

In addition to the novel archaeal DnaG-MCM complex described here, it is also possible that alternative primosome complexes include PriSL as the active primase using GINS to mediate interactions between the MCM helicase, but without evidence of an associated change in activity, it is speculative. Alternatively, Archaea may utilize a dual primase system to initiate DNA replication on the leading and lagging strands with either PriSL or DnaG acting specifically on one strand. Unfortunately, stable associations of DNA primases with members of the replisome are not characteristic and therefore difficult to detect. Hence, future experiments aimed at dissecting stoichiometries, interaction sties, and the specificities of each archaeal primase compared with *in vivo* synthesized RNA primers or Okazaki fragments will be essential in differentiating the roles of these primase enzymes in Archaea.

5.6 CONCLUSION

This chapter describes the discovery and characterization of an archaeal primosome complex. Prior to this, primosomes were primarily observed in bacterial systems between DnaG and the bacterial DnaB helicase. Formation of the bacterial primosome increases both the priming and unwinding activities of DnaG and DnaB, respectively.[22, 24, 29] Here we describe the first observed example of an interaction between a bacterial-type primase (DnaG) and a eukaryotic-like helicase (MCM). The interaction was verified through use of yeast 2-hybrid, fluorescent pulldown assays, and functional studies. However, unlike the observed increase in priming and unwinding

seen for the bacterial primosome, this archaeal primosome shows no increase in priming activity, and has a decreased ability to unwind DNA. These observations have led us to believe that other proteins may be involved in the formation of this complex, which are necessary to produce a fully functional, and stimulated primosome in Archaea.

APPENDIX A: QUANTIFICATION OF ROCK AND SHROOM INTERACTIONS[6]

A.1 SUMMARY

The Rho-associated coiled coil containing protein kinase (Rock) is a well-defined determinant of actin organization and dynamics in animal cells. Regulation of Rock is thought to occur through auto inhibition of the kinase domain through intermolecular interactions with its N-terminus. This regulation can be relieved through a variety of interactions including the recently identified interaction with the Shroom (Shrm) proteins. Through the use of FRET and fluorescence anisotropy have quantified the strength of the interaction between Rock and Shrm in both Humans and D*rosophila*. Additionally we have validated the importance of surface residues in the Rock-Shroom binding domain (SBD) in the interaction between these two proteins.

A.2 BACKGROUND

Cellular processes which change cell and tissue morphology, are often driven by the formation of contractile networks of F-actin and non-muscle myosin II.[(293)] The contractions of this network and the resulting changes to cellular shape are necessary for the development of many types of tissues including heart, gut and central nervous system.[(294-297)] The signaling and mechanistic aspects of the process of apical constriction have been widely studied, having been

[6] Material from this appendix is derived from the following articles:

Das D., Mohan S., **Bauer R.J**., Heroux A., Trakselis M.A., Hildebrand J.D., and VanDemark A.P. (2013) Structure of a Highly Conserved Domain of Rock1 Required for Shroom-Mediated Regulation of Cell Morphology. PLoS ONE 8(12): e81075.

Mohan S., Rizaldy, R., Das, D., **Bauer, R.J**., Heroux, A., Trakselis, M.A., Hildebrand, J.D., and VanDemark, A.P. (2012) Structure of the Shroom Domain 2 Reveals a Three-Segmented Coiled-Coil Required for Dimerization, Rock Binding, and Apical Constriction. *Molecular Biology of the Cell*, 23, 2131-2142.

shown in the context of a variety of systems that apical constriction is driven by the contraction of a mesh of actin bundles. The mechanical force is supplied by myosin II, the motion of which is triggered via signaling pathways resultant from phosphorylation of myosin regulatory light chain (MRLC). MRLC phosphorylation has been reported for several cases, including but not limited to the Rho- associated coiled coil containing protein kinase (Rock). *(298-300)*

Vertebrates have two different Rock proteins, Rock 1 and Rock 2 which share 65% of sequence identity. Both proteins possess an N-terminal kinase domain, a central coiled coil region and C-terminal pleckstrin homology and cysteine rich domains. The Rock kinase domain has a Serene/Threonine kinase fold, similar to protein kinase A, consisting of two kinase lobes linked by a hinge.*(301)* The N and C terminal extensions from the kinase domain aide in dimerization and are required for activity.*(302, 303)* The activity of Rock is tightly controlled by several different mechanisms. The predominant mechanism is relief of intramolecular inhibition of the kinase domain by the C-terminus. The predominant mechanism is relief of intramolecular inhibition of the kinase domain by the C-terminus. This is typically resultant from binding of GTP-bound RhoA to the Rho-binding domain found within the coiled-coil domain of Rock.*(304)* Additionally the Shroom domain 2 (SD2, residues 1563-1968) of the Shroom protein from *Mus musculus* has also been shown to interact with this coiled-coil domain, where binding site was identified on hRock to be within residues 698-947.*(305)*

The Shroom (Shrm) family of actin-binding proteins play essential roles in the development of many tissues including the nervous system, heart, vasculature and gut.*(294, 295, 297)* These proteins have been found to control cell morphology and tissue architecture by regulation of the subcellular distribution of actomyosin networks and use these to cause apical constriction. Shrm proteins are found in both vertebrates and most invertebrates, and analysis of a variety of these proteins suggests that Shrm activity is conserved. In vertebrates there are four different family members of Shroom, with Shrm3 being the most extensively characterized of the group. The interaction between Shrm3 and the Rock protein has been shown to be essential for Shrm3-induced apical constriction.

The Shroom-SD2 is a unique motif not found in any other protein. It has been identified as essential for the apical constriction of neural cells during development of the embryonic nervous system, through interaction between itself and actin.*(306)* It is also capable of causing changes in

cellular structure through interactions with Myosin and γ-Tubulin[307]. Here in the following appendix I detail the characterization of the interaction between Shrm proteins from both the human (hShrm2-SD2) and *Drosophila* (dShrm-SD2) systems and their interactions with their respective Rock binding partners (hRock1 and dRock, respectively).

A.3 MATERIALS AND METHODS

A.3.1 Fluorescence Labeling of dShrm-SD2, dRock and hShrm2-SD2

Purified forms of dShrm-SD2, dRock, were obtained from Andrew VanDemark's laboratory (U. Pittsburgh). dShrm-SD2 was labeled at the N-terminus with Alexa 594 succinimidyl ester (Invitrogen) in amino labeling buffer (20 mM Hepes pH 7.0, 100 mM NaCl, 8% glycerol) or at C1428 of the C1533S mutant with Cy3 or Cy5 maleimide (GE Healthcare) in cysteine labeling buffer (20 mM HEPES, pH 7.6 100 mM NaCl, 8% glycerol). Small (amino acids 821-938) dRock was labeled at C862 with Cy3 maleimide as described. Large dRock (amino acids 724 -938) was labeled at the N-terminus with Cy5 succinimidyl ester (GE Healthcare) in amino labeling buffer. All labeling reactions included 10x molar excess of flourophore, reacted at room temperature for 2h. Labeling of hShrm2-SD2 was performed similarly with Oregon Green 488. Excess flourophore was removed from the samples through extensive dialysis with labeling buffer. The labeling efficiency was quantified using the extinction coefficient of the dye compared with the protein concentration determined from a standard curve using a Bradford assay and found to be essentially 1:1.

A.3.2 FRET Binding Experiments

FRET titrations were performed in dShrm reaction buffer, using a 50 nM Cy3-labeled dShrm-SD2 or dRock and increasing concentrations of Cy5-labeled dRock or dShrm-SD2. Cy3 was excited at 552 nM and the donor emission maximum (563 nm) was corrected for dilution,

normalized and plotted as a function of protein concentration as the average of three independent experiments. Fluorescence quenching (F_Q) titrations were fitted to a single binding equation:

$$F_Q = \frac{\Delta F_Q X\ [dRock]}{K_d + [dRock]} \quad \text{(A.1)}$$

Where ΔF_Q is the normalized change in donor fluorescence intensity and K_d is the dissociation constant.

A.3.3 Fluorescence Anisotropy Binding Experiments

Fluorescence anisotropy measurements were performed in (20 mM Hepes pH 7.4, 100 mM NaCl, 5% glycerol) using 20 nM of N-terminally labeled hShrm2-SD2-Oregon Green 488 and increasing concentrations of hRock1 SBD. Measurements were collected as described previously using a Floromax-3 fluorimeter (Horiba Jobin Yvon).[78]

Labeled proteins were excited at 496 nm and emission was monitored at 524 nm using 5-second integration times for three consecutive readings. The reported anisotropy values (r) are the average of at least three independent experiments and fit to a single binding model:

$$r = \frac{\Delta A * [P]}{K_d + [P]} \quad \text{(A.2)}$$

where A is the amplitude, P is the concentration of hRock1 SBD and K_d is the dissociation constant.

A.4 RESULTS

A.4.1 Characterization of dShrm-SD2/dRock Binding

The first set of experiments were performed on proteins derived from *Drosophila.* We set out to characterize the strength of the interaction between the dShrm-SD2 and dRock. This was achieved through utilizing the quenching of the donor fluorescence from Cy3-labeled dShrm-SD2 with Cy5-labeled dRock. As increasing concentrations of dRock-Cy5 were titrated into a 50 nM sample of dShrm-SD2-Cy3 the fluorescence intensity of the donor was observed to be quenched and the sensitization observed from the Cy5 acceptor dye (**Figure A.1 A**). The donor fluorescene quenching was normalized and the K_d for the interaction between dShrm-SD2 and dRock determined to be 0.58 ± 0.07 μM (**Figure A.1**).

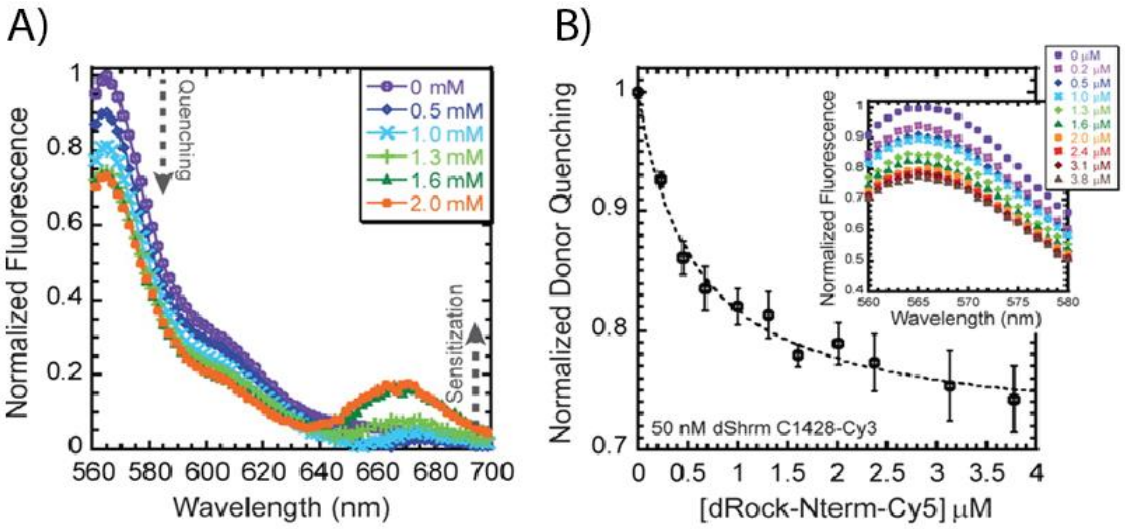

Figure A.1: Characterization of dShrm-SD2 and dRock Binding
A) FRET titration of Cy5-labeled dRock into 50 nM Cy3-labeled dShrm-SD2 (dShrm) showing donor quenching and acceptor sensitization for representative concentrations. B) Donor quenching plotted as a function of Rock concentration and fitted to Equation A.1 to give a K_d value of 0.58 ± 0.07 μM. The error bars show the standard error for the average of at least three independent experiments.

A.4.2 Analysis of the Effect of Mutations to the hRock1 Shrm Binding Domain

Previously the capacity to bind hShrm had been shown for a large central region within the coiled coil domain of hRock1 (residues 648-947). Calculation of disorder profiles indicated that residues 834-913 form a stably folding fragment within this region. Therefore, we also investigated the interaction between the hShroom-2-SD2 domain and a minimal Shrm binding domain (SBD) identified within a portion of the hRock1coiled coil region. Two separate hRock truncations were initially tested for their binding to hShrm2-SD2; hRock (834-913) which contains just the hShrm binding domain and hRock (707-946) which is almost the full size of the previously characterized binding region. Fluorescence anisotropy determined the K_d for the interaction between hShrm2-SD2 and the two hRock1 truncations. A slightly higher K_d was observed for hRock1 (707-946), 1.7 ± 0.2 μM, than for the smaller hRock1 (834-913), 5.3 ± 1.5 μM (**Figure A.2 A**).

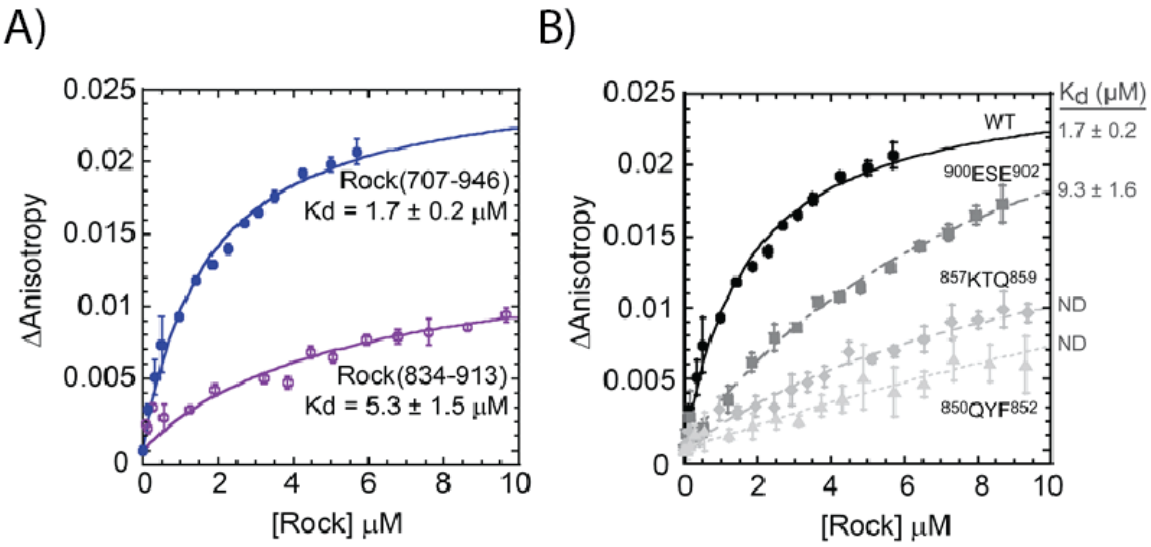

Figure A.2: Fluorescence Anisotropy Binding Curves
A) Rock fragments were assayed for binding to hShrm2-SD2. Increasing concentrations of Rock1 (707-946) or (834-913) were added to a reaction mixture containing 50 nM Oregon-Green labeled hShrm2-SD2 domain in a fluorescence spectrophotometer. The binding isotherm was fit to equation 1 using a non-linear regression to determine binding affinity (K_d). B) Fluorescence anisotropy experiments monitored 50 nM Oregon-green labeled hShrm2-SD2 domain with increasing concentrations of hRock1 (707-946) containing the indicated amino acid substitutions. The change in anisotropy was fit to equation A.2 to determine binding affinities (K_d) as indicated.

To further examine this binding region, and its importance to the interaction with hShrm2-SD2, a series of mutants were created throughout the SBD. The mutants ^{850}QYF^{852}, ^{857}KTQ^{859} and ^{900}ESE^{902}, where all listed residues were mutated to alanine, were chosen to examine the effects these mutations had on the ability of the SBD to bind hShrm2-SD2. While ^{900}ESE^{902} resulted in a modest 5.5 fold decrease in binding affinity, the other two mutations ^{850}QYF^{852}, ^{857}KTQ^{859}, were severely compromised, and prevented the accurate determination of binding affinity. (**Figure A.2 B**). This data helped identify that hRock possesses a single binding site for hShrm2-SD2 located between residues 839-860, with the surface exposed residues 850-859 critical to the interaction between the two proteins.

A.5 DISCUSSION/CONCLUSIONS

This set of collaborative work provided quantitative evidence for the interaction between Rock and Shrm-SD2 proteins in both Humans and D*rosophila*. It served as a method to validate other more qualitative methods, including pull-down and gel-shift assays, from the VanDemark laboratory that initially revealed interactions between the Shrm-SD2 domain and Rock. We quantified both the strength of this interaction in the D*rosophila* and identified specific residues important for binding using the human proteins. The results shown here validated the interaction between Shrm and Rock and formed the basis for further structural studies highlighting this heteroprotein complex.

APPENDIX B: GROWTH, MAINTENANCE, AND TRANSFORMATION OF *SULFOLOBUS* CULTURES[7]

B.1 INTRODUCTION

The *Sulfolobales* are a genus of domain Archaea, which grow optimally at a pH of 3.0 and a temperature of 75-80 °C.[(308)] The availability of the *Sulfolobus* genome, ease by which gene disruption can be achieved through utilization of homologous recombination pathways, and simple growth in the laboratory setting, make the *Sulfolobales* model organisms for the study of a variety of enzymatic processes, most notably DNA replication processes due to high sequence homology between crenarchaeal replication proteins and those found in eukaryotes.[(1, 96, 308-310)] *Sulfolobus acidocaldarius* is commonly utilized for genetic manipulation because the mechanisms of homologous recombination have been deciphered.[(311)] A genetic technique was developed allowing for allele replacement in the *Sulfolobus acidocaldarius* MR31 strain. MR31 are pyrimidine auxotrophs lacking a functional PyrE gene, necessary for the uracil biosynthesis pathway. Homologous recombination can be performed utilizing the PyrE auxotroph to allow for detection of the knockout of target genes on URA^- plates. This technique uses plasmid DNA which has been protected from degradation by *Sulfolobus acidocaldarius* restriction enzymes through altered methylation pattern of a modified *Escherichia coli* strain, ER2566.[(308)] Interestingly, it was found that the methylation of recombined DNA actually reduced the number of recombinantly transformed cells, and that un-methylated linear DNA was actually a preferred substrate.[(308, 312)] Thus genetic knockouts can be achieved through use of a linear, PCR produced, pyrE containing product.

[7] Media preparation referenced/modified from the following:

Robb F.T., and Place A. R. (Eds.), Archaea: A Laboratory Manual, Protocol 19 (Dennis Grogan) Cold Spring Harbor Press, 1995.

Kurosawa, N. and Grogan, D. W. (2005) "Homologous recombination of exogenous DNA with the *Sulfolobus acidocaldarius* genome: properties and uses." FEMS Micro Letters 253, 141-149

B.2 MATERIALS AND METHODS

B.2.1 Materials

Oligonucleotide substrates and primers were purchased from Integrated DNA Technologies (IDT, Coralville, IA) and are listed in **Table B.1**. All commercial enzymes were obtained from NEB (Ipswich, MA) unless otherwise indicated. All chemicals are analytical grade or better.

B.2.2 *Sulfolobus acidocaldarius* Liquid Media

1) Thoroughly rinse all bottles/flasks to be used in the preparation of *Sulfolobus acidocaldarius* media with ddH_2O. Removal of any soap residue is essential for the growth of the archaea.
2) Preparation of the trace mineral solution: combine 5.0 g $FeCl_3$, 0.5 g $CuCl_2$, 0.5 g $CoCl_2$, 0.5 g $MnCl_2$, 0.5 g $ZnCl_2$ into 100 mL 1 N HCl.
3) Preparation of 2X basal media: combine 6.0 g K_2SO_4, 1.0 g NaH_2PO_4, 0.6 g $MgSO_4$•7H_2O, 0.2 g $CaCl_2$•2H_2O, and 40 μL trace mineral solution. Adjust pH to 3.5 with H_2SO_4. Add ddH_2O to reach a final volume of 1 L.
4) Combine, in a 1L bottle: 2 g of D-xylose, 1g of tryptone, 500 mL of 2X basal media, and adjust the pH to 3.5 with H_2SO_4.
5) Dilute the media to 1L total volume with dd$H_2$0. The media cannot be autoclaved.

B.2.3 *Sulfolobus Acidocaldarius* MR31 Liquid Media

1) Thoroughly rinse all bottles/flasks to be used in the preparation of *Sulfolobus acidocaldarius MR31* (MR31 is a pyrimidine auxotroph Lacking a functional PyrE gene and thus media must be supplemented with uracil for growth) media with ddH_2O.
2) Preparation of 50X uracil solution: Weigh out 0.1 g of uracil and add to 100 mL ddH2O in a 100 mL bottle. (Final media uracil concentration should be 20mg/L.)

3) Place 50 mL of 2X basal media (see above) into a 100 mL bottle and add 0.2 g D-xylose and 0.1 g tryptone and 2 mL 50X uracil. Add ddH_2O until total volume is 100 mL. Store the media at 75 °C to prevent contamination, make fresh media every 2 weeks (discoloration of the media will occur as it spoils).

B.2.4 Solid URA- Plate Media

1.) Create concentrated *Sulfolobus acidocaldarius* liquid media (Only steps 1 - 3) as detailed above. Adjust pH to 2.9 with H_2SO_4, add 5 mL 2 M Mg_2SO_4 and 5 mL 500 mM $CaCl_2$, and heat the solution to 60 °C.
2.) In a 1L Flask, add 490 mL H20, heat to 60 °C and begin stirring with a stir bar. Slowly to this add 7 g of Gelrite (add extra slowly, Gelrite clumps). After the addition of all Gelrite, heat until boiling. Once completely dissolved, remove from heat.
3.) Immediately add concentrated media solution from 1) and pour into plates (150 X 15 mm). The plates must be poured while the Gelrite/Media is still hot (above 60 °C) as once it has solidified it cannot be re-melted. Cover the plates and allow them to solidify overnight. Place the plates into a sealed plastic bag, and store at 4 °C.

B.2.6 Growth of *Sulfolobus acidocaldarius* Liquid Cultures

1.) Note: Always start with small 3-5 mL cultures of *Sulfolobus acidocaldarius*, and scale up to larger cultures. The cells will not grow with very low initial cellular densities in liquid cultures.
2.) Place a 50 μL freezer stock of *Sulfolobus acidocaldarius*/*Sulfolobus acidocaldarius MR31* from -80°C storage on ice for 20 minutes.
3.) Place 3-5 mL of hot (75 °C) *Sulfolobus acidocaldarius*/*Sulfolobus acidocaldarius MR31* liquid media into a 50 mL tube, and inoculate with the entire 50 μL stock. If starting *Sulfolobus acidocaldarius* MR31 culture, additional uracil may be necessary in the media (up to 30 g/L). Culture volume must be sufficiently small to allow for adequate aeration of the sample.

4.) Allow for the culture to grow for 24 hours shaking (240 rpm) at 75 °C. Make certain the tube caps are tightly secured.
5.) Cultures must be restarted at least every 5 days. Culture restart is performed as follows: Place 5 mL of respective culture media into a new 50 mL tube, add 100 μL of 50X uracil, and 200 μL of the parent culture. Return the culture to the shaker and incubate at 75 °C.

B.2.7 Preparation of Competent *Sulfolobus acidocaldarius* Freezer Stocks

1) Harvest 5 mL of cells when OD_{540} = 0.3 – 0.5 by centrifugation 4000 x g for 5 minutes at 25 °C.
2) Wash the cells twice in 1.5 mL of cold 20 mM sucrose pH 5.6, pelleting each time as in 1.
3) Resuspend the cells in 750 μL of cold 20 mM sucrose pH 5.6, pellet as in 1.
4) Resuspend the cells in 500 μL of cold 20 mM sucrose pH 5.6, pellet as in 1.
5) Resuspend the cells in 500 μL cold 20 mM sucrose pH 5.6 containing 9% DMSO.
6) Create 50 μL aliquots, freeze in liquid nitrogen and store at -80 °C.
7) Competent cells can be used for transformation or starting new cultures, DMSO does not inhibit initial culture growth.

B.2.8 Electroporation of *Sulfolobus acidocaldarius MR31*

1) Inoculate 50 mL cultures of cells and let grow until OD540 = 0.3 - 0.5 (Approximately 12-15 hours), pellet cells, spinning 5 min 4000 x g 4 °C.
2) Re-suspend the cell pellet in 25 mL cold (4 °C) 20 mM sucrose pH 5.6 and re-pellet as in 1.
3) Re-suspend in 1mL 20 mM sucrose pH 5.6 and transfer to 1.5 mL tube. Pellet the cells for 2.5 min spinning 13,300 RPM, in bench top micro centrifuge at 4 °C. Re-suspend in 100 μL 20 mM sucrose pH 5.6 (this should be enough for 2 electroporation reactions). Final cell concentration should be ~ $1*10^{10}$ cells/mL.
4) Transfer 50 μL of the *Sulfolobus acidocaldarius*/Sucrose solution to a pre-chilled 0.1 -0.2 cm electroporation cuvette. Place on ice.

5) Add to the cells, 800 ng of the DNA sample to be transformed and incubate on ice for 5 min.
6) Electroporate with the following settings: **voltage: 1.5 kV, capacitance: 25 μF, resistance: 400 Ω, with a cuvette gap of 0.2 cm.** This should result in a time constant of ~ 7.4.
7) Immediately add 1 mL of media + uracil and transfer to 1.5 mL microfuge tube, incubate shaking at 75 °C for one hour.
8) Pellet cells in the microfuge for 2.5 min spinning 13,300 RPM at RT. Re-suspend cells into 100 μL fresh media, however lacking uracil (if performing PyrEF-Gene knockout).
9) Repeat step 8 one additional time to ensure removal of residual uracil. Plate the final re-suspended cells onto –URA *Sulfolobus acidocaldarius* plates, and place into a sealed bag which has been lined with dampened paper towels. Make sure the bag is tightly sealed with additional tape (To prevent moisture loss).
10) Place the bag into an additional sealed container (*i.e.* locking Tupperware), and place into the 75 °C incubator.
11) The plates and bag must be checked daily, to ensure the paper towels remain moist.
12) Growth of colonies should be observed within 5-7 days.

B.2.9 Culturing *Sulfolobus solfataricus* in Either DSM88 or 1829 Liquid Media

1) Thoroughly rinse all bottles/flasks to be used in the preparation of *Sulfolobus solfataricus* media with ddH_2O. Removal of any soap residue is essential for the growth of the archaea.
2) Prepare 100X DSM88 metals solution: combine in a 1 L bottle 22 mg $ZnSO_4$•$7H_2O$, 2 mg $CuCl_2$•$2H_2O$, 3 mg Na_2MoO•$2H_2O$ 3 mg $VOSO_4$, 1 mg $CoSO_4$, fill with ddH_2O until total volume reaches 1 L.
3) Prepare DSM88 *Sulfolobus solfataricus* liquid media: combine in a 1 L bottle 1 g yeast extract, 1 g casamino acids 1.3 g $(NH_4)_2SO_4$, 250 mg KH_2PO_4, 250 mg $MgSO_4$•$7H_2O$, 70 mg $CaCl_2$, 1.8 mg $MnCl_2$•$4H_2O$, 4.5 mg $Na_2B_4O_7$•$10H_2O$. 10 ml of 100X metals solution. (Media cannot be autoclaved)
4) Prepare 1829 trace elements solution (SL-10) Combine 100 mL 7.7M HCl, 1.5 g $FeCl_2$•$4H_2O$, 70 mg $ZnCl_2$, 100 mg $MnCl_2$•$4H_2O$, 6 mg H_3BO_3, 190 mg $CoCl_2$•$2H_2O$, 2 mg $CuCl_2$•$2H_2O$,

24 mg $NiCl_2$•$6H_2O$ 36 mg Na_2MoO4•$2H_2O$. Dissolve $FeCl_2$ in the HCl first, dilute the solution in 500 mL ddH_2O, dissolve all remaining salts and add remaining ddH_2O until total volume is 1 L.

5) Prepare 1829 *Sulfolobus solfataricus* Media 1 g yeast extract, 1 g casamino acids, 2.5 g $(NH_4)_2SO_4$, 3.1g KH_2PO_4, 200 mg $MgSO_4$•$7H_2O$, 200 mg $CaCl_2$, 10 mL trace elements solution, Add 500 mL ddH_2O. Adjust PH to 3.5 with H_2SO_4 at room temperature. Add ddH_2O until final volume is 1 L.
6) Note: Always start with small 3-5 mL cultures of *Sulfolobus solfataricus*, and scale up to larger cultures. The cells will not grow with very low initial cellular densities in liquid cultures.
7) Place a 50 μL freezer stock of *Sulfolobus solfataricus* from -80 °C storage on ice for 20 minutes.

6.) Place 3-5 mL of hot (75 °C) *Sulfolobus solfataricus* DSM88 or 1829 liquid media into a 50 mL tube, and inoculate with the entire freezer stock. Culture volume must be sufficiently small to allow for adequate aeration of the sample.

7.) Allow for the culture to grow for 24 hours shaking (240 rpm) at 75 °C. Make certain the tube caps are tightly secured.

B.2.10 DNA Substrates and Preparation of *Sac*PolB3 Knockout Gene

Table B.1: DNA Sequences

DNA Primers	Sequence (5'-3')
*Sac*PolB3 FWD	5'-ATTAGATTAATATGTTAGAGGATTTCTTT
*Sac*PolB3 REV	5'-ATTACTCGAGATTAAAGAATTTTTTTAA
*Sso*PyrEF FWD	5'-ATTAGGGCGGATTGGGCCCGACGTC
*Sso*PyrEF REV	5'-ATTAGCTGAGCTCATTTTTTCTTAA

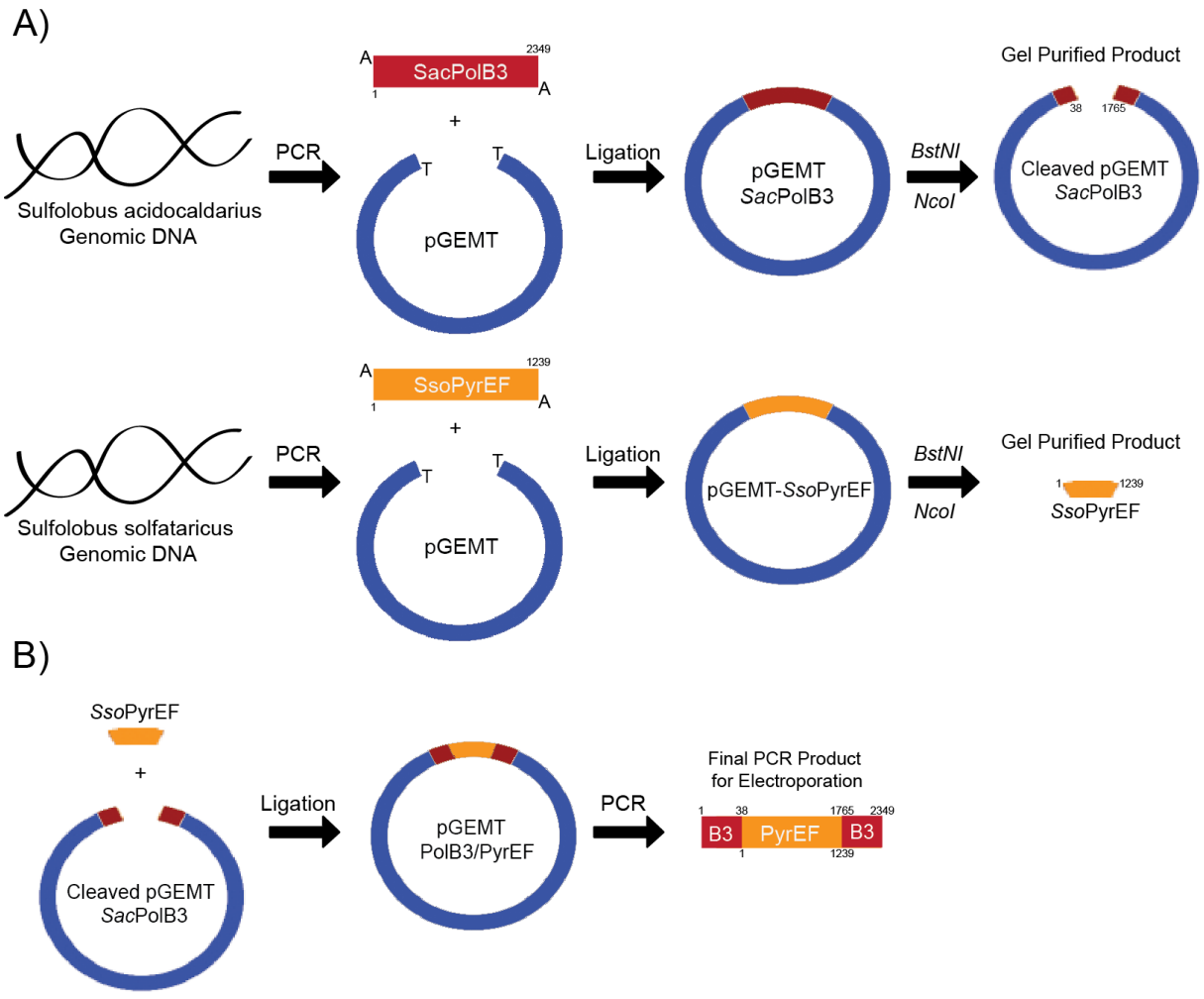

Figure B.1: Schematic of Knockout Gene Creation
A) Amplification of *Sac*PolB3 and *Sso*PyrEF from genomic DNA, ligation into pGemT plasmid, digestion with restriction enzymes and gel purification of the desired DNA product. B.) Ligation of *Sso*PyrEF into the cleaved *Sac*PolB3 gene to create the knockout gene, and final PCR amplification to produce the linear gene product for electroporation.

Sulfolobus acidocaldarius PolB3 was PCR amplified from *Sulfolobus acidocaldarius* Genomic DNA via *Sac*PolB3 FWD and REV primers (**Table B.1**) using KapaHiFi DNA Polymerase (KAPA Biosystems, Woburn, MA), and was inserted into the pGEMT vector (Promega, Madison, WI) by a standard TA-cloning protocol (**Figure B.1 A**) . The *Sulfolobus solfataricus* PyEF genes were PCR amplified from *Sulfolobus solfataricus* genomic DNA via *Sso*PyrEF FWD and REV (**Table B.1**) as detailed for *Sac*PolB3 (**Figure B.1 A**). *Sso*PyrEF was

then inserted into the pGEMT vector through a standard TA-cloning protocol. The plasmids, pGEMT-*Sac*PolB3 and pGEMT-*Sso*PyrEF were cut by the restriction enzymes *NcoI* and *BstNI* (NEB) (included in the *Sso*PyrEF primers, and native to the PolB3 sequence), gel purified, and *Sso*PyrEF was ligated into the cleaved pGEMT-*Sac*PolB3. This process results in the replacement of nucleotides 38-1765 from *Sac*PolB3 with the *Sso*PyrEF gene. The resultant plasmid was named pGEMT-PolB3/PyrEF (**Figure B.1 B**).

B.3 CONCLUSIONS

The experimental procedure described above details the creation of an inactive *Sac*PolB3 gene, where the center of the gene had been replaced by a reporter (*Sso*PyrEF). The *Sso*PyrEF gene allows for the restoration of the uracil synthesis pathway which is deficient in *Sulfolobus acidocaldarius* MR31 cells. Electroporation of the knockout *Sac*PolB3/*Sso*PyrEF construct into these cells allows for replacement of the native genomic PolB3 gene with the mutant construct through a homologous recombination pathway. The knockout cells are selected for through plating on URA- plates, where only *Sulfolobus acidocaldarius* cells which have undergone successful homologous recombination (resulting in the knockout of *Sac*PolB3 activity) will be able to survive, due to the restoration of the uracil synthesis pathway. After numerous attempts, we were unable to detect growth of colonies upon electroporation of the *Sac*PolB3, indicating that *Sac*PolB3 plays essential role in cellular growth processes. It is worth noting, that in these experiments, we lacked a positive control, thus it is possible that either electroporation or growth conditions were not suitable for appropriate detection of transformants. Further experimentation would be required to determine with certainty that *Sac*Dpo3 is essential to the cellular growth process.

REFERENCES

1. Yutin, N., Makarova, K. S., Mekhedov, S. L., Wolf, Y. I., and Koonin, E. V. (2008) The deep archaeal roots of eukaryotes, *Mol. Biol. Evol. 25*, 1619-1630.
2. Forsburg, S. L. (2004) Eukaryotic MCM proteins: Beyond replication initiation, *Microbiol. Mol. Biol. Rev. 68*, 109-131.
3. Lau, E., Tsuji, T., Guo, L., Lu, S.-H., and Jiang, W. (2007) The role of pre-replicative complex (pre-RC) components in oncogenesis, *The FASEB Journal 21*, 3786-3794.
4. Bell, S. P., and Dutta, A. (2002) DNA replication in eukaryotic cells, *Annu. Rev. Biochem. 71*, 333-374.
5. Kelman, Z., and White, M. F. (2005) Archaeal DNA replication and repair, *Curr. Opin. Microbiol. 8*, 669-676.
6. Latterich, M., and Patel, S. (1998) The AAA team: Related ATPases with diverse functions, *Trends in Cell Biol. 8*, 65-71.
7. Fletcher, R. J., Shen, J., Gómez-Llorente, Y., Martín, C. S., Carazo, J. M., and Chen, X. S. (2005) Double hexamer disruption and biochemical activities of *Methanobacterium thermoautotrophicum* MCM, *J. Biol. Chem. 280*, 42405-42410.
8. Barry, E. R., McGeoch, A. T., Kelman, Z., and Bell, S. D. (2007) Archaeal MCM has separable processivity, substrate choice and helicase domains, *Nucl. Acids Res. 35*, 988-998.
9. Brewster, A. S., Wang, G., Yu, X., Greenleaf, W. B., Carazo, J. M., Tjajadia, M., Klein, M. G., and Chen, X. S. (2008) Crystal structure of a near-full-length archaeal MCM: Functional insights for an AAA+ hexameric helicase, *Proc. Natl. Acad. Sci. U.S.A. 105*, 20191-20196.
10. Barry, E. R., Lovett, J. E., Costa, A., Lea, S. M., and Bell, S. D. (2009) Intersubunit allosteric communication mediated by a conserved loop in the MCM helicase, *Proc. Natl. Acad. Sci. U.S.A. 106*, 1051-1056.
11. Kelman, Z., Lee, J.-K., and Hurwitz, J. (1999) The single minichromosome maintenance protein of Methanobacterium thermoautotrophicum ΔH contains DNA helicase activity, *Proc. Natl. Acad. Sci. U.S.A. 96*, 14783-14788.
12. Liu, W., Pucci, B., Rossi, M., Pisani, F. M., and Ladenstein, R. (2008) Structural analysis of the *Sulfolobus solfataricus* MCM protein N-terminal domain, *Nucl. Acids Res. 36*, 3235-3243.
13. Laskey, R. A., and Madine, M. A. (2003) A rotary pumping model for helicase function of MCM proteins at a distance from replication forks, *EMBO Rep. 4*, 26-30.
14. Takahashi, T. S., Wigley, D. B., and Walter, J. C. (2005) Pumps, paradoxes and ploughshares: Mechanism of the MCM2–7 DNA helicase, *Trends Biochem. Sci. 30*, 437-444.
15. Graham, B. W., Schauer, G. D., Leuba, S. H., and Trakselis, M. A. (2011) Steric exclusion and wrapping of the excluded DNA strand occurs along discrete external binding paths during MCM helicase unwinding, *Nucl. Acids Res. 39*, 6585-6595.

16. Aravind, L., Leipe, D. D., and Koonin, E. V. (1998) Toprim--a conserved catalytic domain in type IA and II topoisomerases, DnaG-type primases, OLD family nucleases and RecR proteins, *Nucl. Acids Res. 26*, 4205-4213.
17. Lee, S.-J., Zhu, B., Akabayov, B., and Richardson, C. C. (2012) Zinc-binding domain of the bacteriophage T7 DNA primase modulates binding to the DNA template, *J. Biol. Chem. 287*, 39030-39040.
18. Kusakabe, T., and Richardson, C. C. (1996) The role of the zinc motif in sequence recognition by DNA primases, *J. Biol. Chem. 271*, 19563-19570.
19. Rymer, R. U., Solorio, F. A., Tehranchi, A. K., Chu, C., Corn, J. E., Keck, J. L., Wang, J. D., and Berger, J. M. (2012) Binding mechanism of metal-NTP substrates and stringent-response alarmones to bacterial DnaG-type primases, *Structure 20*, 1478-1489.
20. Corn, J. E., Pelton, J. G., and Berger, J. M. (2008) Identification of a DNA primase template tracking site redefines the geometry of primer synthesis, *Nat. Struct. Mol. Biol. 15*, 163-169.
21. Valentine, A. M., Ishmael, F. T., Shier, V. K., and Benkovic, S. J. (2001) A zinc ribbon protein in DNA replication: Primer synthesis and macromolecular interactions by the bacteriophage T4 primase, *Biochemistry 40*, 15074-15085.
22. Johnson, S. K., Bhattacharyya, S., and Griep, M. A. (2000) DnaB helicase stimulates primer synthesis activity on short oligonucleotide templates, *Biochemistry 39*, 736-744.
23. Corn, J. E., Pease, P. J., Hura, G. L., and Berger, J. M. (2005) Crosstalk between primase subunits can act to regulate primer synthesis in trans, *Mol. Cell 20*, 391-401.
24. Bird, L. E., Pan, H., Soultanas, P., and Wigley, D. B. (2000) Mapping protein-protein interactions within a stable complex of DNA primase and DnaB helicase from *Bacillus stearothermophilus*, *Biochemistry 39*, 171-182.
25. Huang, H., Zhao, K., Arnett, D. R., and Fanning, E. (2010) A specific docking site for DNA polymerase α-primase on the SV40 helicase is required for viral primosome activity, but helicase activity is dispensable, *J. Biol. Chem. 285*, 33475-33484.
26. Wang, G., Klein, M. G., Tokonzaba, E., Zhang, Y., Holden, L. G., and Chen, X. S. (2008) The structure of a DnaB-family replicative helicase and its interactions with primase, *Nat. Struct. Mol. Biol. 15*, 94-100.
27. Bailey, S., Eliason, W. K., and Steitz, T. A. (2007) Structure of hexameric DnaB helicase and its complex with a domain of DnaG primase, *Science 318*, 459-463.
28. VanLoock, M. S., Chen, Y. J., Yu, X., Patel, S. S., and Egelman, E. H. (2001) The primase active site is on the outside of the hexameric bacteriophage T7 gene 4 helicase-primase ring, *J. Mol. Biol. 311*, 951-956.
29. Lu, Y. B., Ratnakar, P. V., Mohanty, B. K., and Bastia, D. (1996) Direct physical interaction between DnaG primase and DnaB helicase of *Escherichia coli* is necessary for optimal synthesis of primer RNA, *Proc. Natl. Acad. Sci. U.S.A. 93*, 12902-12907.
30. Soultanas, P. (2005) The bacterial helicase-primase interaction: A common structural/functional module, *Structure 13*, 839-844.
31. Mitkova, A. V., Khopde, S. M., and Biswas, S. B. (2003) Mechanism and stoichiometry of interaction of DnaG primase with DnaB helicase of *Escherichia coli* in RNA primer synthesis, *J. Biol. Chem. 278*, 52253-52261.

32. Jose, D., Weitzel, S. E., Jing, D., and von Hippel, P. H. (2012) Assembly and subunit stoichiometry of the functional helicase-primase (primosome) complex of bacteriophage T4, *Proc. Natl. Acad. Sci. U.S.A. 109*, 13596-13601.
33. Norcum, M. T., Warrington, J. A., Spiering, M. M., Ishmael, F. T., Trakselis, M. A., and Benkovic, S. J. (2005) Architecture of the bacteriophage T4 primosome: Electron microscopy studies of helicase (gp41) and primase (gp61), *Proc. Natl. Acad. Sci. U.S.A. 102*, 3623-3626.
34. Zechner, E. L., Wu, C. A., and Marians, K. J. (1992) Coordinated leading- and lagging-strand synthesis at the *Escherichia coli* DNA replication fork. III. A polymerase-primase interaction governs primer size, *J. Biol. Chem. 267*, 4054-4063.
35. Zechner, E. L., Wu, C. A., and Marians, K. J. (1992) Coordinated leading- and lagging-strand synthesis at the *Escherichia coli* DNA replication fork. II. Frequency of primer synthesis and efficiency of primer utilization control Okazaki fragment size, *J. Biol. Chem. 267*, 4045-4053.
36. Kuchta, R. D., Reid, B., and Chang, L. M. (1990) DNA primase. Processivity and the primase to polymerase alpha activity switch, *J. Biol. Chem. 265*, 16158-16165.
37. Lee, J. B., Hite, R. K., Hamdan, S. M., Xie, X. S., Richardson, C. C., and van Oijen, A. M. (2006) DNA primase acts as a molecular brake in DNA replication, *Nature 439*, 621-624.
38. Kato, M., Frick, D. N., Lee, J., Tabor, S., Richardson, C. C., and Ellenberger, T. (2001) A complex of the bacteriophage T7 primase-helicase and DNA polymerase directs primer utilization, *J. Biol. Chem. 276*, 21809-21820.
39. Podobnik, M., McInerney, P., O'Donnell, M., and Kuriyan, J. (2000) A TOPRIM domain in the crystal structure of the catalytic core of *Escherichia coli* primase confirms a structural link to DNA topoisomerases, *J. Mol. Biol. 300*, 353-362.
40. Keck, J. L., Roche, D. D., Lynch, A. S., and Berger, J. M. (2000) Structure of the RNA polymerase domain of *E. coli* primase, *Science 287*, 2482-2486.
41. Kusakabe, T., Baradaran, K., Lee, J., and Richardson, C. C. (1998) Roles of the helicase and primase domain of the gene 4 protein of bacteriophage T7 in accessing the primase recognition site, *EMBO J. 17*, 1542-1552.
42. Tougu, K., and Marians, K. J. (1996) The interaction between helicase and primase sets the replication fork clock, *J. Biol. Chem. 271*, 21398-21405.
43. Dracheva, S., Koonin, E. V., and Crute, J. J. (1995) Identification of the primase active site of the herpes simplex virus type 1 helicase-primase, *J. Biol. Chem. 270*, 14148-14153.
44. Tougu, K., Peng, H., and Marians, K. J. (1994) Identification of a domain of *Escherichia coli* primase required for functional interaction with the DnaB helicase at the replication fork, *J. Biol. Chem. 269*, 4675-4682.
45. Pan, H., and Wigley, D. B. (2000) Structure of the zinc-binding domain of *Bacillus stearothermophilus* DNA primase, *Structure 8*, 231-239.
46. Koepsell, S. A., Larson, M. A., Griep, M. A., and Hinrichs, S. H. (2006) *Staphylococcus aureus* helicase but not *Escherichia coli* helicase stimulates *S. aureus* primase activity and maintains initiation specificity, *J. Bacteriol. 188*, 4673-4680.

47. Hou, L., Klug, G., and Evguenieva-Hackenberg, E. (2013) The archaeal DnaG protein needs Csl4 for binding to the exosome and enhances its interaction with adenine-rich RNAs, *RNA Biology 10*, 415-424.
48. Zuo, Z., Rodgers, C. J., Mikheikin, A. L., and Trakselis, M. A. (2010) Characterization of a functional DnaG-type primase in archaea: Implications for a dual-primase system, *J. Mol. Biol. 397*, 664-676.
49. Gotz, D., Paytubi, S., Munro, S., Lundgren, M., Bernander, R., and White, M. F. (2007) Responses of hyperthermophilic crenarchaea to UV irradiation, *Genome Biol. 8*, R220.
50. Andersson, A., Lundgren, M., Eriksson, S., Rosenlund, M., Bernander, R., and Nilsson, P. (2006) Global analysis of mRNA stability in the archaeon *Sulfolobus*, *Genome Biol. 7*, R99.
51. Wurtzel, O., Sapra, R., Chen, F., Zhu, Y., Simmons, B. A., and Sorek, R. (2010) A single-base resolution map of an archaeal transcriptome, *Genome Res. 20*, 133-141.
52. Assiddiq, B. F., Snijders, A. P. L., Chong, P. K., Wright, P. C., and Dickman, M. J. (2008) Identification and characterization of *Sulfolobus solfataricus* P2 proteome using multidimensional liquid phase protein separations, *J. Proteome Res. 7*, 2253-2261.
53. Frick, D. N., and Richardson, C. C. (2001) DNA primases, *Annu. Rev. Biochem. 70*, 39-80.
54. Davey, S. K., and Faust, E. A. (1990) Murine DNA polymerase alpha-primase initiates RNA-primed DNA synthesis preferentially upstream of a 3'-CC(C/A)-5' motif, *J. Biol. Chem. 265*, 3611-3614.
55. Kuchta, R. D., and Stengel, G. (2010) Mechanism and evolution of DNA primases, *Biochimica et Biophysica Acta (BBA) - Proteins and Proteomics 1804*, 1180-1189.
56. Zerbe, L. K., and Kuchta, R. D. (2002) The p58 subunit of human DNA primase is important for primer initiation, elongation, and counting, *Biochemistry 41*, 4891-4900.
57. Sheaff, R. J., and Kuchta, R. D. (1993) Mechanism of calf thymus DNA primase: Slow initiation, rapid polymerization, and intelligent termination, *Biochemistry 32*, 3027-3037.
58. Copeland, W. C., and Wang, T. S. (1993) Enzymatic characterization of the individual mammalian primase subunits reveals a biphasic mechanism for initiation of DNA replication, *J. Biol. Chem. 268*, 26179-26189.
59. Maga, G., Stucki, M., Spadari, S., and Hubscher, U. (2000) DNA polymerase switching: I. Replication factor C displaces DNA polymerase alpha prior to PCNA loading, *J. Mol. Biol. 295*, 791-801.
60. Mossi, R., Keller, R. C., Ferrari, E., and Hubscher, U. (2000) DNA polymerase switching: II. Replication factor C abrogates primer synthesis by DNA polymerase alpha at a critical length, *J. Mol. Biol. 295*, 803-814.
61. Le Breton, M., Henneke, G., Norais, C., Flament, D., Myllykallio, H., Querellou, J., and Raffin, J. P. (2007) The heterodimeric primase from the euryarchaeon *Pyrococcus abyssi*: A multifunctional enzyme for initiation and repair?, *J. Mol. Biol. 374*, 1172-1185.
62. Ito, N., Matsui, I., and Matsui, E. (2007) Molecular basis for the subunit assembly of the primase from an archaeon *Pyrococcus horikoshii*, *FEBS J. 274*, 1340-1351.
63. Chemnitz Galal, W., Pan, M., Kelman, Z., and Hurwitz, J. (2012) Characterization of DNA primase complex isolated from the archaeon, *Thermococcus kodakaraensis*, *J. Biol. Chem. 287*, 16209-16219.

64. Lao-Sirieix, S. H., and Bell, S. D. (2004) The heterodimeric primase of the hyperthermophilic archaeon *Sulfolobus solfataricus* possesses DNA and RNA primase, polymerase and 3'-terminal nucleotidyl transferase activities, *J. Mol. Biol. 344*, 1251-1263.
65. Hu, J., Guo, L., Wu, K., Liu, B., Lang, S., and Huang, L. (2012) Template-dependent polymerization across discontinuous templates by the heterodimeric primase from the hyperthermophilic archaeon *Sulfolobus solfataricus*, *Nucl. Acids Res. 40*, 3470-3483.
66. Lao-Sirieix, S. H., Nookala, R. K., Roversi, P., Bell, S. D., and Pellegrini, L. (2005) Structure of the heterodimeric core primase, *Nat. Struct. Mol. Biol. 12*, 1137-1144.
67. Marinsek, N., Barry, E. R., Makarova, K. S., Dionne, I., Koonin, E. V., and Bell, S. D. (2006) GINS, a central nexus in the archaeal DNA replication fork, *EMBO Rep. 7*, 539-545.
68. Beattie, T. R., and Bell, S. D. (2011) Molecular machines in archaeal DNA replication, *Curr. Opin. Chem. Biol. 15*, 614-619.
69. Augustin, M. A., Huber, R., and Kaiser, J. T. (2001) Crystal structure of a DNA-dependent RNA polymerase (DNA primase), *Nat. Struct. Mol. Biol. 8*, 57-61.
70. Kim, S. W., Kim, D.-U., Kim, J. K., Kang, L.-W., and Cho, H.-S. (2008) Crystal structure of *Pfu*, the high fidelity DNA polymerase from *Pyrococcus furiosus*, *Int. J. Biol. Macromol. 42*, 356-361.
71. Savino, C., Federici, L., Johnson, K. A., Vallone, B., Nastopoulos, V., Rossi, M., Pisani, F. M., and Tsernoglou, D. (2004) Insights into DNA replication: The crystal structure of DNA polymerase B1 from the archaeon *Sulfolobus solfataricus*, *Structure 12*, 2001-2008.
72. Kunkel, T. A., and Bebenek, K. (2000) DNA replication fidelity, *Annu. Rev. Biochem. 69*, 497-529.
73. Jeruzalmi, D., O'Donnell, M., and Kuriyan, J. (2002) Clamp loaders and sliding clamps, *Curr. Opin. Struct. Biol. 12*, 217-224.
74. Pisani, F. M., De, F. M., Manco, G., and Rossi, M. (1998) Domain organization and biochemical features of *Sulfolobus solfataricus* DNA polymerase, *Extremophiles 2*, 171-177.
75. Zhang, L., Brown, J. A., Newmister, S. A., and Suo, Z. (2009) Polymerization fidelity of a replicative DNA polymerase from the hyperthermophilic archaeon *Sulfolobus solfataricus* P2, *Biochemistry 48*, 7492-7501.
76. Prakash, S., Johnson, R. E., and Prakash, L. (2005) Eukaryotic translesion synthesis DNA polymerases: Specificity of structure and function, *Annu. Rev. Biochem. 74*, 317-353.
77. Edgell, D. R., Malik, S. B., and Doolittle, W. F. (1998) Evidence of independent gene duplications during the evolution of archaeal and eukaryotic family B DNA polymerases, *Mol. Biol. Evol. 15*, 1207-1217.
78. Mikheikin, A. L., Lin, H. K., Mehta, P., Jen-Jacobson, L., and Trakselis, M. A. (2009) A trimeric DNA polymerase complex increases the native replication processivity, *Nucl. Acids Res. 37*, 7194-7205.
79. Brown, J. A., and Suo, Z. (2009) Elucidating the kinetic mechanism of DNA polymerization catalyzed by *Sulfolobus solfataricus* P2 DNA polymerase B1, *Biochemistry 48*, 7502-7511.

80. Fidalgo da, S. E., and Reha-Krantz, L. J. (2007) DNA polymerase proofreading: active site switching catalyzed by the bacteriophage T4 DNA polymerase, *Nucl. Acids Res. 35*, 5452-5463.
81. Truniger, V., Lazaro, J. M., Salas, M., and Blanco, L. (1996) A DNA binding motif coordinating synthesis and degradation in proofreading DNA polymerases, *EMBO J. 15*, 3430-3441.
82. Bohlke, K., Pisani, F. M., Vorgias, C. E., Frey, B., Sobek, H., Rossi, M., and Antranikian, G. (2000) PCR performance of the B-type DNA polymerase from the thermophilic euryarchaeon *Thermococcus aggregans* improved by mutations in the Y-GG/A motif, *Nucl. Acids Res. 28*, 3910-3917.
83. Bauer, R. J., Begley, M. T., and Trakselis, M. A. (2012) Kinetics and fidelity of polymerization by DNA polymerase III from *Sulfolobus solfataricus*, *Biochemistry 51*, 1996-2007.
84. Zuo, Z., Lin, H. K., and Trakselis, M. A. (2011) Strand annealing and terminal transferase activities of a B-family DNA polymerase, *Biochemistry 50*, 5379-5390.
85. Dominguez, O., Ruiz, J. F., Lain de, L. T., Garcia-Diaz, M., Gonzalez, M. A., Kirchhoff, T., Martinez, A., Bernad, A., and Blanco, L. (2000) DNA polymerase mu (Pol mu), homologous to TdT, could act as a DNA mutator in eukaryotic cells, *EMBO J. 19*, 1731-1742.
86. Maga, G., Ramadan, K., Locatelli, G. A., Shevelev, I., Spadari, S., and Hubscher, U. (2005) DNA elongation by the human DNA polymerase lambda polymerase and terminal transferase activities are differentially coordinated by proliferating cell nuclear antigen and replication protein A, *J. Biol. Chem. 280*, 1971-1981.
87. Rogozin, I. B., Makarova, K. S., Pavlov, Y. I., and Koonin, E. V. (2008) A highly conserved family of inactivated archaeal B family DNA polymerases, *Biol. Direct 3*, 32.
88. Frols, S., Gordon, P. M., Panlilio, M. A., Duggin, I. G., Bell, S. D., Sensen, C. W., and Schleper, C. (2007) Response of the hyperthermophilic archaeon *Sulfolobus solfataricus* to UV damage, *J. Bacteriol. 189*, 8708-8718.
89. Frols, S., White, M. F., and Schleper, C. (2009) Reactions to UV damage in the model archaeon S*ulfolobus solfataricus*, *Biochem. Soc. Trans. 37*, 36-41.
90. Choi, J. Y., Eoff, R. L., Pence, M. G., Wang, J., Martin, M. V., Kim, E. J., Folkmann, L. M., and Guengerich, F. P. (2011) Roles of the four DNA polymerases of the crenarchaeon *Sulfolobus solfataricus* and accessory proteins in DNA replication, *J. Biol. Chem. 286*, 31180-31193.
91. Iwai, T., Kurosawa, N., Itoh, Y. H., Kimura, N., and Horiuchi, T. (2000) Sequence analysis of three family B DNA polymerases from the thermoacidophilic crenarchaeon *Sulfurisphaera ohwakuensis*, *DNA Research 7*, 243-251.
92. Tahirov, T. H., Makarova, K. S., Rogozin, I. B., Pavlov, Y. I., and Koonin, E. V. (2009) Evolution of DNA polymerases: An inactivated polymerase-exonuclease module in Pol ε and a chimeric origin of eukaryotic polymerases from two classes of archaeal ancestors, *Biol. Direct 4*, 11.
93. Bernad, A., Blanco, L., and Salas, M. (1990) Site-directed mutagenesis of the YCDTDS amino acid motif of the Φ29 DNA polymerase, *Gene 94*, 45-51.

94. Copeland, W. C., and Wang, T. S. (1993) Mutational analysis of the human DNA polymerase alpha. The most conserved region in alpha-like DNA polymerases is involved in metal-specific catalysis, *J. Biol. Chem. 268*, 11028-11040.
95. Edgell, D. R., Klenk, H. P., and Doolittle, W. F. (1997) Gene duplications in evolution of archaeal family B DNA polymerases, *J. Bacteriol. 179*, 2632-2640.
96. She, Q., Singh, R. K., Confalonieri, F., Zivanovic, Y., Allard, G., Awayez, M. J., Chan-Weiher, C. C., Clausen, I. G., Curtis, B. A., De, M. A., Erauso, G., Fletcher, C., Gordon, P. M., Heikamp-de, J. I., Jeffries, A. C., Kozera, C. J., Medina, N., Peng, X., Thi-Ngoc, H. P., Redder, P., Schenk, M. E., Theriault, C., Tolstrup, N., Charlebois, R. L., Doolittle, W. F., Duguet, M., Gaasterland, T., Garrett, R. A., Ragan, M. A., Sensen, C. W., and Van der, O. J. (2001) The complete genome of the crenarchaeon *Sulfolobus solfataricus* P2, *Proc. Natl. Acad. Sci. U.S.A. 98*, 7835-7840.
97. Robinson, N. P., and Bell, S. D. (2005) Origins of DNA replication in the three domains of life, *FEBS J. 272*, 3757-3766.
98. Duggin, I. G., McCallum, S. A., and Bell, S. D. (2008) Chromosome replication dynamics in the archaeon *Sulfolobus acidocaldarius*, *Proc. Natl. Acad. Sci. U.S.A. 105*, 16737-16742.
99. Lundberg, K. S., Shoemaker, D. D., Adams, M. W., Short, J. M., Sorge, J. A., and Mathur, E. J. (1991) High-fidelity amplification using a thermostable DNA polymerase isolated from *Pyrococcus furiosus*, *Gene 108*, 1-6.
100. Hopfner, K. P., Eichinger, A., Engh, R. A., Laue, F., Ankenbauer, W., Huber, R., and Angerer, B. (1999) Crystal structure of a thermostable type B DNA polymerase from *Thermococcus gorgonarius*, *Proc. Natl. Acad. Sci. U.S.A. 96*, 3600-3605.
101. Perler, F. B., Comb, D. G., Jack, W. E., Moran, L. S., Qiang, B., Kucera, R. B., Benner, J., Slatko, B. E., Nwankwo, D. O., and Hempstead, S. K. (1992) Intervening sequences in an archaea DNA polymerase gene, *Proc. Natl. Acad. Sci. U.S.A. 89*, 5577-5581.
102. Hashimoto, H., Nishioka, M., Fujiwara, S., Takagi, M., Imanaka, T., Inoue, T., and Kai, Y. (2001) Crystal structure of DNA polymerase from hyperthermophilic archaeon *Pyrococcus kodakaraensis* KOD1, *J. Mol. Biol. 306*, 469-477.
103. Kuroita, T., Matsumura, H., Yokota, N., Kitabayashi, M., Hashimoto, H., Inoue, T., Imanaka, T., and Kai, Y. (2005) Structural mechanism for coordination of proofreading and polymerase activities in archaeal DNA polymerases, *J. Mol. Biol. 351*, 291-298.
104. Henneke, G., Flament, D., Hubscher, U., Querellou, J., and Raffin, J. P. (2005) The hyperthermophilic euryarchaeota *Pyrococcus abyssi* likely requires the two DNA polymerases D and B for DNA replication, *J. Mol. Biol. 350*, 53-64.
105. Ling, H., Boudsocq, F., Woodgate, R., and Yang, W. (2001) Crystal structure of a Y-family DNA polymerase in action: a mechanism for error-prone and lesion-bypass replication, *Cell 107*, 91-102.
106. McCulloch, S. D., and Kunkel, T. A. (2008) The fidelity of DNA synthesis by eukaryotic replicative and translesion synthesis polymerases, *Cell Res. 18*, 148-161.
107. Perlow-Poehnelt, R. A., Likhterov, I., Scicchitano, D. A., Geacintov, N. E., and Broyde, S. (2004) The spacious active site of a Y-family DNA polymerase facilitates promiscuous nucleotide incorporation opposite a bulky carcinogen-DNA adduct, *J. Biol. Chem. 279*, 36951-36961.

108. Fiala, K. A., Hypes, C. D., and Suo, Z. (2007) Mechanism of abasic lesion bypass catalyzed by a Y-family DNA polymerase, *J. Biol. Chem. 282*, 8188-8198.
109. Ling, H., Boudsocq, F., Woodgate, R., and Yang, W. (2004) Snapshots of replication through an abasic lesion; structural basis for base substitutions and frameshifts, *Mol. Cell 13*, 751-762.
110. Sherrer, S. M., Brown, J. A., Pack, L. R., Jasti, V. P., Fowler, J. D., Basu, A. K., and Suo, Z. (2009) Mechanistic studies of the bypass of a bulky single-base lesion catalyzed by a Y-family DNA polymerase, *J. Biol. Chem. 284*, 6379-6388.
111. Ling, H., Sayer, J. M., Plosky, B. S., Yagi, H., Boudsocq, F., Woodgate, R., Jerina, D. M., and Yang, W. (2004) Crystal structure of a benzo[a]pyrene diol epoxide adduct in a ternary complex with a DNA polymerase, *Proc. Natl. Acad. Sci. U.S.A. 101*, 2265-2269.
112. Rechkoblit, O., Malinina, L., Cheng, Y., Kuryavyi, V., Broyde, S., Geacintov, N. E., and Patel, D. J. (2006) Stepwise translocation of Dpo4 polymerase during error-free bypass of an oxoG lesion, *PLoS Biol. 4*, e11.
113. Zang, H., Irimia, A., Choi, J.-Y., Angel, K. C., Loukachevitch, L. V., Egli, M., and Guengerich, F. P. (2006) Efficient and high fidelity Incorporation of dCTP opposite 7,8-dihydro-8-oxodeoxyguanosine by *Sulfolobus solfataricus* DNA polymerase Dpo4, *J. Biol. Chem. 281*, 2358-2372.
114. Johnson, R. E., Prakash, L., and Prakash, S. (2005) Distinct mechanisms of cis-syn thymine dimer bypass by Dpo4 and DNA polymerase η, *Proc. Natl. Acad. Sci. U.S.A. 102*, 12359-12364.
115. Boudsocq, F., Iwai, S., Hanaoka, F., and Woodgate, R. (2001) *Sulfolobus solfataricus* P2 DNA polymerase IV (Dpo4): An archaeal DinB-like DNA polymerase with lesion-bypass properties akin to eukaryotic polη, *Nucl. Acids Res. 29*, 4607-4616.
116. Vaisman, A., Ling, H., Woodgate, R., and Yang, W. (2005) Fidelity of Dpo4: Effect of metal ions, nucleotide selection and pyrophosphorolysis, *EMBO J. 24*, 2957-2967.
117. Rechkoblit, O., Kolbanovskiy, A., Malinina, L., Geacintov, N. E., Broyde, S., and Patel, D. J. (2010) Mechanism of error-free and semitargeted mutagenic bypass of an aromatic amine lesion by Y-family polymerase Dpo4, *Nat. Struct. Mol. Biol. 17*, 379-388.
118. Strauss, B. S. (1991) The 'A rule' of mutagen specificity: A consequence of DNA polymerase bypass of non-instructional lesions?, *Bioessays 13*, 79-84.
119. Fiala, K. A., and Suo, Z. (2007) Sloppy bypass of an abasic lesion catalyzed by a Y-family DNA polymerase, *J. Biol. Chem. 282*, 8199-8206.
120. Wu, Y., Wilson, R. C., and Pata, J. D. (2011) The Y-family DNA polymerase Dpo4 uses a template slippage mechanism to create single-base deletions, *J. Bacteriol. 193*, 2630-2636.
121. Greagg, M. A., Fogg, M. J., Panayotou, G., Evans, S. J., Connolly, B. A., and Pearl, L. H. (1999) A read-ahead function in archaeal DNA polymerases detects promutagenic template-strand uracil, *Proc. Natl. Acad. Sci. U.S.A. 96*, 9045-9050.
122. Castrec, B., Rouillon, C., Henneke, G., Flament, D., Querellou, J., and Raffin, J.-P. (2009) Binding to PCNA in euryarchaeal DNA replication requires two PIP motifs for DNA polymerase D and one PIP motif for DNA polymerase B, *J. Mol. Biol. 394*, 209-218.

123. Pisani, F. M., De, F. M., Carpentieri, F., and Rossi, M. (2000) Biochemical characterization of a clamp-loader complex homologous to eukaryotic replication factor C from the hyperthermophilic archaeon *Sulfolobus solfataricus*, *J. Mol. Biol. 301*, 61-73.
124. Warbrick, E. (1998) PCNA binding through a conserved motif, *Bioessays 20*, 195-199.
125. Mayanagi, K., Kiyonari, S., Nishida, H., Saito, M., Kohda, D., Ishino, Y., Shirai, T., and Morikawa, K. (2011) Architecture of the DNA polymerase B-proliferating cell nuclear antigen (PCNA)-DNA ternary complex, *Proc. Natl. Acad. Sci. U.S.A. 108*, 1845-1849.
126. Nishida, H., Mayanagi, K., Kiyonari, S., Sato, Y., Oyama, T., Ishino, Y., and Morikawa, K. (2009) Structural determinant for switching between the polymerase and exonuclease modes in the PCNA-replicative DNA polymerase complex, *Proc. Natl. Acad. Sci. U.S.A. 106*, 20693-20698.
127. Bunting, K. A., Roe, S. M., and Pearl, L. H. (2003) Structural basis for recruitment of translesion DNA polymerase Pol IV/DinB to the beta-clamp, *EMBO J. 22*, 5883-5892.
128. Dionne, I., Nookala, R. K., Jackson, S. P., Doherty, A. J., and Bell, S. D. (2003) A heterotrimeric PCNA in the hyperthermophilic archaeon *Sulfolobus solfataricus*, *Mol. Cell 11*, 275-282.
129. Beattie, T. R., and Bell, S. D. (2012) Coordination of multiple enzyme activities by a single PCNA in archaeal Okazaki fragment maturation, *EMBO J. 31*, 1556-1567.
130. Pascal, J. M., Tsodikov, O. V., Hura, G. L., Song, W., Cotner, E. A., Classen, S., Tomkinson, A. E., Tainer, J. A., and Ellenberger, T. (2006) A flexible interface between DNA ligase and PCNA supports conformational switching and efficient ligation of DNA, *Mol. Cell 24*, 279-291.
131. Indiani, C., McInerney, P., Georgescu, R., Goodman, M. F., and O'Donnell, M. (2005) A sliding-clamp toolbelt binds high- and low-fidelity DNA polymerases simultaneously, *Mol. Cell 19*, 805-815.
132. Xing, G., Kirouac, K., Shin, Y. J., Bell, S. D., and Ling, H. (2009) Structural insight into recruitment of translesion DNA polymerase Dpo4 to sliding clamp PCNA, *Mol. Microbiol. 71*, 678-691.
133. Grúz, P., Pisani, F. M., Shimizu, M., Yamada, M., Hayashi, I., Morikawa, K., and Nohmi, T. (2001) Synthetic activity of *Sso* DNA polymerase Y1, an archaeal DinB-like DNA polymerase, is stimulated by processivity factors proliferating cell nuclear antigen and replication factor C, *J. Biol. Chem. 276*, 47394-47401.
134. Dionne, I., Brown, N. J., Woodgate, R., and Bell, S. D. (2008) On the mechanism of loading the PCNA sliding clamp by RFC, *Mol. Microbiol. 68*, 216-222.
135. Lin, L. J., Yoshinaga, A., Lin, Y., Guzman, C., Chen, Y. H., Mei, S., Lagunas, A. M., Koike, S., Iwai, S., Spies, M. A., Nair, S. K., Mackie, R. I., Ishino, Y., and Cann, I. K. (2010) Molecular analyses of an unusual translesion DNA polymerase from *Methanosarcina acetivorans* C2A, *J. Mol. Biol. 397*, 13-30.
136. McInerney, P., Johnson, A., Katz, F., and O'Donnell, M. (2007) Characterization of a triple DNA polymerase replisome, *Mol. Cell 27*, 527-538.
137. Ishmael, F. T., Trakselis, M. A., and Benkovic, S. J. (2003) Protein-protein interactions in the bacteriophage T4 replisome, *J. Biol. Chem. 278*, 3145-3152.
138. Purohit, V., Grindley, N. D. F., and Joyce, C. M. (2003) Use of 2-aminopurine fluorescence to examine conformational changes during nucleotide incorporation by DNA polymerase I (klenow fragment), *Biochemistry 42*, 10200-10211.

139. Lin, H.-K., Chase, S. F., Laue, T. M., Jen-Jacobson, L., and Trakselis, M. A. (2012) Differential temperature-dependent multimeric assemblies of replication and repair polymerases on DNA increase processivity, *Biochemistry 51*, 7367-7382.
140. Yang, J., Zhuang, Z., Roccasecca, R. M., Trakselis, M. A., and Benkovic, S. J. (2004) The dynamic processivity of the T4 DNA polymerase during replication, *Proc. Natl. Acad. Sci. U.S.A. 101*, 8289-8294.
141. Loparo, J. J., Kulczyk, A. W., Richardson, C. C., and van Oijen, A. M. (2011) Simultaneous single-molecule measurements of phage T7 replisome composition and function reveal the mechanism of polymerase exchange, *Proc. Natl. Acad. Sci. U.S.A. 108*, 3584-3589.
142. Grogan, D. W., Carver, G. T., and Drake, J. W. (2001) Genetic fidelity under harsh conditions: analysis of spontaneous mutation in the thermoacidophilic archaeon *Sulfolobus acidocaldarius*, *Proc. Natl. Acad. Sci. U.S.A. 98*, 7928-7933.
143. Sakofsky, C. J., Foster, P. L., and Grogan, D. W. (2012) Roles of the Y-family DNA polymerase Dbh in accurate replication of the *Sulfolobus* genome at high temperature, *DNA Repair (Amst) 11*, 391-400.
144. Furukohri, A., Goodman, M. F., and Maki, H. (2008) A dynamic polymerase exchange with *Escherichia coli* DNA polymerase IV replacing DNA polymerase III on the sliding clamp, *J. Biol. Chem. 283*, 11260-11269.
145. Heltzel, J. M., Maul, R. W., Scouten Ponticelli, S. K., and Sutton, M. D. (2009) A model for DNA polymerase switching involving a single cleft and the rim of the sliding clamp, *Proc. Natl. Acad. Sci. U.S.A. 106*, 12664-12669.
146. Sutton, M. D., Opperman, T., and Walker, G. C. (1999) The Escherichia coli SOS mutagenesis proteins UmuD and UmuD′ interact physically with the replicative DNA polymerase, *Proc. Natl. Acad. Sci. U.S.A. 96*, 12373-12378.
147. Chaurasiya, K. R., Ruslie, C., Silva, M. C., Voortman, L., Nevin, P., Lone, S., Beuning, P. J., and Williams, M. C. (2013) Polymerase manager protein UmuD directly regulates *Escherichia coli* DNA polymerase III α binding to ssDNA, *Nucl. Acids Res. 41*, 8959-8968.
148. De Felice, M., Medagli, B., Esposito, L., De Falco, M., Pucci, B., Rossi, M., Gruz, P., Nohmi, T., and Pisani, F. M. (2007) Biochemical evidence of a physical interaction between *Sulfolobus solfataricus* B-family and Y-family DNA polymerases, *Extremophiles 11*, 277-282.
149. Filee, J., Forterre, P., Sen-Lin, T., and Laurent, J. (2002) Evolution of DNA polymerase families: evidences for multiple gene exchange between cellular and viral proteins, *J. Mol. Evol. 54*, 763-773.
150. Burgers, P. M., Koonin, E. V., Bruford, E., Blanco, L., Burtis, K. C., Christman, M. F., Copeland, W. C., Friedberg, E. C., Hanaoka, F., Hinkle, D. C., Lawrence, C. W., Nakanishi, M., Ohmori, H., Prakash, L., Prakash, S., Reynaud, C. A., Sugino, A., Todo, T., Wang, Z., Weill, J. C., and Woodgate, R. (2001) Eukaryotic DNA polymerases: Proposal for a revised nomenclature, *J. Biol. Chem. 276*, 43487-43490.
151. Hubscher, U., Maga, G., and Spadari, S. (2002) Eukaryotic DNA polymerases, *Annu. Rev. Biochem. 71*, 133-163.
152. Bebenek, K., and Kunkel, T. A. (2004) Functions of DNA polymerases, *Adv. Protein Chem. 69*, 137-165.

153. Nick McElhinny, S. A., Gordenin, D. A., Stith, C. M., Burgers, P. M., and Kunkel, T. A. (2008) Division of labor at the eukaryotic replication fork, *Mol. Cell 30*, 137-144.
154. Beckman, J., Kincaid, K., Hocek, M., Spratt, T., Engels, J., Cosstick, R., and Kuchta, R. D. (2007) Human DNA polymerase alpha uses a combination of positive and negative selectivity to polymerize purine dNTPs with high fidelity, *Biochemistry 46*, 448-460.
155. Burgers, P. M. (2009) Polymerase dynamics at the eukaryotic DNA replication fork, *J. Biol. Chem. 284*, 4041-4045.
156. Stillman, B. (2008) DNA polymerases at the replication fork in eukaryotes, *Mol. Cell 30*, 259-260.
157. Grabowski, B., and Kelman, Z. (2003) Archeal DNA replication: Eukaryal proteins in a bacterial context, *Annu. Rev. Microbiol. 57*, 487-516.
158. Barry, E. R., and Bell, S. D. (2006) DNA replication in the Archaea, *Microbiol. Mol. Biol. Rev. 70*, 876-887.
159. Majernik, A. I., Jenkinson, E. R., and Chong, J. P. (2004) DNA replication in thermophiles, *Biochem. Soc. Trans. 32*, 236-239.
160. Leipe, D. D., Aravind, L., and Koonin, E. V. (1999) Did DNA replication evolve twice independently?, *Nucl. Acids Res. 27*, 3389-3401.
161. Cann, I. K. O., Komori, K., Toh, H., Kanai, S., and Ishino, Y. (1998) A heterodimeric DNA polymerase: Evidence that members of Euryarchaeota possess a distinct DNA polymerase, *Proc. Natl. Acad. Sci. U.S.A. 95*, 14250-14255.
162. Kulaeva, O. I., Koonin, E. V., McDonald, J. P., Randall, S. K., Rabinovich, N., Connaughton, J. F., Levine, A. S., and Woodgate, R. (1996) Identification of a DinB/UmuC homolog in the archeon *Sulfolobus solfataricus*, *Mutat. Res. 357*, 245-253.
163. Gruz, P., Shimizu, M., Pisani, F. M., De, F. M., Kanke, Y., and Nohmi, T. (2003) Processing of DNA lesions by archaeal DNA polymerases from *Sulfolobus solfataricus*, *Nucl. Acids Res. 31*, 4024-4030.
164. Fiala, K. A., and Suo, Z. (2004) Mechanism of DNA polymerization catalyzed by *Sulfolobus solfataricus* P2 DNA polymerase IV, *Biochemistry 43*, 2116-2125.
165. Fiala, K. A., and Suo, Z. (2004) Pre-steady-state kinetic studies of the fidelity of *Sulfolobus solfataricus* P2 DNA polymerase IV, *Biochemistry 43*, 2106-2115.
166. Prangishvili, D., and Klenk, H. P. (1993) Nucleotide sequence of the gene for a 74 kDa DNA polymerase from the archaeon *Sulfolobus solfataricus*, *Nucl. Acids Res. 21*, 2768.
167. Sambrook, J. a. D. W. R. (2001) *Molecular Cloning: A Laboratory Manual*, Vol. 1-3, CSHL Press, Cold Spring Harbor.
168. Studier, F. W. (2005) Protein production by auto-induction in high density shaking cultures, *Protein Expression Purif. 41*, 207-234.
169. Gill, S. C., and von Hippel, P. H. (1989) Calculation of protein extinction coefficients from amino acid sequence data, *Anal. Biochem. 182*, 319-326.
170. Marky, L. A., and Breslauer, K. J. (1987) Calculating thermodynamic data for transitions of any molecularity from equilibrium melting curves, *Biopolymers 26*, 1601-1620.
171. Arnold, K., Bordoli, L., Kopp, J., and Schwede, T. (2006) The SWISS-MODEL workspace: a web-based environment for protein structure homology modelling, *Bioinformatics 22*, 195-201.
172. Franklin, M. C., Wang, J., and Steitz, T. A. (2001) Structure of the replicating complex of a pol alpha family DNA polymerase, *Cell 105*, 657-667.

173. Hillebrand, G. G., and Beattie, K. (1984) Template–dependent variation in the relative fidelity of DNA polymerase I of *Escherichia coli* in the presence of Mg^{2+} versus Mn^{2+}, *Nucl. Acids Res. 12*, 3173-3183.
174. Polesky, A. H., Steitz, T. A., Grindley, N. D., and Joyce, C. M. (1990) Identification of residues critical for the polymerase activity of the Klenow fragment of DNA polymerase I from *Escherichia coli*, *J. Biol. Chem. 265*, 14579-14591.
175. Dua, R., Levy, D. L., and Campbell, J. L. (1999) Analysis of the essential functions of the C-terminal protein/protein interaction domain of *Saccharomyces cerevisiae* pol epsilon and its unexpected ability to support growth in the absence of the DNA polymerase domain, *J. Biol. Chem. 274*, 22283-22288.
176. Lowe, L. G., and Guengerich, F. P. (1996) Steady-state and pre-steady-state kinetic analysis of dNTP insertion opposite 8-oxo-7,8-dihydroguanine by *Escherichia coli* polymerases I exo- and II exo, *Biochemistry 35*, 9840-9849.
177. Korona, D. A., Lecompte, K. G., and Pursell, Z. F. (2011) The high fidelity and unique error signature of human DNA polymerase epsilon, *Nucl. Acids Res. 39*, 1763-1773.
178. Bebenek, A., Dressman, H. K., Carver, G. T., Ng, S., Petrov, V., Yang, G., Konigsberg, W. H., Karam, J. D., and Drake, J. W. (2001) Interacting fidelity defects in the replicative DNA polymerase of bacteriophage RB69, *J. Biol. Chem. 276*, 10387-10397.
179. Fazlieva, R., Spittle, C. S., Morrissey, D., Hayashi, H., Yan, H., and Matsumoto, Y. (2009) Proofreading exonuclease activity of human DNA polymerase δ and its effects on lesion-bypass DNA synthesis, *Nucl. Acids Res. 37*, 2854-2866.
180. Dieckman, L. M., Johnson, R. E., Prakash, S., and Washington, M. T. (2010) Pre-steady state kinetic studies of the fidelity of nucleotide incorporation by yeast DNA polymerase delta, *Biochemistry 49*, 7344-7350.
181. Zhong, X., Pedersen, L. C., and Kunkel, T. A. (2008) Characterization of a replicative DNA polymerase mutant with reduced fidelity and increased translesion synthesis capacity, *Nucl. Acids Res. 36*, 3892-3904.
182. Blasco, M. A., Bernad, A., Blanco, L., and Salas, M. (1991) Characterization and mapping of the pyrophosphorolytic activity of the phage phi 29 DNA polymerase. Involvement of amino acid motifs highly conserved in alpha-like DNA polymerases, *J. Biol. Chem. 266*, 7904-7909.
183. Swan, M. K., Johnson, R. E., Prakash, L., Prakash, S., and Aggarwal, A. K. (2009) Structural basis of high-fidelity DNA synthesis by yeast DNA polymerase delta, *Nat. Struct. Mol. Biol. 16*, 979-U107.
184. Zahn, K. E., Tchesnokov, E. P., Gotte, M., and Doublie, S. (2011) Phosphonoformic acid inhibits viral replication by trapping the closed form of the DNA polymerase, *J. Biol. Chem. 286*, 25246-25255.
185. Xia, S., Wang, M., Blaha, G., Konigsberg, W. H., and Wang, J. (2011) Structural insights into complete metal ion coordination from ternary complexes of B family RB69 DNA polymerase, *Biochemistry 50*, 9114-9124.
186. Saturno, J., Lazaro, J. M., Blanco, L., and Salas, M. (1998) Role of the first aspartate residue of the "YxDTDS" motif of phi29 DNA polymerase as a metal ligand during both TP-primed and DNA-primed DNA synthesis, *J. Mol. Biol. 283*, 633-642.

187. Kennedy, E. M., Hergott, C., Dewhurst, S., and Kim, B. (2009) The mechanistic architecture of thermostable *Pyrococcus furiosus* family B DNA polymerase motif A and its interaction with the dNTP substrate, *Biochemistry 48*, 11161-11168.
188. Johnson, K. A. (1992) Transient-state kinetic analysis of enzyme reaction pathways, In *The Enzymes* (David, S. S., Ed.), pp 1-61, Academic Press.
189. Pisani, F. M., De, F. M., and Rossi, M. (1998) Amino acid residues involved in determining the processivity of the 3'-5' exonuclease activity in a family B DNA polymerase from the thermoacidophilic archaeon *Sulfolobus solfataricus*, *Biochemistry 37*, 15005-15012.
190. Duggin, I. G., and Bell, S. D. (2006) The chromosome replication machinery of the archaeon *Sulfolobus solfataricus*, *J. Biol. Chem. 281*, 15029-15032.
191. Matsunaga, F., Norais, C., Forterre, P., and Myllykallio, H. (2003) Identification of short 'eukaryotic' Okazaki fragments synthesized from a prokaryotic replication origin, *EMBO Rep. 4*, 154-158.
192. Kong, X. P., Onrust, R., O'Donnell, M., and Kuriyan, J. (1992) Three-dimensional structure of the beta subunit of *E. coli* DNA polymerase III holoenzyme: A sliding DNA clamp, *Cell 69*, 425-437.
193. Krishna, T. S., Kong, X. P., Gary, S., Burgers, P. M., and Kuriyan, J. (1994) Crystal structure of the eukaryotic DNA polymerase processivity factor PCNA, *Cell 79*, 1233-1243.
194. Paschall, C. O., Thompson, J. A., Marzahn, M. R., Chiraniya, A., Hayner, J. N., O'Donnell, M., Robbins, A. H., McKenna, R., and Bloom, L. B. (2011) The *E. coli* clamp loader can actively pry open the beta-sliding clamp, *J. Biol. Chem. 286*, 42704-42714.
195. Jeruzalmi, D., Yurieva, O., Zhao, Y., Young, M., Stewart, J., Hingorani, M., O'Donnell, M., and Kuriyan, J. (2001) Mechanism of processivity clamp opening by the delta subunit wrench of the clamp loader complex of *E. coli* DNA polymerase III, *Cell 106*, 417-428.
196. Trakselis, M. A., and Benkovic, S. J. (2001) Intricacies in ATP-dependent clamp loading: Variations across replication systems, *Structure 9*, 999-1004.
197. Bloom, L. B. (2009) Loading clamps for DNA replication and repair, *DNA Repair (Amst) 8*, 570-578.
198. Trakselis, M. A., Alley, S. C., Abel-Santos, E., and Benkovic, S. J. (2001) Creating a dynamic picture of the sliding clamp during T4 DNA polymerase holoenzyme assembly by using fluorescence resonance energy transfer, *Proc. Natl. Acad. Sci. U.S.A. 98*, 8368-8375.
199. Smiley, R. D., Zhuang, Z., Benkovic, S. J., and Hammes, G. G. (2006) Single-molecule investigation of the T4 bacteriophage DNA polymerase holoenzyme: Multiple pathways of holoenzyme formation, *Biochemistry 45*, 7990-7997.
200. Trakselis, M. A., Berdis, A. J., and Benkovic, S. J. (2003) Examination of the role of the clamp-loader and ATP hydrolysis in the formation of the bacteriophage T4 polymerase holoenzyme, *J. Mol. Biol. 326*, 435-451.
201. Thompson, J. A., Paschall, C. O., O'Donnell, M., and Bloom, L. B. (2009) A slow ATP-induced conformational change limits the rate of DNA binding but not the rate of beta clamp binding by the *Escherichia coli* gamma complex clamp loader, *J. Biol. Chem. 284*, 32147-32157.

202. Bertram, J. G., Bloom, L. B., Hingorani, M. M., Beechem, J. M., O'Donnell, M., and Goodman, M. F. (2000) Molecular mechanism and energetics of clamp assembly in *Escherichia coli*. The role of ATP hydrolysis when gamma complex loads beta on DNA, *J. Biol. Chem. 275*, 28413-28420.
203. Hayner, J. N., and Bloom, L. B. (2013) The beta sliding clamp closes around DNA prior to release by the *Escherichia coli* clamp loader gamma complex, *J. Biol. Chem. 288*, 1162-1170.
204. Thompson, J. A., Marzahn, M. R., O'Donnell, M., and Bloom, L. B. (2012) Replication factor C is a more effective proliferating cell nuclear antigen (PCNA) opener than the checkpoint clamp loader, Rad24-RFC, *J. Biol. Chem. 287*, 2203-2209.
205. Yao, N. Y., Johnson, A., Bowman, G. D., Kuriyan, J., and O'Donnell, M. (2006) Mechanism of proliferating cell nuclear antigen clamp opening by replication factor C, *J. Biol. Chem. 281*, 17528-17539.
206. Gomes, X. V., and Burgers, P. M. (2001) ATP utilization by yeast replication factor C. I. ATP-mediated interaction with DNA and with proliferating cell nuclear antigen, *J. Biol. Chem. 276*, 34768-34775.
207. Hedglin, M., Perumal, S. K., Hu, Z., and Benkovic, S. (2013) Stepwise assembly of the human replicative polymerase holoenzyme, *Elife 2*, e00278.
208. Erzberger, J. P., and Berger, J. M. (2006) Evolutionary relationships and structural mechanisms of AAA^+ proteins, *Annu. Rev. Biophys. Biomol. Struct. 35*, 93-114.
209. Neuwald, A. F., Aravind, L., Spouge, J. L., and Koonin, E. V. (1999) AAA^+: A class of chaperone-like ATPases associated with the assembly, operation, and disassembly of protein complexes, *Genome Res. 9*, 27-43.
210. Turner, J., Hingorani, M. M., Kelman, Z., and O'Donnell, M. (1999) The internal workings of a DNA polymerase clamp-loading machine, *EMBO J. 18*, 771-783.
211. Hingorani, M. M., and O'Donnell, M. (1998) ATP binding to the *Escherichia coli* clamp loader powers opening of the ring-shaped clamp of DNA polymerase III holoenzyme, *J. Biol. Chem. 273*, 24550-24563.
212. Bertram, J. G., Bloom, L. B., Turner, J., O'Donnell, M., Beechem, J. M., and Goodman, M. F. (1998) Pre-steady state analysis of the assembly of wild type and mutant circular clamps of *Escherichia coli* DNA polymerase III onto DNA, *J. Biol. Chem. 273*, 24564-24574.
213. Hingorani, M. M., Bloom, L. B., Goodman, M. F., and O'Donnell, M. (1999) Division of labor--sequential ATP hydrolysis drives assembly of a DNA polymerase sliding clamp around DNA, *EMBO J. 18*, 5131-5144.
214. Downey, C. D., Crooke, E., and McHenry, C. S. (2011) Polymerase chaperoning and multiple ATPase sites enable the *E. coli* DNA polymerase III holoenzyme to rapidly form initiation complexes, *J. Mol. Biol. 412*, 340-353.
215. Mossi, R., and Hubscher, U. (1998) Clamping down on clamps and clamp loaders - The eukaryotic replication factor C, *Eur. J. Biochem. 254*, 209-216.
216. Bowman, G. D., O'Donnell, M., and Kuriyan, J. (2004) Structural analysis of a eukaryotic sliding DNA clamp-clamp loader complex, *Nature 429*, 724-730.
217. Jeruzalmi, D., O'Donnell, M., and Kuriyan, J. (2001) Crystal structure of the processivity clamp loader gamma complex of *E. coli* DNA polymerase III, *Cell 106*, 429-441.

218. Yao, N. Y., and O'Donnell, M. (2012) The RFC clamp loader: Structure and function, *Subcell Biochem. 62*, 259-279.
219. Gulbis, J. M., Kelman, Z., Hurwitz, J., O'Donnell, M., and Kuriyan, J. (1996) Structure of the C-terminal region of p21(WAF1/CIP1) complexed with human PCNA, *Cell 87*, 297-306.
220. Moldovan, G. L., Pfander, B., and Jentsch, S. (2007) PCNA, the maestro of the replication fork, *Cell 129*, 665-679.
221. Dalrymple, B. P., Kongsuwan, K., Wijffels, G., Dixon, N. E., and Jennings, P. A. (2001) A universal protein-protein interaction motif in the eubacterial DNA replication and repair systems, *Proc. Natl. Acad. Sci. U.S.A. 98*, 11627-11632.
222. Wijffels, G., Dalrymple, B. P., Prosselkov, P., Kongsuwan, K., Epa, V. C., Lilley, P. E., Jergic, S., Buchardt, J., Brown, S. E., Alewood, P. F., Jennings, P. A., and Dixon, N. E. (2004) Inhibition of protein interactions with the beta 2 sliding clamp of *Escherichia coli* DNA polymerase III by peptides from beta 2-binding proteins, *Biochemistry 43*, 5661-5671.
223. Shamoo, Y., and Steitz, T. A. (1999) Building a replisome from interacting pieces: Sliding clamp complexed to a peptide from DNA polymerase and a polymerase editing complex, *Cell 99*, 155-166.
224. Seybert, A., and Wigley, D. B. (2004) Distinct roles for ATP binding and hydrolysis at individual subunits of an archaeal clamp loader, *EMBO J. 23*, 1360-1371.
225. Seybert, A., Scott, D. J., Scaife, S., Singleton, M. R., and Wigley, D. B. (2002) Biochemical characterisation of the clamp/clamp loader proteins from the euryarchaeon *Archaeoglobus fulgidus*, *Nucl. Acids Res. 30*, 4329-4338.
226. Miyata, T., Suzuki, H., Oyama, T., Mayanagi, K., Ishino, Y., and Morikawa, K. (2005) Open clamp structure in the clamp-loading complex visualized by electron microscopic image analysis, *Proc. Natl. Acad. Sci. U.S.A. 102*, 13795-13800.
227. Miyata, T., Oyama, T., Mayanagi, K., Ishino, S., Ishino, Y., and Morikawa, K. (2004) The clamp-loading complex for processive DNA replication, *Nat. Struct. Mol. Biol. 11*, 632-636.
228. Yao, N. Y., Georgescu, R. E., Finkelstein, J., and O'Donnell, M. E. (2009) Single-molecule analysis reveals that the lagging strand increases replisome processivity but slows replication fork progression, *Proc. Natl. Acad. Sci. U.S.A. 106*, 13236-13241.
229. Hu, Z., Perumal, S. K., Yue, H., and Benkovic, S. J. (2012) The human lagging strand DNA polymerase delta holoenzyme is distributive, *J. Biol. Chem. 287*, 38442-38448.
230. Langston, L. D., and O'Donnell, M. (2008) DNA polymerase delta is highly processive with proliferating cell nuclear antigen and undergoes collision release upon completing DNA, *J. Biol. Chem. 283*, 29522-29531.
231. Bauer, R. J., Graham, B. W., and Trakselis, M. A. (2013) Novel interaction of the bacterial-Like DnaG primase with the MCM helicase in archaea, *J. Mol. Biol. 425*, 1259-1273.
232. McGeoch, A. T., Trakselis, M. A., Laskey, R. A., and Bell, S. D. (2005) Organization of the archaeal MCM complex on DNA and implications for the helicase mechanism, *Nat. Struct. Mol. Biol. 12*, 756-762.
233. Svergun, D. I., Petoukhov, M. V., and Koch, M. H. (2001) Determination of domain structure of proteins from X-ray solution scattering, *Biophys J 80*, 2946-2953.

234. Svergun, D. I. (1999) Restoring low resolution structure of biological macromolecules from solution scattering using simulated annealing, *Biophys J 76*, 2879-2886.
235. Volkov, V. V., and Svergun, D. I. (2003) Uniqueness of *ab initio* shape determination in small-angle scattering, *J. Appl. Cryst. 36*, 860-864.
236. Cann, I. K., Ishino, S., Yuasa, M., Daiyasu, H., Toh, H., and Ishino, Y. (2001) Biochemical analysis of replication factor C from the hyperthermophilic archaeon *Pyrococcus furiosus*, *J. Bacteriol. 183*, 2614-2623.
237. von Hippel, P. H., Fairfield, F. R., and Dolejsi, M. K. (1994) On the processivity of polymerases, *Ann. N.Y. Acad. Sci. 726*, 118-131.
238. Hacker, K. J., and Alberts, B. M. (1994) The slow dissociation of the T4 DNA polymerase holoenzyme when stalled by nucleotide omission. An indication of a highly processive enzyme, *J. Biol. Chem. 269*, 24209-24220.
239. Svergun, D. I. (1992) Determination of the regularization parameter in indirect-transform methods using perceptual criteria, *J. Appl. Cryst. 25*, 495-503.
240. Debyser, Z., Tabor, S., and Richardson, C. C. (1994) Coordination of leading and lagging strand DNA synthesis at the replication fork of bacteriophage T7, *Cell 77*, 157-166.
241. Kadyrov, F. A., and Drake, J. W. (2001) Conditional coupling of leading-strand and lagging-strand DNA synthesis at bacteriophage T4 replication forks, *J. Biol. Chem. 276*, 29559-29566.
242. Kim, S., Dallmann, H. G., McHenry, C. S., and Marians, K. J. (1996) tau couples the leading- and lagging-strand polymerases at the *Escherichia coli* DNA replication fork, *J. Biol. Chem. 271*, 21406-21412.
243. Alley, S. C., Abel-Santos, E., and Benkovic, S. J. (2000) Tracking sliding clamp opening and closing during bacteriophage T4 DNA polymerase holoenzyme assembly, *Biochemistry 39*, 3076-3090.
244. Kumar, R., Nashine, V. C., Mishra, P. P., Benkovic, S. J., and Lee, T. H. (2010) Stepwise loading of yeast clamp revealed by ensemble and single-molecule studies, *Proc. Natl. Acad. Sci. U.S.A. 107*, 19736-19741.
245. Perumal, S. K., Ren, W., Lee, T. H., and Benkovic, S. J. (2013) How a holoenzyme for DNA replication is formed, *Proc. Natl. Acad. Sci. U.S.A. 110*, 99-104.
246. Gomes, X. V., Schmidt, S. L., and Burgers, P. M. (2001) ATP utilization by yeast replication factor C. II. Multiple stepwise ATP binding events are required to load proliferating cell nuclear antigen onto primed DNA, *J. Biol. Chem. 276*, 34776-34783.
247. Chen, S., Levin, M. K., Sakato, M., Zhou, Y., and Hingorani, M. M. (2009) Mechanism of ATP-driven PCNA clamp loading by *S. cerevisiae* RFC, *J. Mol. Biol. 388*, 431-442.
248. Anderson, S. G., Thompson, J. A., Paschall, C. O., O'Donnell, M., and Bloom, L. B. (2009) Temporal correlation of DNA binding, ATP hydrolysis, and clamp release in the clamp loading reaction catalyzed by the *Escherichia coli* gamma complex, *Biochemistry 48*, 8516-8527.
249. Kaboord, B. F., and Benkovic, S. J. (1996) Dual role of the 44/62 protein as a matchmaker protein and DNA polymerase chaperone during assembly of the bacteriophage T4 holoenzyme complex, *Biochemistry 35*, 1084-1092.
250. Hlinkova, V., Xing, G., Bauer, J., Shin, Y. J., Dionne, I., Rajashankar, K. R., Bell, S. D., and Ling, H. (2008) Structures of monomeric, dimeric and trimeric PCNA: PCNA-ring assembly and opening, *Acta Crystallogr. D Biol. Crystallogr. 64*, 941-949.

251. Williams, G. J., Johnson, K., Rudolf, J., McMahon, S. A., Carter, L., Oke, M., Liu, H., Taylor, G. L., White, M. F., and Naismith, J. H. (2006) Structure of the heterotrimeric PCNA from *Sulfolobus solfataricus*, *Acta Crystallograph. Sect. F. Struct. Biol. Cryst. Commun. 62*, 944-948.
252. Winter, J. A., and Bunting, K. A. (2012) Rings in the extreme: PCNA interactions and adaptations in the archaea, *Archaea 2012*, 951010.
253. Zhuang, Z., and Ai, Y. (2010) Processivity factor of DNA polymerase and its expanding role in normal and translesion DNA synthesis, *Biochimica et Biophysica Acta (BBA) - Proteins and Proteomics 1804*, 1081-1093.
254. Mace, D. C., and Alberts, B. M. (1984) T4 DNA polymerase: Rates and processivity on single-stranded DNA templates, *J. Mol. Biol. 177*, 295-311.
255. Bauer, R. J., Wolff, I. D., Zuo, X., Lin, H.-K., and Trakselis, M. A. (2013) Assembly and Distributive Action of an Archaeal DNA Polymerase Holoenzyme, *J. Mol. Biol. 425*, 4820-4836.
256. Clausen, A. R., Murray, M. S., Passer, A. R., Pedersen, L. C., and Kunkel, T. A. (2013) Structure–function analysis of ribonucleotide bypass by B family DNA replicases, *Proc. Natl. Acad. Sci. U.S.A. 110*, 16802-16807.
257. Acharya, N., Johnson, R. E., Prakash, S., and Prakash, L. (2006) Complex formation with Rev1 enhances the proficiency of *Saccharomyces cerevisiae* DNA polymerase ζ for mismatch extension and for extension opposite from DNA lesions, *Mol. Cell. Biol. 26*, 9555-9563.
258. Lawrence, C. W. (2002) Cellular roles of DNA polymerase ζ and Rev1 protein, *DNA Repair 1*, 425-435.
259. Wood, A., Garg, P., and Burgers, P. M. J. (2007) A ubiquitin-binding motif in the translesion DNA polymerase Rev1 mediates Its essential functional interaction with ubiquitinated proliferating cell nuclear antigen in response to DNA damage, *J. Biol. Chem. 282*, 20256-20263.
260. Pages V, F. R. (2002) How DNA lesions are turnd into mutations within cells?, *Oncogene 21*, 8957-8966.
261. Heltzel, J. M. H., Maul, R. W., Wolff, D. W., and Sutton, M. D. (2012) *Escherichia coli* DNA polymerase IV (pol IV), but not pol II, dynamically switches with a stalled pol III* replicase, *J. Bacteriol. 194*, 3589-3600.
262. Comeau, S. R., Gatchell, D. W., Vajda, S., and Camacho, C. J. (2004) ClusPro: A fully automated algorithm for protein–protein docking, *Nucl. Acids Res. 32*, W96-W99.
263. Daraba, A., Gali, V. K., Halmai, M., Haracska, L., and Unk, I. (2014) Def1 Promotes the Degradation of Pol3 for Polymerase Exchange to Occur During DNA-Damage–Induced Mutagenesis in *Saccharomyces cerevisiae*, *PLoS Biol. 12*, e1001771.
264. Rouillon, C., Henneke, G., Flament, D., Querellou, J., and Raffin, J.-P. (2007) DNA polymerase switching on homotrimeric PCNA at the replication fork of the euryarchaea *Pyrococcus abyssi*, *J. Mol. Biol. 369*, 343-355.
265. Pisani, F. M., Manco, G., Carratore, V., and Rossi, M. (1996) Domain organization and DNA-induced conformational changes of an archaeal family B DNA polymerase†, *Biochemistry 35*, 9158-9166.

266. Iyer, L. M., Koonin, E. V., Leipe, D. D., and Aravind, L. (2005) Origin and evolution of the archaeo-eukaryotic primase superfamily and related palm-domain proteins: Structural insights and new members, *Nucl. Acids Res. 33*, 3875-3896.
267. Walter, P., Klein, F., Lorentzen, E., Ilchmann, A., Klug, G., and Evguenieva-Hackenberg, E. (2006) Characterization of native and reconstituted exosome complexes from the hyperthermophilic archaeon *Sulfolobus solfataricus*, *Mol. Microbiol. 62*, 1076-1089.
268. Yuzhakov, A., Turner, J., and O'Donnell, M. (1996) Replisome assembly reveals the basis for asymmetric function in leading and lagging strand replication, *Cell 86*, 877-886.
269. Kaplan, D. L., and Steitz, T. A. (1999) DnaB from *Thermus aquaticus* unwinds forked duplex DNA with an asymmetric tail length dependence, *J. Biol. Chem. 274*, 6889-6897.
270. Rothenberg, E., Trakselis, M. A., Bell, S. D., and Ha, T. (2007) MCM forked substrate specificity involves dynamic interaction with the 5'-tail, *J. Biol. Chem. 282*, 34229-34234.
271. Wu, K., Lai, X., Guo, X., Hu, J., Xiang, X., and Huang, L. (2007) Interplay between primase and replication factor C in the hyperthermophilic archaeon *Sulfolobus solfataricus*, *Mol. Microbiol. 63*, 826-837.
272. Chong, J. P., Hayashi, M. K., Simon, M. N., Xu, R. M., and Stillman, B. (2000) A double-hexamer archaeal minichromosome maintenance protein is an ATP-dependent DNA helicase, *Proc. Natl. Acad. Sci. U.S.A. 97*, 1530-1535.
273. Godson, G. N., Schoenich, J., Sun, W., and Mustaev, A. A. (2000) Identification of the magnesium ion binding site in the catalytic center of *Escherichia coli* primase by iron cleavage, *Biochemistry 39*, 332-339.
274. Rodina, A., and Godson, G. N. (2006) Role of conserved amino acids in the catalytic activity of *Escherichia coli* primase, *J. Bacteriol. 188*, 3614-3621.
275. Chang, P., and Marians, K. J. (2000) Identification of a region of *Escherichia coli* DnaB required for functional interaction with DnaG at the replication fork, *J. Biol. Chem. 275*, 26187-26195.
276. Chintakayala, K., Larson, M. A., Griep, M. A., Hinrichs, S. H., and Soultanas, P. (2008) Conserved residues of the C-terminal p16 domain of primase are involved in modulating the activity of the bacterial primosome, *Mol. Microbiol. 68*, 360-371.
277. De Falco, M., Ferrari, E., De Felice, M., Rossi, M., Hubscher, U., and Pisani, F. M. (2007) The human GINS complex binds to and specifically stimulates human DNA polymerase alpha-primase, *EMBO Rep. 8*, 99-103.
278. Bermudez, V. P., Farina, A., Raghavan, V., Tappin, I., and Hurwitz, J. (2011) Studies on human DNA polymerase epsilon and GINS complex and their role in DNA replication, *J. Biol. Chem. 286*, 28963-28977.
279. McGeoch, A. T., and Bell, S. D. (2005) Eukaryotic/archaeal primase and MCM proteins encoded in a bacteriophage genome, *Cell 120*, 167-168.
280. Samuels, M., Gulati, G., Shin, J. H., Opara, R., McSweeney, E., Sekedat, M., Long, S., Kelman, Z., and Jeruzalmi, D. (2009) A biochemically active MCM-like helicase in *Bacillus cereus*, *Nucl. Acids Res. 37*, 4441-4452.
281. Zhou, B., Arnett, D. R., Yu, X., Brewster, A., Sowd, G. A., Xie, C. L., Vila, S., Gai, D., Fanning, E., and Chen, X. S. (2012) Structural basis for the interaction of a hexameric

replicative helicase with the regulatory subunit of human DNA polymerase alpha-primase, *J. Biol. Chem. 287*, 26854-26866.
282. Kirk, B. W., and Kuchta, R. D. (1999) Arg304 of human DNA primase is a key contributor to catalysis and NTP binding: Primase and the family X polymerases share significant sequence homology, *Biochemistry 38*, 7727-7736.
283. Li, Z., Santangelo, T. J., Čuboňová, Ľ., Reeve, J. N., and Kelman, Z. (2010) Affinity purification of an archaeal DNA replication protein network, *mBio 1*.
284. Lao-Sirieix, S. H., Pellegrini, L., and Bell, S. D. (2005) The promiscuous primase, *Trends Genet. 21*, 568-572.
285. Evguenieva-Hackenberg, E., Walter, P., Hochleitner, E., Lottspeich, F., and Klug, G. (2003) An exosome-like complex in *Sulfolobus solfataricus*, *EMBO Rep. 4*, 889-893.
286. Witharana, C., Roppelt, V., Lochnit, G., Klug, G., and Evguenieva-Hackenberg, E. (2012) Heterogeneous complexes of the RNA exosome in *Sulfolobus solfataricus*, *Biochimie 94*, 1578-1587.
287. Evguenieva-Hackenberg, E., Roppelt, V., Lassek, C., and Klug, G. (2011) Subcellular localization of RNA degrading proteins and protein complexes in prokaryotes, *RNA Biology 8*, 49-54.
288. Roppelt, V., Hobel, C. F. V., Albers, S. V., Lassek, C., Schwarz, H., Klug, G., and Evguenieva-Hackenberg, E. (2010) The archaeal exosome localizes to the membrane, *FEBS Lett. 584*, 2791-2795.
289. Gristwood, T., Duggin, I. G., Wagner, M., Albers, S. V., and Bell, S. D. (2012) The sub-cellular localization of *Sulfolobus* DNA replication, *Nucl. Acids Res. 40*, 5487-5496.
290. Bernstein, J. A., and Richardson, C. C. (1989) Characterization of the helicase and primase activities of the 63-kDa component of the bacteriophage T7 gene 4 protein, *J. Biol. Chem. 264*, 13066-13073.
291. Bhattacharyya, S., and Griep, M. A. (2000) DnaB helicase affects the initiation specificity of *Escherichia coli* primase on single-stranded DNA templates, *Biochemistry 39*, 745-752.
292. Pandey, M., Syed, S., Donmez, I., Patel, G., Ha, T., and Patel, S. S. (2009) Coordinating DNA replication by means of priming loop and differential synthesis rate, *Nature 462*, 940-943.
293. Heisenberg, C.-P., and Bellaïche, Y. (2013) Forces in Tissue Morphogenesis and Patterning, *Cell 153*, 948-962.
294. Chung, M.-I., Nascone-Yoder, N. M., Grover, S. A., Drysdale, T. A., and Wallingford, J. B. (2010) Direct activation of Shroom3 transcription by Pitx proteins drives epithelial morphogenesis in the developing gut, *Development 137*, 1339-1349.
295. Hildebrand, J. D., and Soriano, P. (1999) Shroom, a PDZ domain–containing actin-binding protein, Is required for neural tube morphogenesis in mice, *Cell 99*, 485-497.
296. Tullio, A. N., Accili, D., Ferrans, V. J., Yu, Z.-X., Takeda, K., Grinberg, A., Westphal, H., Preston, Y. A., and Adelstein, R. S. (1997) Nonmuscle myosin II-B is required for normal development of the mouse heart, *Proc. Natl. Acad. Sci. U.S.A. 94*, 12407-12412.
297. Lee, C., Le, M.-P., and Wallingford, J. B. (2009) The shroom family proteins play broad roles in the morphogenesis of thickened epithelial sheets, *Dev. Dynam. 238*, 1480-1491.

298. Sawyer, J. M., Harrell, J. R., Shemer, G., Sullivan-Brown, J., Roh-Johnson, M., and Goldstein, B. (2010) Apical constriction: A cell shape change that can drive morphogenesis, *Dev. Biol. 341*, 5-19.
299. Amano, M., Ito, M., Kimura, K., Fukata, Y., Chihara, K., Nakano, T., Matsuura, Y., and Kaibuchi, K. (1996) Phosphorylation and activation of myosin by rho-associated kinase (rho-kinase), *J. Biol. Chem. 271*, 20246-20249.
300. Ikebe, M., Hartshorne, D. J., and Elzinga, M. (1987) Phosphorylation of the 20,000-dalton light chain of smooth muscle myosin by the calcium-activated, phospholipid-dependent protein kinase. Phosphorylation sites and effects of phosphorylation, *J. Biol. Chem. 262*, 9569-9573.
301. Jacobs, M., Hayakawa, K., Swenson, L., Bellon, S., Fleming, M., Taslimi, P., and Doran, J. (2006) The structure of dimeric Rock I reveals the mechanism for ligand selectivity, *J. Biol. Chem. 281*, 260-268.
302. Leung, T., Chen, X. Q., Manser, E., and Lim, L. (1996) The p160 RhoA-binding kinase ROK alpha is a member of a kinase family and is involved in the reorganization of the cytoskeleton, *Mol. Cell. Biol. 16*, 5313-5327.
303. Yamaguchi, H., Kasa, M., Amano, M., Kaibuchi, K., and Hakoshima, T. (2006) Molecular mechanism for the regulation of rho-kinase by dimerization and its inhibition by fasudil, *Structure 14*, 589-600.
304. Ishizaki T, M. M., Fujisawa K, Okawa K, Iwamatsu A, Fujita A, Watanabe N, Saito Y, Kakizuka A Morii N, and Narumiya S. (1996) The small GTP-binding protein Rho binds to and activates a 160 kDa Ser/Thr protein kinase homologous to myotonic dystrophy kinase, *EMBO J. 15*, 1885–1893.
305. Nishimura, T., and Takeichi, M. (2008) Shroom3-mediated recruitment of Rho kinases to the apical cell junctions regulates epithelial and neuroepithelial planar remodeling, *Development 135*, 1493-1502.
306. Dye, D. E., Karlen, S., Rohrbach, B., Staub, O., Braathen, L. R., Eidne, K. A., and Coombe, D. R. (2009) hShroom1 links a membrane bound protein to the actin cytoskeleton, *Cell Mol Life Sci 66*, 681-696.
307. Lee, C., Scherr, H. M., and Wallingford, J. B. (2007) Shroom family proteins regulate γ-tubulin distribution and microtubule architecture during epithelial cell shape change, *Development 134*, 1431-1441.
308. Kurosawa, N., and Grogan, D. W. (2005) Homologous recombination of exogenous DNA with the *Sulfolobus acidocaldarius* genome: Properties and uses, *FEMS Microbiol. Lett. 253*, 141-149.
309. Chen, L., Brügger, K., Skovgaard, M., Redder, P., She, Q., Torarinsson, E., Greve, B., Awayez, M., Zibat, A., Klenk, H.-P., and Garrett, R. A. (2005) The genome of *Sulfolobus acidocaldarius*, a model organism of the crenarchaeota, *J. Bacteriol. 187*, 4992-4999.
310. Grogan, D. W. (1996) Exchange of genetic markers at extremely high temperatures in the archaeon *Sulfolobus acidocaldarius*, *J. Bacteriol. 178*, 3207-3211.
311. Hansen, J. E., Dill, A. C., and Grogan, D. W. (2005) Conjugational genetic exchange in the hyperthermophilic archaeon *Sulfolobus acidocaldarius*: Intragenic recombination with minimal dependence on marker separation, *J. Bacteriol. 187*, 805-809.
312. Grogan, D. W. (2009) Homologous recombination in *Sulfolobus acidocaldarius*: Genetic assays and functional properties, *Biochem. Soc. Trans. 37*, 88-91.